NASA Contractor Report 179506

Oil Film Thickness Measurement and Analysis for an Angular Contact Ball Bearing Operating in Parched Elastohydrodynamic Lubrication

Scott D. Hunter

Case Western Reserve University
Cleveland, Ohio

September 1986

Prepared for
Lewis Research Center
Under Grant NCC 3-30

National Aeronautics and
Space Administration

OIL FILM THICKNESS MEASUREMENT AND ANALYSIS FOR AN ANGULAR CONTACT BALL BEARING OPERATING IN PARCHED ELASTOHYDRODYNAMIC LUBRICATION

by

Scott D. Hunter

The capacitance method is used to estimate the oil film thickness in the Hertzian contact zone of an angular contact ball bearing operating in parched elastohydrodynamic lubrication. The parched elastohydrodynamic lubrication regime is characterized by a transient film thickness and basic speed ratio (ball spin rate over combined race speed) and the formation of a friction polymer. The experimental apparatus tests 40 mm 108 H ball bearings in the counter rotating race mode at loads of 200 and 300 lb, a film parameter of 1.6 and nominal inner and outer race speeds of 38 and 26 rps, respectively. Experimental results are presented for the capacitance, thickness and conductance of the oil film as functions of elapsed time and for the basic speed ratio as a function of elapsed time, load and amount of lubricant applied to the test bearing.

Results indicate that a friction polymer formed from the initial lubricant has an effect on the capacitance and basic speed ratio measurements. Based on a secondary ion mass spectroscopy and

emission infrared spectroscopy analyses, the polymer contains carbon, carbon-hydrogen groups, possibly nitrogen and phosphate and forms a carboneous material during failure. The basic speed ratio shows a rapid increase before bearing failure due to the formation of the friction polymer which reduces the slip between the balls and races. The capacitance measurements also signify an approaching failure through a sudden decrease in capacitance and increase in conductance of the oil film due to the presence of surface metal in the film.

ACKNOWLEDGMENTS

I wish to thank Dr. Joseph M. Prahl for his advice, patience and support throughout this work and Edward Kingsbury of Stark Draper Laboratories for his advice and knowledge in the areas of parched EHL and the test rig.

TABLE OF CONTENTS

ABSTRACT	i
ACKNOWLEDGMENTS	iii
LIST OF SYMBOLS	vii
CHAPTER I - INTRODUCTION	1
1.1 Lubrication Regimes	1
1.2 Parched EHL	4
1.3 Basic Speed Ratio and Fluid Film Degradation	5
1.4 Fluid Film Analysis	9
1.5 Fluid Film Thickness Measurement	12
CHAPTER II - EXPERIMENTAL APPARATUS	23
2.1 BSR Test Rig	23
2.2 Initial Oil Film Thickness	29
2.3 Lubricants	32
2.4 Capacitance Measurement	32
2.5 Test Bearings	37
2.6 Outline of Different Tests	37
CHAPTER III - RESULTS AND DISCUSSION	55
3.1 Oil Film Thickness Calculation	55
3.2 Calibration Procedure	61
3.3 BSR and Capacitance Versus Initial Film Thickness	64
3.4 BSR Comparison at Different Loads	69
3.5 Tests to Failure	69
3.6 Film Thickness Time Study Tests	74
3.7 Friction Polymer Analysis	78
3.8 Conclusion	80
REFERENCES	146
APPENDIX A - BASIC SPEED RATIO CALCULATIONS WITH NO SLIP	148
APPENDIX B - ERROR ANALYSIS FOR BALL SPEED MEASUREMENT AND BASIC SPEED RATIO	160

APPENDIX C - ERROR ANALYSIS FOR INITIAL OIL FILM THICKNESS 163

APPENDIX D - EXPERIMENTAL DATA FOR TEST TO FAILURE NO. 1 166

APPENDIX E - EXPERIMENTAL DATA FOR TEST TO FAILURE NO. 2 172

APPENDIX F - EXPERIMENTAL DATA FOR BSR VERSUS OIL/FREON CONCENTRATION NO. 1 182

APPENDIX G - EXPERIMENTAL DATA FOR BSR VERSUS OIL/FREON CONCENTRATION NO. 2 193

APPENDIX H - EXPERIMENTAL DATA FOR TIME STUDY NO. 1 218

APPENDIX I - EXPERIMENTAL DATA FOR TIME STUDY NO. 2 232

LIST OF SYMBOLS

A	area of contact ellipse
a	radius of contact ellipse along y-axis
BSR	basic speed ratio
b	radius of contact ellipse along x-axis
$\tilde{C}$	capacitance across two flat plates
C_H	capacitance across Hertzian contact zone
C_L	capacitance across region in the plane perpendicular to direction of motion
C_M	total measured capacitance across bearing races
C_S	capacitance measured with no balls or lubricant in test bearing
C_T	capacitance across Hertzian contact zone and surrounding region
C_i	ball-inner race contact capacitance
C_o	ball-outer race contact capacitance
$\tilde{C}_a$	capacitance of air across two flat plates
$\tilde{C}_o$	capacitance of oil across two flat plates
C_1	capacitance across surfaces in the inlet region
C_2	capacitance across surfaces in the outlet region
D	distance between race curvature centers
d	ball diameter
$\tilde{d}$	distance between two flat plates
d_e	pitch diameter
E	modulus of elasticity
$\tilde{E}$	activation energy for the average degradation reaction

E' reduced modulus of elasticity

e error

F applied load to one ball

$\tilde{F}$ normal force

$\mathcal{F}$ $(\pi/2) + q \ln \alpha$

F_T total applied load

f_b rms surface finish of ball

f_i inner race conformity ratio

f_o outer race conformity ratio

f_r rms surface finish of race

h oil film thickness

h_o average oil film thickness

K $\pi k E'(R \tilde{\varepsilon}/4.5\mathcal{F})$

k ellipticity parameter, a/b

m_o mass of oil

n number of balls in bearing

P_d diametral clearance

p pressure

q $(\pi/2) - 1$

R radius of relative curvature

$\tilde{R}$ rate of degradation

R_a radius of surface a

R_b radius of surface b

S algebraic difference of the inner and outer race angular velocities

$\tilde{S}$ shear energy dissipated in elastohydrodynamic contact

$\tilde{T}$ tangential (friction) force

T' contact transit time

t time

u slip velocity

X $b^2\varepsilon_o/2\ R\ h_o\ \varepsilon_a$

x upstream miniscus position

x_o position that separates starvation from fully flooded

Y $(\varepsilon_o\ \varepsilon_a/h_o)^{-1/2}\ C_{1,2}$

y distance from edge of a flat plate

$\ddot{y}$ acceleration

z number of balls in bearing

α radius ratio

α' pressure-viscosity coefficient

β contact angle under an applied load

β_f free contact angle

γ_i inner race grove radius

γ_o outer race groove radius

δ initial oil film thickness

$\dot{\delta}$ ball spin-about-its-own-center angular velocity

$\hat{\delta x}$ dimensional error associated with quantity x

δ' total elastic deformation

ε $1 + q/\alpha$

$\tilde{\varepsilon}$ dielectric constant

ε_a dielectric constant of air

ε_o dielectric constant of SRG 200 oil

ε_0' dielectric constant of oil in Hertzian contact zone

ζ $1/\xi$

η dynamic viscosity

η_0 dynamic viscosity at atmospheric pressure

Λ film parameter

μ coefficient of friction

ν kinematic viscosity

ν' Poisson's ratio

ξ x/b

ρ_0 density of oil

τ limiting shear stress

ω_B ball angular velocity about its own center

ω_C ball separator angular velocity

ω_i inner race angular velocity

ω_o outer race angular velocity

CHAPTER I

INTRODUCTION

Lubrication and wear are two important fundamental aspects of all machinery and processes that must be dealt with on a continuous basis. As noted by Hamrock [1], even before the birth of Christ, stones were used in plough shares and in the soles of Roman military sandals to reduce wear. But it wasn't until the 20th century that four distinct modes of lubrication were recognized.

1.1 LUBRICATION REGIMES

The four lubrication regimes in order of decreasing film thickness between surfaces in relative motion are hydrodynamic or fluid film, elastohydrodynamic, mixed and boundary lubrication. Stribeck distinguished the different regimes from one another by their coefficient of friction μ and film parameter Λ as noted by Hamrock [1]:

$$\mu = \frac{\tilde{T}}{\tilde{F}} \tag{1}$$

where $\tilde{T}$ is the tangential (friction) force and $\tilde{F}$ is the normal force and

$$\Lambda = \frac{h}{\left(f_r^2 + f_b^2\right)^{1/2}} \tag{2}$$

where f_r is the rms surface finish of the race and f_b is the rms surface finish of the ball. Fig. 1.1 shows the coefficient of

friction as a function of film parameter for the different regimes.

Osborne Reynolds in 1886 [2] showed that a load could be supported by the pressure built up in the converging section of a journal bearing. The two surfaces transmitting the load are completely separated by a fluid film normally greater than 10^{-6} m thick with very low frictional shear. Reynolds called this mode fluid film or hydrodynamic lubrication and it is now known that the physical properties of the lubricant control the characteristics of the bearing.

The second mode of lubrication is elastohydrodynamic lubrication (EHL). In rolling element bearings and gears, fluid film lubrication exists in the contact zone where high pressures are generated and the bearing surfaces elastically distort but no asperity contact occurs. In EHL the physical properties of the lubricant are important and the fluid film thickness is between 10^{-7} and 10^{-6} m.

Mixed lubrication lies between EHL and boundary lubrication and is characterized by some asperity contact and partial fluid film lubrication action that develops in the bulk space between the surfaces. The film thickness in a mixed lubrication contact is between 10^{-6} and 10^{-8} m.

William Harding introduced boundary lubrication in the early 1920's. He proposed that very thin films adhering to surfaces were often sufficient to allow easy relative motion of those surfaces and that the chemical properties of the films and surfaces dictate

their performance. Door hinges and diamond pivots in instruments are examples of boundary lubrication where the surface films vary in thickness from 5×10^{-9} to 10^{-8} m and asperity contact does occur.

The shape of the curve in fig. 1.1 is explained by looking at how the normal force $\tilde{F}$ and tangential force $\tilde{T}$ vary with h. In hydrodynamic lubrication, $\tilde{F}$ is proportional to $1/h^2$ whereas h has little effect on the normal force in EHL so that $\tilde{F}$ is virtually independent of h. In hydrodynamic and EHL, $\tilde{T}$ is proportional to $1/h$ so that

$$(\mu)_{HL} \propto \frac{\frac{1}{h}}{\left(\frac{1}{h}\right)^2} \propto h \tag{3}$$

$$(\mu)_{EHL} \propto \frac{\frac{1}{h}}{\text{constant}} \propto \frac{1}{h} \tag{4}$$

which explains the form of fig. 1.1 as noted by Hamrock [1].

EHL can be further subdivided into three different regimes - fully flooded, starved and parched. In the fully flooded regime, there is an ample supply of free bulk oil outside the contact zone, the bearing operates with no asperity contact and will, in theory, run indefinitely. In the starved regime, there is less free bulk oil than in the fully flooded regime but enough to keep the bearing operating with a steady state behavior. Hamrock [1] notes that the fully flooded EHL film thickness predictions can be modified to predict film thicknesses in the starved regime:

$$\frac{h_{starved}}{h_{fully\ flooded}} = \left[\frac{\frac{x}{b} - 1}{\frac{x_o}{b} - 1}\right]^{0.29} \qquad (5)$$

where h is the film thickness, x is the upstream miniscus position, x_o is the position that separates starvation from fully flooded and b is the Hertz halfwidth in the direction of rolling. When less lubricant is used than in the starved regime and there is no free bulk oil outside the contact zone, the above equation becomes invalid and the parched EHL regime is reached.

1.2 PARCHED EHL

The parched EHL regime is introduced because fully flooded and starved EHL fail to describe the conditions and subsequent fluid film thickness transient when there is very little or no free bulk oil as in instrument ball bearings. Parched EHL is defined by Kingsbury [3] as having no flow anywhere in the system except inside the Hertzian contacts due to the lack of free bulk oil which doesn't replenish the amount forced out of the contact zone as the bearing operates. Even though parched EHL doesn't seem like it provides the best operating conditions for instrument ball bearings, it does produce the least driving torque and best possible spin definition for stability and yet the bearings can operate for years as noted by Kingsbury [3].

To show that the oil films outside the contact zone are immobile in a ball bearing operating in parched EHL, Singleterry [4] looked at the Jeffreys equation for drainage from an accelerated flat plate:

$$h = \sqrt{\frac{y\nu}{\ddot{y}t}} \tag{6}$$

where h is the film thickness at a distance y from the edge of the plate. The flat plate is accelerated at $\ddot{y}$ for time t and is covered with an oil of kinematic viscosity ν. For a plate covered with an oil of $\nu = 7.5$ cm^2/sec, Kingsbury [3] calculated that the film thickness is 9×10^{-5} cm, 1 cm from the edge and decreasing in thickness at 4×10^{-9} cm each second for an acceleration of 100 g's. Based on this analysis, one can deduce that there is no flow back into the contact zone between ball passes in a ball bearing operating in parched EHL.

1.3 BASIC SPEED RATIO (BSR) AND FLUID FILM DEGRADATION

As the fluid film thickness in parched EHL decreases with time, the high pressure and shear stresses in the contact zone cause the oil to breakdown and turn into a friction polymer. This polymer adheres to the bearing surfaces and changes the operating characteristics of the ball bearing. A characteristic number associated with every angular contact ball bearing is the basic speed ratio (BSR)

$$BSR = \frac{\dot{\delta}}{S} \tag{7}$$

where $\dot{\delta}$ is the ball-spin-about-its-own-center angular velocity and S is the algebraic difference of the race angular velocities. The BSR is a sensitive measure of the ball-lubricant-race coupling or slip in a ball bearing. For an angular contact ball bearing with

no slip at the ball-inner and ball-outer contacts, and equal inner and outer contact angles, the following is obtained

$$BSR = \frac{d_e^2 - d^2 \cos^2 \beta}{2 d_e d} \tag{8}$$

where d_e is the pitch diameter, d is the ball diameter, and β is the bearing contact angle. See appendix A for detailed calculations. Note that the BSR with no slip is a function of bearing geometry only and applies to inner, outer, and mutual race rotation modes equally as described by Kingsbury [5].

In parched EHL the film thickness decreases with time due to no inflow into the Hertzian contact zone which reduces the amount of rheologic slip between the balls and races, leading to an increase in BSR. Due to the kinematic slip, the shear increases as the oil film becomes thinner, leading to a higher lubricant degradation rate, the formation of friction polymer and hence a higher BSR. Fig. 1.2 shows a plot of the BSR versus time for an angular contact ball bearing operating in parched EHL. The data scatter at the beginning is typical as the bearing settles in. The gradual increase in BSR leads into a more rapid increase caused by the formation of the polymer. Examination of the balls after the test shows a band of polymer in the wear track as in fig. 1.3. Whereas the oil that was initially applied can be washed away with Freon, the polymer cannot be washed away as shown in fig. 1.4 and is removed only after wiping the film on the ball with a cloth. If the test is stopped before asperity contact takes place, no surface

damage occurs and the balls can be used again after being cleaned but if the film gets too thin, metal-to-metal contact occurs and the bearing fails, as in fig. 1.5. A magnified view of the wear track is shown in fig. 1.6, verifying the surface damage to the ball bearing.

In normal EHL films, the degradation of the lubricant film is negligible but when the films get too thin, the degradation can be very rapid. Kingsbury suggests that the rate of degradation can be represented by

$$\tilde{R} = (\text{constant}) \exp\left[\frac{-\tilde{E}}{\tilde{S}}\right] \tag{9}$$

where $\tilde{E}$ is an activation energy for the average degradation reaction and $\tilde{S}$ is the shear energy dissipated in the EHL contact. The shear energy dissipated for constant pivoting kinematic slip is

$$\tilde{S} = \frac{uT'\tau}{h} \tag{10}$$

where u is the slip velocity, h the film thickness, T' the contact transit time and τ the limiting shear stress. Taking the ratio of two rates as the film thickness goes from h_1 to h_2

$$\frac{R_1}{R_2} = \exp\left[\frac{-\tilde{E}}{uT'\tau}(h_1 - h_2)\right] \tag{11}$$

For $\tilde{E} = 3\text{x}10^{+8}$ J/m^3 (energy required to add a CH2 group to many organic forms), $\tau = 3\text{x}10^{+7}$ Pa [6], $u = 0.04$ m/sec [7], $T'' = 3\text{x}10^{-5}$ sec and for a film difference of $4\text{x}10^{-7}$ m (10 μin.) [8], the degradation is 25 times faster in the thinner film. As the film gets thinner, the degradation rate increases significantly as noted by Kingsbury [8].

Besides time, the BSR is effected by load, temperature and the amount of oil initially applied to the bearing. A higher load decreases the film thickness and changes the contact angle, causing a reduction in slip and increase in the BSR. There have been instances reported where the film thickness has remained the same with increased applied load. Hamrock [1] notes that in 1893 Barus proposed the following formula for the isothermal viscosity of liquids as a function of pressure

$$\eta = \eta_0 e^{\alpha' p} \tag{12}$$

where α' is the pressure-viscosity coefficient, η_0 is the dynamic viscosity at atmospheric pressure and η is the dynamic viscosity at pressure p. As the load increases, the pressure will increase and cause an exponential rise in the viscosity which increases the load carrying capacity of the bearing at a constant film thickness and occasionally results in a larger film thickness. Also, elastic deformation of the surfaces can increase the area of the Hertzian contact zone at heavier loads, further increasing the load carrying capacity of the bearing at constant or even thicker film thicknesses.

A temperature increase causes a thinning of the lubricant making it less effective and more sensitive to degradation, leading to thinner films and hence higher BSR's.

The amount of oil initially applied to the ball bearing has a dramatic effect on the BSR. When the initial oil film thickness is increased, the BSR decreases to a point where even if more oil is introduced, the BSR remains the same or levels out, corresponding

more to fully flooded or starved EHL. When the initial oil film thickness is decreased, the BSR increases to a point corresponding to no lubrication. The bearing cannot operate without any lubricant so that eq. (8) must be used for this value based on the geometry of the ball bearing.

1.4 FLUID FILM ANALYSIS

The friction polymer that adheres to the races and balls as a ball bearing operates in parched EHL is different from the oil that is initially applied. An analysis to determine the difference between the polymer and the oil will aid in explaining the fluid degradation and operating phenomena of parched EHL. Two aspects to consider are the actual chemical composition of the film and a film thickness time study to see when the polymer starts to form during a test run.

There are many tools available for elemental and chemical analyses of the polymer film as described by Ferrante [14] but only a few are available and applicable to the film that is deposited. The problems encountered with the film are that it is opaque, relatively thin (of order of a few hundred Angstroms) and insoluable in most chemicals that are used in the instruments. The elemental and chemical analysis methods can be divided into several categories - spectroscopy analysis by electron levels, by mass, by absorption, and through examination of macroscopic features.

There are two available chemical analysis by electron level techniques - Auger Electron Spectroscopy and X-Ray Photoelectron

Spectroscopy. Auger Electron Spectroscopy or AES involves bombarding the surface to be analyzed with electrons and detecting and analyzing the energy of the secondary electrons that are emitted. The results give the elemental composition of the surface and can provide chemical analysis in some instances. The technique is surface sensitive which means that less than ten atomic layers are effected.

The X-Ray Photoelectron Spectroscopy technique or XPS bombards the surface with X-rays and the photo-emitted core and valence electrons are detected. The technique gives chemical and elemental analysis and is surface sensitive.

Secondary Ion Mass Spectroscopy or SIMS is the chemical analysis by mass tool. The surface to be analyzed is hit with a beam of ions and the sputtered charged particles are analyzed for mass. The technique will give elemental and compound information and is surface sensitive.

Fieser [15] describes three types of radiation spectroscopy that can be used. The first is nuclear magnetic resonance spectroscopy which requires that the sample be soluble in a limited number of chemicals. The solution is irradiated with radio frequency energy (60 MHz) between the faces of a strong permanent or electromagnet (14 000 G). The absorption of radio frequency energy is plotted versus magnetic field strength to produce a spectrum which gives the number, kind and relative location of certain atoms, primarily hydrogen, in the molecule.

Infrared spectroscopy produces a spectrum that shows the absorption of electromagnetic radiation by the sample in the 4000 to 650 wavenumber region. The absorption of infrared radiation by an organic molecule causes its vibrational amplitude to change. The important peaks that are obtained in the spectrum result from changes in the frequencies of bond stretching or bending.

Ultraviolet spectroscopy differs from infrared spectroscopy in that information about the molecule's electronic transitions are obtained. Electrons move from one electron level to another due to the absorption of high energy, short wavelength ultraviolet radiation. Besides covering the ultraviolet wavelength region (200 to 400 nm), the technique generally will include the visible region (400 to 800 nm) as well.

The Scanning Electron Microscope or SEM will show macroscopic features of the surface and, if properly equipped, can give elemental information. A highly focused electron beam is incident onto the surface and the secondary electrons emitted from the surface are picked up. SEM will give an approximation of the film thickness and a detailed magnified view of the surface.

Besides the SEM, other techniques to measure the film thickness include interference, optical and acoustic microscopes.

There are a few facts about the friction polymer that should be considered before an analysis is attempted. The term friction polymer was coined by Hermance and Egan at the Bell Laboratories in 1958 after finding an organic polymer deposit on electric relay

contacts. A polymer is defined by its long chain-like structure and high molecular weight but there have been instances where the polymer formed into a more viscous lubricant and then hardened into a resin [16]. Besides this form of the polymer, there seems to be as many different "polymers" as there are ways to generate them, not all having a chain-like structure as noted by Lauer [17]. These friction polymers are only generated with certain lubricant/metal surface combinations, are associated with both a reduction and increase in wear, depending on the conditions and can be formed in EHL and boundary lubrication. Even though it has been almost 30 years since the discovery of friction polymers, few general conclusions can be drawn about them.

Based on the above facts, a chemical rather than elemental analysis is required to compare the oil to the polymer that is formed. The oil and the polymer seem to contain the same elements but are rearranged into different structures so that an elemental analysis may not be helpful. The most promising techniques for analyzing the polymer and those pursued in this work are Auger Electron and X-Ray Photoelectron spectroscopies, SIMS and infrared spectroscopy. The Scanning Electron Microscope gives detailed images of the surfaces of the bearings which will be useful in seeing the polymer build-up and surface damage.

1.5 FLUID FILM THICKNESS MEASUREMENT

One characteristic that helps to distinguish between the different lubrication regimes is the fluid film thickness between

the surfaces moving relative to each other. The BSR gives a relative indication of the film thickness - as the film thickness decreases, there is a reduction in slip and an increase in BSR but at this time there is no direct relation between film thickness and BSR.

As noted by Seth [13], techniques for measuring the lubricant film thickness in EHL contacts can be classified into four categories - mechanical, electrical, X-ray, and optical. One must be careful in using any of these techniques since each has its limitations. The minimum film thickness in the contact zone is much harder to determine than the average because viscosity, temperature, and other properties of the lubricant and surfaces are effected by the high pressure gradients and the precise position of the minimum film thickness is hard to locate. Most of the techniques rely on a calibration against known gaps so that caution must be exercised in the calibration procedure because the films are generally thinner than most accurate standards.

Of the two mechanical techniques, the first is the strain gauge method. A strain gauge is mounted on the outside of the outer race of a ball bearing to detect the maximum tensile strain that occurs when a ball is directly under the strain gauge. The load imposed on each ball in the radial direction by the races is related to the difference in the maximum and minimum strains. Knowing the relation between the diametral interference (outer raceway diameter - inner raceway diameter - 2 x ball diameter) and

the load, the average film thickness can be determined. The disadvantages of this method are that its accuracy is reduced in dynamic operating conditions over that in steady state and is greatly effected by the type of lubricant used.

The second mechanical method is the spring dynamometer technique which incorporates a dynamometer spring compression as a measure of the film thickness. The technique is applied to two concentric, contrarotating plates with three equally spaced balls between them. This technique measures an average film thickness and has a large data scatter because the films are thinner than measurements of the displacement of mechanical components.

Optical methods fall into two categories - interferometry and laser-beam diffraction. The interference technique is widely used and is based upon the observation of interference fringes in the contact zone between two rolling bodies. One of the structural component members is transparent and the film thickness can be calculated from the interference pattern of the reflected rays from the contact zone. The major disadvantage of the interferometric technique is that one of the surfaces must be flat and transparent and so is limited to simple geometries and light loads.

The laser-beam diffraction technique is based on the diffraction pattern produced when a beam of light is passed through a small gap. Once oil is introduced into the gap, the diffraction pattern becomes distorted and even worse as the gap size becomes small ($<10^{-6}$ m) because the diffraction pattern bandwidth is

inversely proportional to the film thickness, limiting the method to simple geometries and lightly loaded operating conditions.

The X-ray technique is used for film thickness measurements between two flat disks. A Geiger counter measures the rate of transmission of the X-rays before the test is started at a known gap and then under the actual EHL conditions. The technique is sensitive to small changes in the film thickness but is expensive, limited to simple geometries and calibration is carried out in unloaded conditions so that accuracy can be low when test conditions are extreme, due to changes in lubricant and surface properties.

The fourth and final techniques are the electrical methods. The resistance technique is useful when asperity contact occurs because the method doesn't actually measure the film thickness but only the amount of asperity contact. This technique is used predominantly to indicate lubricant film breakdown and for surface roughness studies.

The second electrical technique utilizes the change in capacitance of the lubricant with film thickness. The capacitance between two separated surfaces varies inversely with the distance between them, so that the film thickness in a ball bearing is estimated by measuring the capacitance between the races. The method requires that the two surfaces be finely finished and electrically insulated from each other. A voltage is applied across the inner and outer races via a brush and slip ring system

and the capacitance is measured using a capacitance bridge. This technique gives an average film thickness and the geometry of the ball-race contact is required to calculate the shape of the film for the film thickness calculations. The properties of the lubricant, particularly its dielectric constant, should be known as a function of pressure and temperature in extreme operating conditions as noted by Dyson [9] and Allen [10].

For an angular contact ball bearing operating in parched EHL, the capacitance technique is the most applicable and the method pursued in this work. The other methods are not suitable because of the complex geometry, highly loaded operating conditions and thin film thicknesses in the Hertzian contact zone of the ball bearings tested.

The BSR is used as an indirect film thickness measurement because as the film thickness in the Hertzian contact zone decreases, there is a reduction in the amount of slip and the BSR increases. This is demonstrated in fig. 1.2 where the BSR is increasing slightly in the middle of the test. The BSR cannot give a quantitative value of the film thickness but only an indication that it is changing. Friction polymer is forming during the test which will affect the BSR due to the differences in properties between the oil and polymer. The polymer is more viscous than the oil so that the slip decreases as the polymer forms causing an increase in BSR.

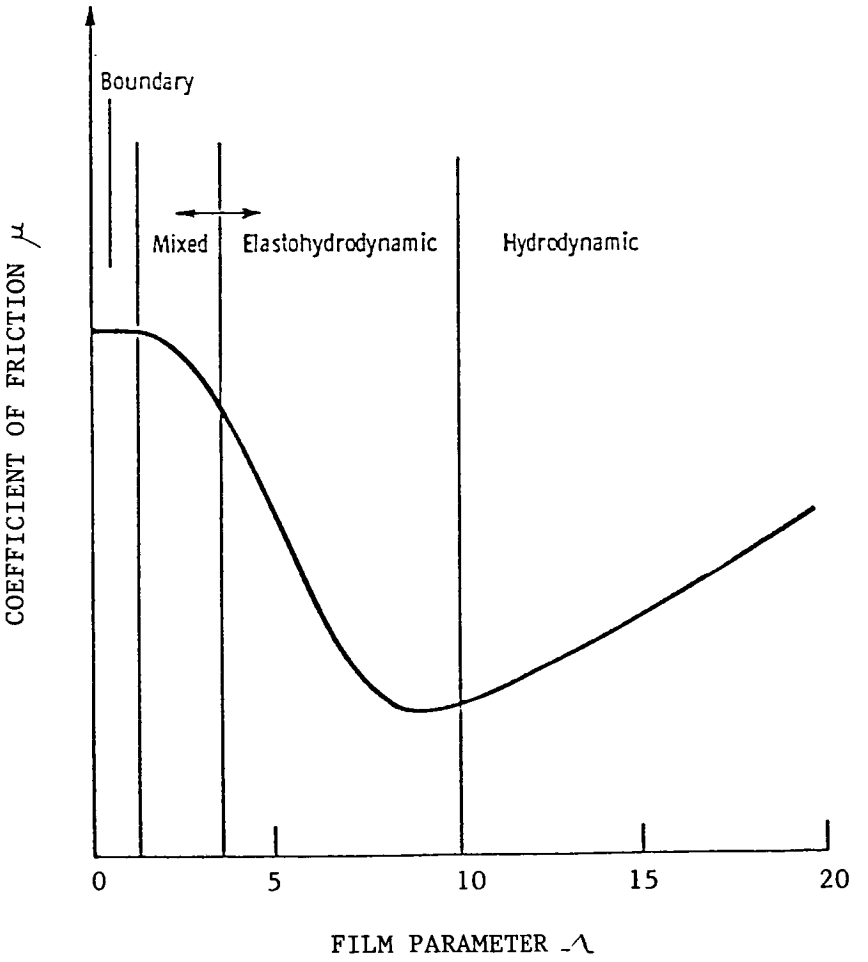

Fig. 1.1 Coefficient of friction as a function of film parameter.

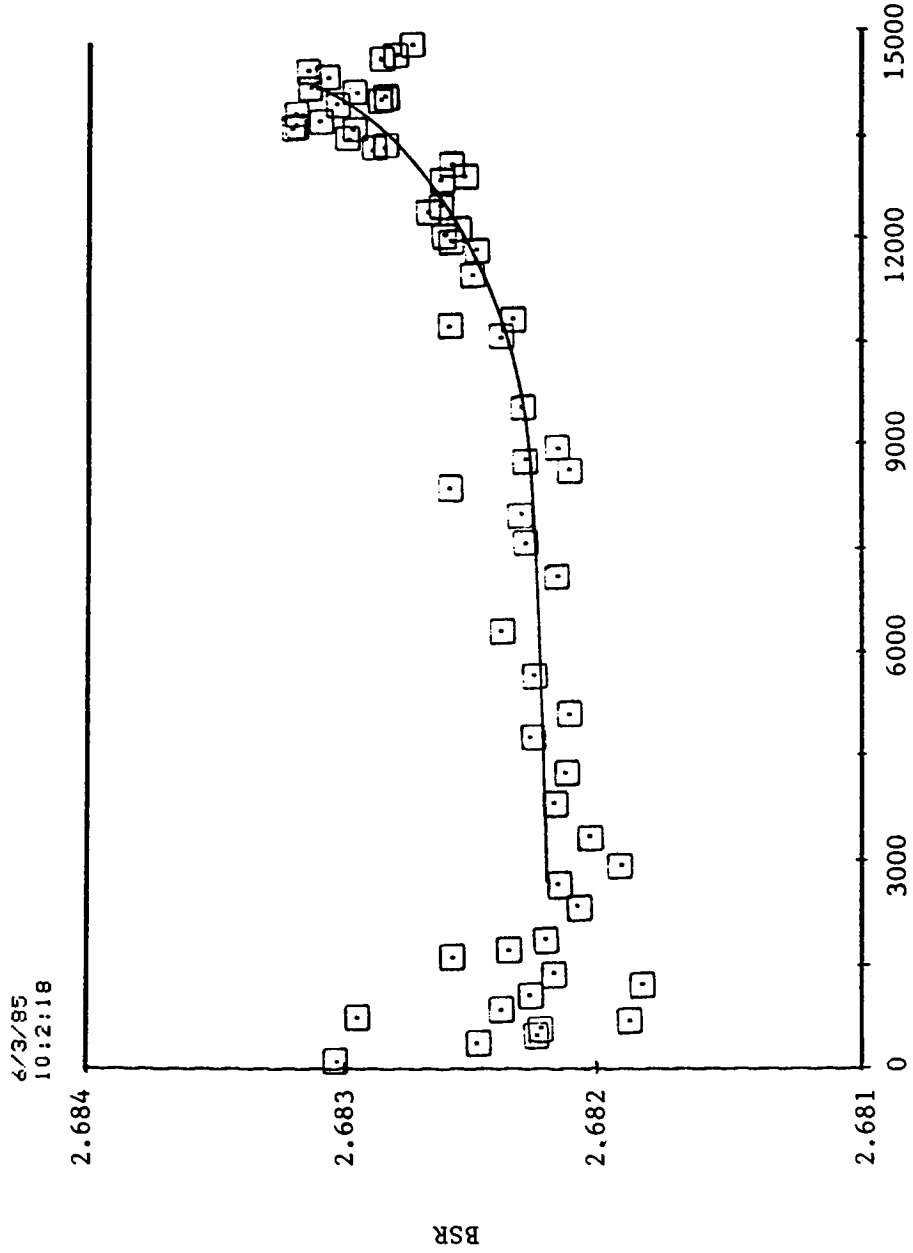

Fig. 1.2 BSR vs. elapsed time for ITI 8990-A test bearing, 300 lb load, 0.010 SRG 200 oil/freon concentration.

Fig. 1.3 Uncleaned ball from ITI 8990-A test bearing, 300 lb load, 0.002 SRG 200 oil/freon concentration.

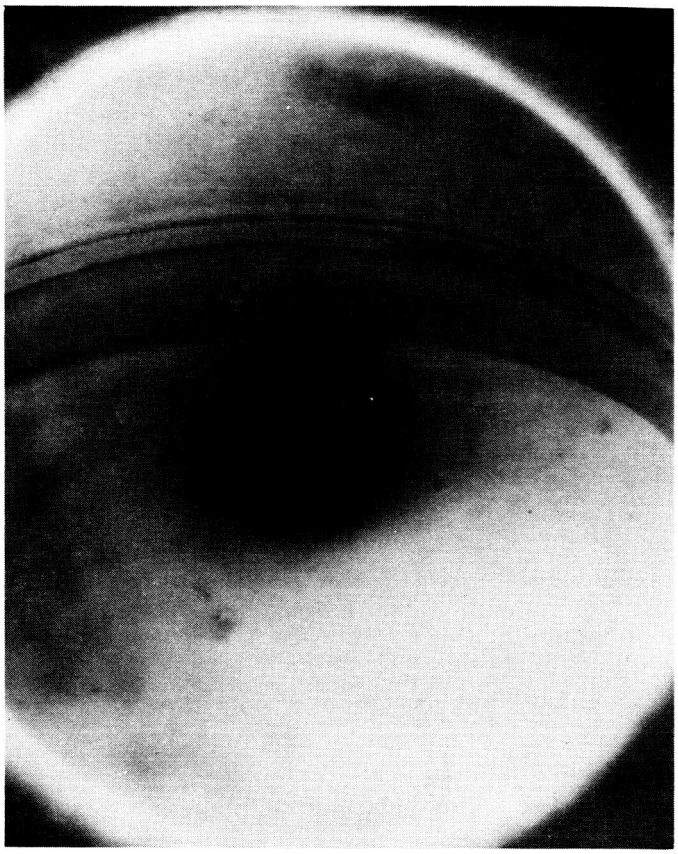

Fig. 1.4 Freon cleaned ball from ITI 8990-A test bearing, 300 lb load, 0.002 SRG 200 oil/freon concentration.

Fig. 1.5 Wiped ball from ITI 8990-A test bearing, 300 lb load, 0.002 SRG 200 oil/freon concentration.

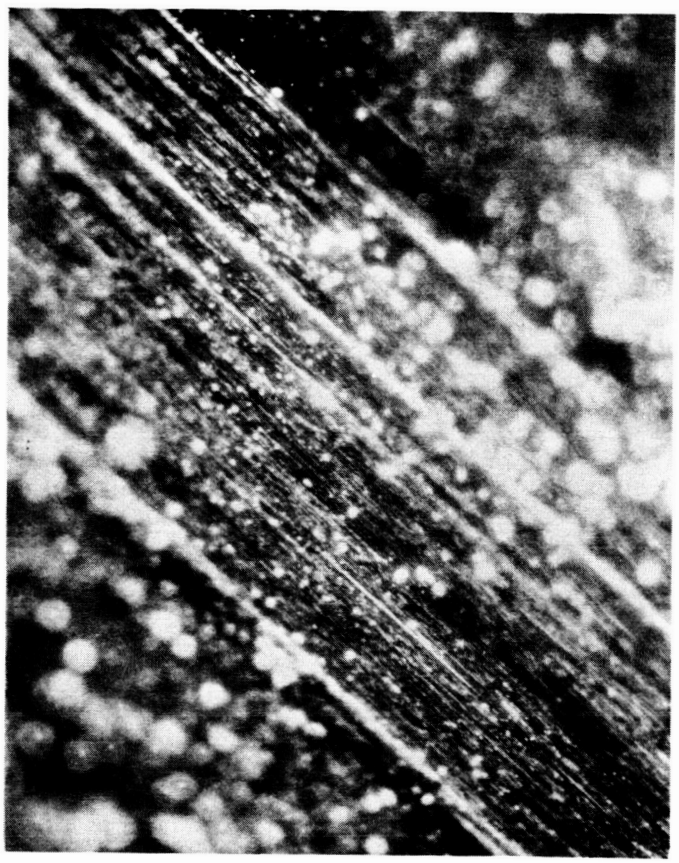

Fig. 1.6 Magnified view of wear track of wiped ball from ITI 8990-A test bearing, 300 lb load, 0.002 SRG 200 oil/freon concentration.

CHAPTER II

EXPERIMENTAL APPARATUS

The purpose of this chapter is to describe the test rig and general apparatus. The primary focus is to measure the basic speed ratio (BSR) and the capacitance across the races and balls of an angular contact ball bearing operating in the parched EHL regime.

Kingsbury [3][5][11] has been successful at measuring the BSR in an angular contact ball bearing, especially for bearings operating in parched EHL. The BSR is a characteristic number of an angular contact ball bearing defined as the ball spin rate over the difference in race angular velocities. To measure the ball spin rate without difficulty, the ball complement orbital velocity must be zero so that a counter-rotating race mode is used.

Measuring the capacitance to find the oil film thickness was first attempted in simple geometries such as between rotating cylinders by Dyson [9]. Application to an actual ball bearing by Allen [10] has also been successful.

2.1 BSR TEST RIG

A schematic of the test rig is shown in fig. 2.1. Kingsbury [3] developed the test rig at NASA-Lewis Research Center for use in parched EHL research. The test rig was originally designed to measure the BSR and is modified to measure the capacitance across the races for this study.

The 40 mm test bearing with no separator or cage and a seventeen 3/8" diameter ball complement is located at the top of the rig. Fig. 2.2 shows the test bearing disassembled and fig. 2.3 displays the assembled test bearing in the mount. Four working bearings are used to support the spindle and mounting assembly. The test and support bearings run with no apparent problems even without the separator.

The races are counter-rotated to enable the ball complement orbital velocity to be zero. Adjustable power supplies control variable speed motors attached to the inner and outer races by way of belts, as shown in fig. 2.4. The two power supplies, one for each motor, must have fine control over the motors because the ball complement must be held extremely steady to obtain good BSR data. The range of the BSR in fig. 1.2 gives an indication of how sensitive the instruments and apparatus are. The power supplies are manufactured by Elgar (model 1001B) and provide the AC power needed to control the motors. The units consist of 2 DC power supplies and a direct coupled amplifier driving an output transformer. The output power frequency is controlled by a plug-in oscillator with a range of 45 Hz to 5 kHz and a resolution of 0.0001 percent. The power output ranges from 0 to 1000 VA.

The motors that are powered by the power supplies are Electrical Indicator Company model GNFRNT-1148 hysteresis synchronous motors and can be operated at up to 12 000 rpm with a maximum of 3.65 A and 208 V for an output of 1.4 hp. The tests are

normally run at about 2.8 A to stay well away from the maximum operating parameters of the motors.

The motors have 1-7/8 in. 75 tooth aluminum gears mounted on their output shafts as shown in fig. 2.10. Toothed drive belts of unknown manufacturer (model SDP 6G6-400031) are used to connect the motors to the test rig which has 3-7/8 in. 150 tooth aluminum gears mounted on it to drive the inner and outer races as shown in figs. 2.1 and 2.10.

The ball spin rate is measured using a signal generator, stroboscope, external lamp and digital counter. A ball in the test bearing is marked with a star-shaped figure using a fine marking pen. As shown in fig. 2.5, the low power microscope (7X, Spencer Lens Company), and external lamp (General Radio type 1538-P2) are placed on top of the clear plexiglas cover box to view three balls of the 17 ball complement. The motors are started simultaneously by two switches connected together with a bar. The inner and outer race speeds are adjusted to bring the ball complement into an approximately stationary position.

The marked ball is brought into the field of view of the microscope by adjusting the outer race speed and the external lamp is pointed at the marked ball. Besides aiding in viewing the marked ball, the microscope allows the observer to see how steady the ball complement is. If the marked ball starts to wander out of the field of view or tumble in spin orientation, the outer race

speed is adjusted to bring the ball compliment to a more stationary arrangement.

The tumbling of the balls, which occurs near bearing failure, is evident from the behavior of the mark on the ball. The mark is normally positioned on the top of the ball but begins to shift off the top and even out of view as tumbling occurs. As failure approaches, the tumbling cannot be controlled by the outer race, indicating surface damage and the rig is shut down.

Once the orbital speed of the ball complement is zero and the marked ball is in view, the signal generator (Krohn-Hite model 2200) that controls the stroboscope and external lamp is adjusted to bring the star on the marked ball to a stationary position. The signal generator is used as the input to the external trigger to give fine control of the strobascope (General Radio type 1358-A). The signal sent to the strobascope from the signal generator is a square wave of nominally 170 Hz.

The ball and race speeds are measured with Eldorado model 1411 universal digital preset counters. The ball speed is measured on a counter that is connected to the signal generator and the counters for the race speeds are attached directly to the power supplies. The synchronous motors run exactly at a multiple of the supply frequency without slip so that the race speed is available exactly by counting the supply frequency. When the star on the marked ball is brought to a stationary position, the ball and outer race speeds are read from the digital counters and entered into an Apple-Isaac

computer system. The inner race speed is input into the computer at the start of a test run and adjusted periodically which eliminates the need to input the inner race speed at every reading. The Basic computer program, executed when the test is started, converts the counter readings into angular velocities, calculates the BSR and an internal clock assigns an elapsed time to the data. The data is stored on a disk and a hard copy is obtained from the printer. Typical nominal values of the ball, inner and outer race speeds are 170, 38, and 26 rps, respectively.

The ball speed measuring scheme is calibrated in order to determine the error associated with it. The calibration procedure involves finding a shaft rotating at a known speed and comparing it to readings taken with the ball measuring scheme. A proximity probe is mounted onto a Dayton model 27846A permanent magnet DC motor to measure the rotational speed of the output shaft. A 60-tooth gear is placed on the shaft to trigger the proximity probe which is powered by 18 V from a Sorensen model SAL 20-12 power supply (25 V maximum). The proximity probe output is measured by an Eldorado model 1411 digital counter. The accuracy of the probe is only limited by the counter so that the probe is more accurate than the ball speed measuring scheme. A series of points were taken to compare the output of the ball speed measuring scheme to the probe output. Finding that the ball speed measuring scheme has an accuracy of 0.003 percent and the race speeds 0.0015 percent, the

BSR error is 0.003 percent. See appendix B for statistical and error analysis.

The four support bearings on the test rig are critical to the smooth operation of the test rig. Alignment of the whole shaft and spindle assembly is important in eliminating unwanted vibrations and unsteady behavior of the test bearing itself. The test rig is taken apart periodically (every 2 to 3 months) to check for wear and lack of lubrication. The support bearings are BMC 12692 40 mm ball bearings with 3/8 in. diameter grade 5 balls and are lubricated with SRG 100 oil. SRG 100 oil is used because of its viscous properties and resistance to forming the polymer film. The bottom three support bearings tend to exhibit less wear while the top support bearing needs to be cleaned and relubricated more often. The whole upper mounting assembly with the test bearing and top support bearing comes off as one piece and is removed after every test causing the top support bearing to collect more dust and debris. The other support bearings are protected from dust and contaminates by a cover plate and were only replaced once in an 18 month period. The top support bearing was replaced approximately once every 3 months, depending on the number of tests run and their duration.

The thrust load is applied to the bearing via a cable, lever arm, and jack as shown in fig. 2.6. The scissors jack is manufactured by Huffy (model 2072) and has a lifting capacity of 3000 lbs. A horseshoe force gauge (Dillon model X) is mounted

between the end of the lever arm and the top of the jack and has been calibrated to read the load that is applied to the test rig. The lever arm is attached to the test table using a bracket and pin.

The thrust load that is applied to the test bearing is set before the test is started but during the course of a test, the load has to be reset periodically (3 or 4 times per test). The tests are run at loads of 200 and 300 lb.

2.2 INITIAL OIL FILM APPLICATION

Since the tests are run in parched EHL, a limited amount of oil must be applied to the balls and races. The method to use in applying the oil involves coating the balls with a thin film of oil.

A solution of Freon and oil is prepared using between 0.1 and 1.5 ($\pm$0.01) ml of oil per 50 ($\pm$0.1) ml of Freon. A high grade of laboratory Freon 113 (see table I for specifications) is used because the oil is soluble in it, the Freon evaporates rapidly out of the oil once the solution is applied to the balls and any debris in the oil will effect the operation of the bearing due to the thin oil films applied (approximately 20 μin.). The balls and races are cleaned by initially wiping them with a Freon-soaked lint-free cloth. The races and balls are then soaked in a Freon bath, rinsed with Freon over a vacuum, soaked in a fresh Freon bath, rinsed, and soaked again.

In order to estimate the initial film thickness on the balls, the mass of the oil applied to the balls is measured. Knowing this

weight and assuming that the oil film forms evenly around the ball, the initial oil film thickness is estimated:

$$m_o = \rho_o \frac{4\pi}{3}\left(\frac{3}{4} d^2\delta + \frac{3}{2}\delta^2 d + \delta^3\right) \tag{13}$$

$$m_o = \rho_o \pi\delta d^2 \tag{14}$$

where m_o is the mass of the oil, ρ_o is the oil density, d is the ball diameter, and δ is the initial film thickness. Equation (14) is a good approximation to eq. (13) because d is 3/8 in. and δ is of the order of 10^{-6} in., causing the last two terms to be negligible compared to the first term in the brackets.

The mass of oil on the balls is determined by weighing the balls before and after application of the oil. Fine mesh stainless steel screens, used to hold 18 test balls, are cleaned with Freon, dried over a vacuum and weighed on a balance. The solution of oil and Freon is prepared by measuring out the oil using a syringe and the Freon in a graduated cylinder. Combining the two in a 100 ml beaker, the solution is mixed in an ultrasonic mixer for approximately 5 min. Eighteen grade 10 test balls are cleaned as described above and placed onto the clean screens. The ball and screen combination is weighed on a Mettler analytical balance (type B5C1000, 1000 g maximum weight) to $\pm$0.1 mg.

Once the solution is mixed thoroughly, the balls are placed into the solution. Up to this point, the balls have been handled using standard laboratory metal tongs with indentations to hold the

balls more securely. In order to minimize damage to the oil film that coats the balls, a pair of tweezers with tygon tubing on the ends are used to handle the oil coated balls. The balls are taken out of the solution using the tygon tweezers, dried over a vacuum to remove the Freon, and placed on the screens. Once all of the balls are coated and on the screens, the assembly is weighed. The balls are used in the assembling of the test bearing which is pressed into the top of the test rig. Some of the oil on the balls may have been transferred to the screens so that the screens are reweighed without the balls. Taking the difference in the weights of the oil coated and clean balls and correcting for the amount of oil transferred to the screens, the mass of the oil on the balls and the initial oil film thickness is estimated. All of the above weight measurements are made on the Mettler balance and repeated four times or more. An error analysis for this procedure is presented in appendix C.

The above procedure is time consuming and all of the oil/Freon concentrations are in a certain range so that a graph of initial film thickness versus oil/Freon concentration is developed, as shown in fig. 2.7. The data has a fair amount of scatter in the film thickness variable because the initial film thickness is only accurate to 7.1 percent (see appendix C). The initial film thickness is not used in any calculations and the plot is used to give an estimate of the initial film thickness for a given test.

2.3 LUBRICANTS

The lubricants used come from the SRG homologous oil series which consists of SRG 10, SRG 20, SRG 30, SRG 40, SRG 60, KG 80, SRG 100, SRG 160, SRG 200, SRG 300, and SRG 800. The oils above and including SRG 60 are refined from the same Pennsylvania crude stock, differing primarily in viscosity. The number in each name indicates the nominal viscosity in SUS at 210 °F [11].

The oils used in testing are SRG 100 and SRG 200. The SRG 200 lubricant is used primarily due to its tendency to have a greater polymer build up than all of the others. Both of the lubricants are not molecularly distilled unlike KG 80 and SRG 160. SRG 200 uses a light resin (insoluble when in contact with propane) as raw material and is percolated through bauxite in refining to remove aromatics, sulphur, nitrogen and oxygen [11].

All of the lubricants in the SRG series have 1/2 percent hindered phynl antioxident and 1 percent tricresyl phosphate antiwear added [11].

2.4 CAPACITANCE MEASUREMENT

The capacitance measurement technique is the most suitable method for determining the oil film thickness in the Hertzian contact zone of an angular contact ball bearing operating in parched EHL. A ball bearing has the same electrical system as a parallel arrangement of series-connected pairs of capacitors. The Hertzian contact zones between the balls and the races form the capacitors where the oil is the dielectric. Fig. 2.8 shows a

bearing and the equivalent electrical system. Based on the geometry of the surfaces in the test ball bearing, the average film thickness in the Hertzian contact zone is estimated from the total capacitance across the bearing.

In order to measure the capacitance, the inner and outer races are electrically insulated from one another. As shown in fig. 2.9, Bakelite is used as an insulator to separate the outer race from the test rig. The inner race is grounded with the rest of the rig so that there is no need to insulate it. The Bakelite ring between the inner race and test rig is used to firmly hold the inner race electrical contact. Bakelite is incorporated because it is relatively easy to machine and has good insulating characteristics.

The capacitance and conductance are measured using a Hewlett Packard 4270A automatic capacitance bridge which has a measuring rate of 70 msec and a balance time of 0.5 sec. Coaxial cables (RG-59) are used to connect the capacitance bridge to the brush assembly. The inner race signal and its cable shield are grounded to the capacitance bridge ground while the outer race signal comes from the high terminal of the bridge.

The voltage, supplied by the capacitance bridge, is applied across the test bearing and has a magnitude of 0.5 Vrms ($\pm$10 percent) and a frequency of 10 kHz. Electrical contact is made through a brush and slip ring system. Fig. 2.10 shows the slip ring assembly in place and figs. 2.11 and 2.12 display the brush assembly.

The slip rings are made out of stock metal and coated with silver to increase the conductivity at the surface. The rings are embedded in Bakelite holders which are mounted in brackets to hold the rings in place. One end of the wires that run between the slip rings and the races are wedged between the slip rings and Bakelite. The other end of the inner race wire is placed between the inner race upper surface and a Bakelite ring on the center spindle assembly and is held in place by the applied thrust load. The other end of the outer race wire is connected to the outer race by way of a Bakelite block (fig. 2.9) that holds the wire against the upper edge of the race.

The brush assembly is positioned over the top of the slip ring system and held stationary relative to the slip rings during a test, as shown in fig. 2.4. A cross sectional view of the spring-loaded brush is shown in fig. 2.13. The brushes are made of oil-impregnated graphite to reduce the wear of the brushes and slip rings. The wire is connected to the spring which sends the signal to the graphite brush.

Although the brush assembly is placed into position before a test is started, the brushes are not placed into contact with the slip ring system until after the test rig is running. This procedure ensures that no damage occurs to the graphite brushes as a test is started. Once the test begins, the brushes are aligned and lowered onto the slip ring assembly. The brushes are spring loaded so that they follow the contour of the slip rings. The

voltage from the capacitance bridge goes through the coaxial cables (RG-59) to the top of the brush assembly. Wires (22 gauge) connected to the springs inside the brushes (fig. 2.13) bring the signal from the coaxial cables. The graphite rides on the slip ring and passes the signal to it. The silver coated slip rings are connected to the races with the same 22 gauge wire.

A copper shield is placed between the two brushes to reduce interference between the inner and outer race signals. Approximately 500 g of assorted laboratory weights are placed on top of the lightweight platform of the brush assembly to keep it in a fixed position and ensure that the brushes are in contact with the slip rings. The platform that holds the brushes is made of a clear plexiglass so that the microscope can be placed over it and the observer can still see the ball complement. A box made of the same clear plexiglass is placed over the test rig during a test for safety purposes and to support the external lamp and capacitance brush assembly. A hole was cut into the center of the box to allow the test bearing to be accessible and easier to view. Soft rubber feet are attached to the ends of the legs of the platform to keep the platform from moving over the surface of the box during a test. The legs of the brush platform are threaded to allow for height adjustment of the platform and are fitted with locking nuts that are tightened against the platform once the platform is at the desired height. The slot cut into the platform allows the external

lamp to be placed as close as possible to the ball complement without interfering with the rest of the test rig.

Other brush systems were tried with the same slip ring system but the graphite brushes are the most convenient to use and give consistent data. The first and simplest brush was a wire that rubbed against the slip rings. This gave inconsistent data because the wire didn't follow the surface of the slip rings well and shed debris which fell into the bearing.

The second brush system used vacuum cleaner brushes which are displayed in fig. 2.14. These are fragile, tended to wear very quickly during the course of a test and gave inconsistent and erratic data.

The capacitance and conductance are measured at the same time as the ball and outer race speeds and are entered into the computer together. The film thickness calculation is an iterative process and the computer is relatively slow at performing this operation so that the film thicknesses are calculated after the test is completed. After the data at one point is input, the computer's built-in timer assigns an elapsed time to it and the data is stored on a disk. The computer plots BSR, capacitance, conductance and outer race speed versus elapsed time following a test. Once the film thickness is calculated, the computer plots the thickness versus elapsed time.

2.5 TEST BEARINGS

Two different sets of 40 mm 108H ball bearings manufactured by Industrial Tectronics Inc. are used for the various tests. Specifications for each test bearing are in appendix A and show that the bearings differ only in conformity ratios and diametral pitch. The grade 10 3/8 in. diameter balls used are made of 440C stainless steel, the same material as the races which have a minimum Rockwell hardness of 58. The rms surface roughness values of the races and balls are 3 and 1 μin., respectively.

2.6 OUTLINE OF DIFFERENT TESTS

There were several different tests run on the test rig to observe different characteristics of parched EHL. Although the tests differ, they all have a few things in common. All of the balls are coated with oil in the same manner as described in the introduction. The load is applied to the test bearing once it is in the test rig and the rig is operated for approximately 10 sec. After stopping the rig, one of the balls is marked with the marking pen and the slip ring assembly is attached. The rig is started and shut down to bring the balls into their preferred orientation. This ensures that the mark placed on top of the one ball will remain on top during the test so that it may be observed more easily. A clear plastic shield is mounted on top of the test bearing mount to keep out debris from the brushes and surrounding atmosphere. The nominal speeds of the inner and outer races and

balls are kept approximately the same for each test and are given in table II for the two different test bearings.

In the first test, a bearing is run at a known initial film thickness and observations are made of the BSR, capacitance and conductance until the bearing fails. The test bearings are relatively expensive and can't be used afterwards so few of these tests are run. The tests show how the BSR, capacitance and conductance are related for the entire operating regime of the bearing - start-up, mild transient, and failure characteristics as shown in fig. 1.2 for the BSR.

The second test looks at the "steady state" BSR as a function of initial film thickness or solution concentration of oil and Freon. Fig. 1.2 shows the mild transient region of the BSR as the bearing operates in parched EHL. The BSR changes only slightly in this region and an average value can be calculated once the bearing operates in this area for a period of time. For a bearing operating with a thick initial film thickness, the "steady state" BSR should be at a lower value due to the higher degree of slip. But as the initial film thickness decreases, the slip is reduced and the BSR increases. Once the bearing is run at thin film thicknesses, a comparison between the calculated no slip BSR and the "steady state" BSR can be made. If possible, a "steady state" film thickness can be investigated at the same time.

The friction polymer that is formed is of high interest so that a time study of the build up of the polymer is run. Does the polymer build up gradually or all at once just before the bearing fails? This test involves running a test bearing at the same initial film thickness and load for different time intervals. After each interval, a few of the balls are observed with a scanning electron microscope to see how much polymer has formed. This would explain any unexpected behavior in the capacitance and BSR readings. If the polymer dielectric constant is different from the oil, this will have an effect on the readings and not give an accurate film thickness estimate as the polymer builds up.

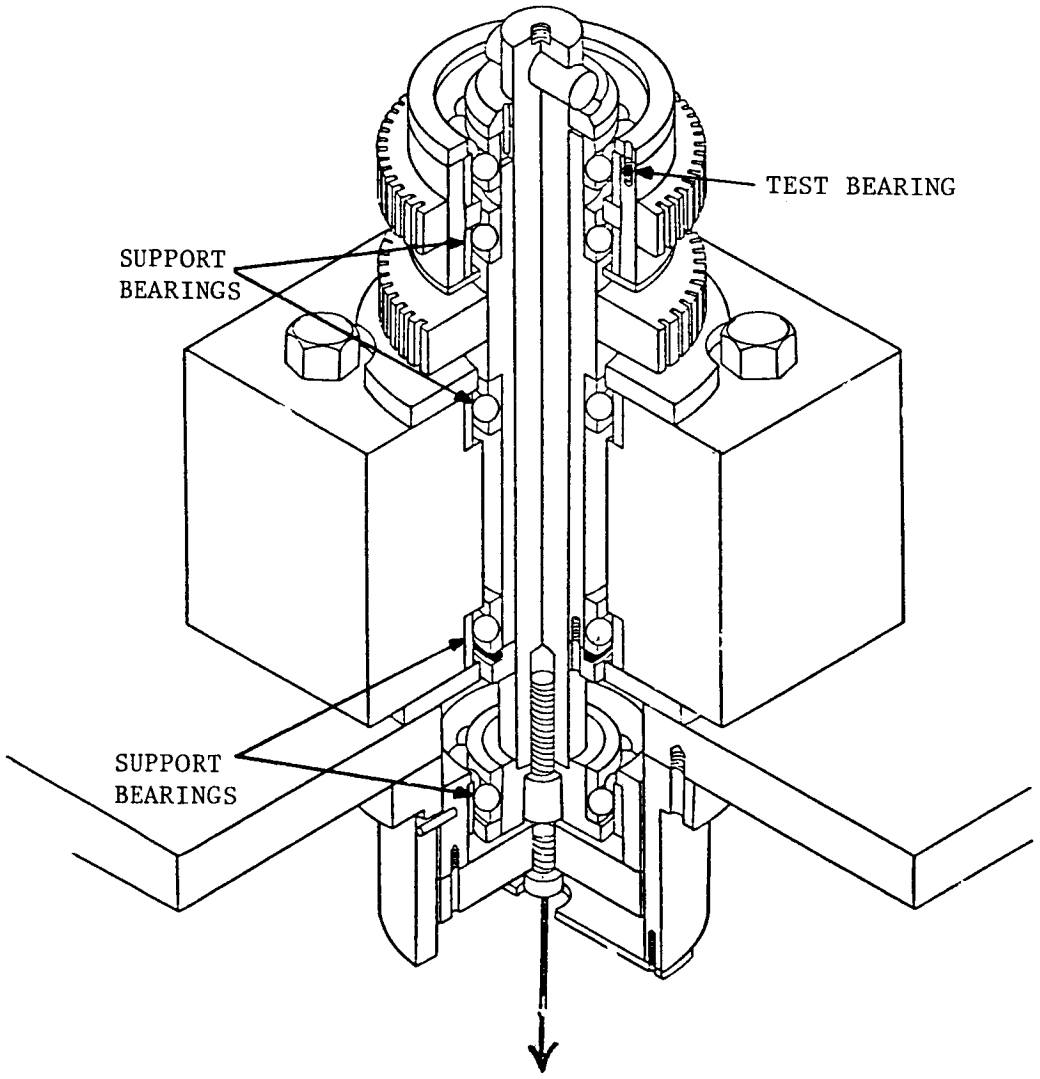

Fig. 2.1 Parched elastohydrodynamic test rig.

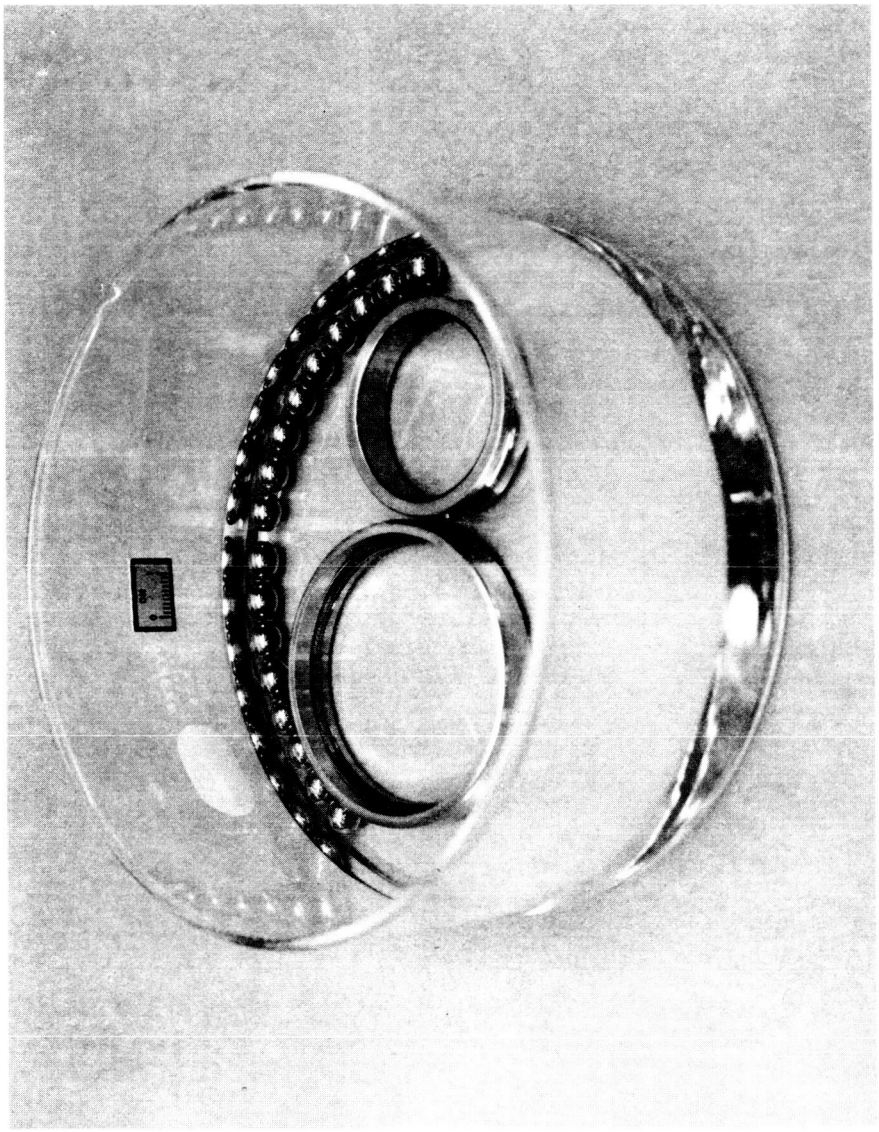

Fig. 2.2 Disassembled 40 mm test bearing with 17 grade 10 balls.

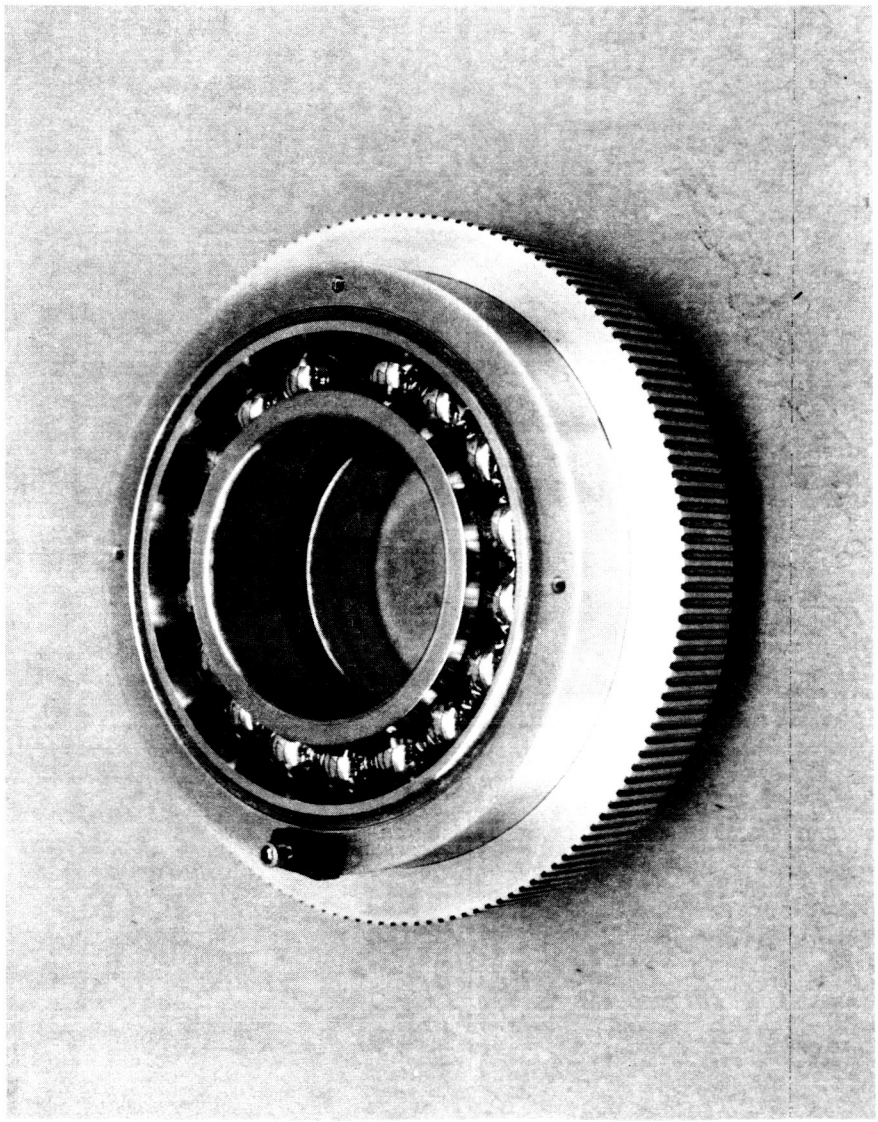

Fig. 2.3 Assembled 40 mm test bearing with 17 grade 10 balls.

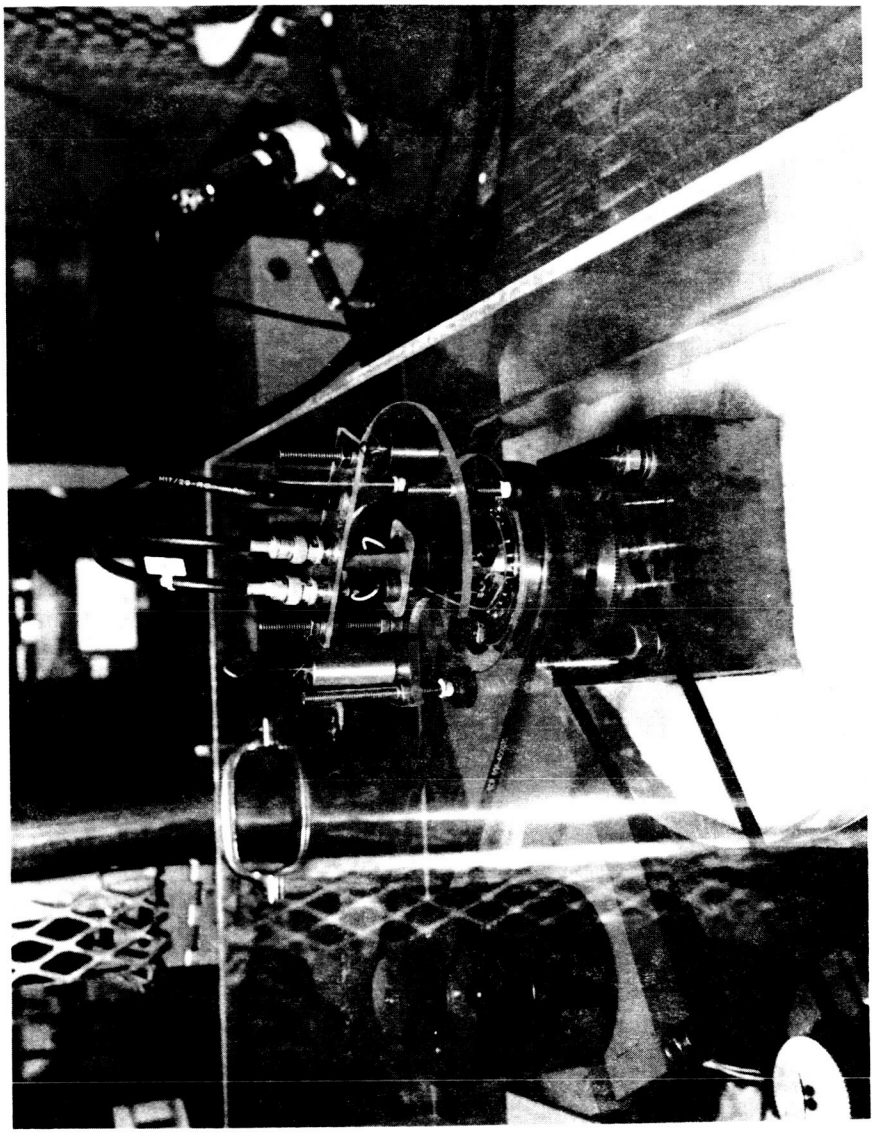

Fig. 2.4 Test rig with capacitance brush assembly in place.

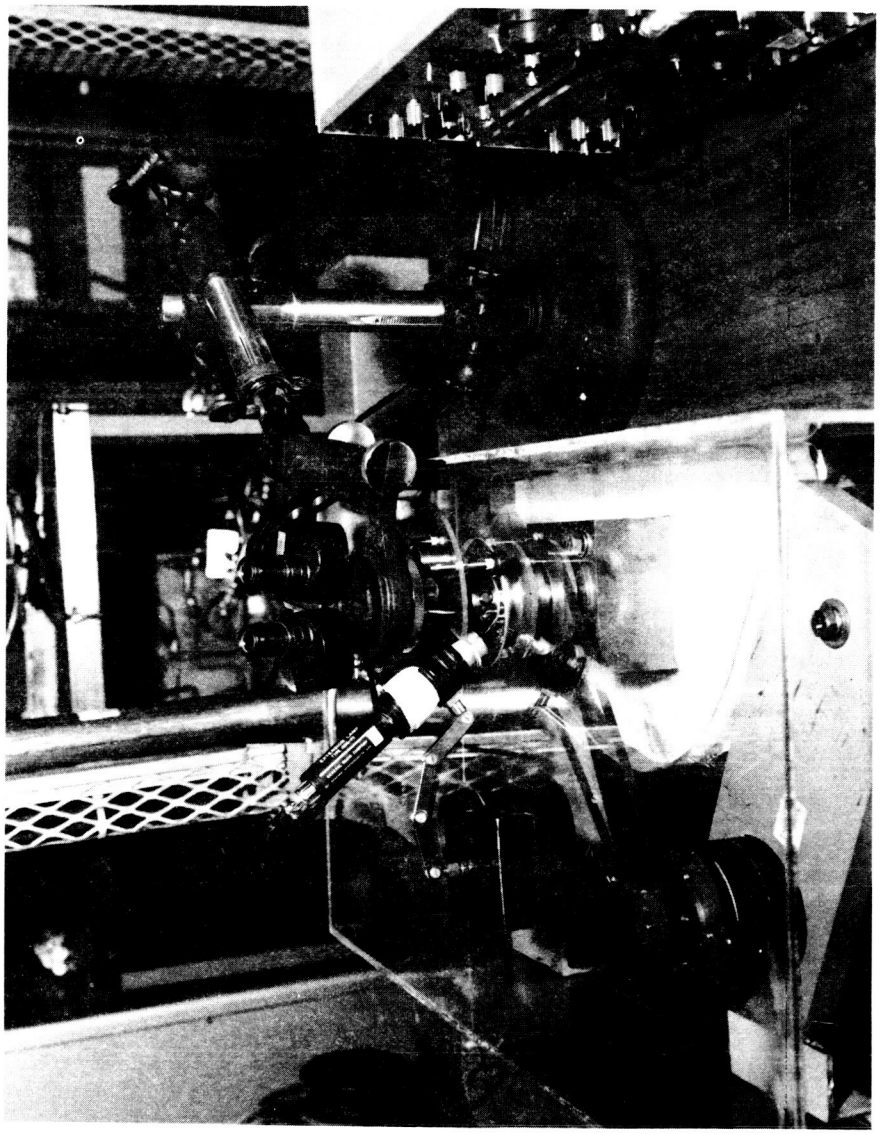

Fig. 2.5 Test rig with capacitance brush assembly and ball speed measuring apparatus in place.

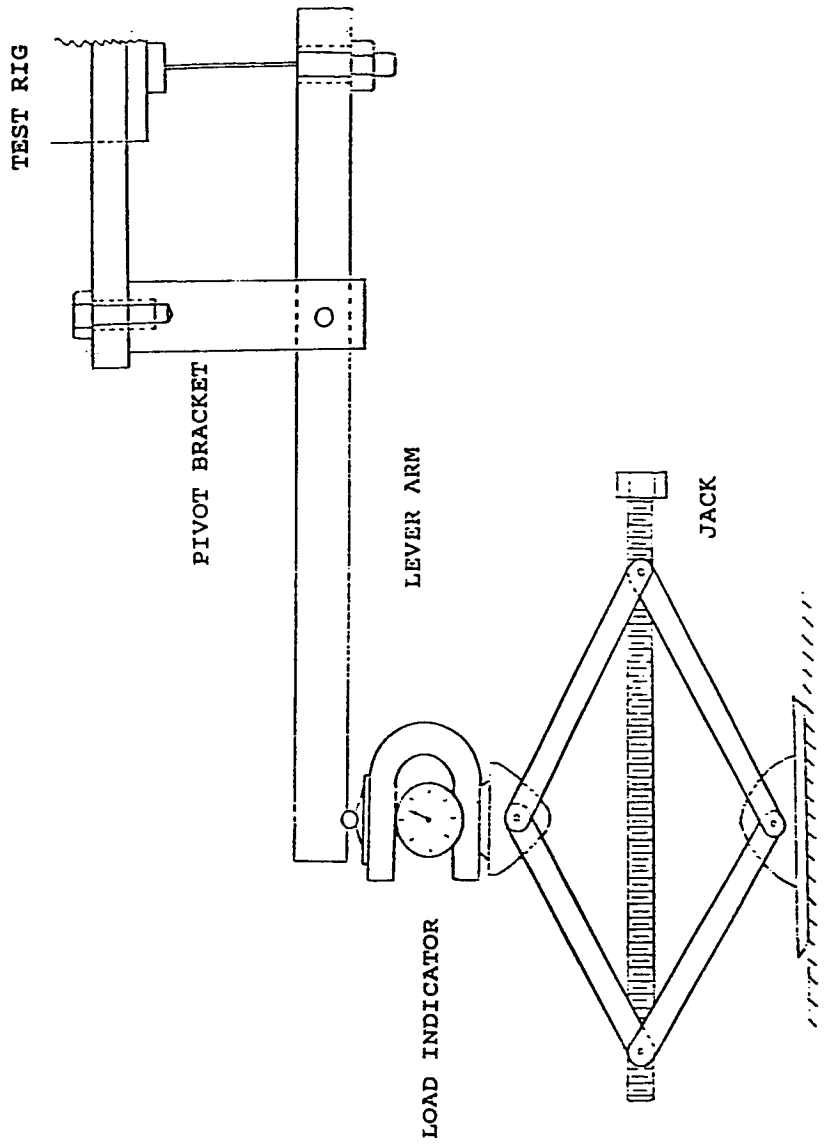

Fig. 2.6 Diagram of load application mechanism.

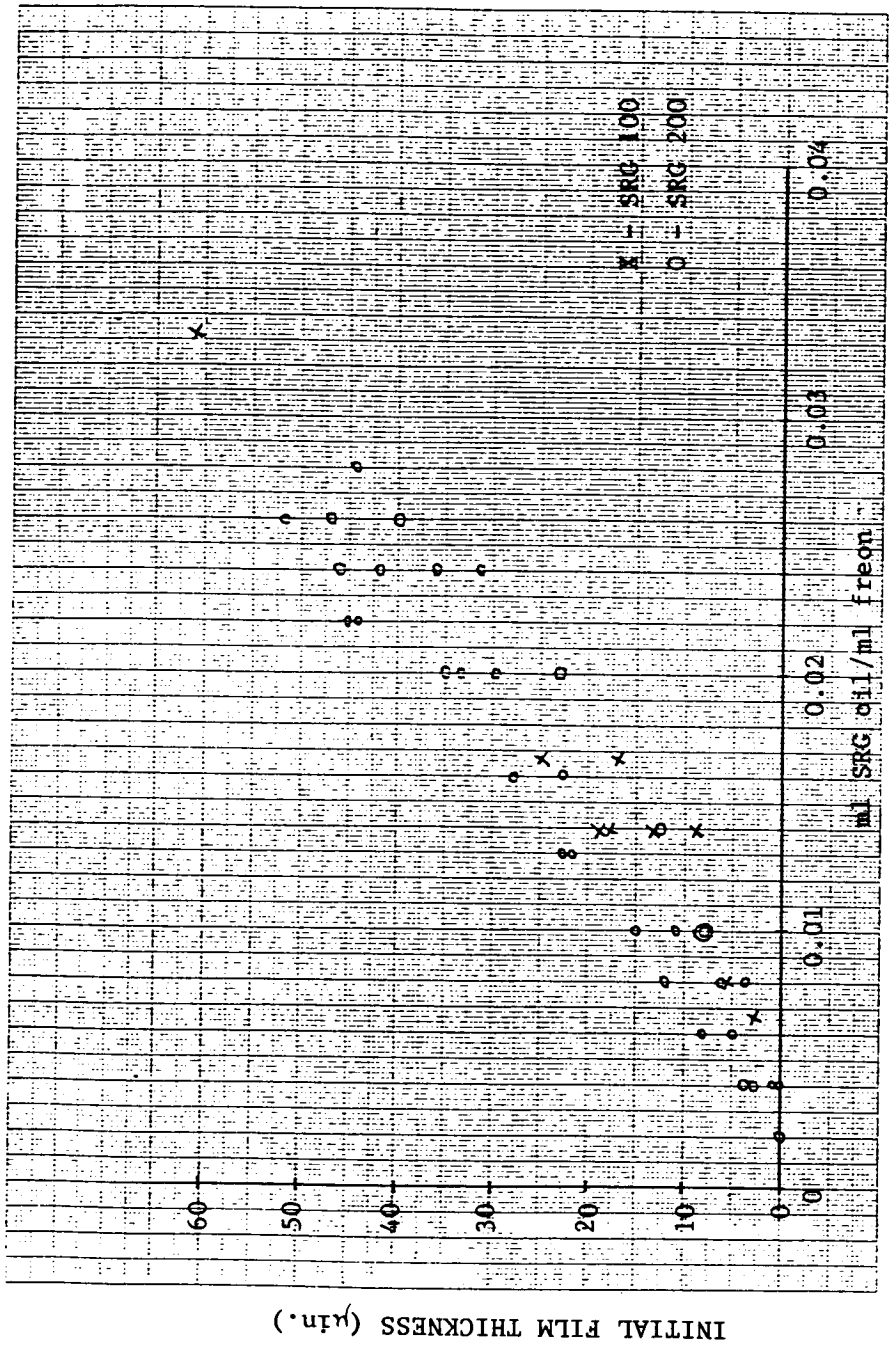

Fig. 2.7 Initial oil film thickness vs. SRG oil/freon concentration.

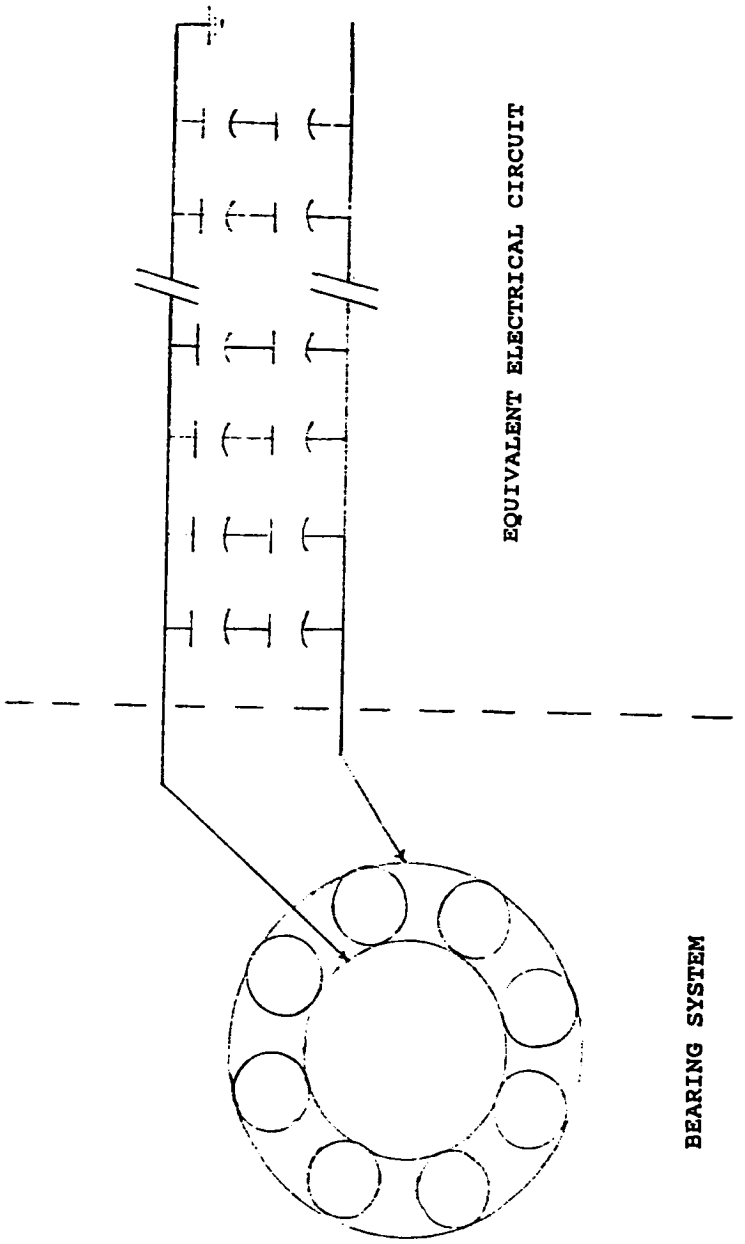

Fig. 2.8 Equivalent electrical system for a ball bearing.

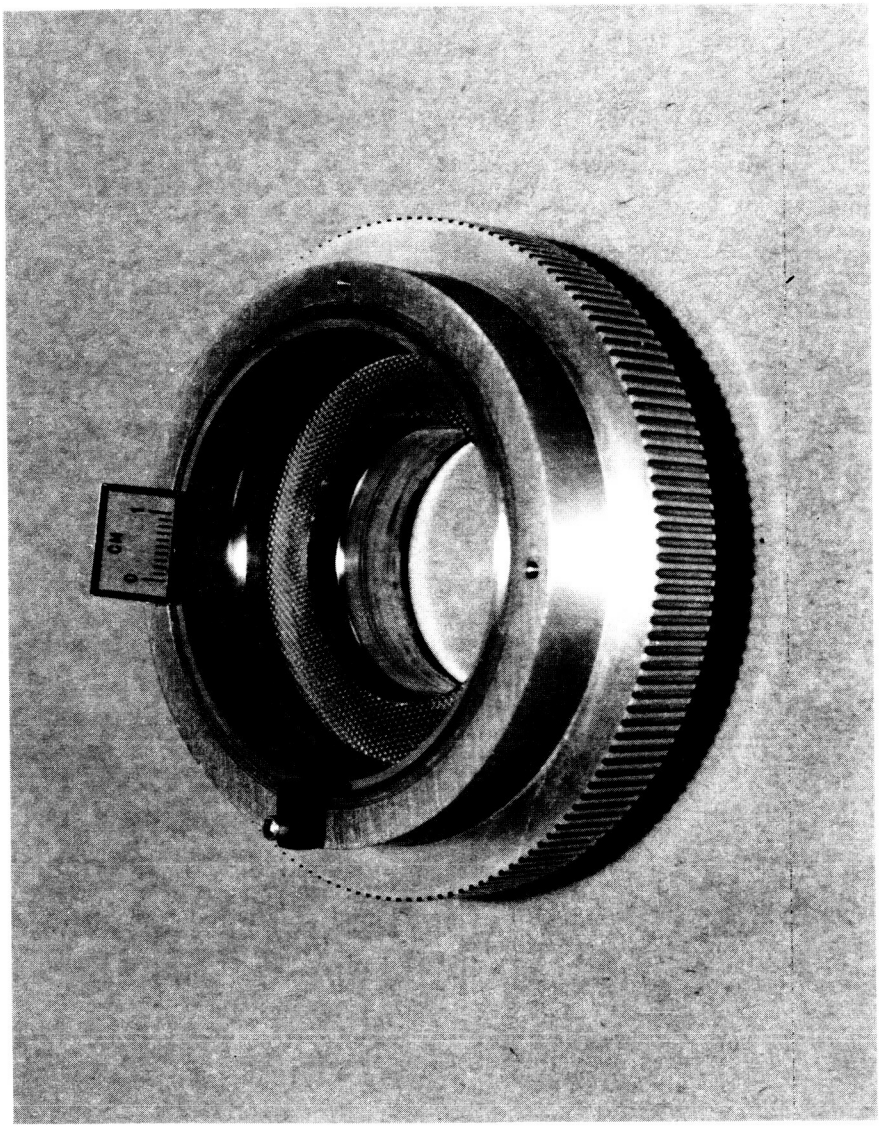

Fig. 2.9 Test bearing mount showing outer race and insulating Bakelite seperators.

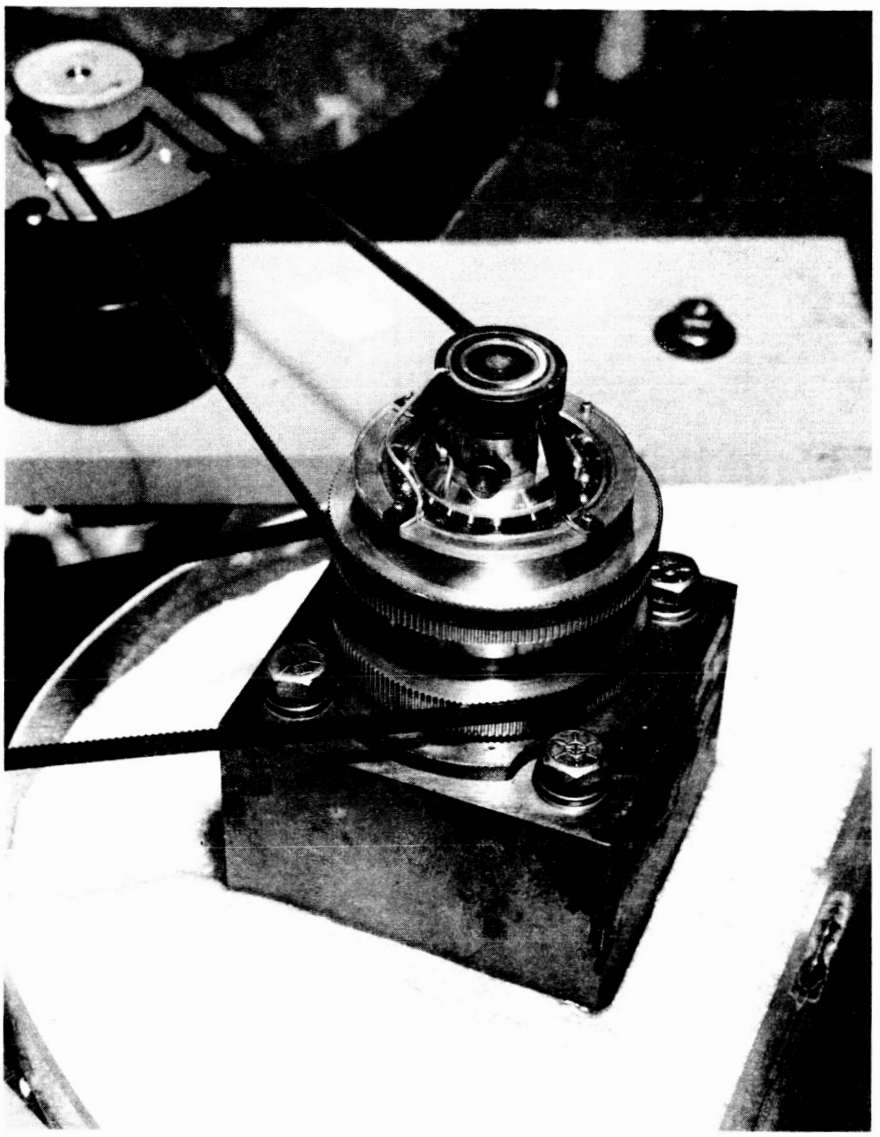

Fig. 2.10 Slip ring assembly in place.

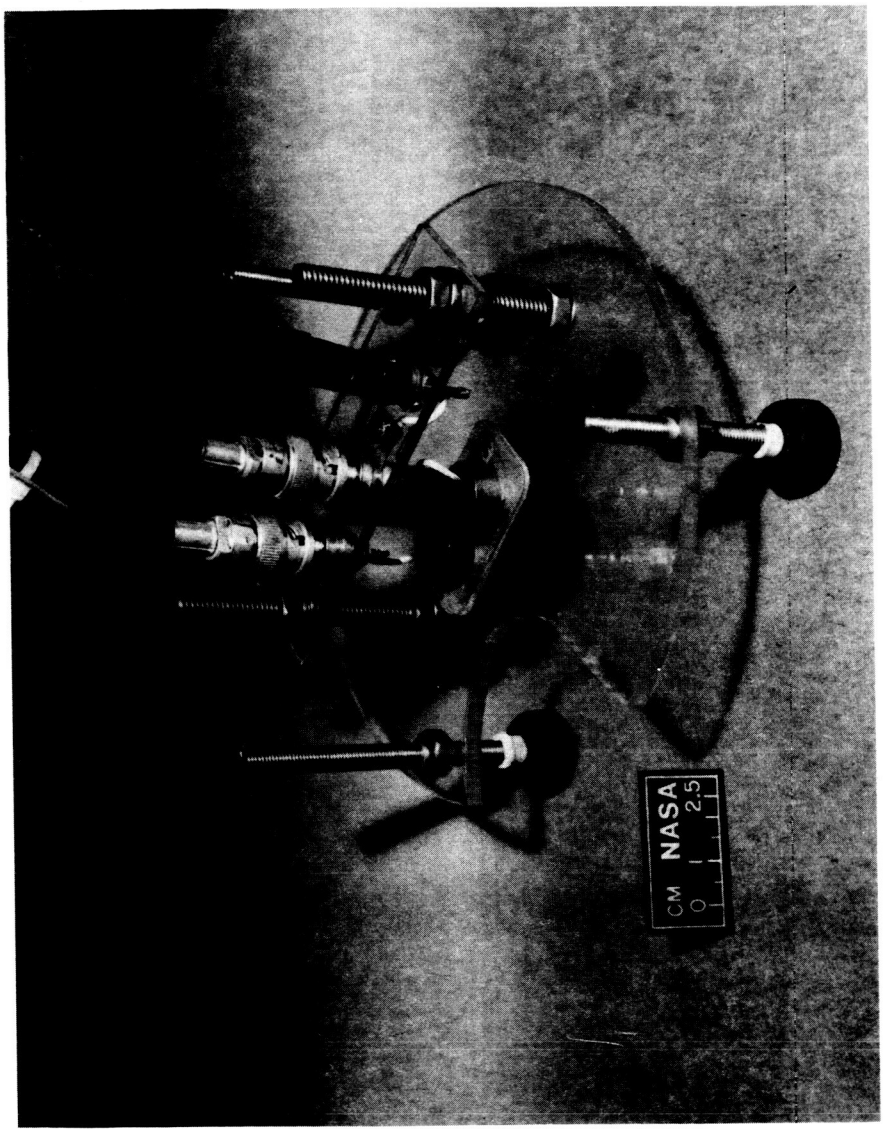

Fig. 2.11 Top view of brush assembly.

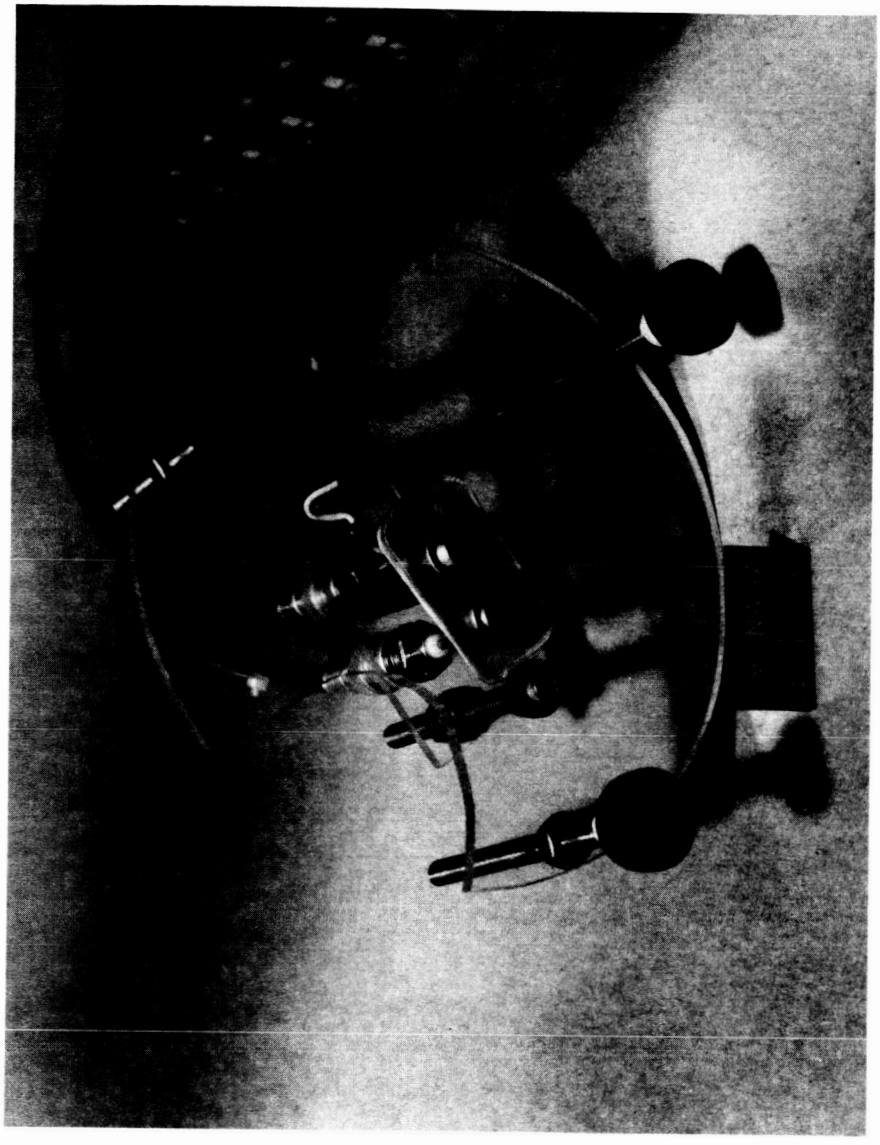

Fig. 2.12 Bottom view of brush assembly.

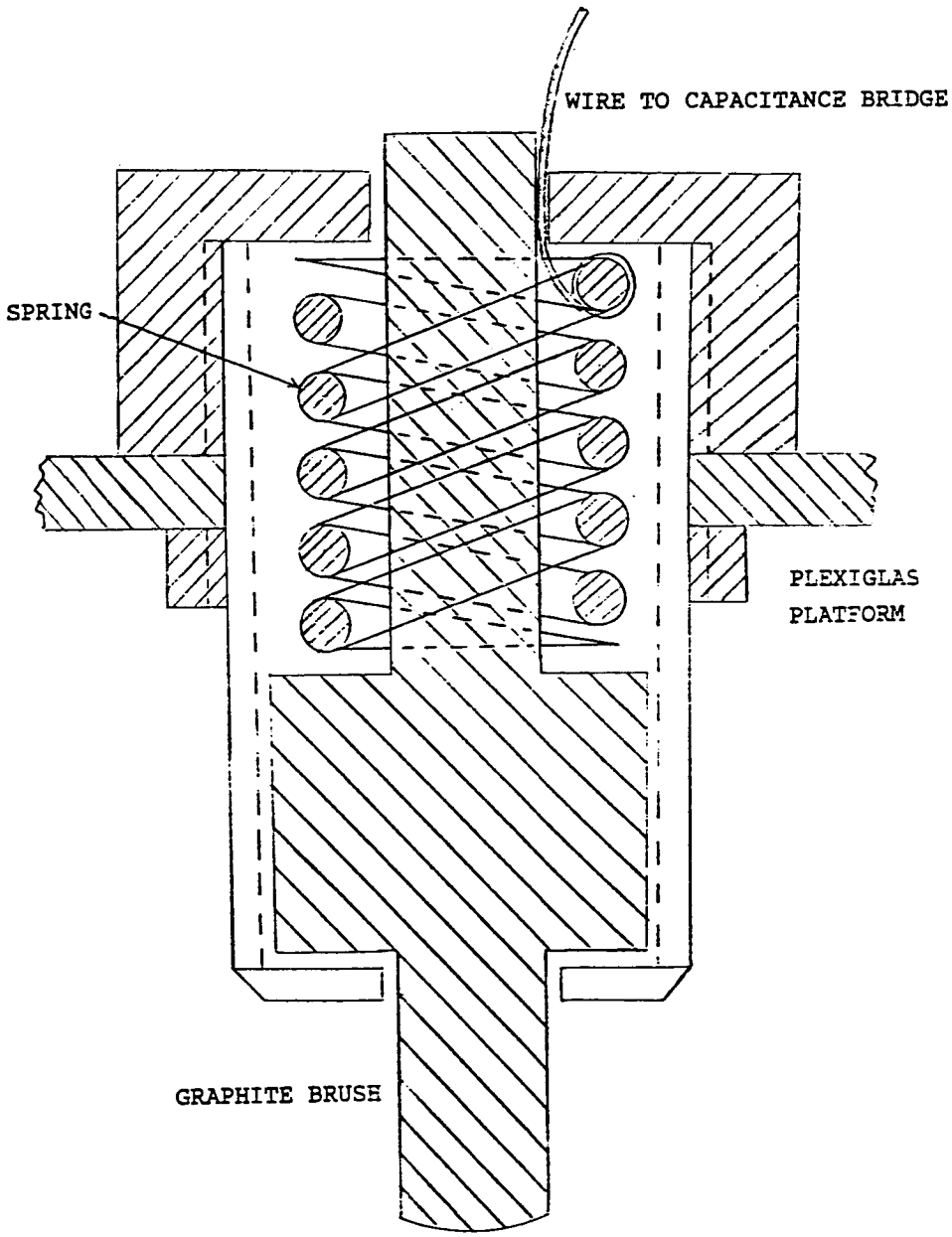

Fig. 2.13 Cross sectional view of brush.

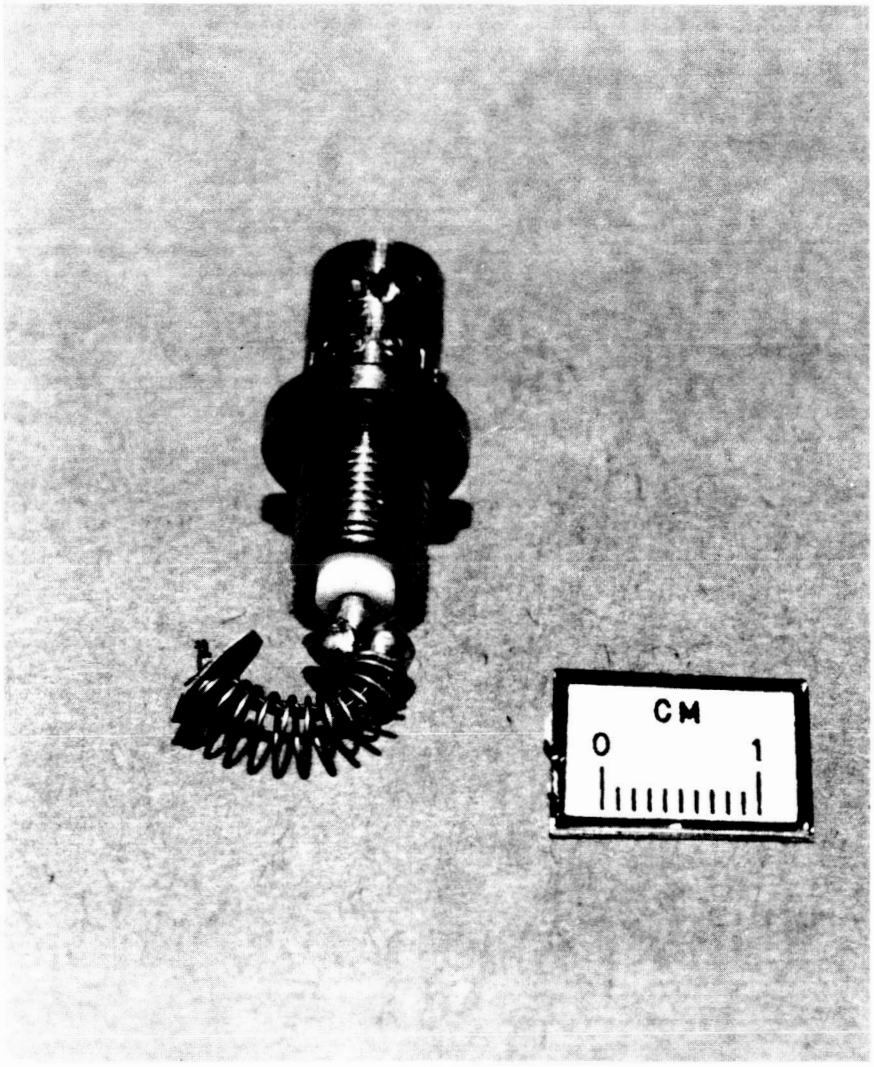

Fig. 2.14 Vacuum cleaner style brush.

TABLE I. - FREON 113 SPECIFICATIONS

Material name:	Trichlorotriflouroethane
Trade name:	Arklone P-113, Blaco-tron TF, Freon TF, Freon 113, Frigen 113TR-T, Genetron 113, Genesolv D, Isotron 113, Refrigerant 113, Ucon 113.
Boiling point, (1 atm)	117.6 °F
Vapor pressure at 70 °F	285 mm Hg
Solubility in H_2O AT 70 °F	0.028 percent
Specific gravity	1.57
Evaporation rate (acetone = 1)	-0.45
Melting point	-35 to -36 °C
Molecular weight	187.39

TABLE II. - NOMINAL ANGULAR VELOCITIES FOR TEST BEARINGS USED

	ITI 11532-A	ITI 8990-A
Inner race speed, rps	36 to 37	38
Outer race speed, rps	25 to 26	25 to 26
Ball speed, rps	167 to 173	168 to 170

CHAPTER III

RESULTS AND DISCUSSION

3.1 OIL FILM THICKNESS CALCULATION

The average oil film thickness in an angular contact ball bearing operating in parched EHL is calculated based on the capacitance between the inner and outer races. The film thickness is estimated based on the capacitance technique of Dyson [9]. Although this method was developed for lubricated cylinders, Allen [10] successfully applied it to ball bearings. Following Allen [10], the assumptions are:

1. The shape of the Hertzian contact zone is assumed to be the same as in dry contact with the addition of the average oil film thickness h_o.
2. There is no free bulk oil outside the contact zone so the oil film is assumed to be in two parts at the inlet and outlet. This implies that an oil film of thickness $h_o/2$ adheres to the ball and race with the remainder of the inlet and outlet sections composed of air.
3. The film thicknesses between the ball and inner race and between the ball and outer race are equal. It has been shown that the two thicknesses differ by only about 5 percent as noted by Allen [10].

4. The surfaces in the Hertzian contact zone are parallel planes.

A correction for capacitance effects perpendicular to the plane of motion is included.

Fig. 3.1 shows two stationary spherical surfaces in contact under light load (no elastic deformation) with the space between the surfaces filled with oil. The film thickness for small values of x is represented by

$$h_1 \simeq \frac{x^2}{2R} \quad . \quad . \quad . \tag{15}$$

where R is the radius of relative curvature, defined as

$$\frac{1}{R} = \frac{1}{R_a} + \frac{1}{R_b} \tag{16}$$

When a normal load is applied to the stationary surfaces they elastically deform and a Hertzian contact area is formed where the surfaces meet as illustrated in fig. 3.2. The Hertzian contact area formed is shown in fig. 3.3 where a and b are defined by Hamrock [18] as:

$$a = \left(\frac{6\, k^2 \varepsilon\, F\, R}{\pi\, E'} \right)^{1/3} \tag{17}$$

$$b = \left(\frac{6\, \varepsilon\, F\, R}{\pi k\, E'} \right)^{1/3} \tag{18}$$

where F is the applied load and E' is the reduced modulus of elasticity:

$$E' = \frac{2}{\frac{1 - \tilde{\nu}_a^2}{E_a} + \frac{1 - \tilde{\nu}_b^2}{E_b}} \tag{19}$$

where $\tilde{\nu}_a$ and $\tilde{\nu}_a$ are the Poisson's ratios for each surface and E_a and E_b are the Young's moduli of the two surfaces. The other parameters that define a and b are dependent on the ratio of R_a and R_b [18]. The shape of the oil film outside of the Hertzian contact zone is

$$h_2 = \frac{b^2}{2R} \left\{ |\xi\sqrt{\xi^2 - 1}| - \ln\left[|\xi| + |\sqrt{\xi^2 - 1}| \right] \right\} \tag{20}$$

where $\xi = x/b$ [9]. Note that as b goes to zero, h_2 reduces to h_1 and eq. (20) becomes eq. (15).

When the surfaces are set into motion under a heavy load, a fluid film builds up between the surfaces as shown in fig. 3.4. The surfaces are assumed to have the same shape as in fig. 3.2 with the addition of a constant film thickness h_o that is normally of the same order as the elastic deformation of the surfaces so that this assumption is applicable. The oil films in the inlet and outlet regions are assumed to separate into equal parts, each of thickness $h_o/2$ with the remaining volume filled with air.

The capacitance across the Hertzian contact and surrounding region is represented by

$$C_T = C_1 + C_H + C_2 + C_L \tag{21}$$

where

C_1 = the capacitance across the surfaces in the inlet region.

C_H = the capacitance across the Hertzian contact.

$C_2 = C_1$ = the capacitance across surfaces in the outlet region.

C_L = capacitance across the region in the plane perpendicular to the direction of motion.

Letting C_i and C_o equal the inner and outer race contact capacitances

$$C_i = C_{1i} + C_{Hi} + C_{2i} + C_{Li} \tag{22}$$

and

$$C_o = C_{1o} + C_{Ho} + C_{2o} + C_{Lo} \tag{23}$$

the total capacitance C_T is

$$C_T = Z\left[\frac{C_i\ C_o}{C_i + C_o}\right] \tag{24}$$

where Z is the number of ball in the bearing.

The capacitance in picofarads in the Hertzian contact zone as given by Allen [10] is:

$$C_H \cong \frac{\varepsilon_o' b}{2\pi h_o} \tag{25}$$

where ε_o' is the dielectric constant of the oil in the Hertzian contact zone. The capacitance across the inlet and outlet regions is given by

$$C_{1,2} = \int_{\pm b}^{\infty} \frac{dx}{\left[4\pi\left(\frac{h_o}{\varepsilon_o} + \frac{h_2}{\varepsilon_a}\right)\right]} \tag{26}$$

where ε_o is the dielectric constant of the oil at atmospheric pressure. The inlet and outlet have air and oil and not just oil so that ε_a is equal to 1.

The equation for h_2 is substituted into eq. (26) and the following is obtained:

$$C_{1,2} = \frac{\varepsilon_o b}{4\pi h_o} \int_1^\infty \frac{d\xi}{1 + X\left\{|\xi\sqrt{\xi^2 - 1}| - \ln\left[|\xi| + |\sqrt{\xi^2 - 1}|\right]\right\}} \tag{27}$$

where

$$X \equiv \frac{b^2}{2R\, h_o} \frac{\varepsilon_o}{\varepsilon_a} \tag{28}$$

The variable is changed to

$$\zeta = \frac{1}{\xi} \tag{29}$$

to avoid infinity at the limits and eq. (27) becomes

$$Y = \frac{2^{1/2}}{4\pi} X^{1/2} \int_0^1 \frac{d\zeta}{\zeta^2 + X\left\{|\sqrt{1 - \zeta^2}| - \zeta^2 \ln\left[\left|\frac{1}{\zeta}\right| + |\sqrt{\frac{1}{\zeta^2} - 1}|\right]\right\}} \tag{30}$$

where

$$Y = \left(\frac{\varepsilon_o\, \varepsilon_a R}{h_o}\right)^{-1/2} C_{1,2} \tag{31}$$

This integral was evaluated numerically by Dyson [9] with the results shown in fig. 3.5 and table III.

The capacitances in the different regions, according to Allen [10], are represented by the following:

$$C_{Hi} = \frac{\epsilon_o A_i}{4\pi h_o}\left(\frac{2.54}{0.9}\right) \tag{32}$$

$$C_{Ho} = \frac{\epsilon_o A_o}{4\pi h_o}\left(\frac{2.54}{0.9}\right) \tag{33}$$

$$C_{1i} = C_{2i} = \left(2a_i\right) Y_{1i} \sqrt{\frac{R_i \epsilon_o}{h_o}}\left(\frac{2.54}{0.9}\right) \tag{34}$$

$$C_{1o} = C_{2o} = \left(2a_o\right) Y_{1o} \sqrt{\frac{R_o \epsilon_o}{h_o}}\left(\frac{2.54}{0.9}\right) \tag{35}$$

$$C_{Li} = (2b_i) Y_{Li} \epsilon_o \sqrt{\frac{R_L}{h_o}}\left(\frac{2.54}{0.9}\right) \tag{36}$$

$$C_{Lo} = (2b_o) Y_{Li} \epsilon_o \sqrt{\frac{R_L}{h_o}}\left(\frac{2.54}{0.9}\right) \tag{37}$$

where

$$R_i = \frac{d\ \gamma_i}{d + \gamma_i} \tag{38}$$

$$R_o = \frac{d\ \gamma_o}{d + \gamma_o} \tag{39}$$

$$R_L = \frac{d\ \gamma_g}{d + \gamma_g} \tag{40}$$

γ_i and γ_o are the inner and outer race track radii, respectively and γ_g is the groove radius.

The capacitance for a given film thickness h_o can be readily found. The value of h is substituted into eq. (31) to obtain the different X's and the Y's are found either from

fig. 3.5 or table III and used in the appropriate capacitance equations given on the previous page. The values of C_i and C_o are calculated and eq. (24) is used to get the total capacitance.

Calculating a film thickness for a given capacitance is not as straight forward. An iterative scheme is used where a film thickness is chosen and a capacitance is calculated. This capacitance is compared to the given capacitance and a new film thickness is chosen. The process is repeated until the calculated and given capacitances are equal.

3.2 CALIBRATION PROCEDURE

It is difficult to calibrate the test rig with a material of known thickness and dielectric constant due to the geometry of the test bearing and characteristics of the test rig. A calibration curve in the form of a graph of calculated film thickness versus total capacitance C_T is plotted, as shown in fig. 3.9 for a 200 lb load. Note that all of the capacitance data is for a load of 200 lb . The dielectric constant is chosen to be 2.1 and assumed to remain constant which is a good approximation because the dielectric constant seems to vary little over a pressure range of 0 to 50 000 lb/in.^{2} (5 percent) for a similar oil used by Dyson [9].

The effect of temperature on the dielectric constant is determined experimentally for the SRG 200 oil. Two 2 in. by 3 in. nonwarping 3/8 in. thick tool steel parallel plates are separated

at the edges by a thin plastic sheet of known thickness. The tool steel bar was manufactured by Teledyne Pittsburgh Tool Steel and the surfaces of the plates were polished to a fine finish. The plates are placed in a Thelco model 26 laboratory oven and connected to the Hewlett Packard capacitance bridge by way of RG-59 coaxial cables as shown in fig. 3.6.

The capacitance between the plates with air as the dielectric is found to be 305.2 pF. Based on the area of the plates A (5.93 $in.^2$), the separation distance of the plates (0.0043 in.) and the dielectric constant of air ε_a (approximately 1.0), the calculated capacitance is 309.4 pF from the following formula:

$$\tilde{C} = \varepsilon_a \frac{\tilde{\varepsilon}_p A}{4\pi \tilde{d}} \tag{41}$$

where $\tilde{\varepsilon}_p$ is the permittivity constant, $\tilde{C}$ is the capacitance and $\tilde{d}$ is the distance between the plates. This confirms that the measurement scheme will give a good approximation of the dielectric constant of the oil because the theoretical and measured air capacitances vary by approximately 1 percent.

The measuring of the capacitance of the oil uses the same test set-up as for the air capacitance so that the gap and area of the plates are the same. The above equation is rewritten as

$$\frac{\tilde{C}_o}{\tilde{C}_a} = \frac{\varepsilon_o}{\varepsilon_a} \tag{42}$$

where $\tilde{C}_o$ is the capacitance of the oil and ε_o is the oil dielectric constant.

The temperature of the test bearing after a test is always low enough so that it can held in the hand with no discomfort. The dielectric constant of the oil is determined for temperatures ranging from 27 to 76 °C using an API Instruments analog temperature measuring system (IC type J) as shown in figs. 3.7 and 3.8. The oven is adjusted to a higher temperature after a reading is taken and the next reading is not taken until the oven has settled out at the desired temperature. The data for a 10 hr time period is displayed in table IV.

The dielectric constant of the SRG 200 oil is chosen to be 2.1 for the film thickness calculation because the dielectric experiment is not felt to be extremely accurate and the bearing operates at the higher temperature range of the dielectric experiment. This agrees well with the tabulated mineral oil dielectric constant of 2.24. The SRG oil series is mineral oil with other chemicals added that can have a significant effect on such properties as the dielectric constant. An error analysis is not attempted because the capacitance data is sensitive to the position of the plates which are lined up by eye. The experiment is only used to estimate the dielectric constant of the SRG 200 oil.

The total capacitance C_T is the electrical capacitance between the inner race, balls and outer race separated by an oil film. The capacitance that is measured C_M includes all stray capacitances that occur between the terminals of the capacitance bridge. This effect can be corrected for by measuring the

capacitance between the races when no balls or lubricant are present. Calling this capacitance C_s, the total capacitance is equal to $C_M - C_s$. The value of C_s is found to be approximately 0.5 pF which is a small percentage of the capacitance readings, typically ranging between 200 and 400 pF.

The error in the capacitance readings is ±5 pF based on the ability to read the capacitance bridge and enter the BSR, capacitance and conductance data into the computer at the same time. This causes the film thickness to vary by less than 3 percent even at lower capacitance values. The error is lower at higher capacitance values due to the shape of the graph in fig. 3.9.

The loss or conductance measurement is important to the analysis of the film thickness and polymer degradation. One expects the conductance of the polymer to be less than that of the oil because polymers are in general better insulators relative to oil. If metal is pulled away from the surface as the oil film thickness decreases, the conductance would increase due to the presence of the metal in the oil film. The conductance is measured with the capacitance on the capacitance bridge and has units of μ℧ (micromho). The error in the conductance measurement is approximately ±0.2 μ℧ based on the same reasoning as in the capacitance measurement.

3.3 BSR AND CAPACITANCE VERSUS INITIAL FILM THICKNESS

The amount of oil applied to the bearing initially has a significant effect on the BSR. A test bearing has essentially

three operation modes during a test as shown in fig. 1.2 in which the BSR is plotted versus elapsed time. The bearing has erratic BSR values initially due to the "settling in" of the test bearing which has been observed only with mineral oil. During this period the balls come to their preferred orientation and the oil is redistributed. Another reason for the erratic data is a result of the data taking method. At the start of a test, the outer race speed is adjusted to stop the ball complement and it usually takes a few readings to get an outer race speed that keeps a constant group of balls in the view field of the microscope. A typical plot of outer race speed versus elapsed time is shown in fig. 3.20 showing that the outer race is changing at the beginning as an outer race speed that makes the ball complement more stationary is sought. Eventually, a constant outer race speed is attained.

After the settling in period, the bearing reaches a point where the BSR becomes approximately constant. This value of BSR is affected by the initial concentration of the solution of oil and Freon that the balls are dipped into. As the amount of oil initially put on the bearing decreases, this steady state BSR increases because the oil film initially applied is thinner which reduces the amount of rheologic slip between the races and balls and causes an increase in BSR.

As the amount of oil initially applied increases, the bearing begins to leave the parched EHL regime and enters into the starved and fully flooded regimes. This causes the BSR to reach a constant

value because the film thickness becomes relatively thick and has less affect on the rheologic slip.

The amount of oil applied to the bearing has an effect on the capacitance as shown in fig. 3.10 where capacitance is plotted versus elapsed time. This is highlighted in fig. 3.11 as the bearing starts to approach steady state. The capacitance increases initially indicating a reduction in film thickness (fig. 3.12) and then reaches a constant value.

The BSR as a function of the amount of oil applied or oil/Freon solution concentration for two ITI 8990-A test bearings operating at a 300 lb. load is shown in figs. 3.13 and 3.14. The data is plotted versus oil/Freon concentration because the initial film thickness is only 7.1 percent accurate while the solution concentration has an error of only 1 percent (see appendix C). As the amount of applied oil or the initial film thickness increases, the BSR reaches a constant value which is slightly different for each bearing. For one bearing the constant BSR is approximately 2.6821 while the other is 2.6831. These bearings are suppose to be identical but the BSRs are not, even though the BSRs only vary by 1/1000. This indicates that the BSR is sensitive to differences in geometry, slight as they may be. This is confirmed in fig. 3.15 where different bearings having the same part number, ITI 11532-A, are compared at varying amounts of applied oil. This plot shows that the BSR can vary noticeably between bearings having the same part number. The steady state BSR data is the average of the

BSR after the bearing has settled in with a typical test run shown in fig. 3.18.

As the amount of oil applied or the initial film thickness is reduced, the BSR increases toward the calculated no-slip BSR because the rheologic slip decreases as the film thickness decreases. For the bearings used, ITI 8990-A, the no-slip BSR at 300 lb. is 2.6844 which is where the bearing in fig. 3.13 is headed. The BSR of the bearing in fig. 3.14 at 0.002 initial concentration of oil to Freon is 2.68528 which is already above the no-slip BSR of 2.6844. The BSR is a sensitive function of geometry so that the calculated no-slip BSR is a reference value only. The general shape of the curves in figs. 3.13 and 3.14 is the same indicating the same behavior in BSR as the initial film thickness decreases.

The steady state capacitance is a function of slight changes in geometry as shown in fig. 3.16 which displays the steady state capacitance of different bearings of the same part number at various oil/Freon concentrations. Most of the bearings exhibit a steady state capacitance of approximately 280 pF except the one bearing that has a capacitance of around 375 pF. All of the bearings are operated at a 200 lb. load and approximately the same speed so that the bearing at the higher capacitance appears to have a greater difference in geometry than the others. The average calculated film thicknesses for 280 and 375 pF are 5.5 and 3.9 μin., respectively.

The elastohydrodynamic lubrication regime has characteristic film thicknesses between 10^{-7} and 10^{-6} m or 4 and 40 μin. Parched EHL is in the region of thinnest films of the elastohydrodynamic lubrication regime so that the bearing is operating in parched EHL. The balls and races have rms surface finishes of 1 and 3 μin. respectively and a typical film thickness is 5 μin so that the film parameter defined by eq. (2) is

$$\Lambda = \frac{h}{(f_r^2 + f_b^2)^{1/2}} = 1.6 \qquad (43)$$

From fig. 1.1, a film parameter of 1.6 is in the mixed lubrication regime indicating that some asperity contact does occur at the lower initial film thicknesses. During the course of a test at a thinner initial film thickness, there are sudden jumps in the conductance which indicate asperity contact.

The plot of the capacitance in fig. 3.16 shows an increasing trend as the initial film thickness is decreased for the bearing operating at the higher capacitance indicating a reduction in film thickness as the initial film thickness is decreased. The capacitance method does not give consistent data when the oil/Freon concentration is lowered below 0.008 so that the curve could not be completed but the BSR can be measured down to 0.002. Asperity contact is the probable cause of the erratic readings in the capacitance at the very thin initial film thicknesses which reduces the film parameter toward the mixed and even boundary lubrication regimes.

3.4 BSR COMPARISON AT DIFFERENT LOADS

The first series of tests were run to see how the BSR varies with the applied load. The tests were run with balls dipped in a solution of SRG 100 oil and Freon with a concentration of 0.014 ml of oil to milliliter of Freon corresponding to an initial film thickness of approximately 14 μin. The same ITI 8990-A test bearing was used for all of these tests.

The data along with the calculated no-slip BSR values are shown in table V. Note the difference in the BSR values between loads and the no-slip values. The applied film thickness is relatively thick which explains the large discrepancy between the test and no-slip BSR values but the general trend of increasing BSR with increasing load is common to the data and the no-slip BSR. The no-slip BSR increases over a smaller range which is probably due to the existence of the oil film in the actual bearing. A smaller initial film thickness has less distance to compress relative to a larger film thickness so that the slip or BSR has a smaller range of variation at different loads.

3.5 TESTS TO FAILURE

Several tests were run to see how the test bearing operated up to failure which occurs when the film between the balls and races becomes so thin that the asperities of each surface contact. Surface damage results and the operating characteristics of the rig change dramatically. Before failure occurs, the mark on top of the ball begins to oscillate and tumble over to different positions on

the ball. The ball complement is less stationary so that the outer race speed must be adjusted more often until failure occurs at which time the outer race has no control over the ball complement.

Before a failure occurs, the BSR starts to increase at a rapid rate as shown in fig. 3.19 for an ITI 8990-A test bearing operating at a 300 lb load and 0.01 concentration of oil to Freon. The BSR starts to increase due to the degradation of the oil into the friction polymer which has different viscous properties than the oil. The test rig is shut down right after the bearing fails and the test bearing is disassembled. A photograph of a ball taken straight out of a bearing from a similar test is shown in fig. 1.3. Note the appearance of the polymer band that forms in the wear track of the ball. The oil is soluble in Freon so that the oil washes away from the ball as shown in fig. 1.4 but the polymer band remains indicating that the polymer is different than the oil. Fig. 1.5 shows the ball after it has been wiped with a Freon soaked cloth exposing a wear track with definite surface damage. A magnified view of the surface in fig. 1.6 verifies the damage to the ball.

A typical plot of the outer race speed as a function of elapsed time is shown in fig. 3.20 for the test in fig. 3.19. The outer race speed is initially adjusted to bring the ball complement to a stationary position and then reaches a constant value similar to the BSR in fig. 3.19. At about the same time that the BSR starts to increase at a rapid rate, the outer race speed begins to

decrease significantly in an effort to try and keep the ball complement stationary. This occurs because there is less slip between the balls and the races and the outer race slows down to keep the ball complement stationary.

A test can be stopped before surface damage occurs to the balls and races and the test bearing can be used again, confirming the observations of Kingsbury [3][12]. To avoid surface damage, a test is stopped as soon as the BSR starts to increase and the balls start to tumble. Several tests were run on the same bearing in figs. 3.19 and 3.20 where the BSR increased but no surface damage occurred. Fig. 3.21 shows the BSR versus time for a load of 300 lb and an oil/Freon concentration of 0.004. The amount of oil applied is relatively small so that the bearing settles in very quickly and exhibits only a short period of constant BSR. The BSR begins to increase at a rapid rate at which time the test rig is shut down. An even less amount of oil is applied to the test bearing of fig. 3.22 which is run at a 300 lb load and oil/Freon concentration of 0.002. The BSR settles in rapidly and then starts to increase almost immediately afterwards. The polymer was wiped off the test bearing and the bearing was used again until the failure displayed in fig. 3.19 occurred.

Sometimes as a bearing starts to fail, the balls will tumble over to a new orientation and the BSR will drop as shown in fig. 3.23. This ITI 8990-A test bearing was run at a 200 lb load and at 0.014 oil/Freon concentration. A photo of a ball after this

test shows multiple wear tracks as displayed in fig. 3.24. Just before the BSR suddenly drops after the first BSR increase, the balls shift their orientation slightly. After the bearing fails and the ball complement cannot be controlled, the ball complement suddenly becomes stationary for a few seconds and then goes out of control again. This occurs a few times after which the bearing started to seize, showing that the bearing looses its original orientation and is forced to a less stable one. The balls and races are operating across damaged surfaces which damages the new wear track causing repeated surface wear.

The capacitance and film thickness versus elapsed time for the same bearing are shown in figs. 3.25 and 3.26. The capacitance changes significantly at the point where the BSR starts to rise the first time. The capacitance is increasing indicating a reduction in average film thickness up to the point where the BSR suddenly decreases. The capacitance begins to decrease steadily until the bearing fails at which time it drops rapidly. The decrease in the capacitance is possibly due to the presence of surface metal in the film after the BSR increased the first time. The surface damage that occurs just before failure causes the capacitance to drop to zero which corresponds to a sudden sharp increase in conductance or loss as shown in fig. 3.27. The oil film has so much metal in it from the bearing surfaces that the oil shorts out causing the capacitance to drop.

The conductance versus elapsed time is important for a few reasons. As mentioned above, it can indicate metal present in the oil film. The oil used probably has a different conductivity than the polymer that forms so the conductance can indicate polymer build-up. A magnified view of fig. 3.27 is shown in fig. 3.28. The conductance suddenly drops before the BSR increases the first time which could indicate the sudden formation of polymer. This is not likely because the polymer probably wouldn't form that fast. There is an increase and then decrease after the BSR drops back down. The conductance continues to decrease, which is a more realistic indication that polymer is forming, and rapidly increases as the bearing fails, indicating surface wear.

An ITI 11532-A test bearing was run until it failed at a load of 200 lb and an oil/Freon concentration of 0.008. The BSR as a function of elapsed time is plotted in fig. 3.29 and shows the typical behavior as the bearing settles in, goes through a mild transient and increases rapidly just before failure. The capacitance plot in fig. 3.30 shows an increase indicating a reduction in oil film thickness (fig. 3.31) but then suddenly decreases. The sudden decrease is due the metal that is worn away from the surfaces as the bearing surfaces are damaged. The conductance is plotted in fig. 3.32 and shows a gradual decrease as the polymer forms and a sudden increase before failure due to the presence of metal in the oil film. The outer race speed is plotted in fig. 3.33 and shows the typical decrease as the BSR increases before failure.

3.6 FILM THICKNESS TIME STUDY TESTS

Two series of tests were run to see how the polymer formed as a function of time. ITI 11532-A test bearings were run for tests of different lengths. The first test lasts for 10 minutes and each subsequent test for 10 minutes longer than the previous one (tests of 10, 20, 30 min ...) with the bearing cleaned and relubricated for each test. After each test, the wear tracks of two balls are examined with a scanning electron microscope to see how much, if any, polymer and/or surface damage had developed. The two balls cannot be used again after the analysis so that two new balls are used in their place. The two series of tests were run at 0.008 and 0.016 SRG 200 oil/Freon concentrations and a 200 lb load.

The first time study was run for tests of 10, 20, 30, 40 and 50 minutes at a SRG 200 oil/Freon concentration of 0.016. Figs. 3.34 and 3.35 show the BSR and average film thickness, respectively, versus time for the 10 minute test. The initial film thickness at 0.016 is approximately 20 μin. while the operating calculated film thickness is 4.5 μin. indicating that the excess is squeezed out as the bearing settles in. The BSR for all of the tests behaves in the same manner as it settles in and reaches a constant value of approximately 2.749. The average film thickness exhibits the same behavior for all of the tests as it decreases initially and reaches a constant value of approximately 4.5 μin. The 50 minute test shows the same behavior in the BSR and average film thickness as shown in figs. 3.36 and 3.37 but the conductance did not. The

conductance for the 50 minute test, plotted in fig. 3.38, starts out in the same manner of other tests as it decreases from about 6 $\mu\mho$ but instead of reaching a constant value it steadily increases from 5.5 $\mu\mho$ to 8.5 $\mu\mho$ at the end of the test. This indicates the presence of metal in the oil film as the test progresses. The BSR shows a wider data scatter than other tests due to the unsteady behavior of the ball complement.

The scanning electron microscope (SEM) photographs from the 50 minute test show a wear track with pits where the metal was pulled away from the surface as shown in fig. 3.39, taken at a magnification of 2000x. The dark areas are the pits and the dark lines are wear marks in the surface. The photographs from the other tests show no surface wear or polymer build-up except the 40 minute test photos which show significantly less pitting. A ball that has never been used is shown in fig. 3.40 and shows no pits and only light indentations. A 60 minute test was attempted but the balls tumbled throughout the test and the bearing failed after 25 min.

The darker areas around the lines and pits in fig. 3.39 indicate polymer build-up. Fig. 3.41 shows a higher magnification (5060x) of one of the pits. The light area is a cavity in the surface from where metal is pulled away from the surface and the darker areas around the edge of the cavity are friction polymer. The edge of the cavity is raised due to the pulling away of the metal so that as the bearing operates, the pressure at the edge of the cavity is higher. This increases the degradation rate of the oil which causes the polymer to form faster in these areas.

The second time study was run for the same type of bearing and load but at a SRG 200 oil/Freon concentration of 0.008 or half that of the first time study. Figs. 3.42 and 3.43 show the BSR and average film thickness for a typical test run. The initial film thickness at 0.008 is approximately 10 μin. while the operating film thickness is 4.2 μin. The two time study test bearings settle into different film thicknesses due to the different initial film thicknesses. The BSR is higher due to the decreased initial film thickness and different bearing and the average film thickness is about 4.2 μin. which is thinner than for the bearing in the first time study.

The polymer starts to form and pits begin to appear at the end of the 60 minute test as shown in fig. 3.44 taken at a magnification of 2010x showing the same type of wear as in the first time study. The SEM photos of the 50 minute test show a few pits and patches of polymer build-up. Just before the end of the 60 minute test, the BSR increased but then decreased as shown in fig. 3.45. The average film thickness and conductance exhibit a periodic behavior that was not observed in any other tests, as shown in figs. 3.46 and 3.47. This periodic motion is due in part to the metal that is worn away from the surface. The wear track for this test is larger than the previous tests so that after the ball experiences surface wear, it shifts slightly to a new orientation until surface wear again occurs. Each time the ball shifts, it operates on a different film of oil with less metal in it which explains the periodic motion of the

film thickness and conductance. Every time the conductance increases, the average film thickness decreases. The 70 minute test does not show periodic behavior but more polymer build-up is evident as shown in fig. 3.48 (magnified 2100x). The 80 minute test shows periodic behavior in the conductance only as shown in fig. 3.49.

A 90 minute test was attempted but the bearing failed after 60 minute. The conductance, fig. 3.50, increases from the start of the test as it does in the 50 minute test for the first time study. The BSR readings are not consistent due to ball tumbling and loss of the ball mark. The SEM photos in figs. 3.51 (1000x) and 3.52 (1970x) show surface damage and fig. 3.52 indicates that the polymer film is thicker (dark areas are darker than other tests) and more concentrated.

These tests indicate that the polymer builds up around the pits formed in the surface when metal is removed. A SEM photo of the polymer film from a test where a continuous polymer film builds up on an inner race is shown in fig. 3.53. The film is between the two arrows and the dark points outside the film are contaminants. The ridge in the middle of the film is magnified 254x in fig. 3.54 and shows the distinct cut off between the polymer film and the race surface. The line pointed out by the arrow is magnified 2010x in fig. 3.55 and is a crack in the race surface with polymer build-up around it. An end view of the edge of the film is displayed in fig. 3.56 (1990x) and 3.57 (9950x). At this magnification, the polymer has waves in it and is more rough than

the race surface in the foreground. From fig. 3.57 the film thickness is estimated to be between 0.5 and 0.75 μm which is almost four times the measured film thickness in the bearing, showing that the polymer replaces the oil in the Hertzian contact zone and causes the bearing to fail. Fig. 3.58 shows the film away from the ridge and the surface pitting is not as severe as in the time study tests so that the polymer forms a continuous film. The larger pits increase the surface roughness, causing the polymer to concentrate in these areas.

SEM photographs taken of three balls out of another failed test bearing are shown in figs. 3.59, 3.60, and 3.61. All of the photos are taken at a magnification of 1000x but show different surface damage. The surface in fig. 3.59 shows heavy surface damage with polymer deposited in the surface scars. The surface in fig. 3.60 shows light surface wear as indicated by the vertical lines (the crater formations are residues of the Freon used to clean off the oil). Fig. 3.61 displays a surface with heavy polymer build-up but light surface damage. This indicates that the balls are different in size which causes the surfaces to wear differently. The ball with light wear and no polymer is probably undersized and floats in the bearing while other balls carry the load, such as the ball in fig. 3.59. The size of the ball in fig. 3.61 is between the other two and shows wear characteristics of both.

3.7 FRICTION POLYMER ANALYSIS

An analysis of the friction polymer that forms from the SRG 200 oil for an ITI 8990-A test bearing, 300 lb load and 0.002

oil/Freon concentration is attempted using the emission infrared spectroscopy and secondary ion mass spectroscopy techniques. The Auger Electron spectroscopy technique is not successful because it only offers an elemental analysis while the X-ray Photoelectron spectroscopy technique recognizes oxidation states and requires a larger area of analysis than the film has.

The emission infrared spectroscopy analysis showed the presence of a small amount of phosphate. The SRG series of mineral oils contain one percent tri cresyl phosphate antiwear which diffuses out of the oil and coats the bearing surfaces to reduce wear.

The SIMS analysis indicates a substantial amount of carbon, carbon-hydrogen groups and possibly nitrogen as shown in fig. 3.62 for a typical spectrum. There appears to be two steps in the degradation of the SRG 200 oil. The first is a mechanochemical polymerization of the oil where high mechanical shear stresses and pressure in the Hertzian contact zone degrade the oil and form a polymer as indicated by the carbon-hydrogen groups. The SIMS method bombards the film surface with ions which fragment the polymeric chain causing several carbon-hydrogen groups to be detected. The polymer is probably cross-linked in structure rather than chained or branched because of the insolubility of the film.

The second step in the degradation of the oil is the formation of carbonaceous material from the polymer as indicated by the large amounts of carbon present in the SIMS analysis. The film is relatively translucent before failure but is black in appearance

after failure due to the presence of carbon. During the SIMS analysis the relative amount of carbon and carbon-hydrogen groups is extremely sensitive to the position of the ion beam. The areas of high concentration occur in small patches which supports the SEM photographs where the polymer builds up around surface pits and scars. The film appears uniform but the surface determines where the oil degrades at a faster rate.

The presence of nitrogen in the film is from the surrounding atmospheric air that the bearing is operated in. There are traces of iron in the film which is worn away from the bearing surfaces and a few spectra have higher molecular weight molecules indicating longer polmeric chains.

3.8 CONCLUSION

Based on the experimental data, the capacitance technique is suitable for the measurement of the oil film thickness in angular contact ball bearing operating in parched EHL. The results are questionable when the friction polymer starts to form because the difference between the dielectric constant of the oil and polymer is not known. When the surface starts to wear and loose surface metal, the capacitance technique is not accurate because the oil film conductivity increases due to the metal particles and the capacitance decreases or the film thickness increases, the opposite of what is expected before failure.

The BSR measurements show the three modes of operation - setting in, mild transient and failure. The mild transient mode

allows an average BSR to be taken so that the BSR for different initial film thicknesses or oil/Freon concentration of the solution that the balls are dipped into is plotted. This shows that as the initial film thickness is decreased the BSR increases due to the reduction in rheologic slip toward the no-slip calculated values for the particular bearing. The starved or fully flooded EHL regime is reached as the initial film thickness is increased because free bulk oil starts to develop outside the contact zone. As the bearing settles in, the BSR and calculated film thickness do reach constant values but no direct relation is apparent.

The failure of a bearing is characterized by a rapid increase in BSR and tumbling motion of the balls. The test rig can be shut down at the first sign of BSR increase and the balls can be used again. If the bearing is allow to run, the BSR keeps increasing and the ball tumbling becomes more severe until heavy surface damage occurs and control of the ball complement is lost. There are instances when the BSR rises but the balls shift to a new orientation and the BSR drops suddenly. The bearing continues to operate at the lower BSR and exhibits another increase in BSR at a later time.

The SRG 200 oil applied to the bearing degrades at a moderate rate and deposits on the surfaces as the bearing operates. As failure starts to occur the polymer builds up more rapidly to a thickness of the same order of magnitude as the operating oil film thickness at failure. If the test is stopped before surface damage

occurs, the polymer is wiped off indicating that it can be formed with no metal-to-metal contact and the bearing is used for another test. If the test is not stopped, surface damage occurs and the bearing cannot be used again.

The conductance of the oil film is measured and indicates the presence of metal in the film and possible polymer build-up. The conductance increases significantly before failure showing the presence of metal worn away from the surfaces.

An emission infrared spectroscopy analysis of the deposited polymer film shows a small concentration of phosphate which is added to the SRG series of oils as tri cresyl phosphate antiwear. A SIMS analysis shows the presence of carbon, carbon-hydrogen groups and possibly nitrogen indicating a two-step degradation process. The oil degrades into a polymer through a mechanochemical reaction due to the high pressure and shear stresses in the contact area. As failure starts to occur the translucent polymer film turns black in appearance indicating the presence of carbon which is verified by the SIMS analysis. Relatively small traces of iron worn away from the bearing surfaces are brought out by the SIMS technique. The concentration of the carbonaceous material and polymer is variable throughout the film due to the presence of pits and scars in the surface which increase the degradation rate in those areas.

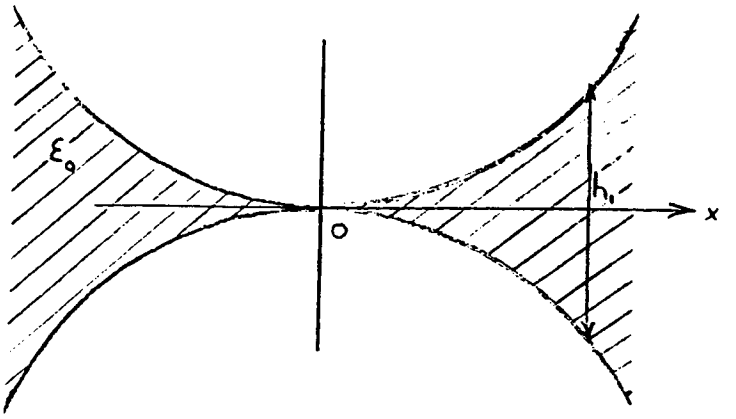

Fig. 3.1 Stationary surfaces under light load.

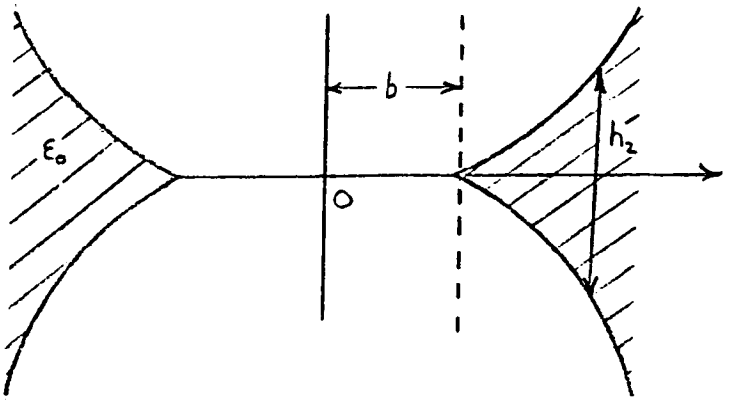

Fig. 3.2 Stationary surfaces under heavy load.

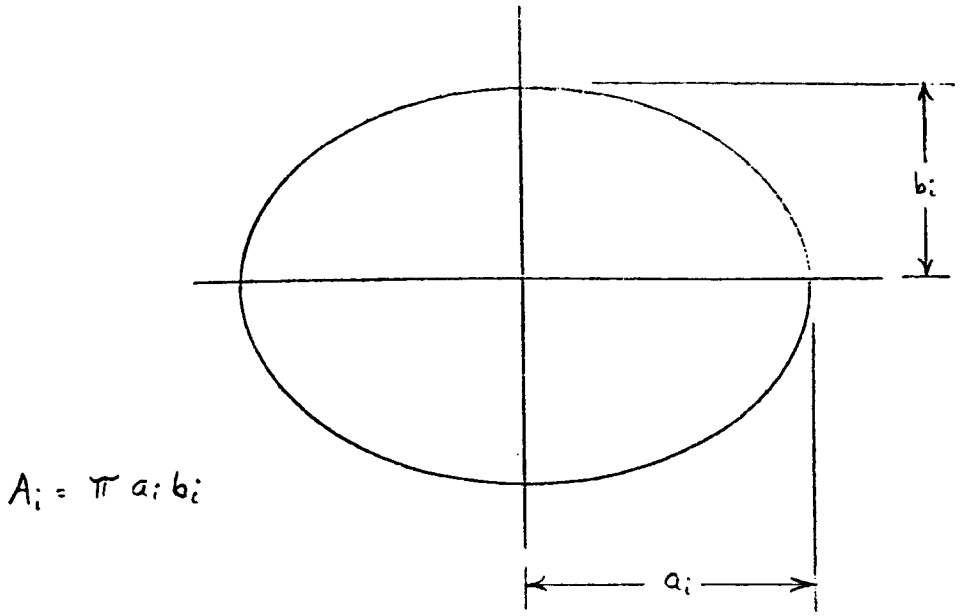

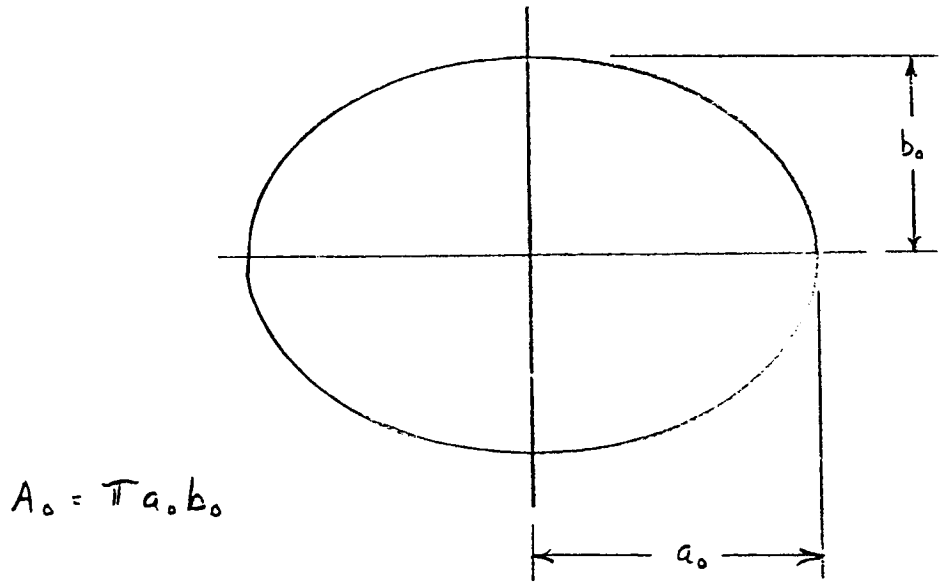

Fig. 3.3 Inner and outer contact ellipses.

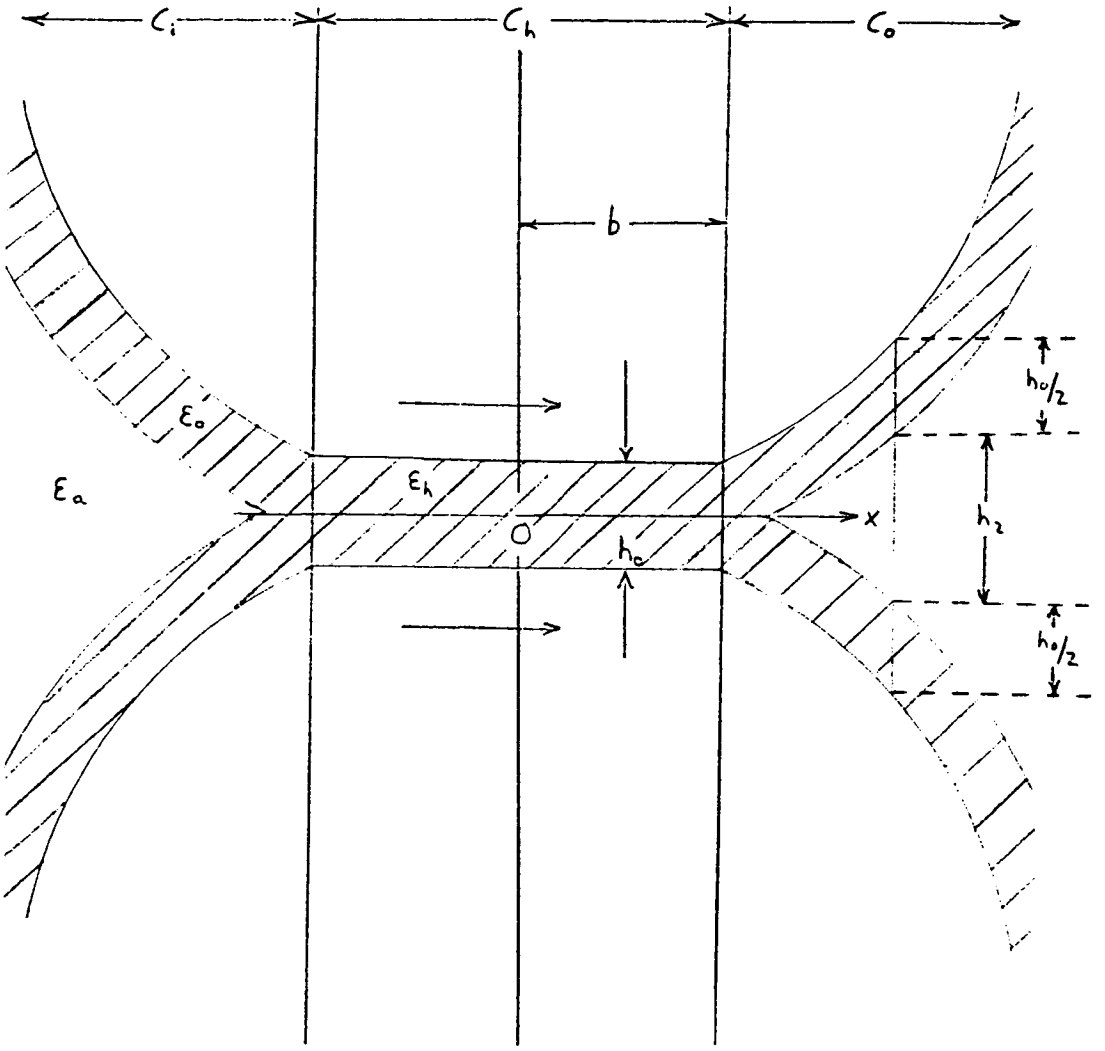

Fig. 3.4 Surfaces in motion under heavy load.

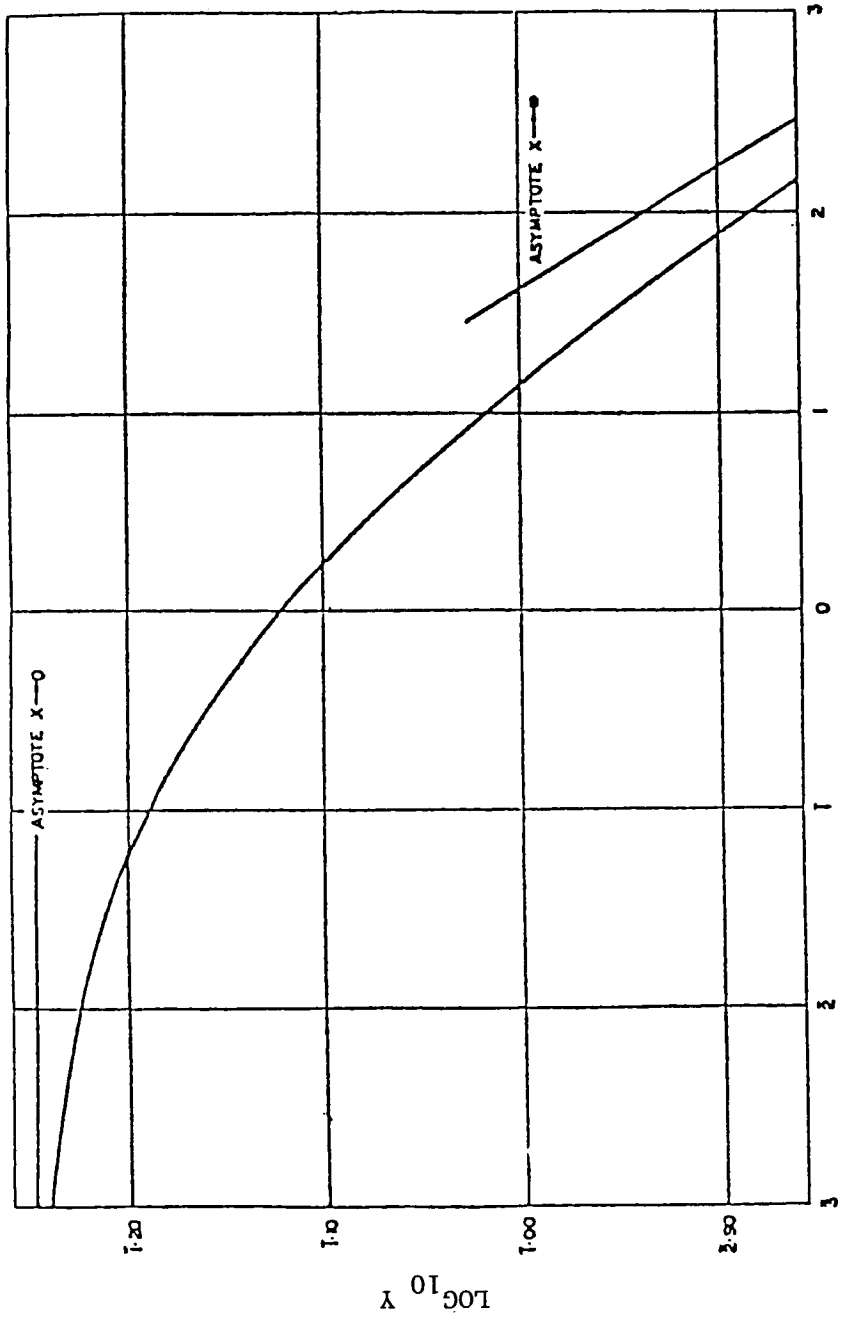

Fig. 3.5 Relationship between Y and X used in determination of capacitance of inlet and outlet sections.

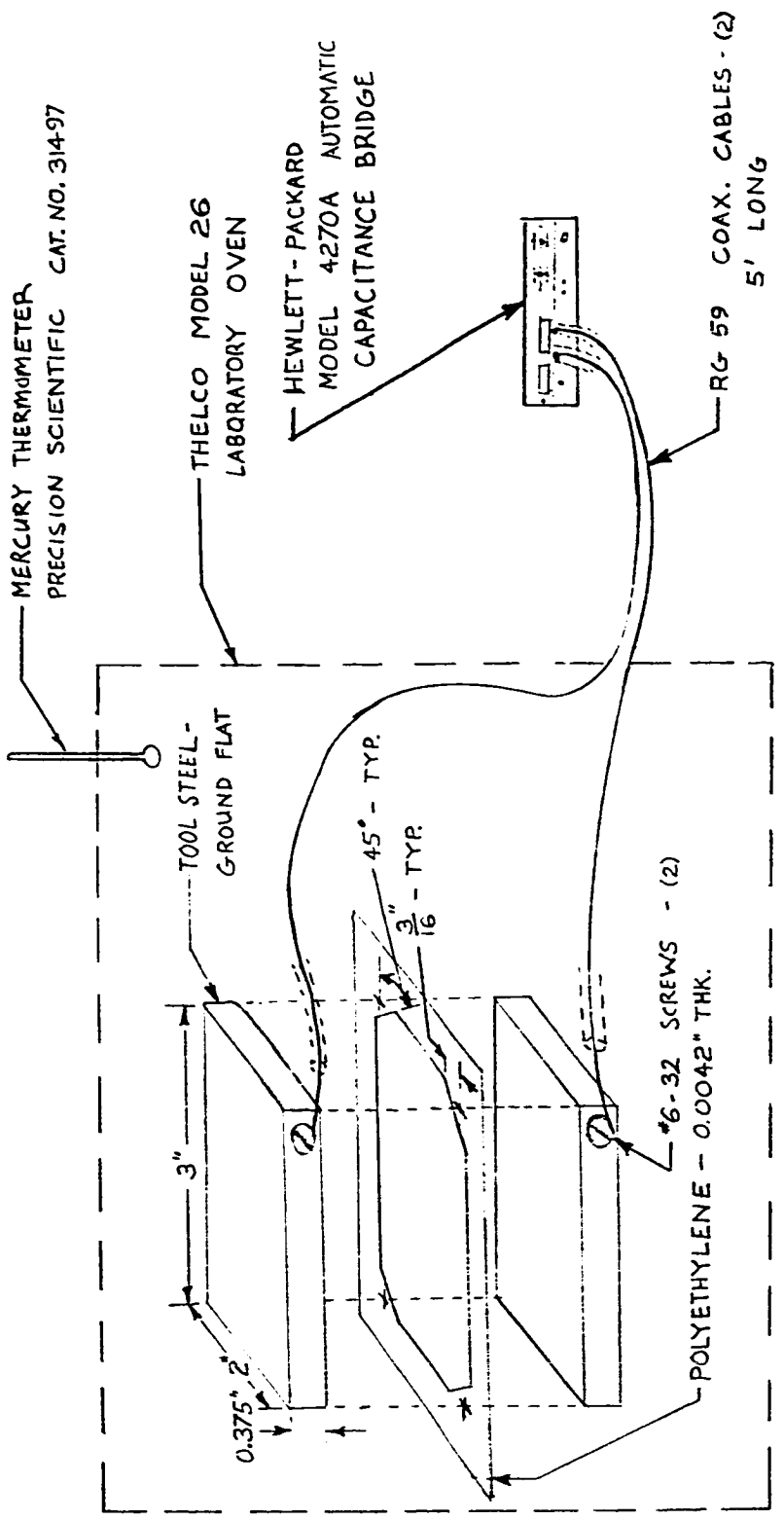

Fig. 3.6 Experimental set-up for determination of SRG 200 dielectric constant.

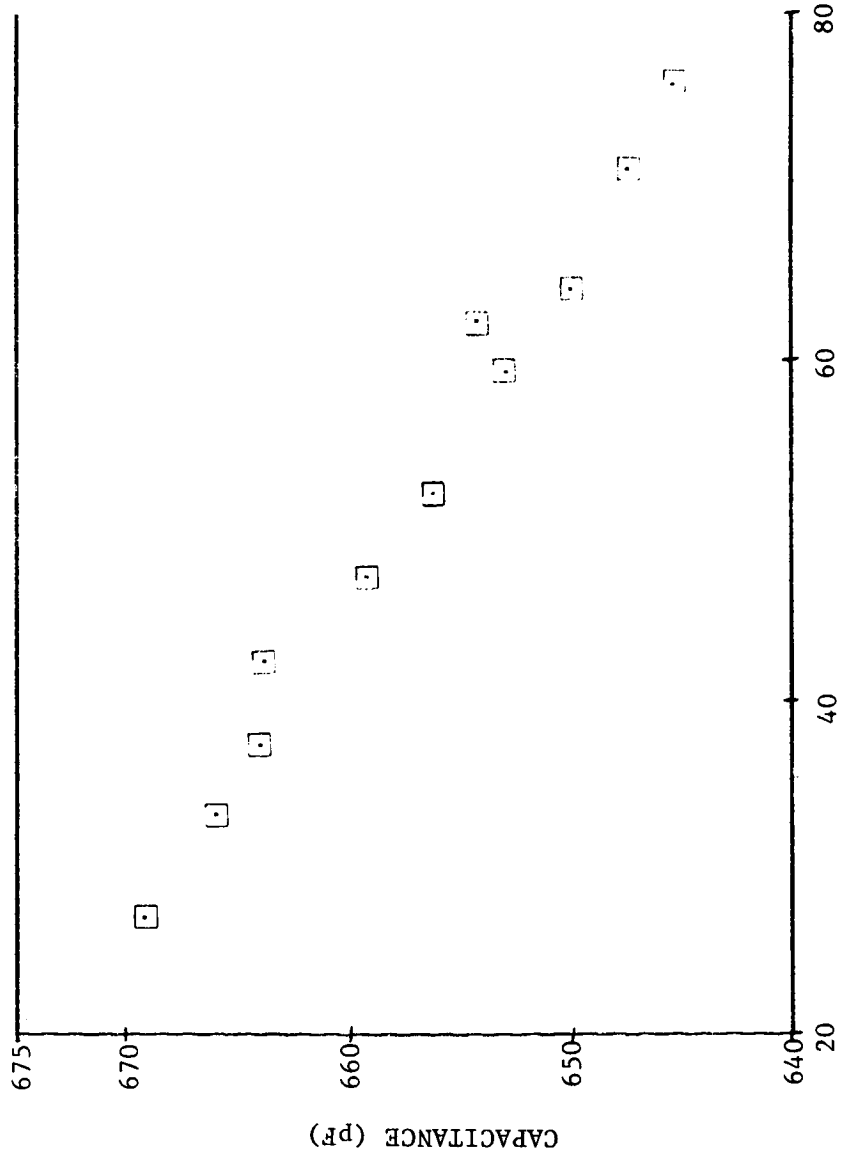

Fig. 3.7 Capacitance vs. temperature for SRG 200 oil dielectric constant experiment. Pressure = 1 atm.

C-2

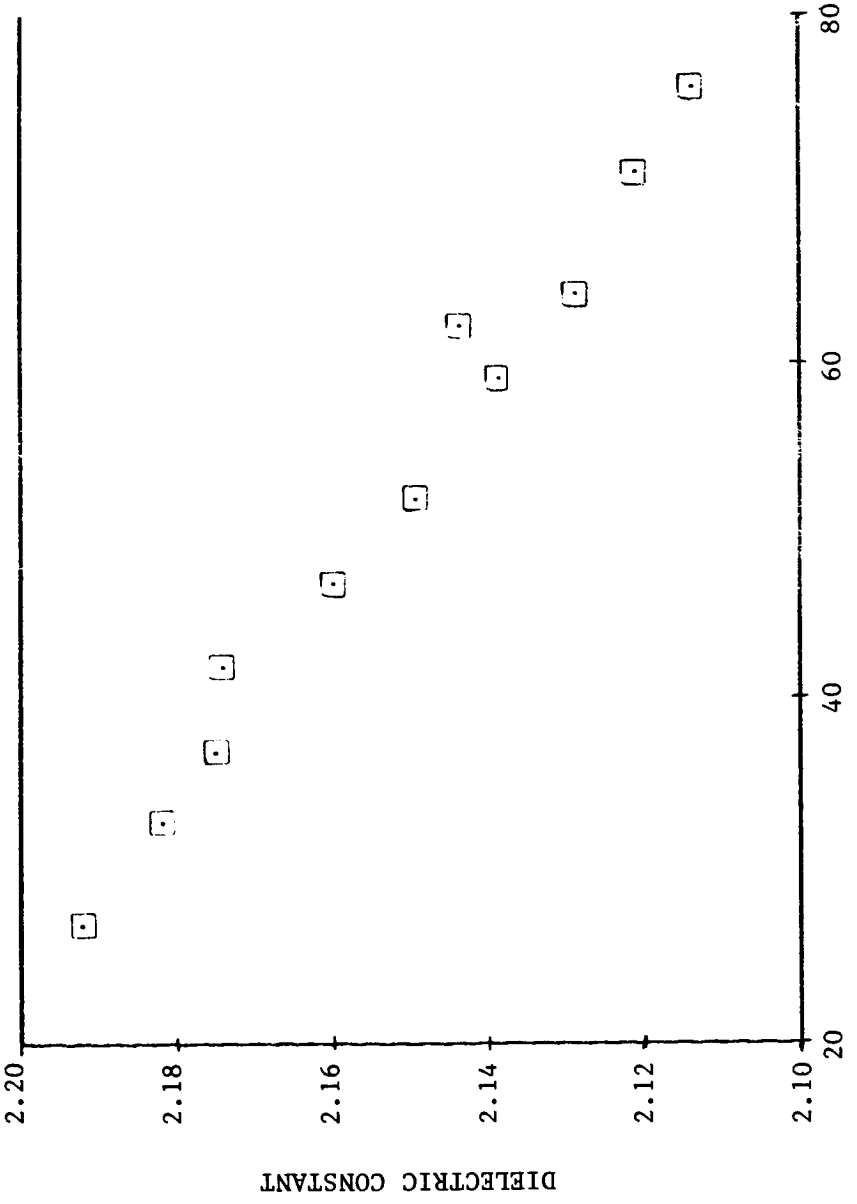

Fig. 3.8 SRG 200 oil dielectric constant vs. temperature. Pressure = 1 atm.

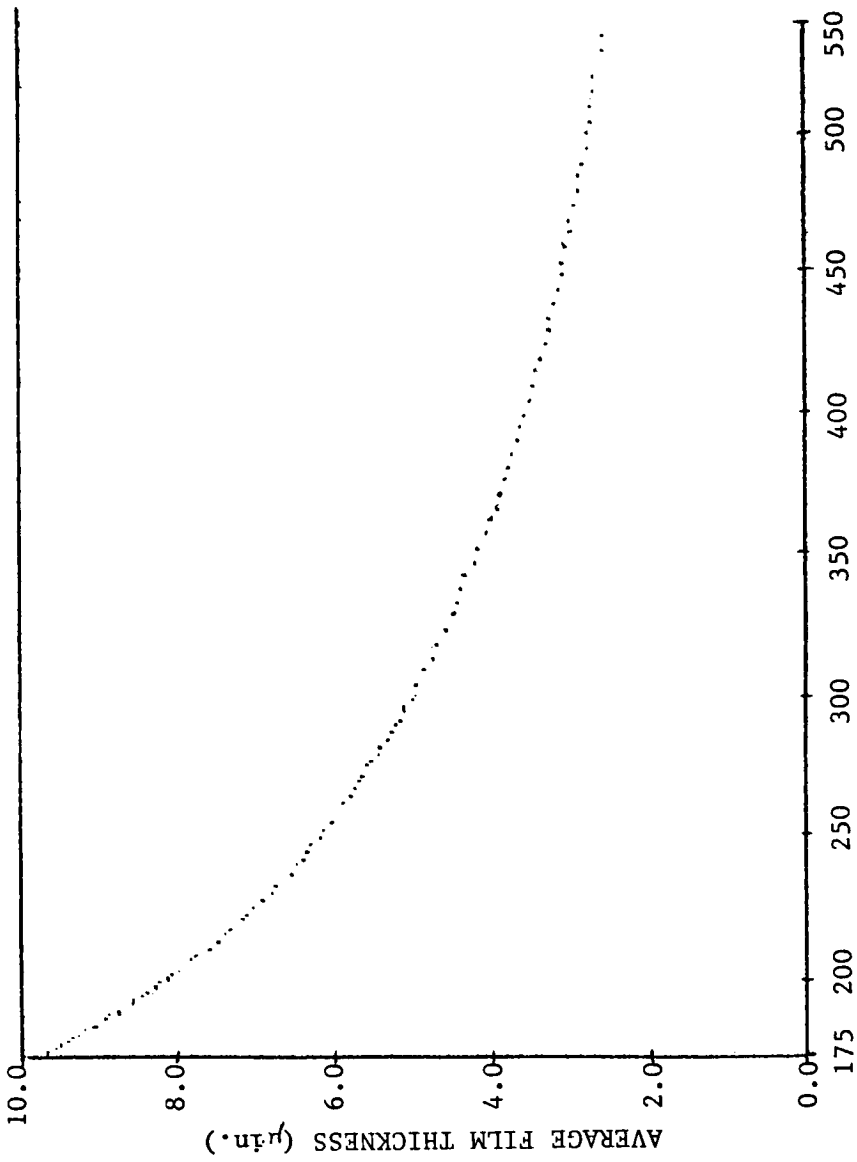

Fig. 3.9 Average film thickness vs. capacitance for both test bearings, 200 lb load, SRG 200 oil.

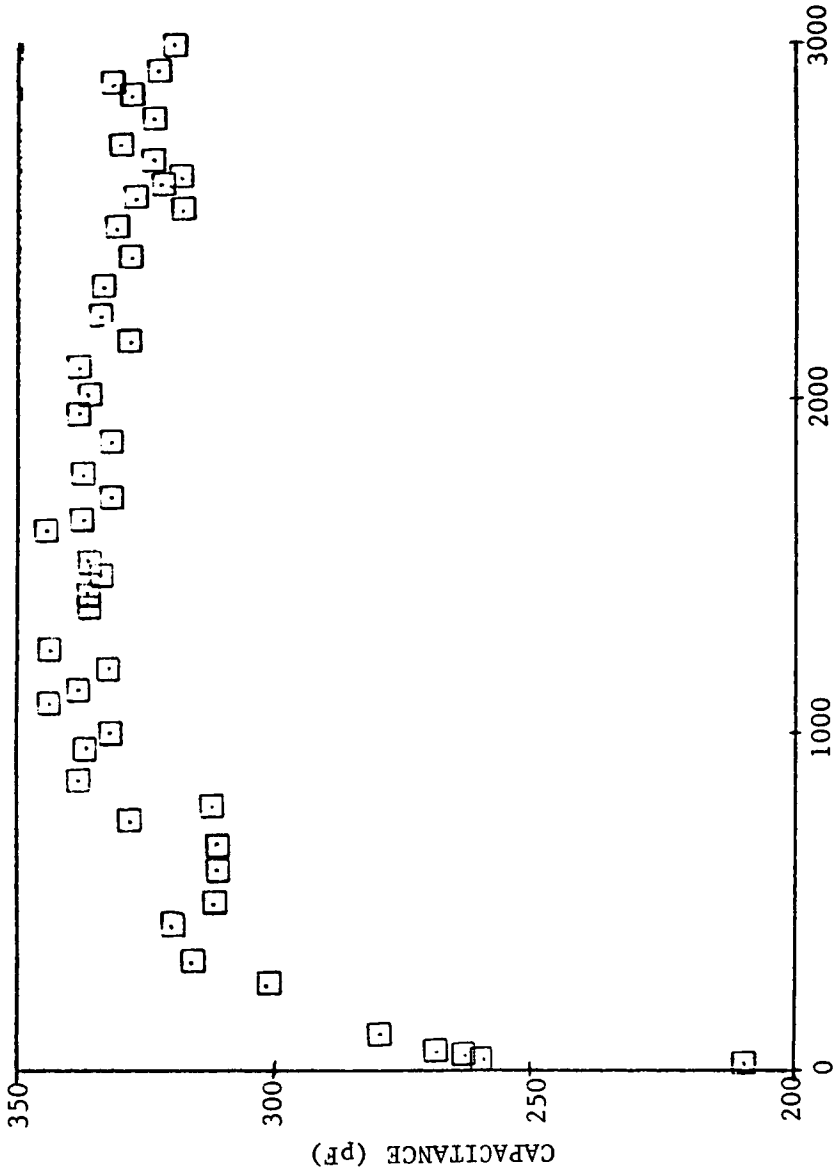

Fig. 3.10 Capacitance vs. elapsed time for ITI 11532-A test bearing, 200 lb load, 0.016 SRG 200 oil/freon concentration.

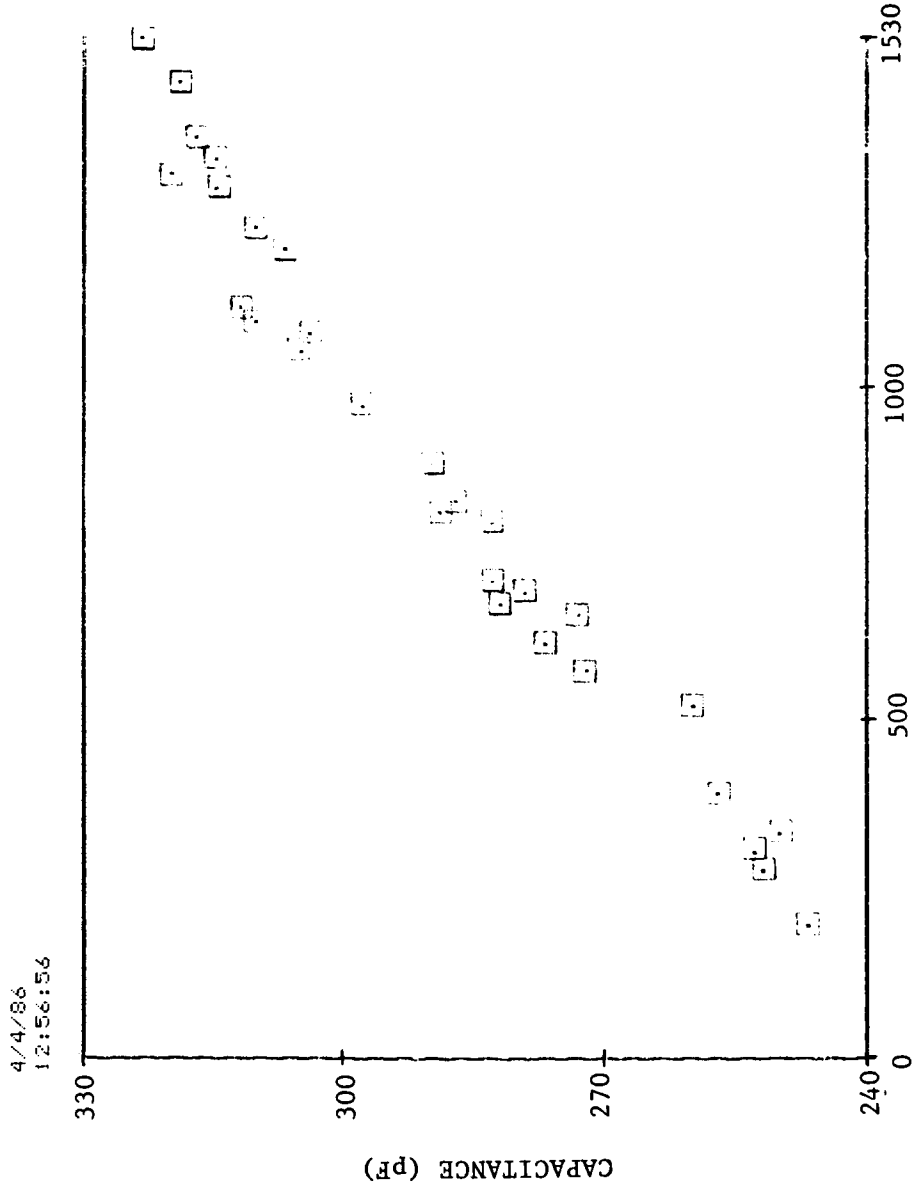

Fig. 3.11 Capacitance vs. elapsed time for ITI 11532-A test bearing, 200 lb load, 0.022 SRG 200 oil/freon concnetration.

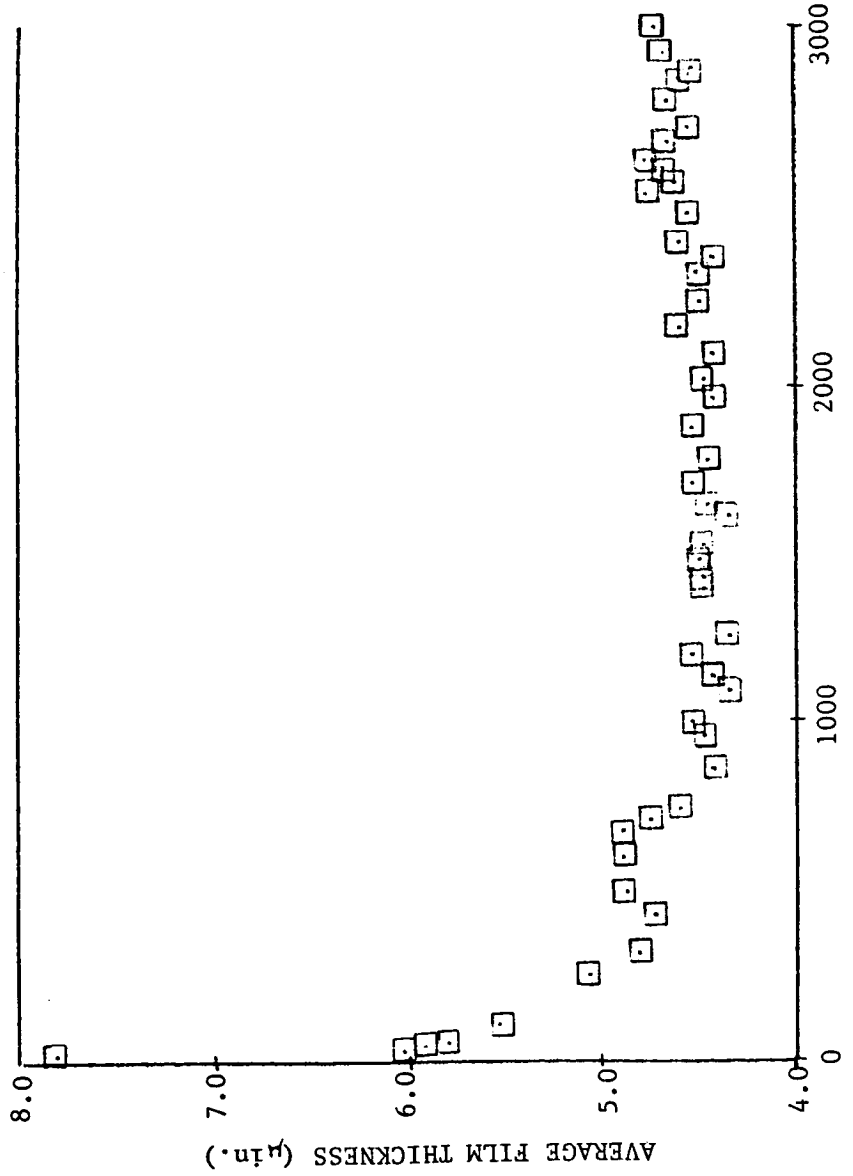

Fig. 3.12 Average film thickness vs. elapsed time for ITI 11532-A test bearing, 200 lb load, 0.016 SRG 200 oil/freon concentration.

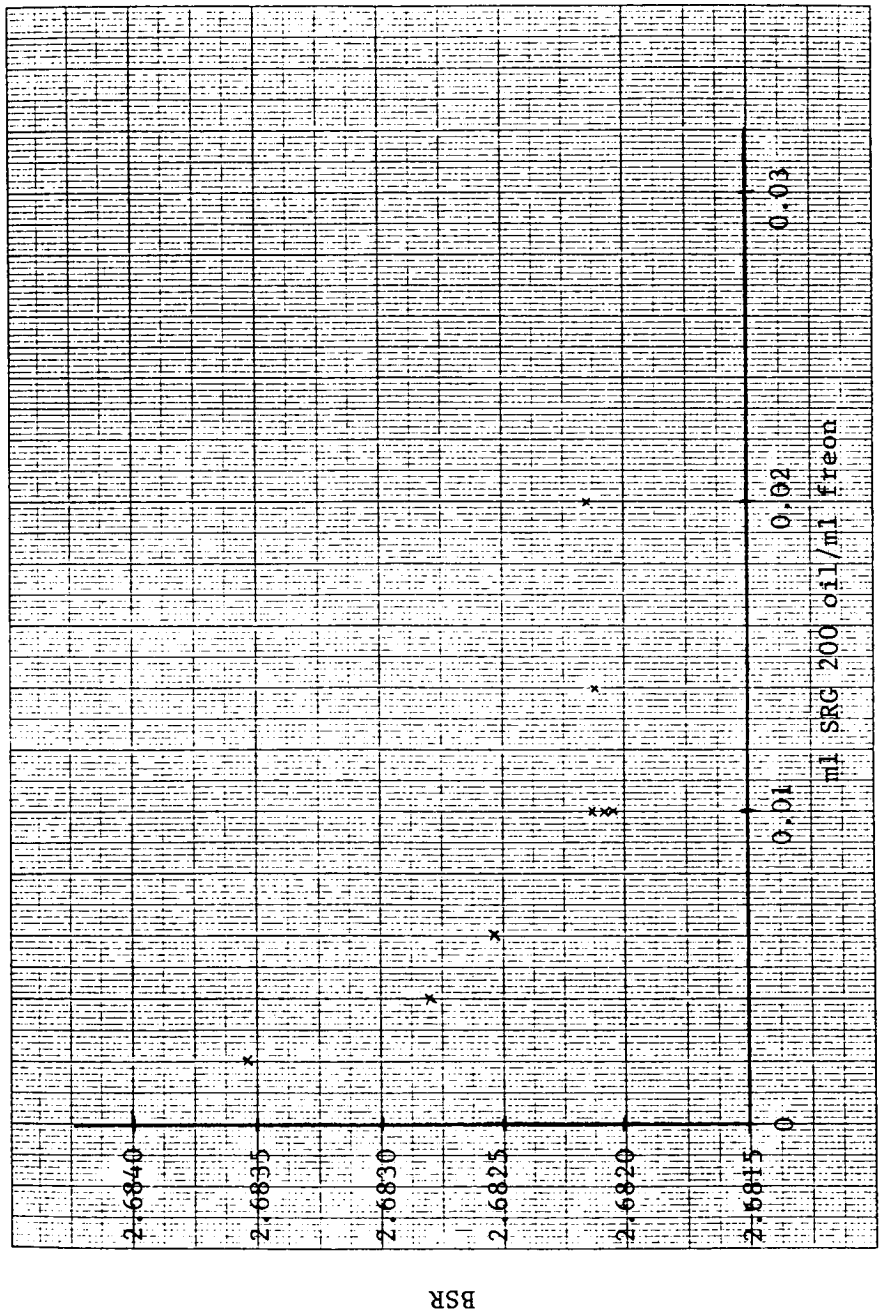

Fig. 3.13 BSR vs. SRG 200 oil/freon concentration for ITI 8990-A test bearing, 300 lb load.

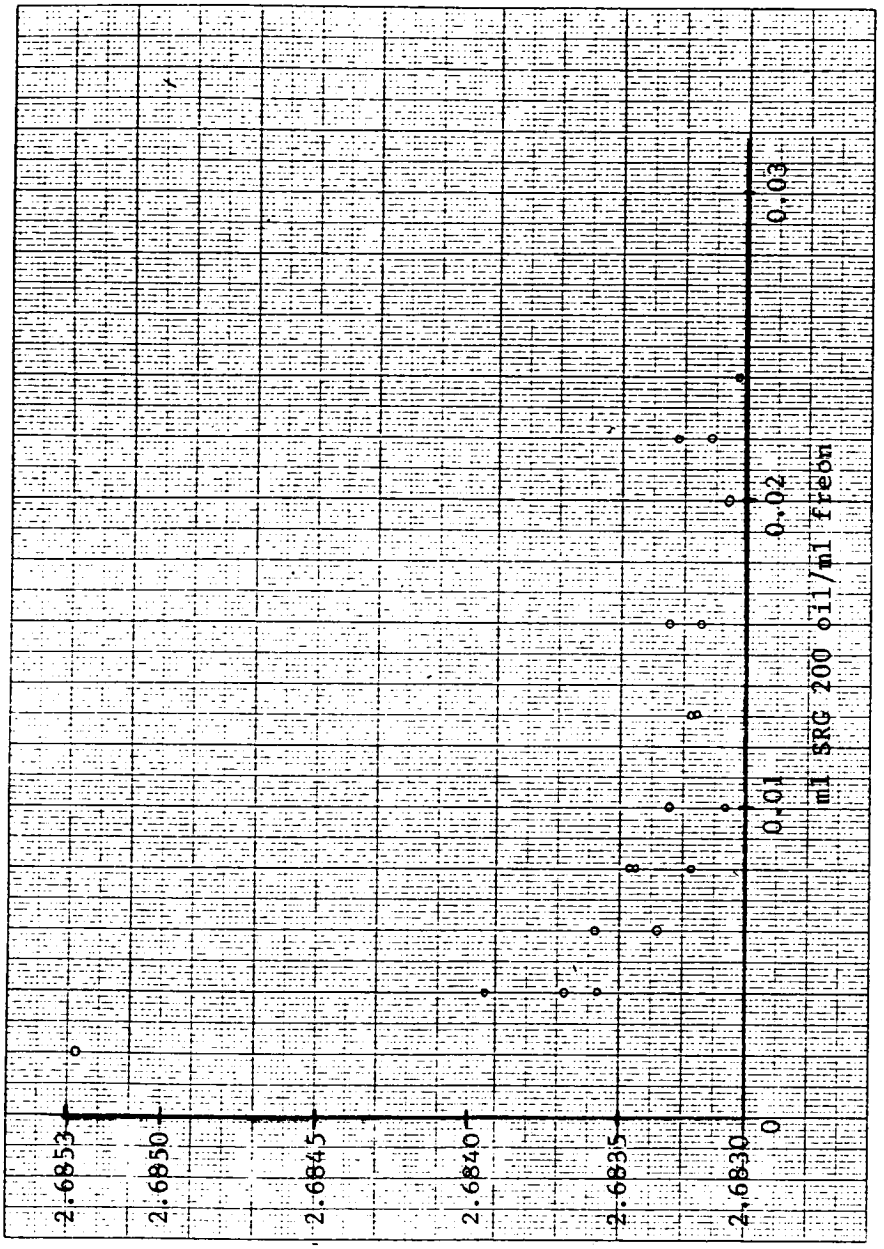

Fig. 3.14 BSR vs. SRG 200 oil/freon concentration for ITI 8990-A test bearing, 300 lb load.

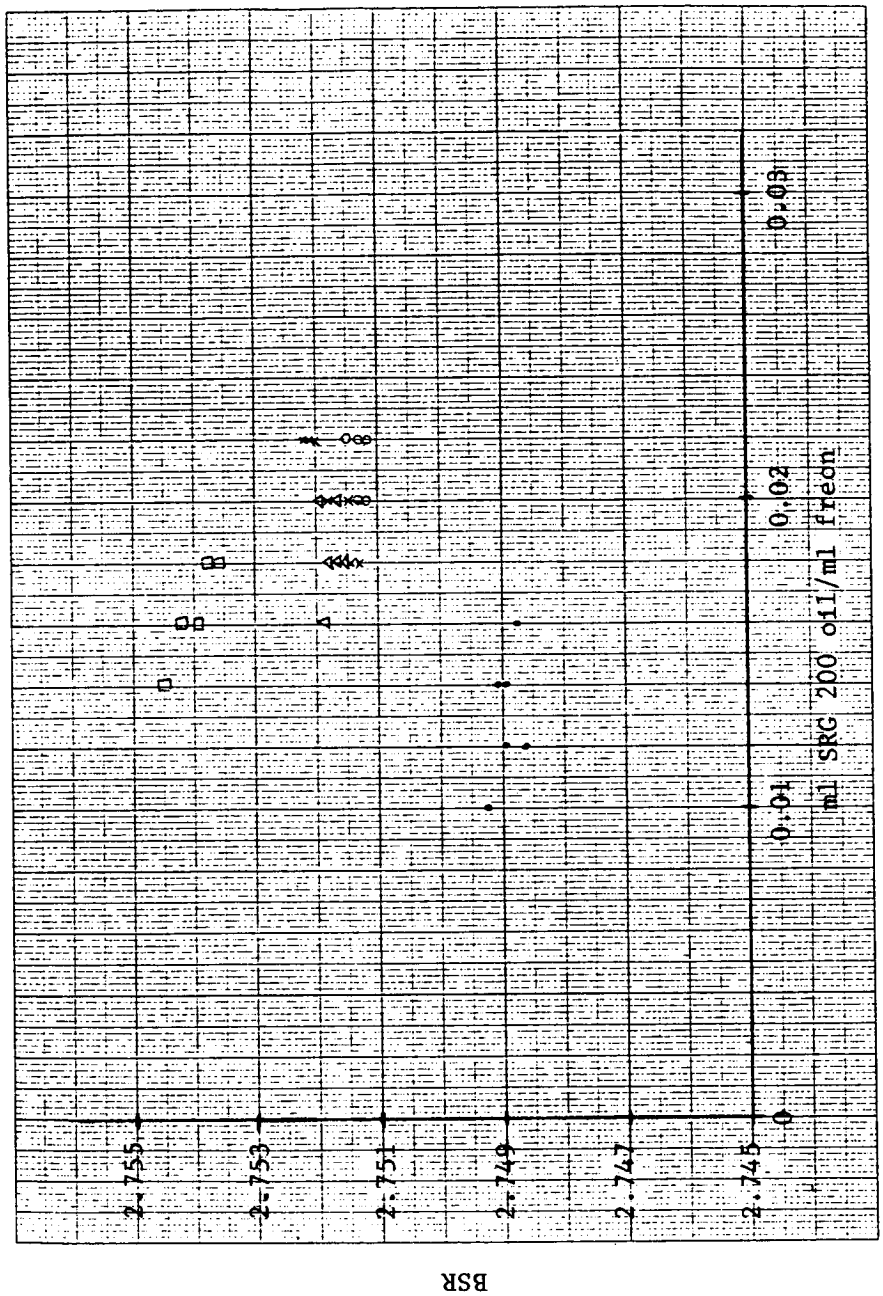

Fig. 3.15 BSR vs. SRG 200 oil/freon concentration for various ITI 11532-A test bearings, 200 lb load.

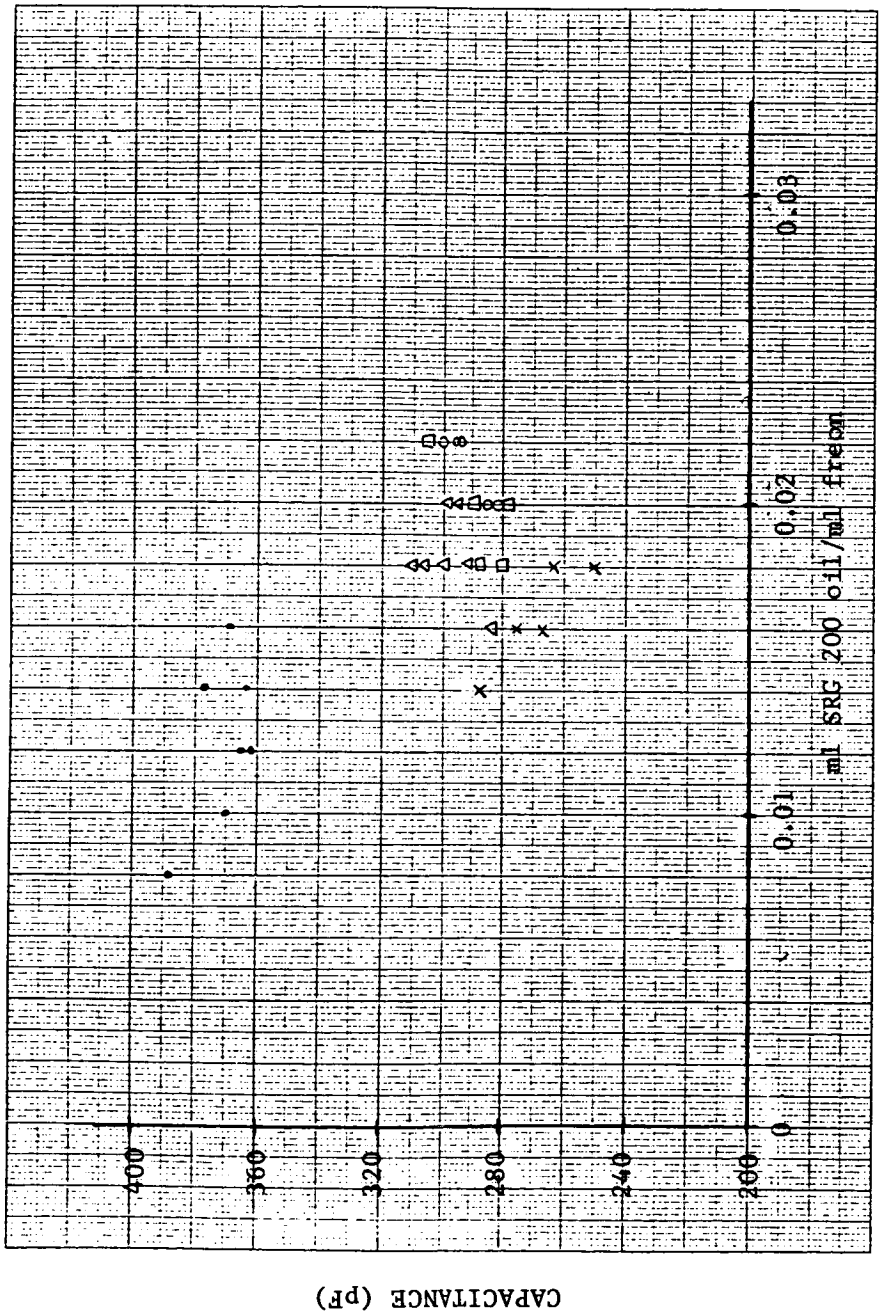

Fig. 3.16 Capacitance vs. SRG 200 oil/freon concentration for various ITI 11532-A test bearings, 200 lb load.

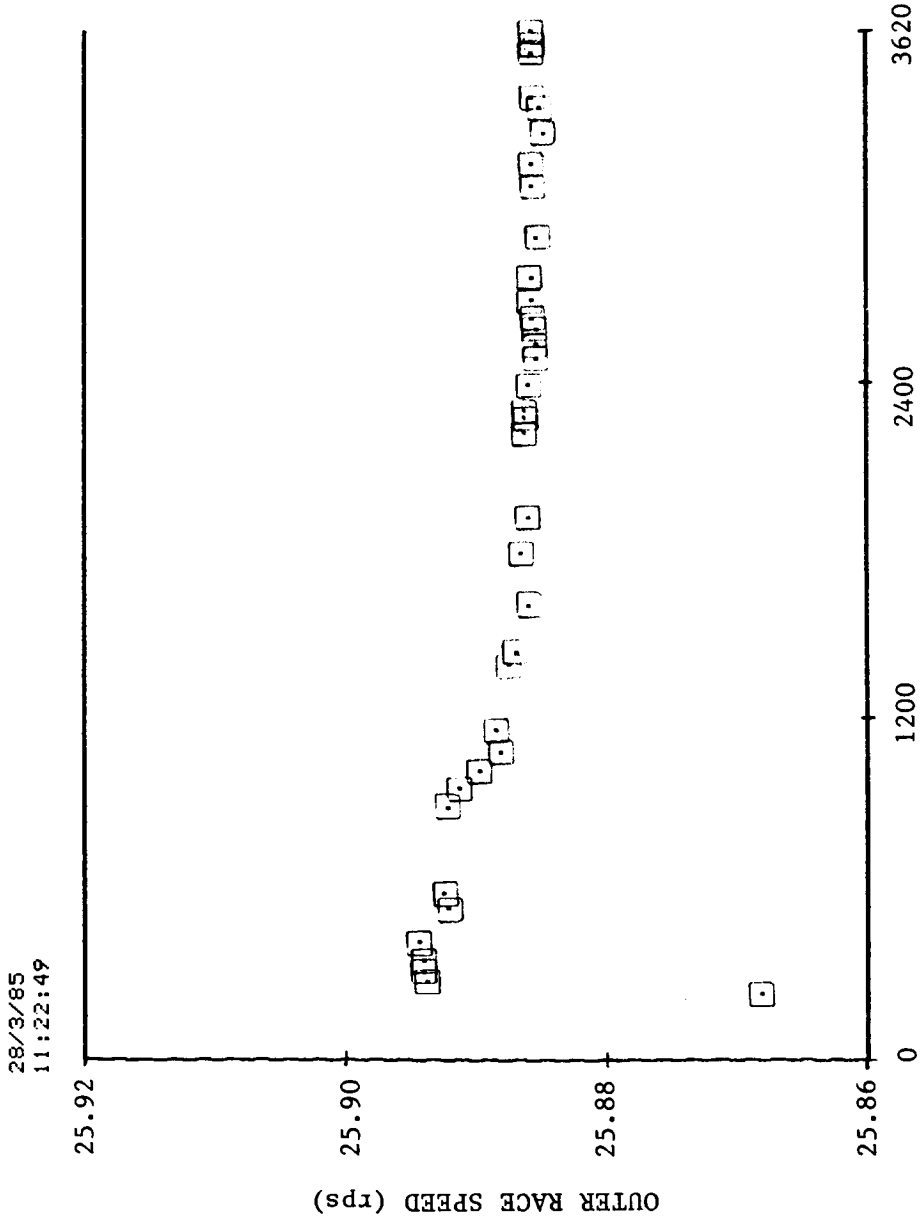

Fig. 3.17 Outer race speed vs. elapsed time for ITI 8990-A test bearing, 300 lb load, 0.026 SRG 200 oil/freon concentration.

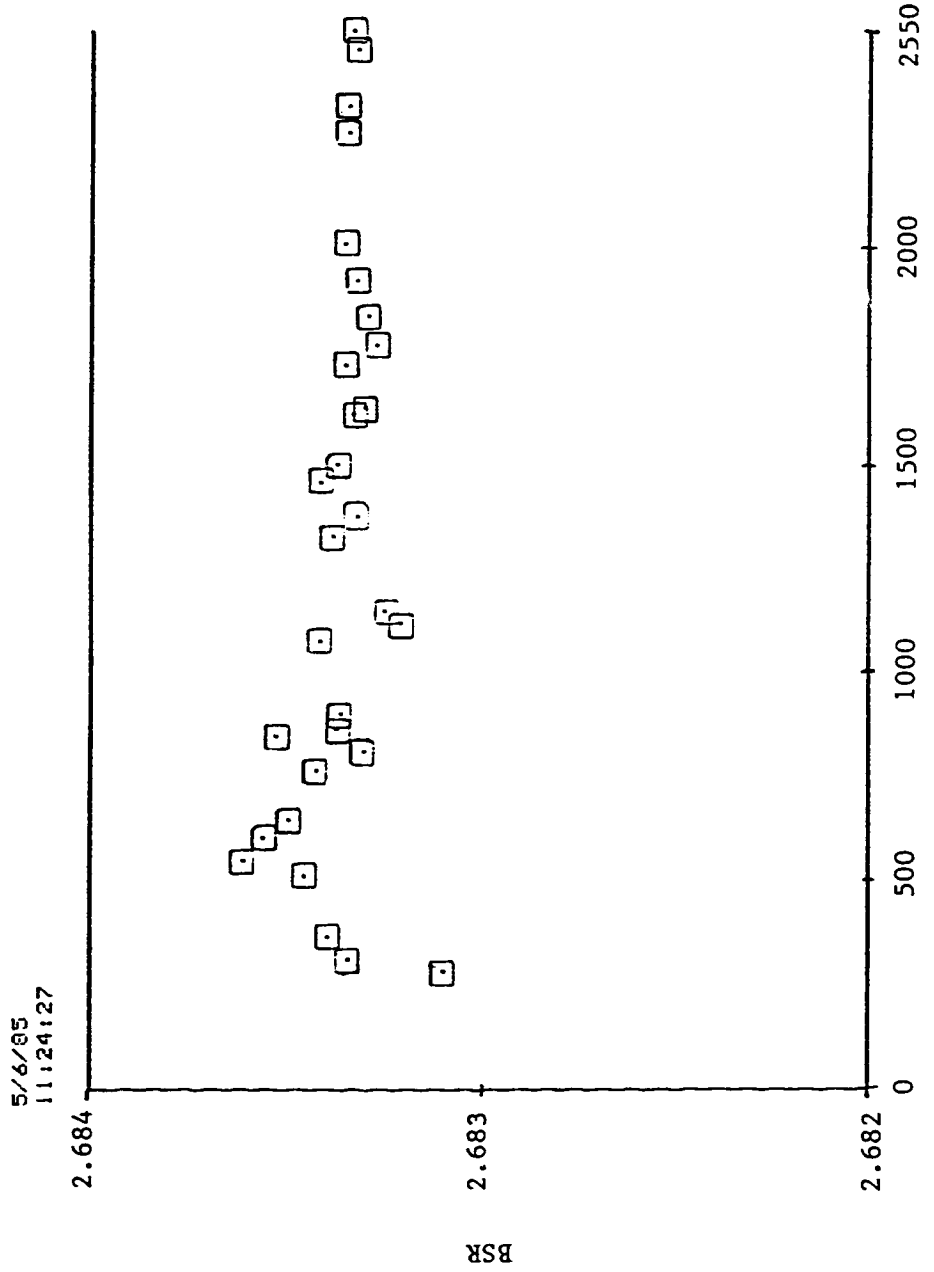

Fig. 3.18 BSR vs. elapsed time for ITI 8990-A test bearing, 300 lb load, 0.022 SRG 200 oil/freon concentration.

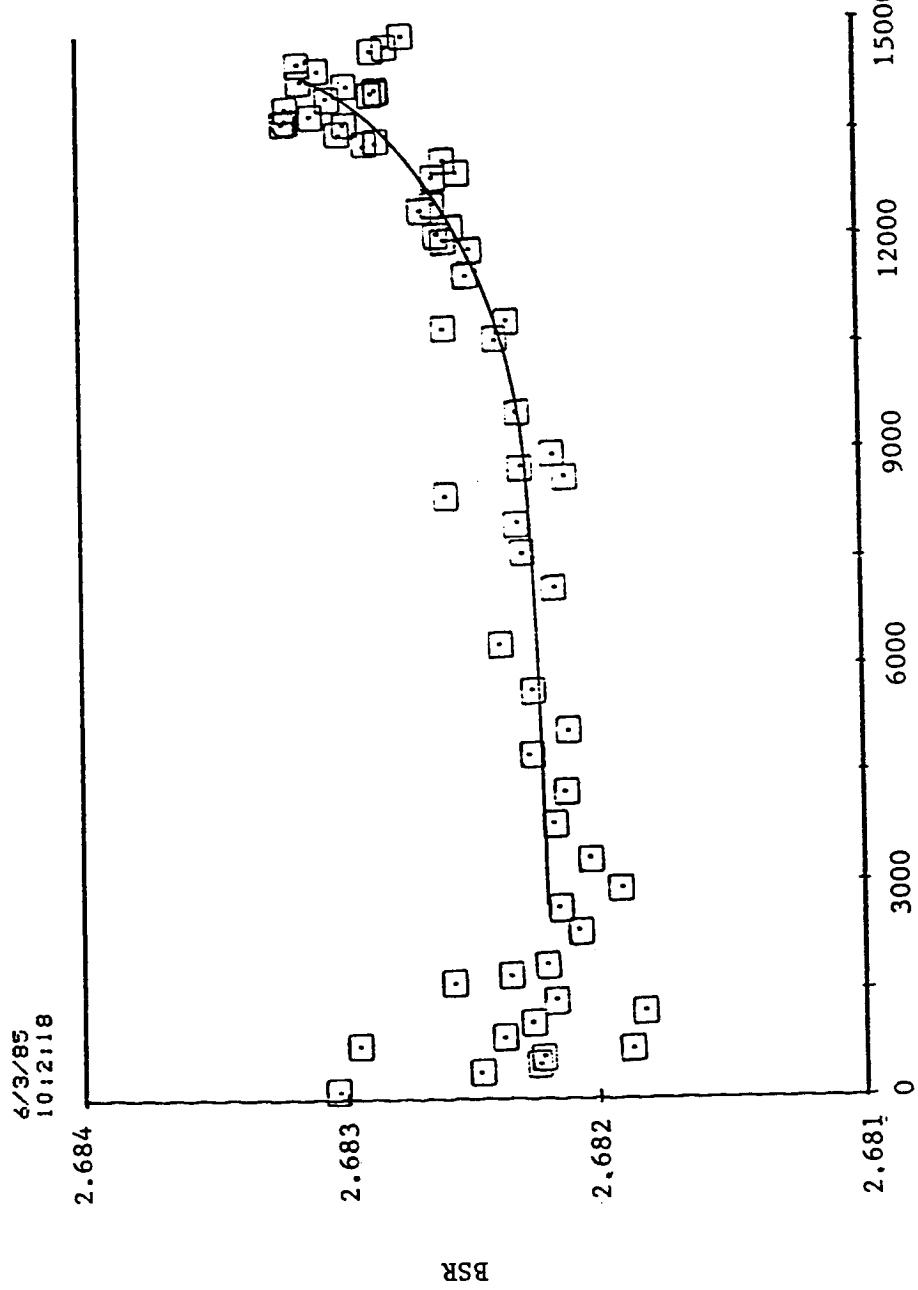

Fig. 3.19 BSR vs. elapsed time for ITI 8990-A test bearing, 300 lb load, 0.010 SRG 200 oil/freon concentration.

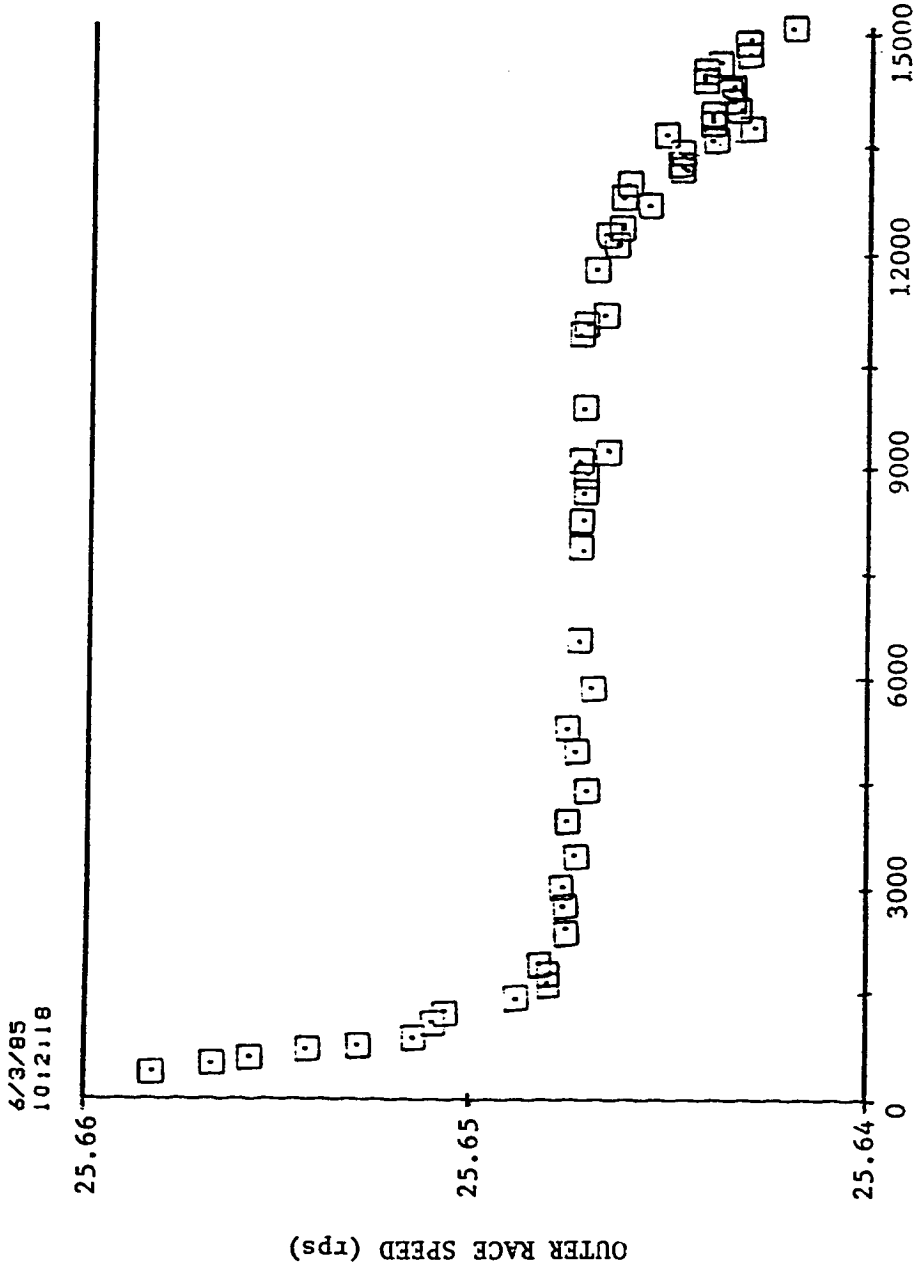

Fig. 3.20 Outer race speed vs. elapsed time for ITI 8990-A test bearing, 300 lb load, 0.010 SRC 200 oil/freon concentration.

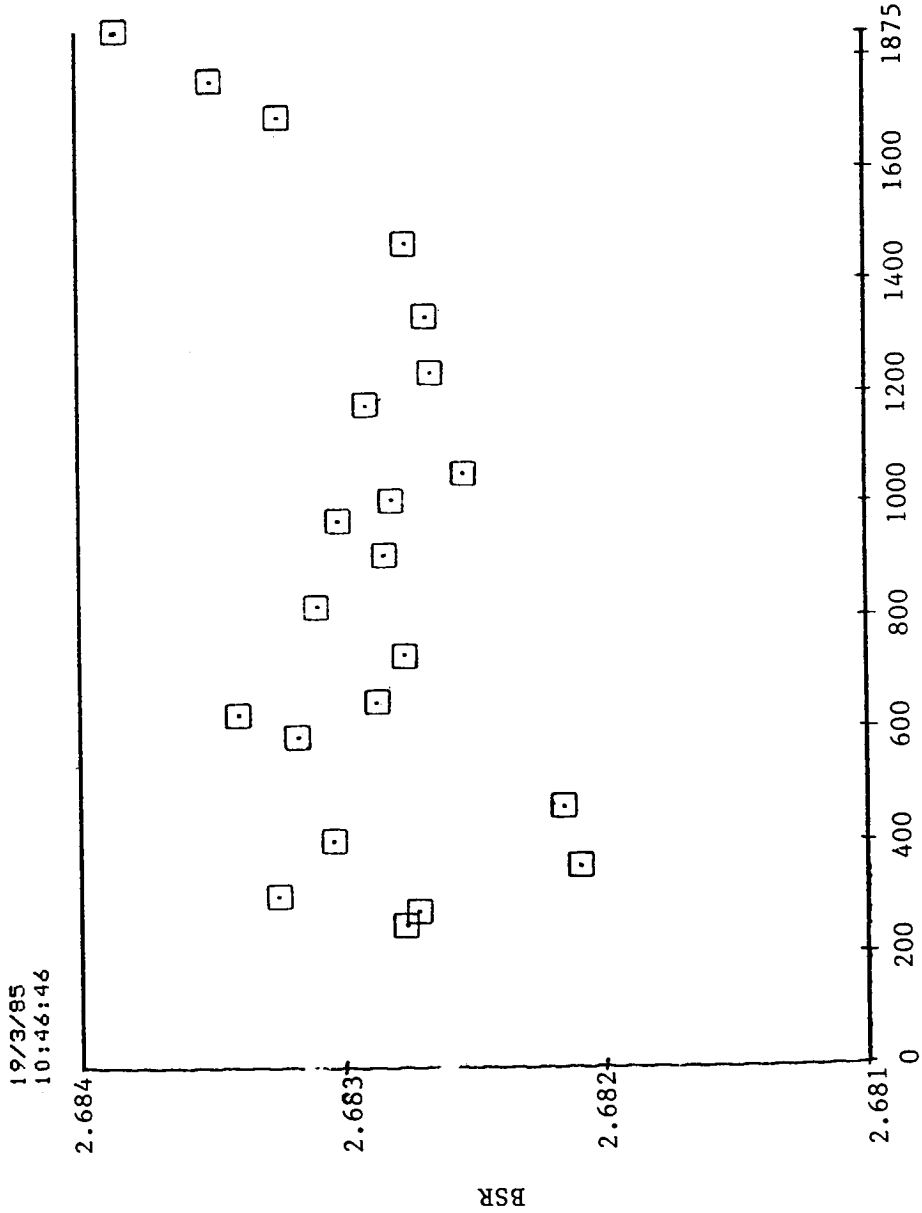

Fig. 3.21 BSR vs. elapsed time for ITI 8990-A test bearing, 300 lb load, 0.004 SRG 200 oil/freon concentration.

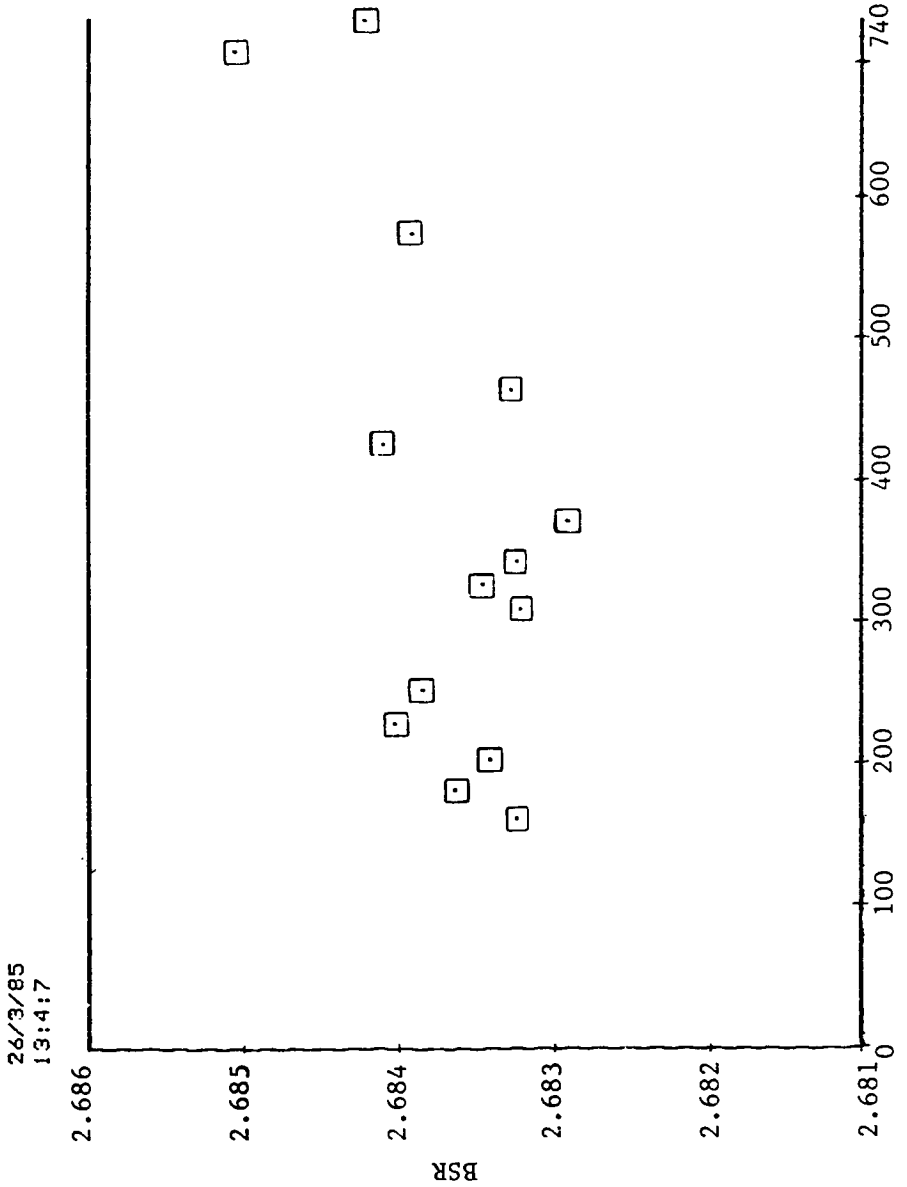

Fig. 3.22 BSR vs. elapsed time for ITI 8990-A test bearing, 300 lb load, 0.002 SRG 200 oil/freon concentration.

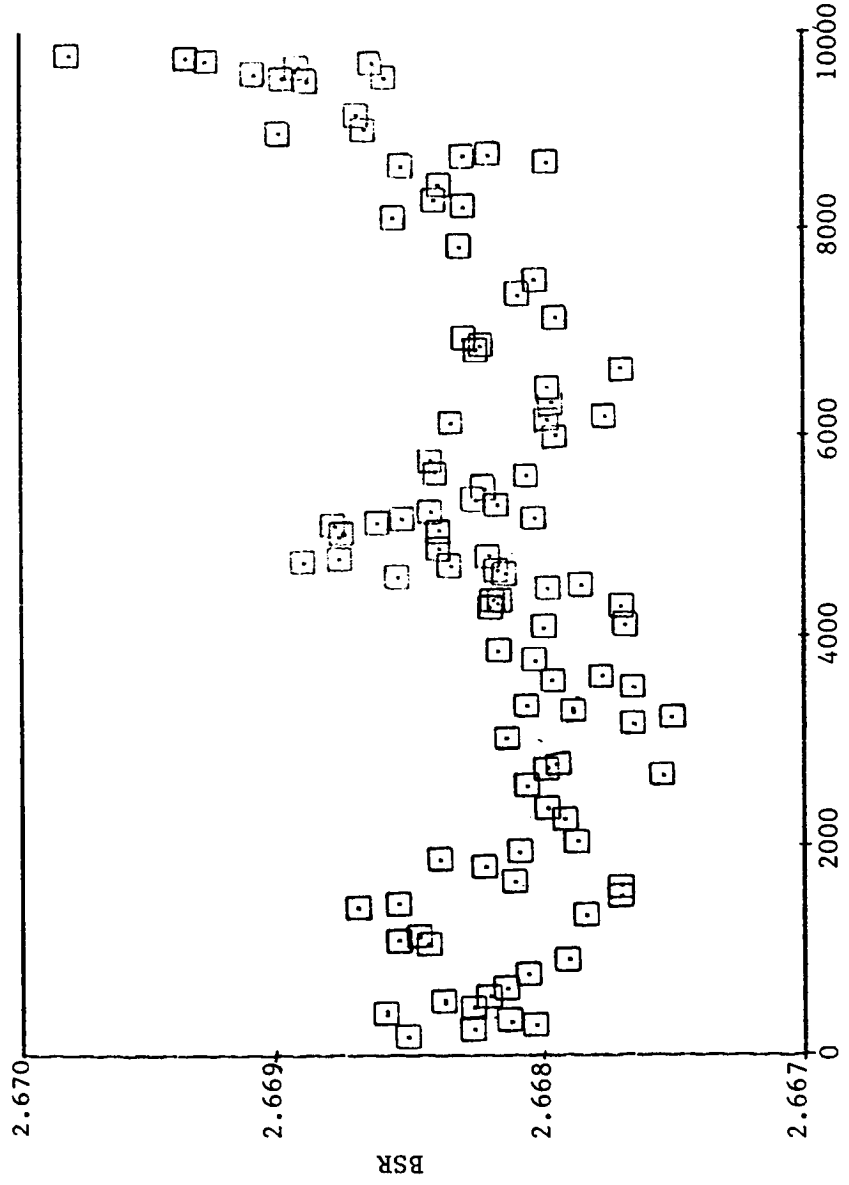

Fig. 3.23 BSR vs. elapsed time for ITI 8990-A test bearing, 200 lb load, 0.014 SRG 200 oil/freon concentration.

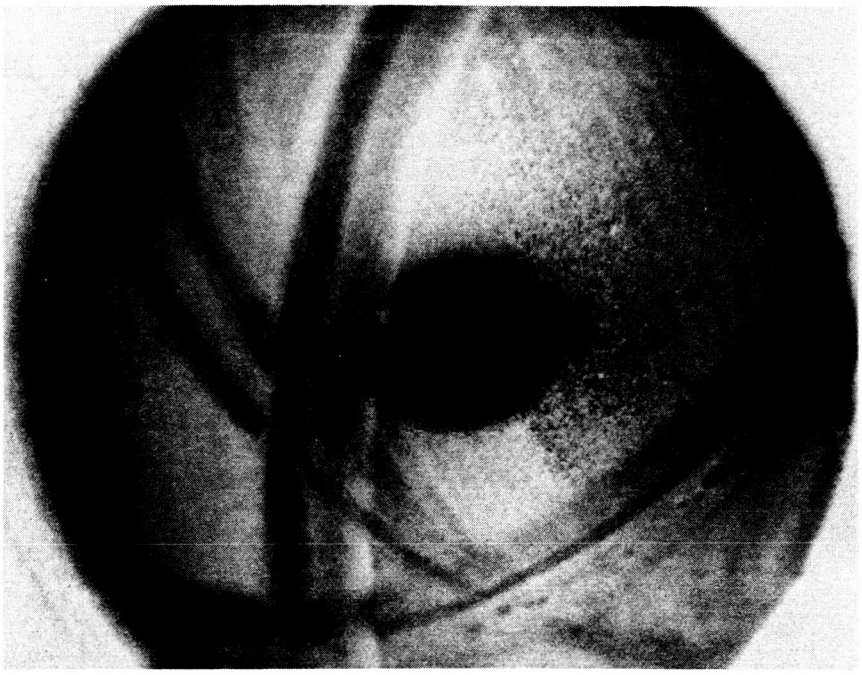

Fig. 3.24 Multiple wear tracks on wiped ball from ITI 8990-A test bearing, 200 lb load, 0.014 SRG 200 oil/freon concentration.

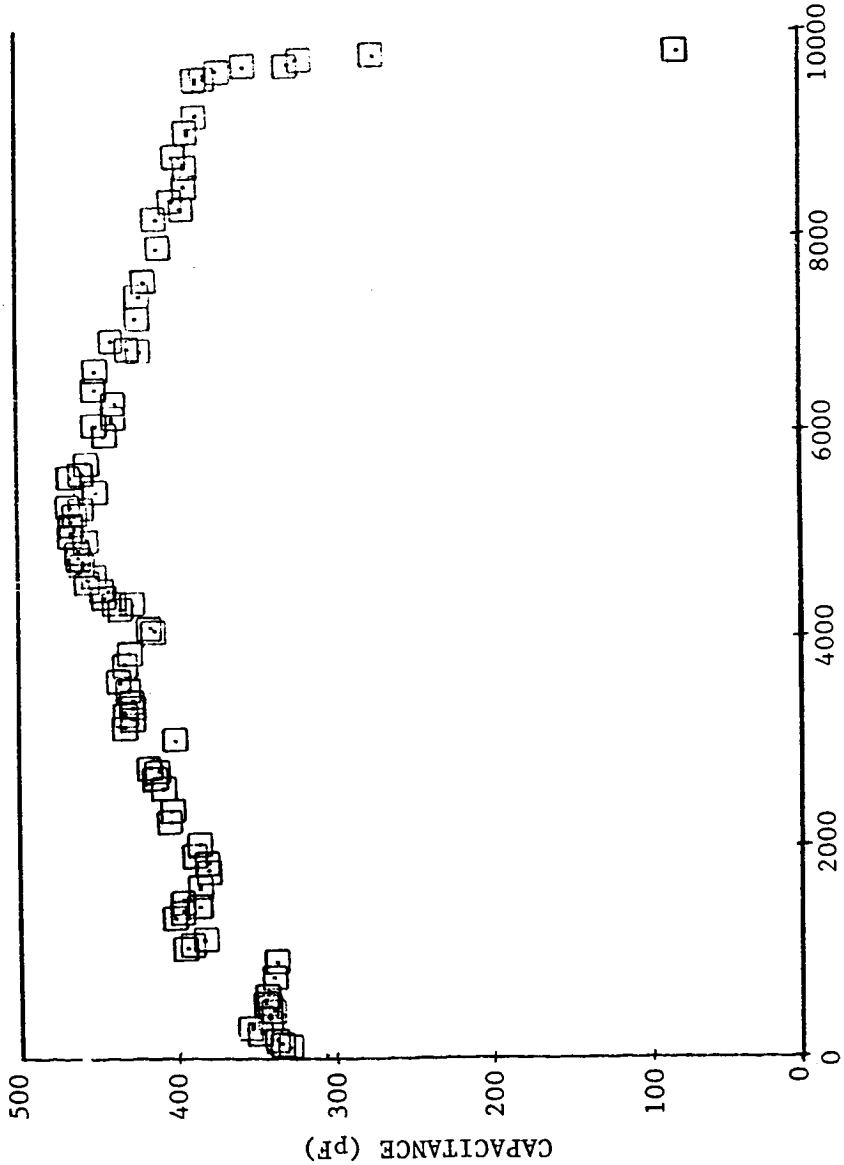

Fig. 3.25 Capacitance vs. elapsed time for ITI 8990-A test bearing, 200 lb load, 0.014 SRG 200 oil/freon concentration.

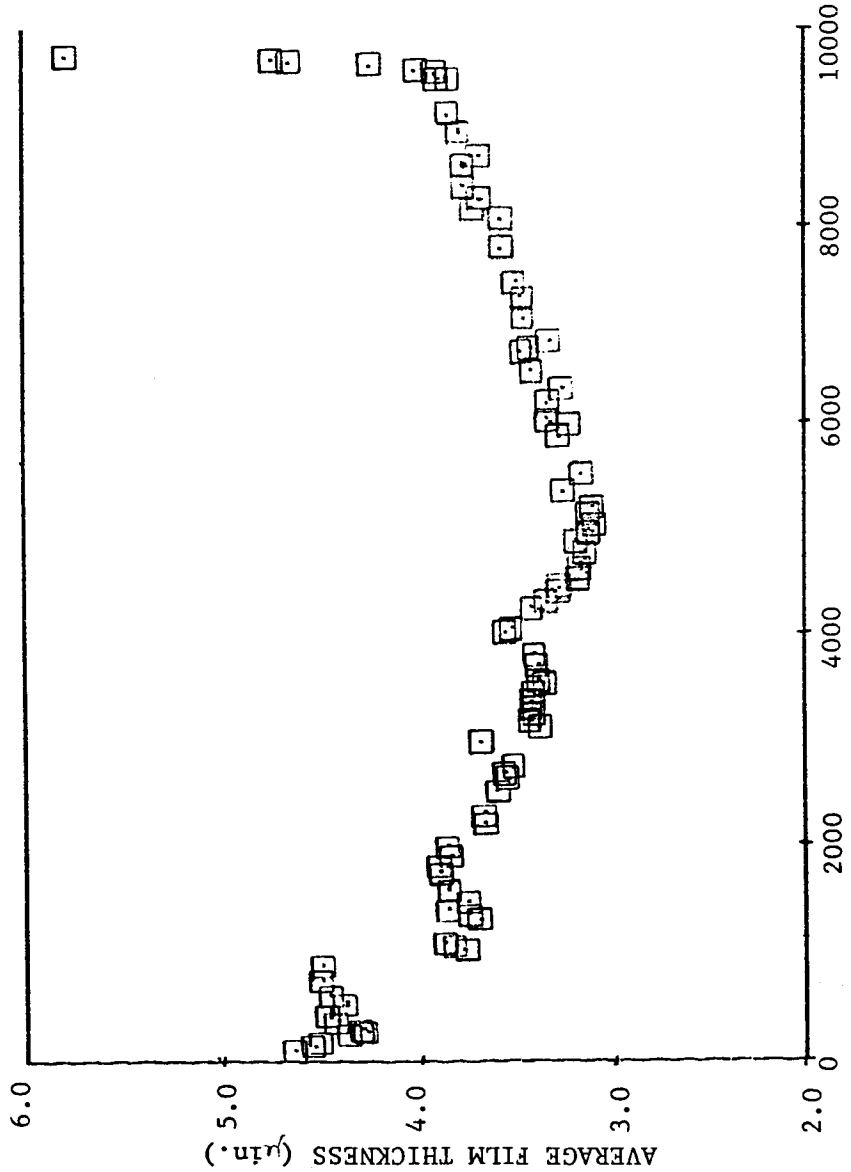

Fig. 3.26 Average film thickness vs. elapsed time for ITI 8990-A test bearing, 200 lb load, 0.014 SRG 200 oil/freon concentration.

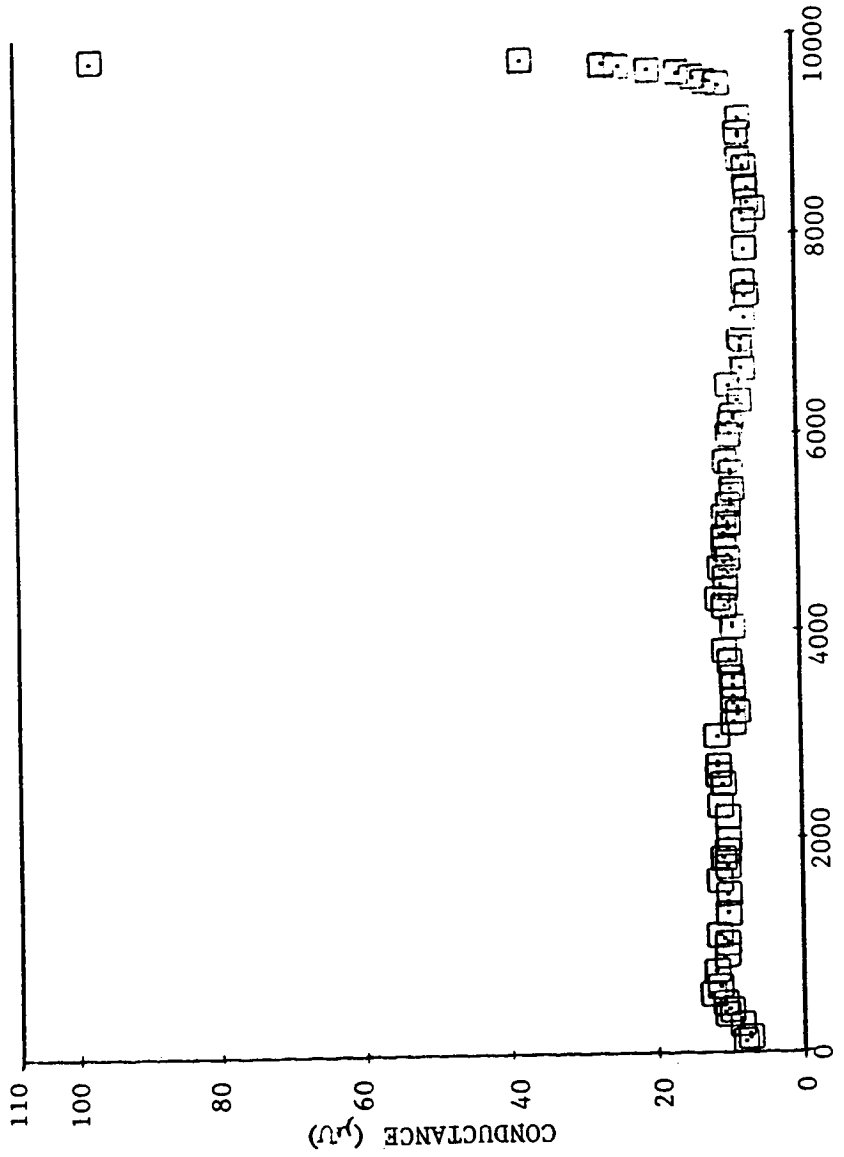

Fig. 3.27 Conductance vs. elapsed time for ITI 8990-A test bearing, 200 lb load, 0.014 SRG 200 oil/freon concentration.

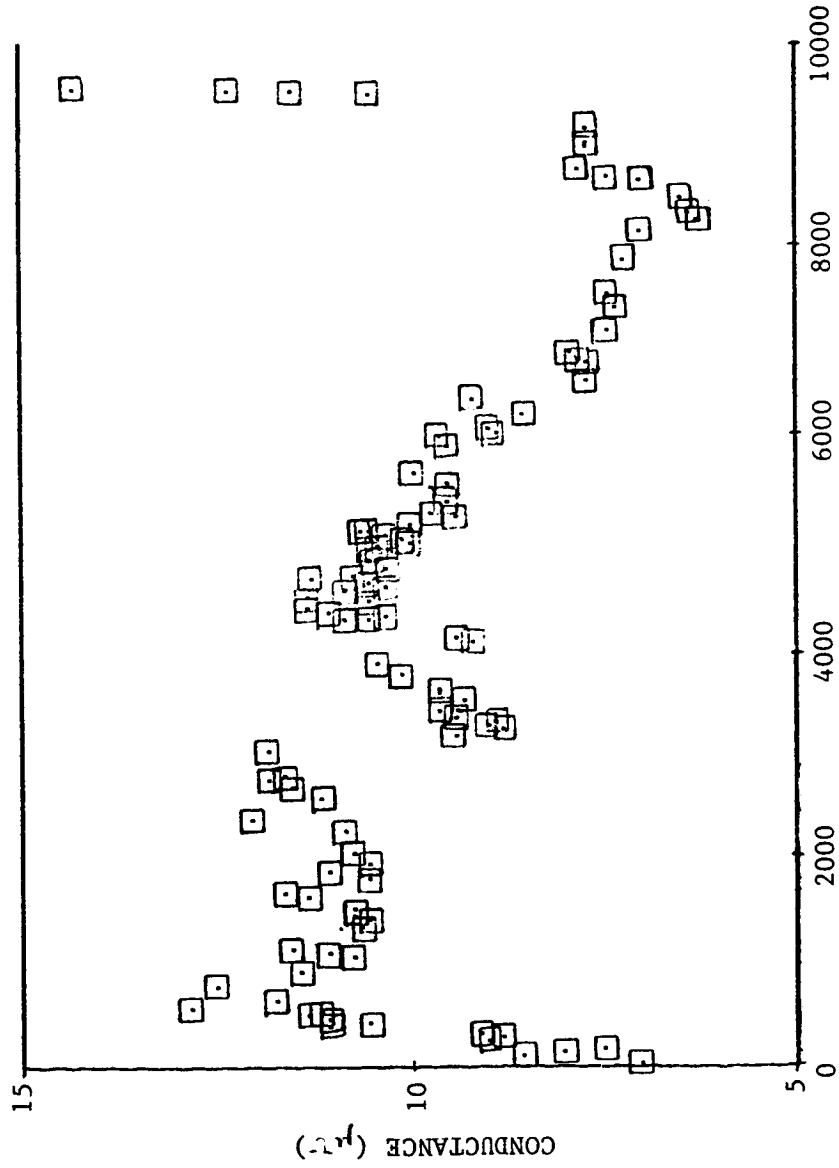

Fig. 3.28 Conductance vs. elapsed time for ITI 8990-A test bearing, 200 lb load, 0.014 SRG 200 oil/freon concentration.

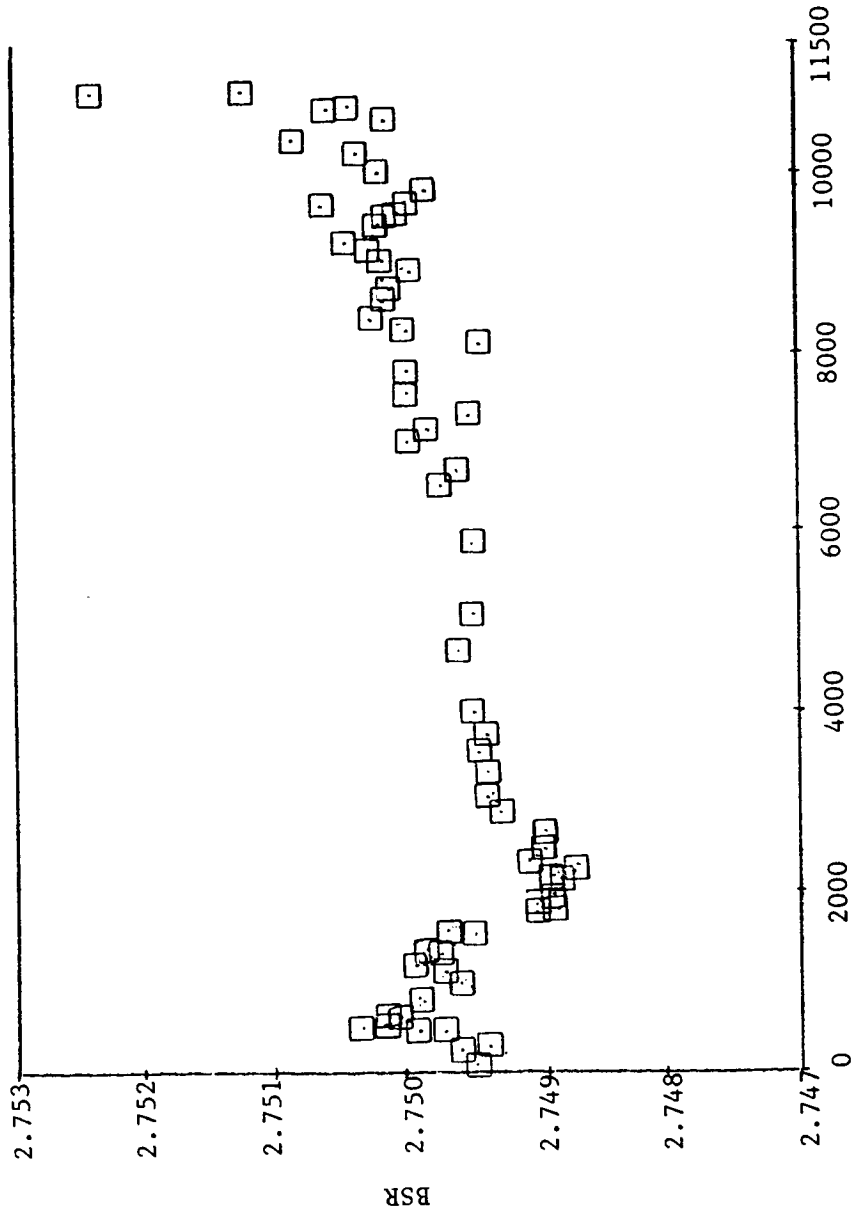

Fig. 3.29 BSR vs. elapsed time for ITI 11532-A test bearing, 200 lb load, 0.008 SRG 200 oil/freon concentration.

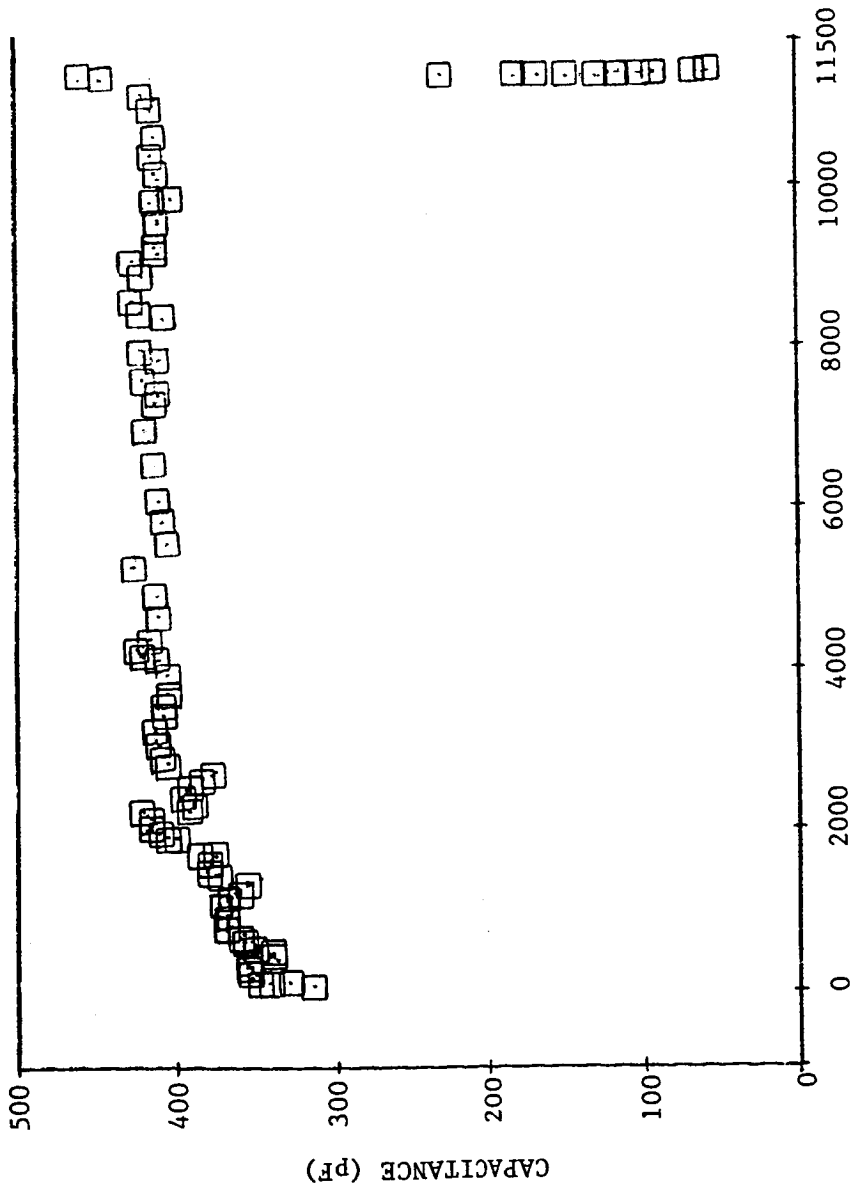

Fig. 3.30 Capacitance vs. elapsed time for ITI 11532-A test bearing, 200 lb load, 0.008 SRG 200 oil/freon concentration.

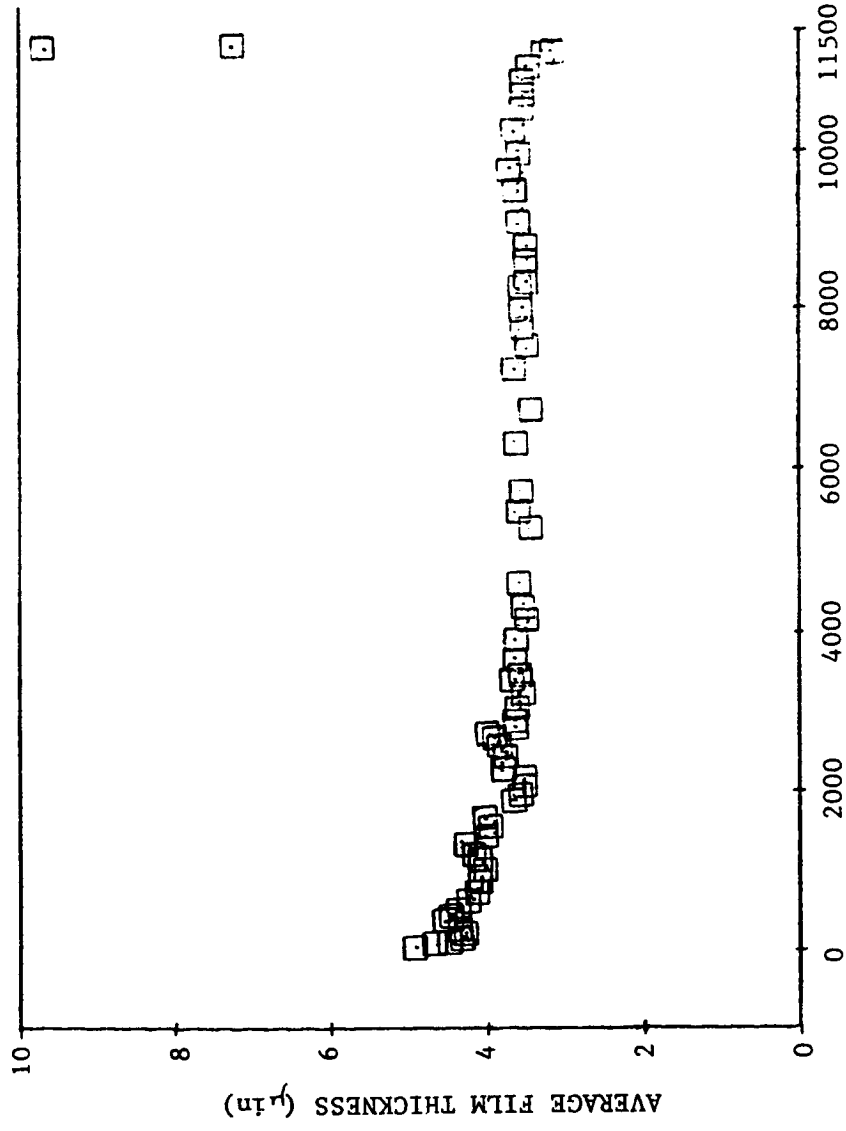

Fig. 3.31 Average film thickness vs. elapsed time for ITI 11532-A test bearing, 200 lb load, 0.008 SRG 200 oil/freon concentration.

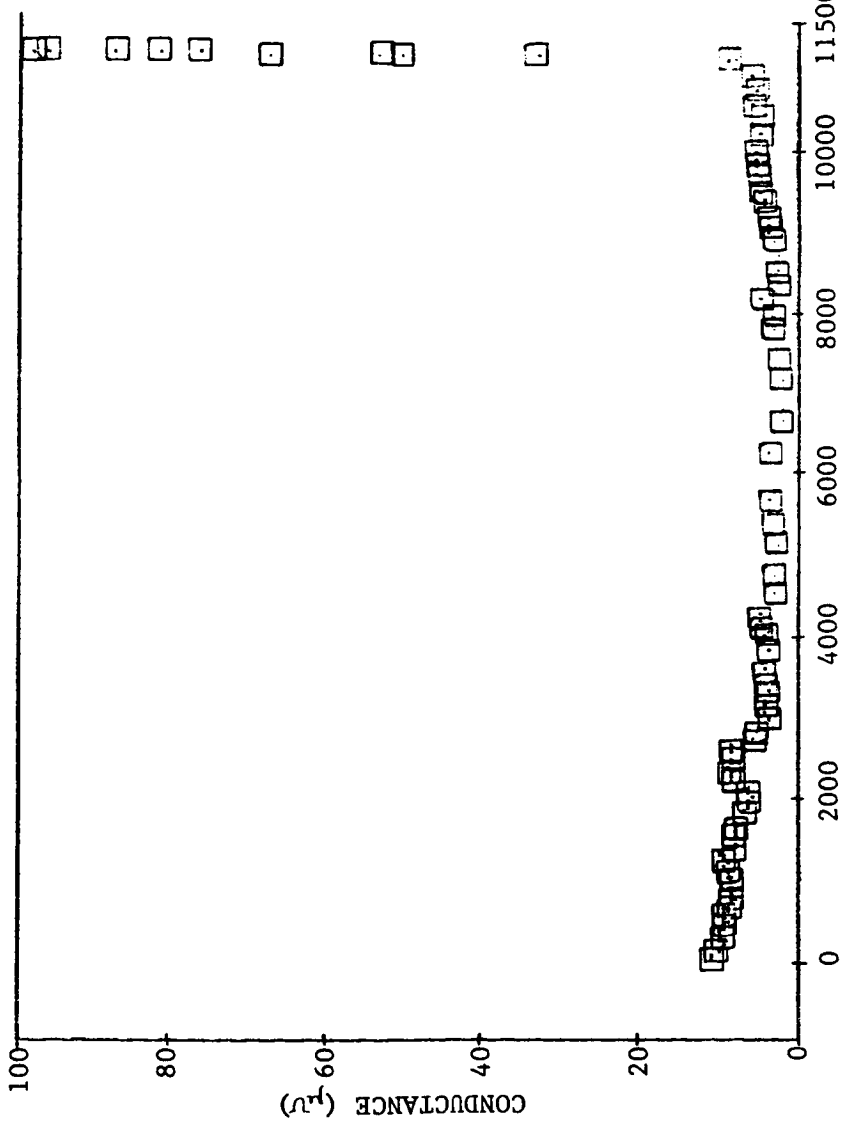

Fig. 3.32 Conductance vs. elapsed time for ITI 11532-A test bearing, 200 lb load, 0.008 SRG 200 oil/freon concentration.

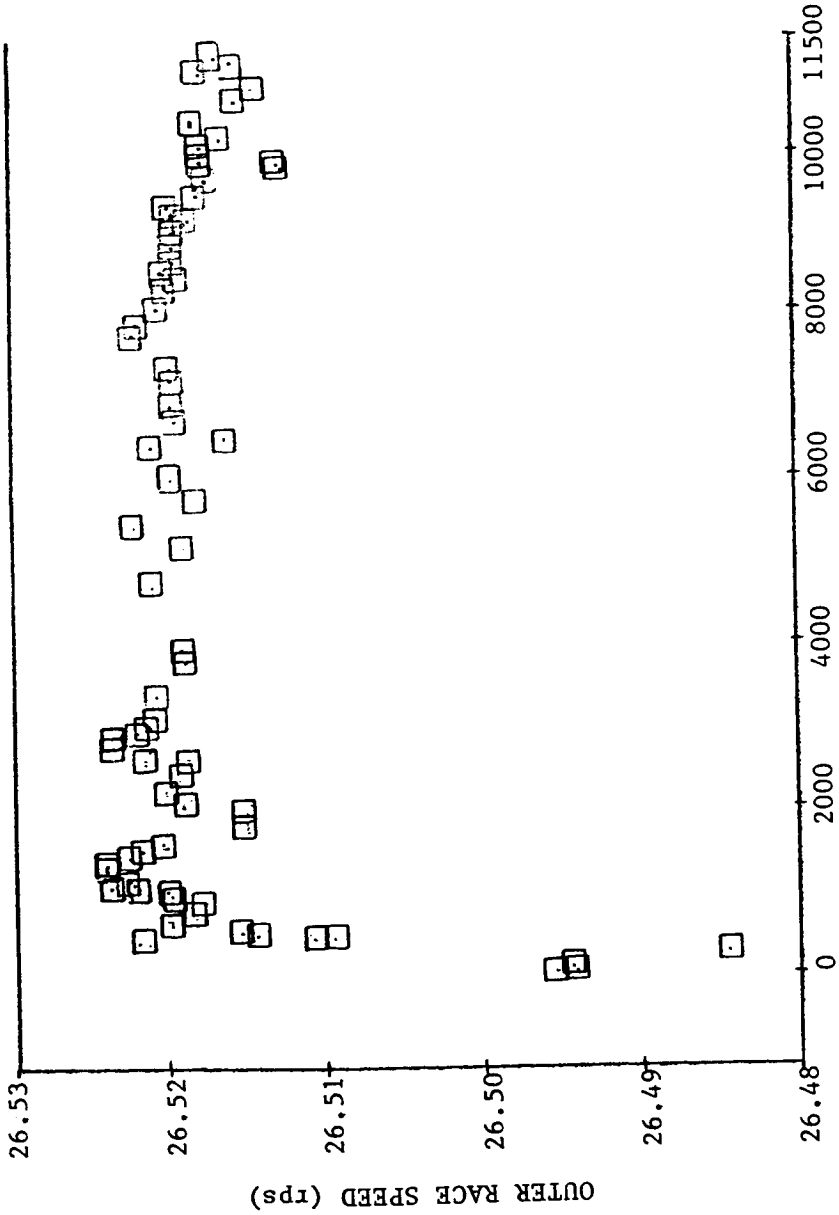

Fig. 3.33 Outer race speed vs. elapsed time for ITI 11532-A test bearing, 200 lb load, 0.008 SRG 200 oil/freon concentration.

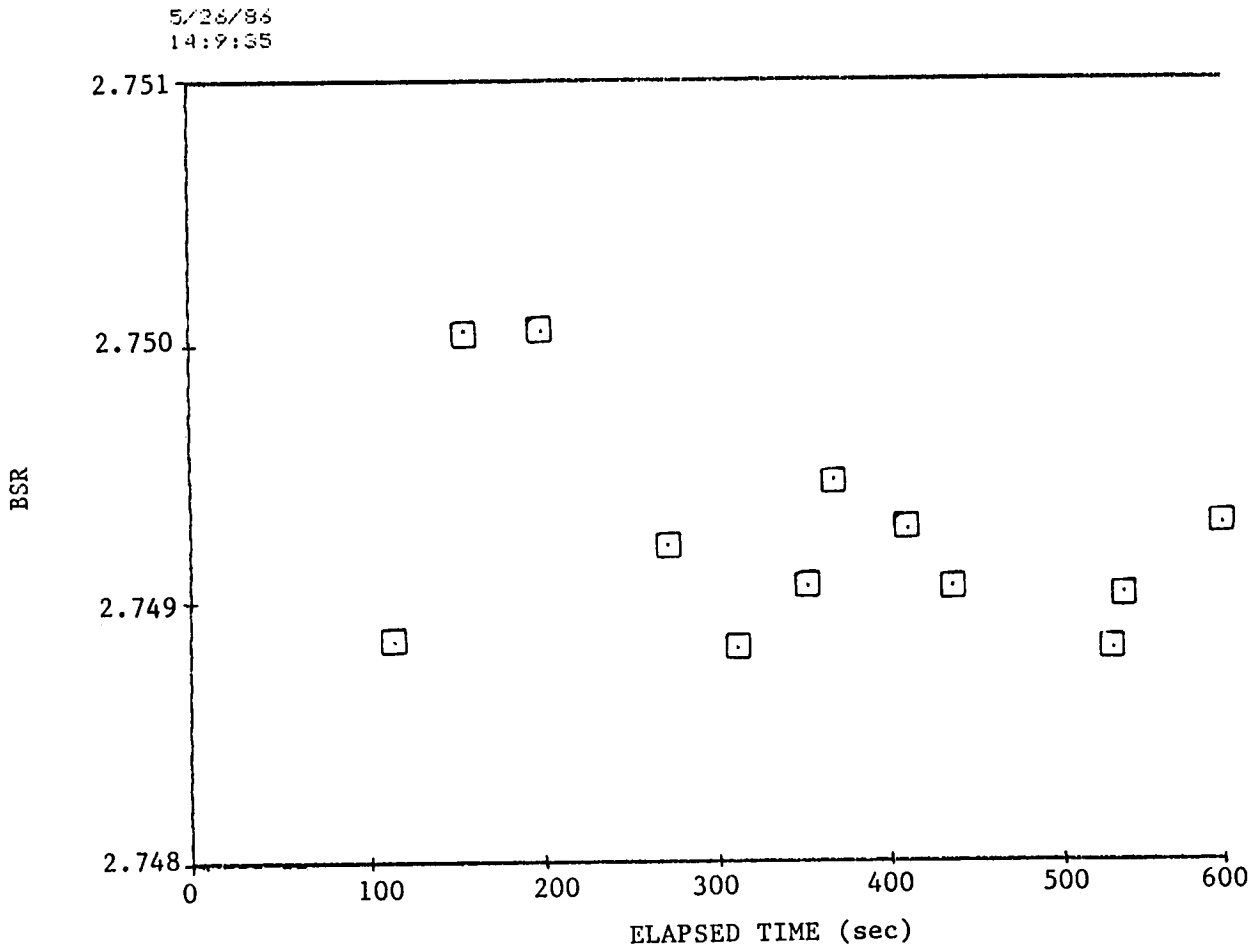

Fig. 3.34 BSR vs. elapsed time for ITI 11532-A test bearing, 200 lb load, time study #1 - 10 min., 0.016 SRG 200 oil/freon concentration.

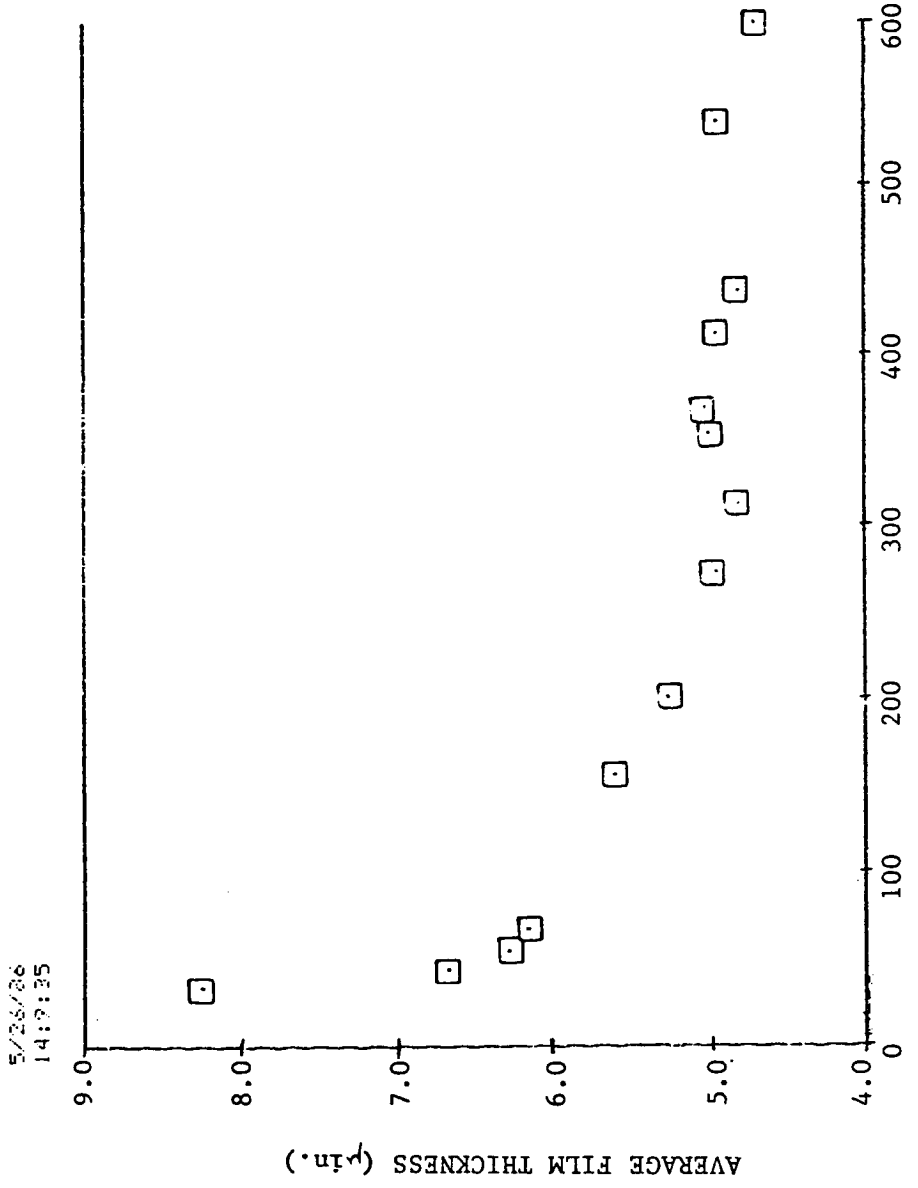

Fig. 3.35 Average film thickness for ITI 11532-A test bearing, 200 lb load, time study #1 - 10 min., 0.016 SRG 200 oil/freon concentration.

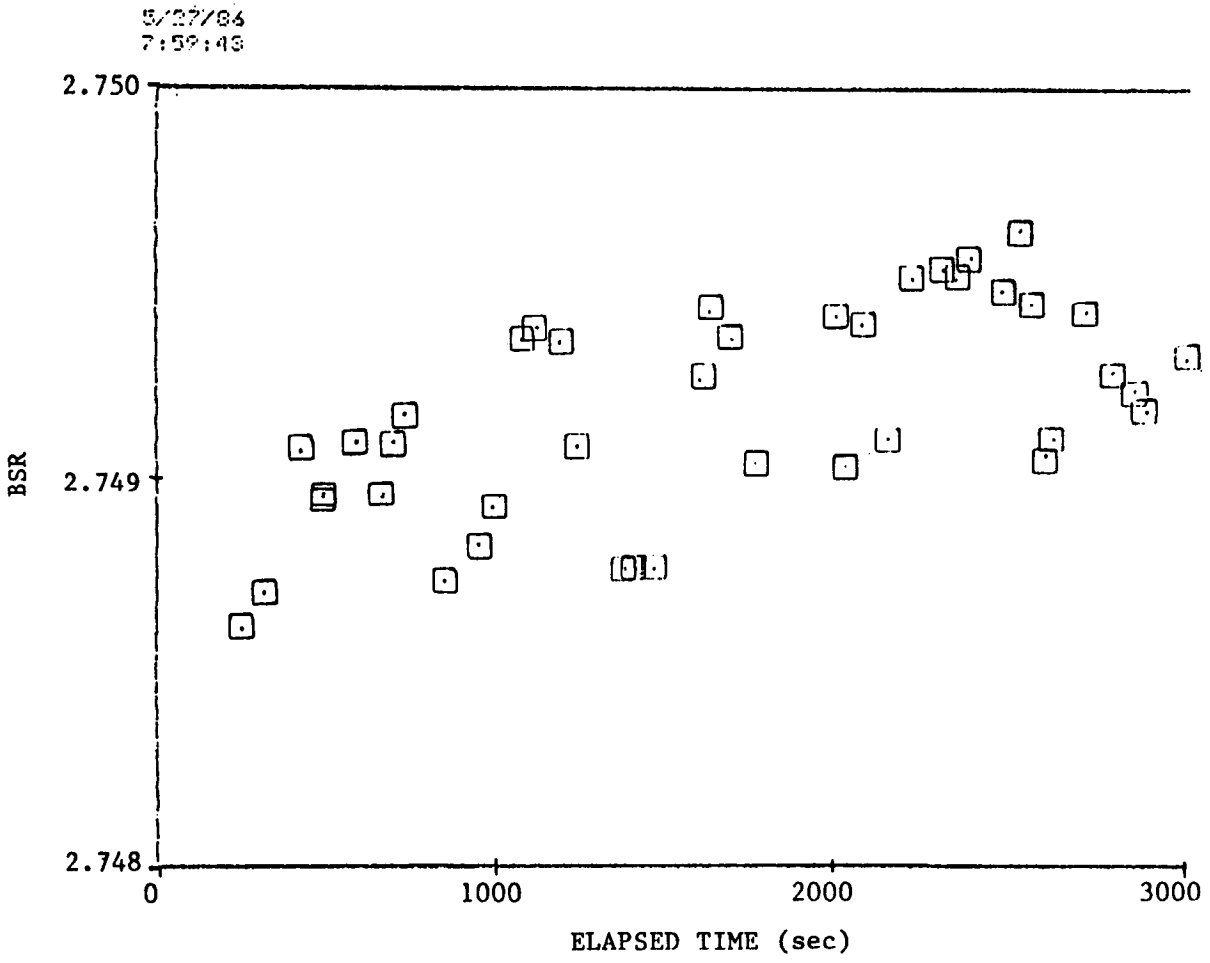

Fig. 3.36 BSR vs. elapsed time for ITI 11532-A test bearing, 200 lb load, time study #1 - 50 min., 0.016 SRG 200 oil/freon concentration.

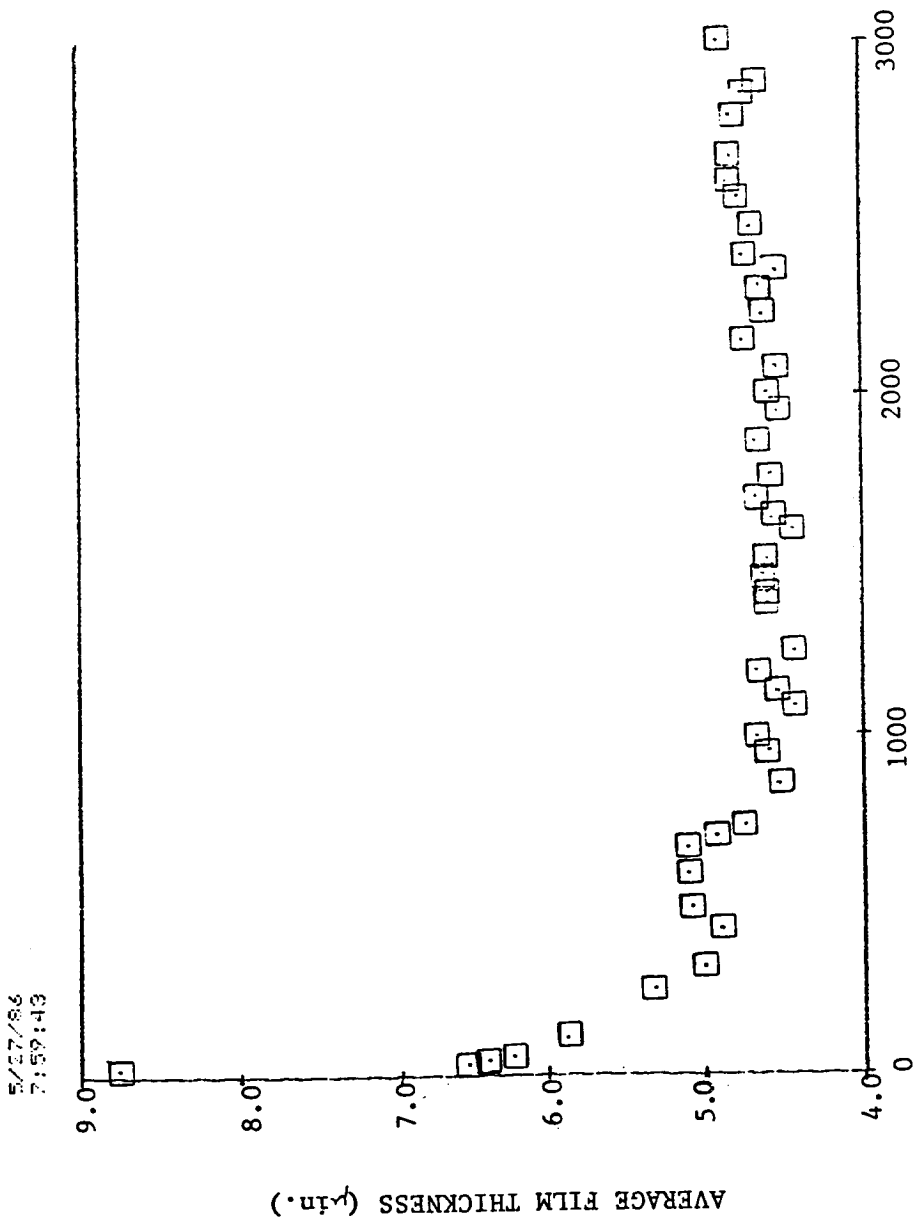

Fig. 3.37 Average film thickness vs. elapsed time for ITI 11532-A test bearing, 200 lb load, time study #1 - 50 min., 0.016 SRG 200 oil/freon concentration.

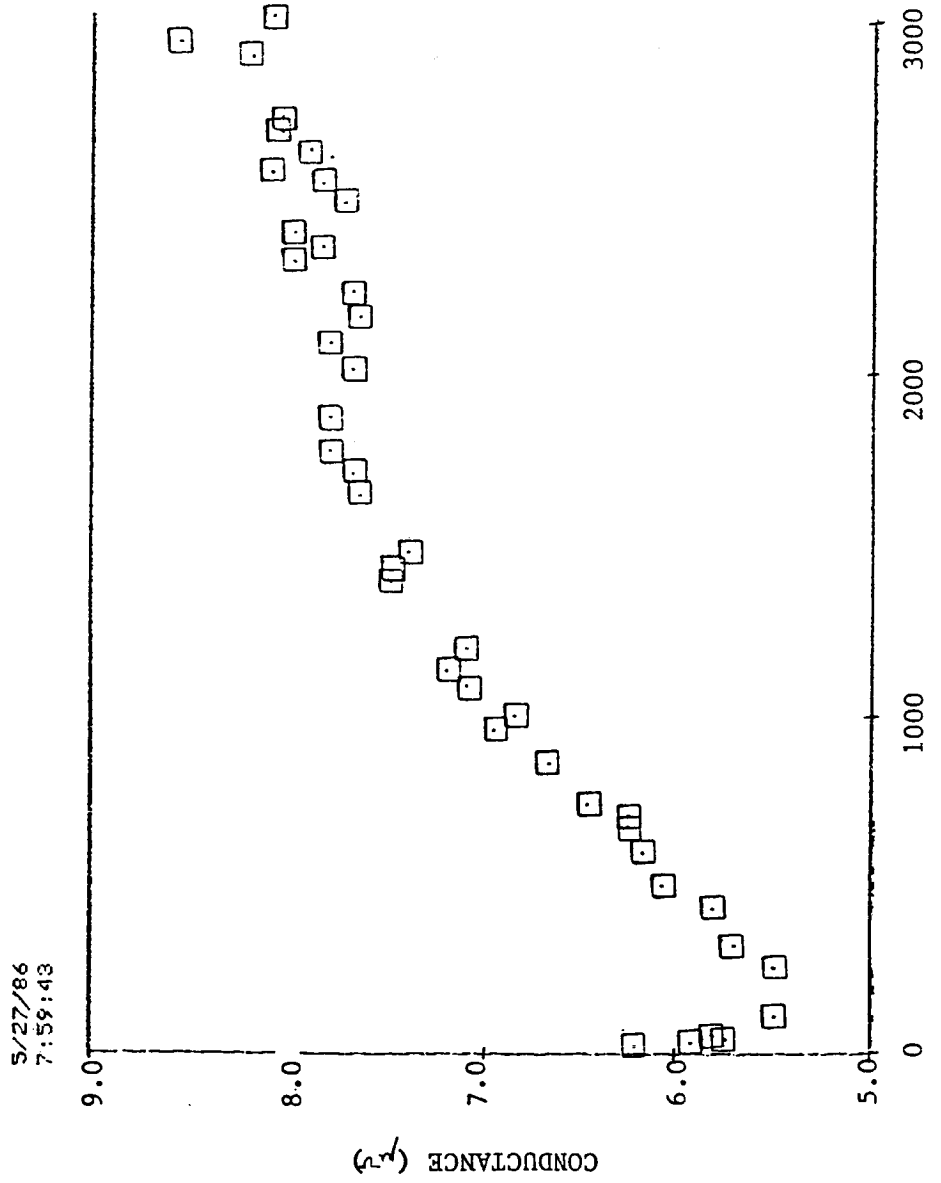

Fig. 3.38 Conductance vs. elapsed time for ITI 11532-A test bearing, 200 lb load, time study #1 - 50 min., 0.016 SRG 200 oil/freon concentration.

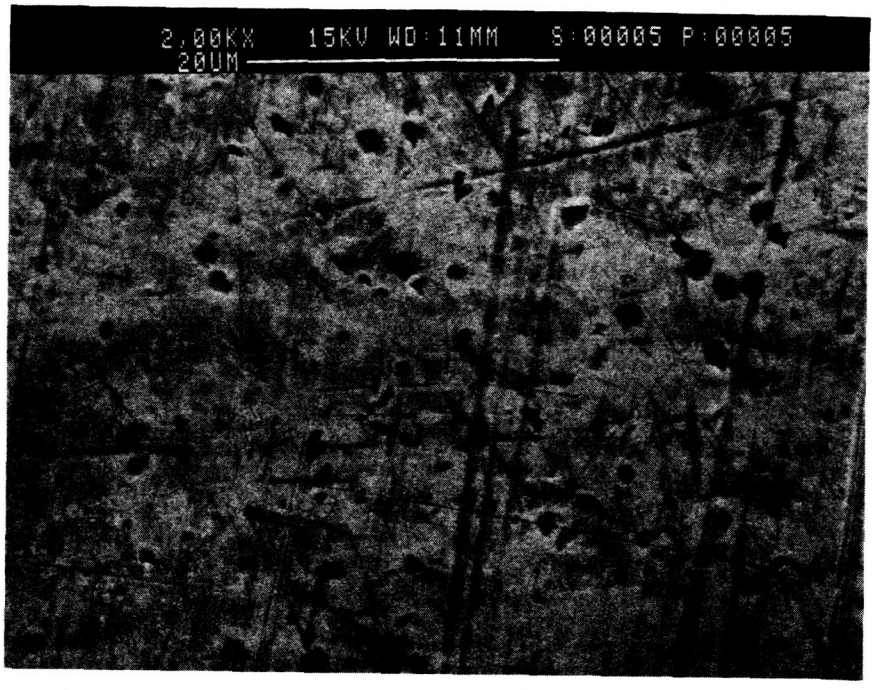

Fig. 3.39 Surface wear track magnified 2000x for grade 10 ball, 200 lb load, time study #1 - 50 min., 0.016 SRG 200 oil/freon concentration.

ORIGINAL PAGE IS
OF POOR QUALITY

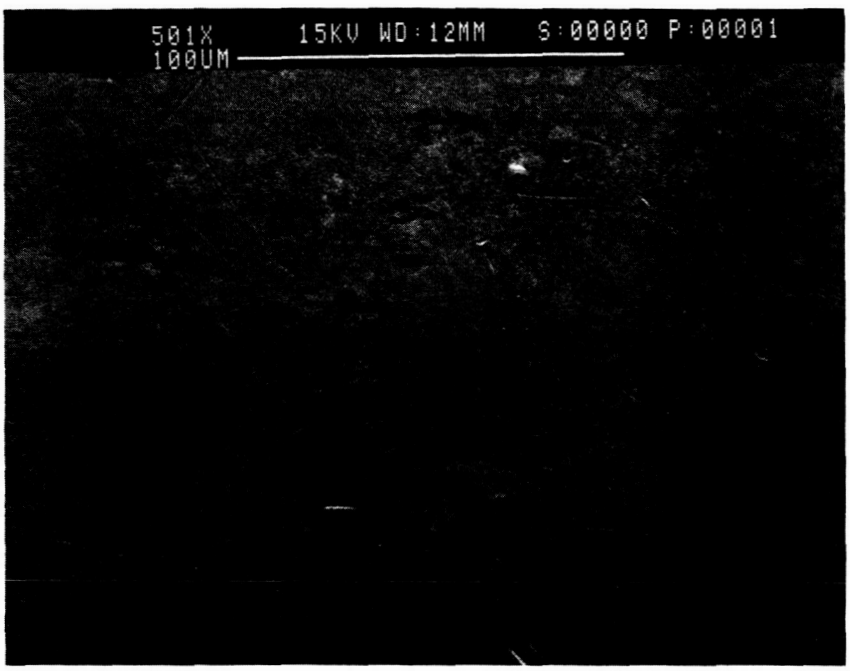

Fig. 3.40 Surface of grade 10 ball magnified 501x as received.

Fig. 3.41 Surface wear track magnified 5060x for grade 10 ball, 200 lb load, time study #1 - 50 min., 0.016 SRG 200 oil/freon concentration.

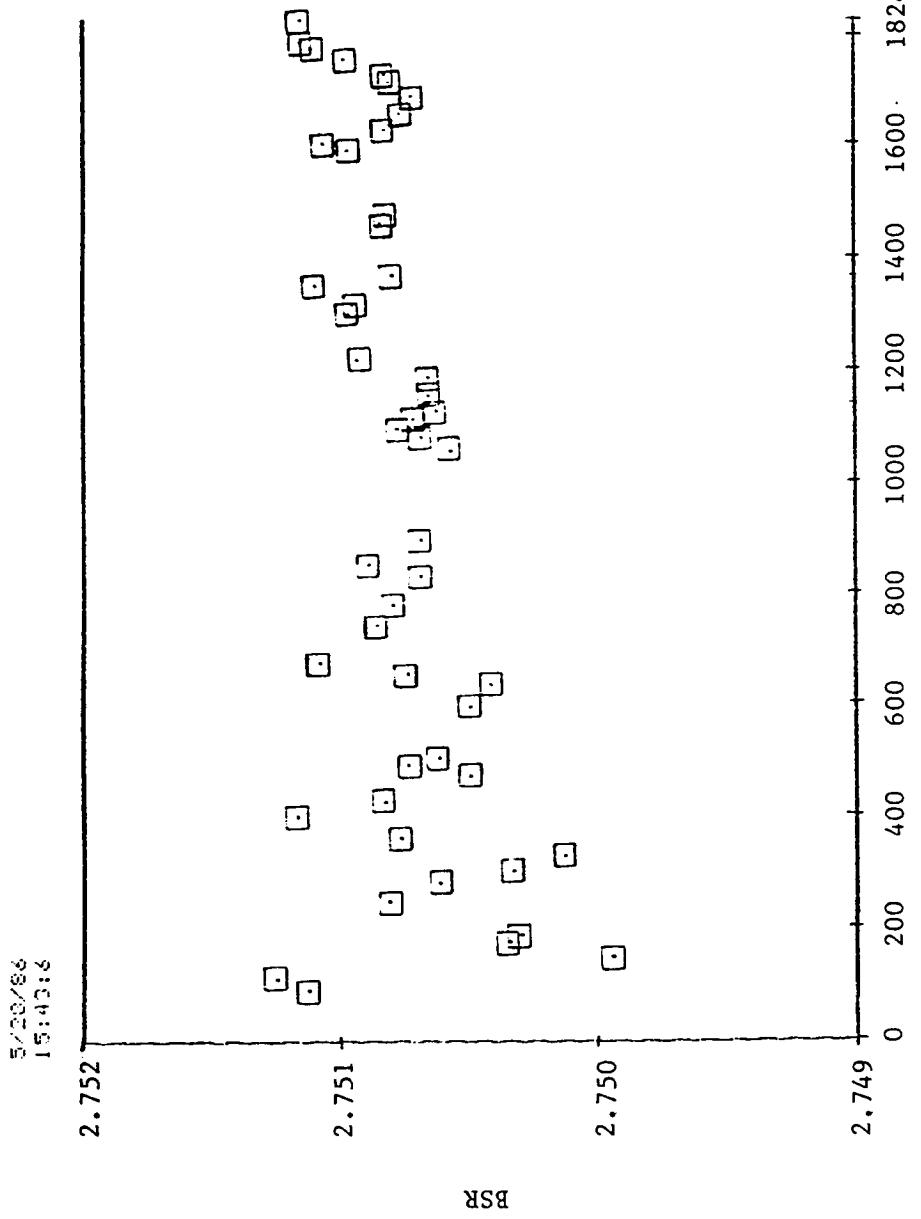

Fig. 3.42 BSR vs. elpased time for ITI 11532-A test bearing, 200 lb load, time study #2 - 30 min., 0.008 SRG 200 oil/freon concentration.

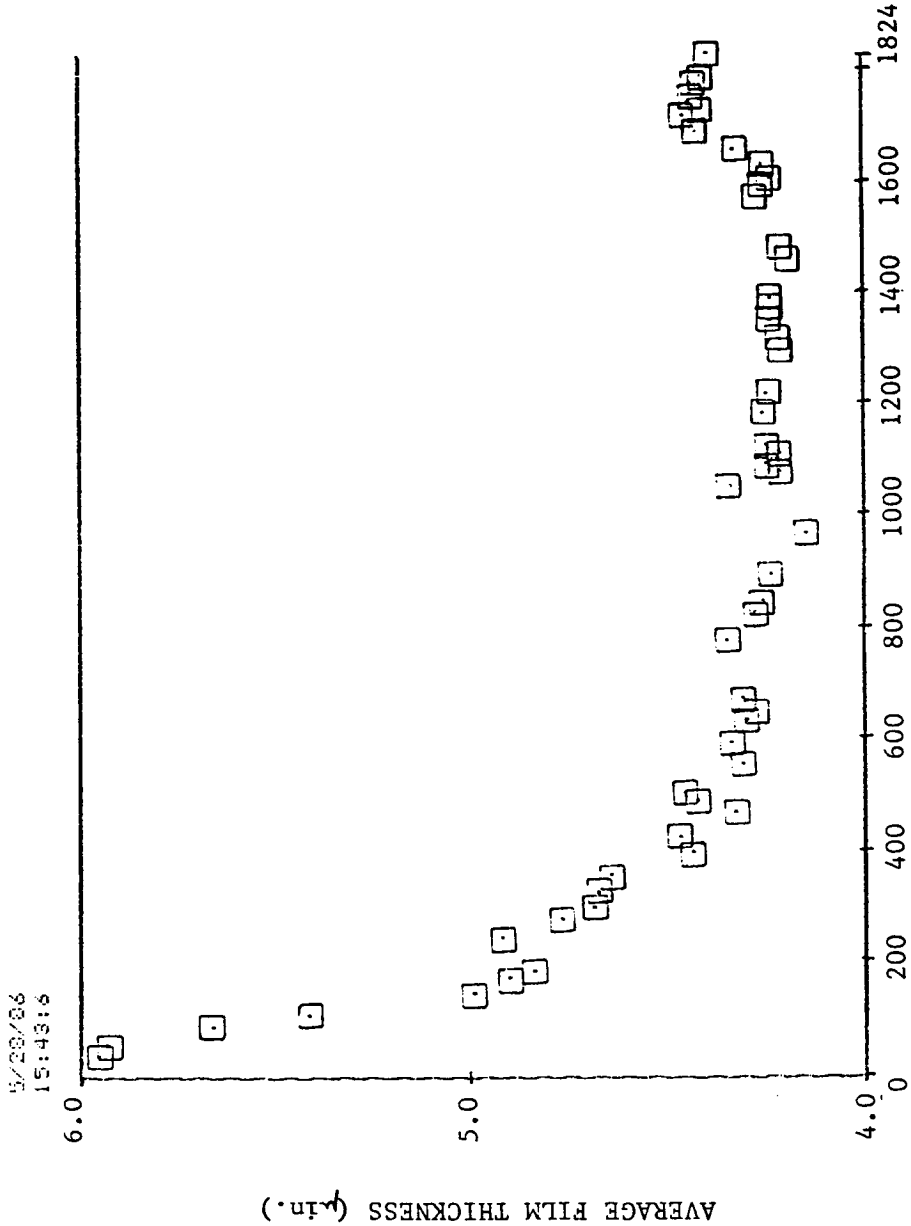

Fig. 3.43 Average film thickness vs.elapsed time for ITI 11532-A test bearing, 200 lb load, time study #2 - 30 min., 0.008 SRG 200 oil/freon concentration.

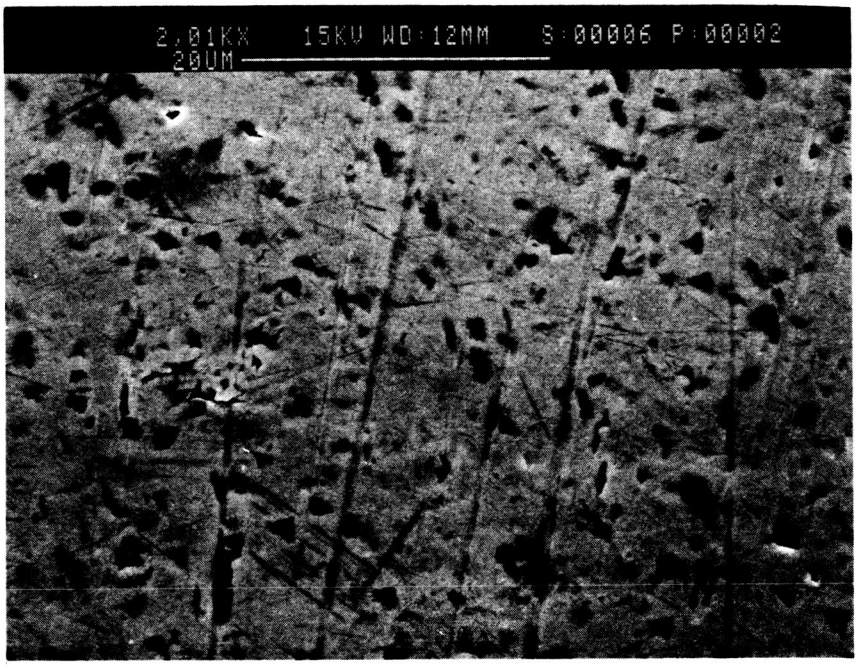

Fig. 3.44 Surface wear track magnified 2010x for grade 10 ball, 200 lb load, time study #2 - 60 min., 0.008 SRG 200 oil/freon concentration.

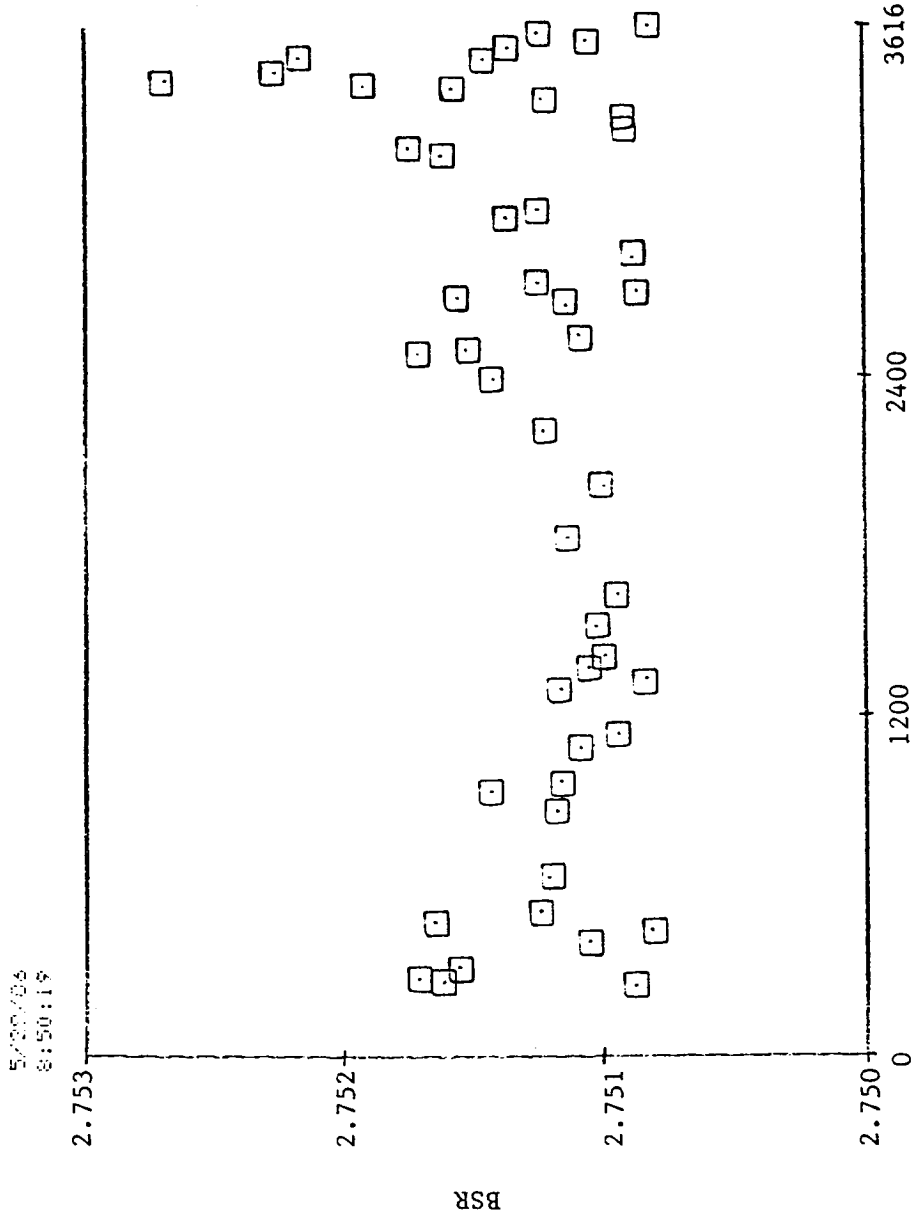

Fig. 3.45 BSR vs. elapsed time for ITI 11532-A test bearing, 200 lb load, time study #2 - 60 min., 0.008 SRG 200 oil/freon concentration.

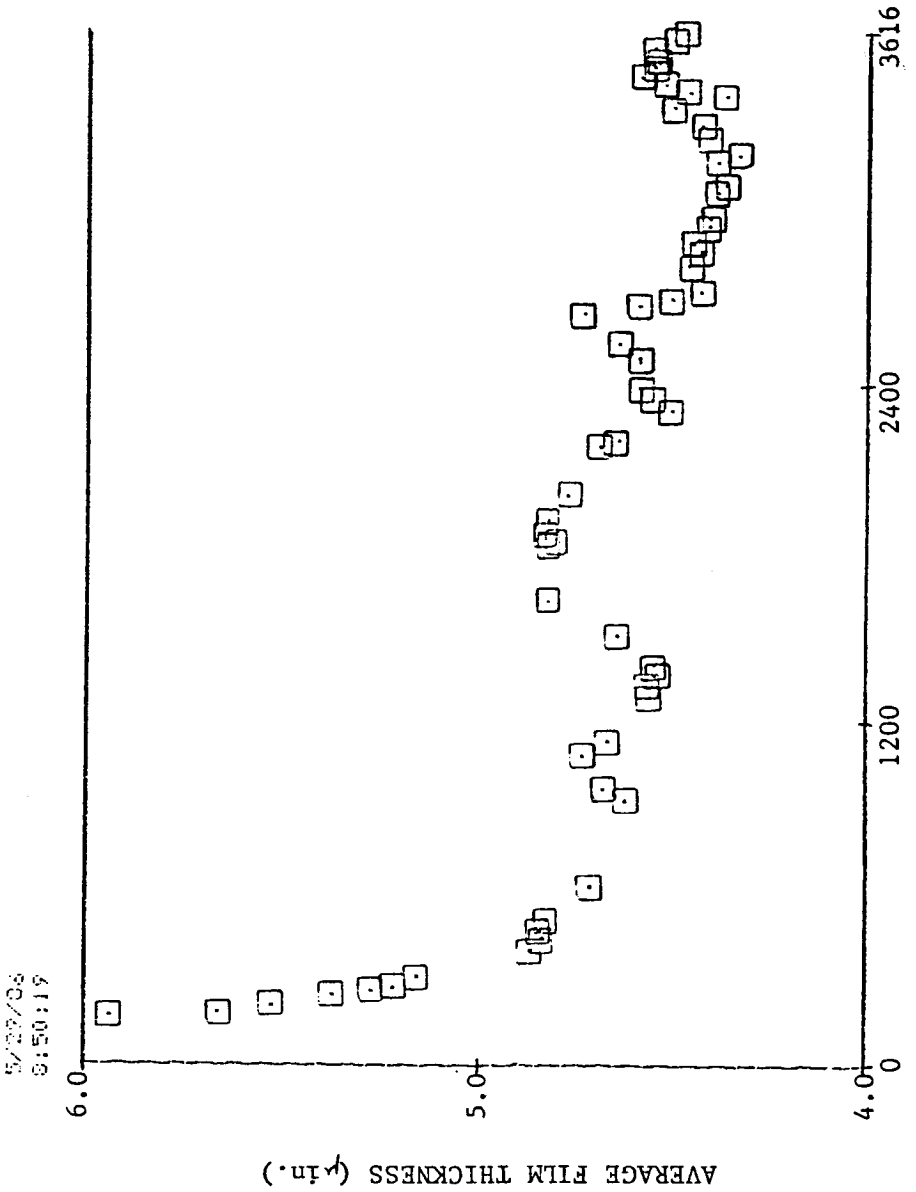

Fig. 3.46 Average film thickness vs. elasped time for ITI 11532 test bearing, 200 lb load, time study #2 - 60 min., 0.008 SRG 200 oil/freon concentration.

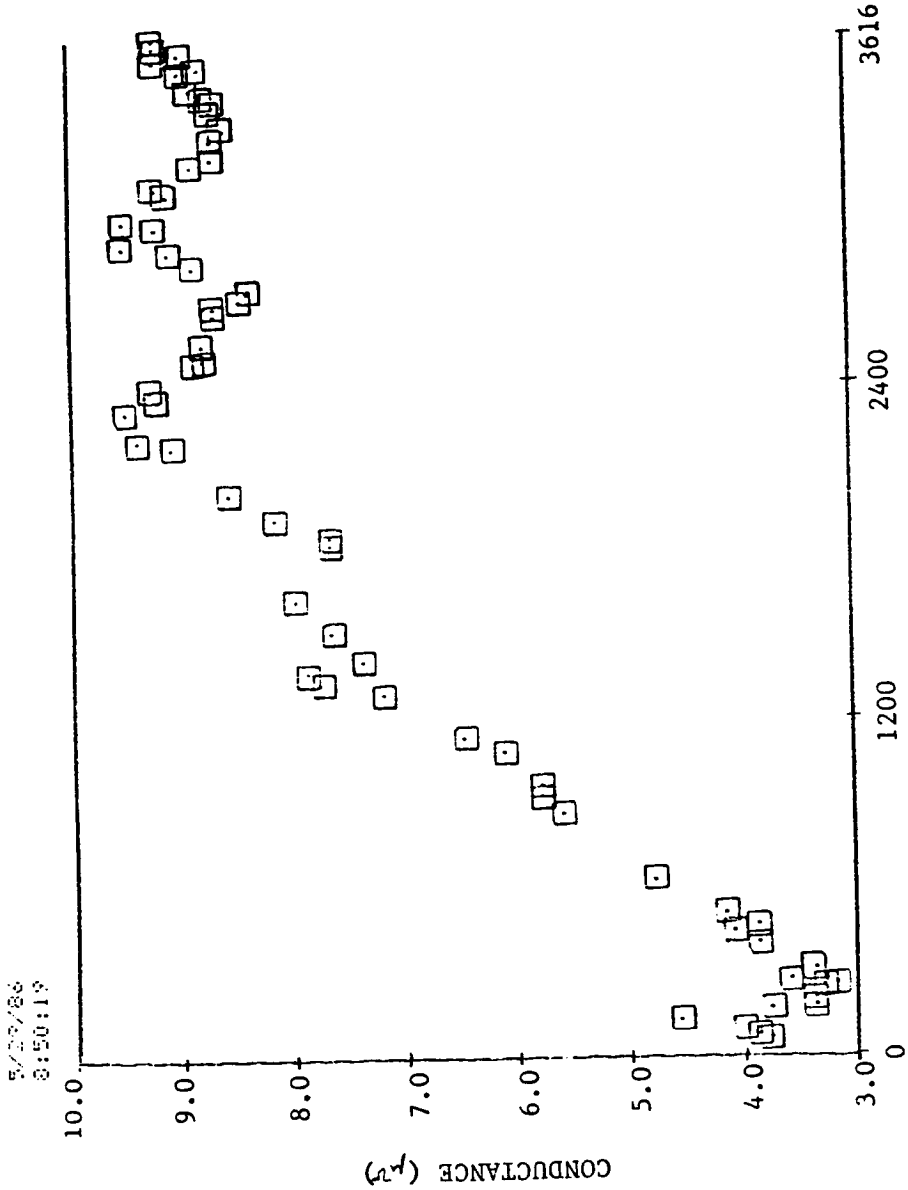

Fig. 3.47 Conductance vs. elapsed time for ITI 11532-A test bearing, 200 lb load, time study #2 - 60 min., 0.008 SRG 200 oil/freon concentration.

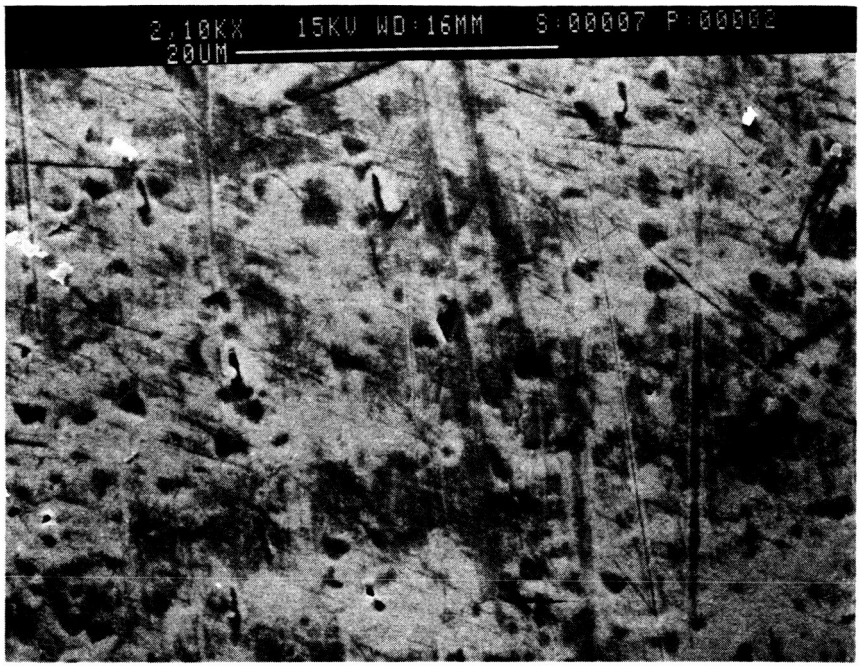

Fig. 3.48 Surface wear track magnified 2100x for grade 10 ball, 200 lb load, time study #2 - 70 min., 0.008 SRG 200 oil/freon concentration.

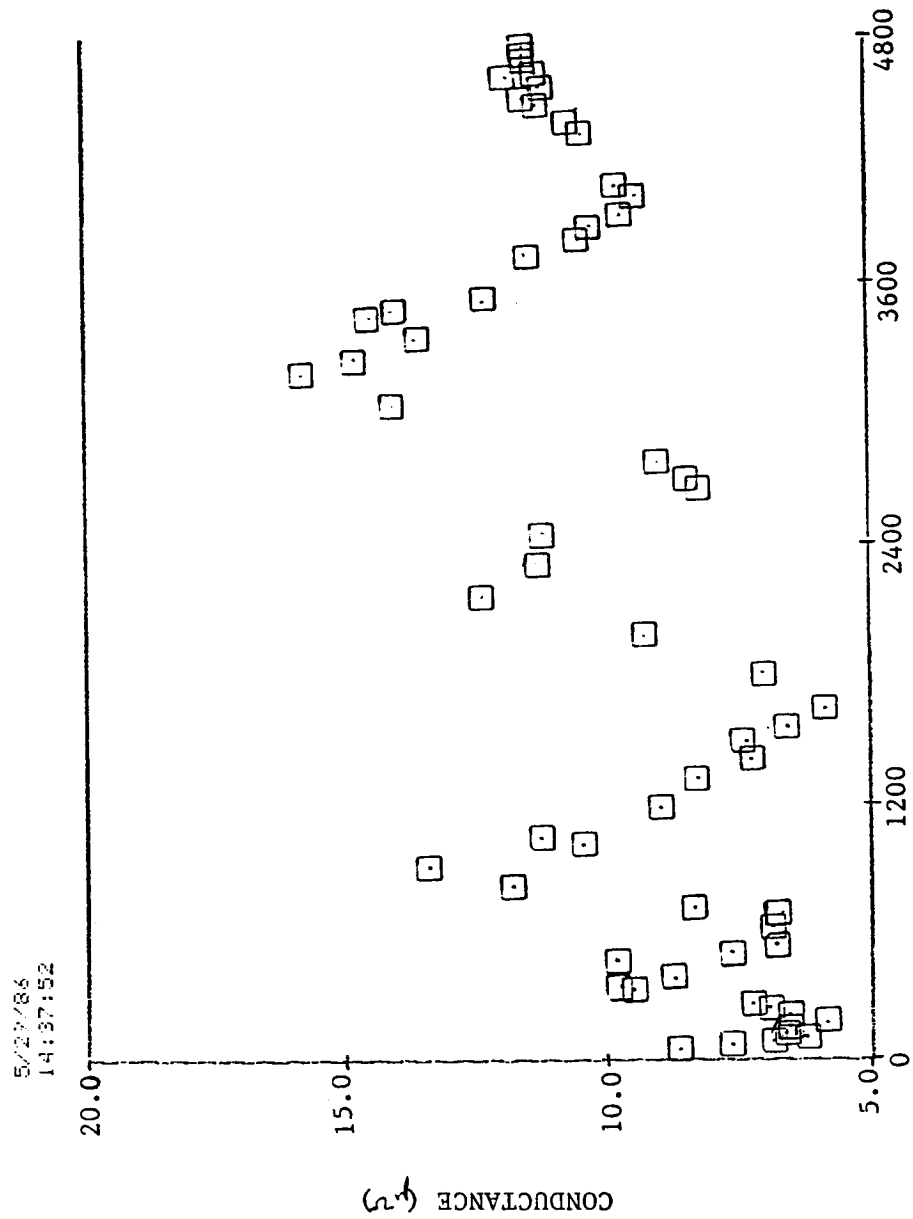

Fig. 3.49 Conductance vs elapsed time for ITI 11532-A test bearing, 200 lb load, time study #2 - 80 min., 0.008 SRG 200 oil/freon concentration.

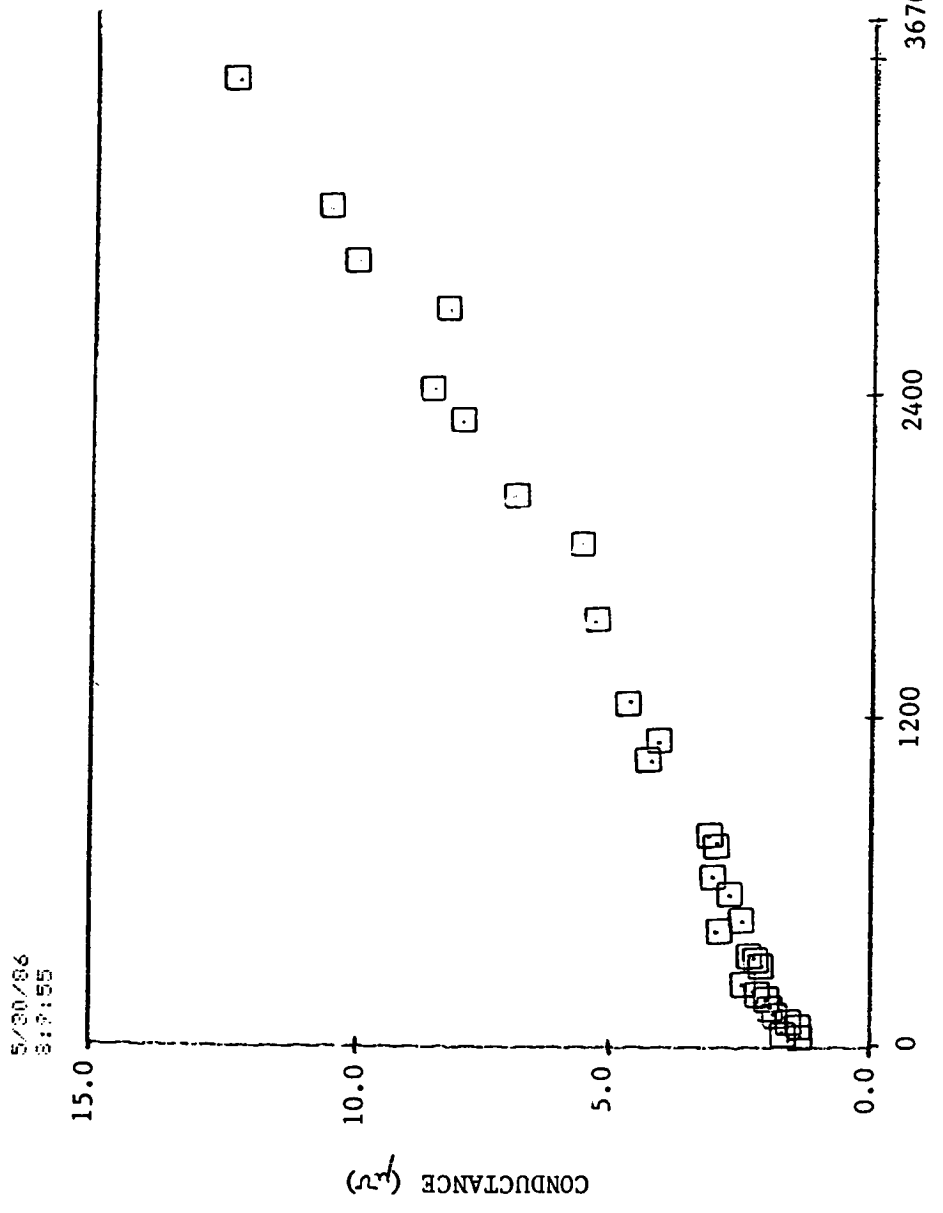

Fig. 3.50 Conductance vs. elapsed time for ITI 11532-A test bearing, 200 lb load, time study #2 - 90 min., 0.008 SRG 200 oil/freon concentration.

* - test bearing failed

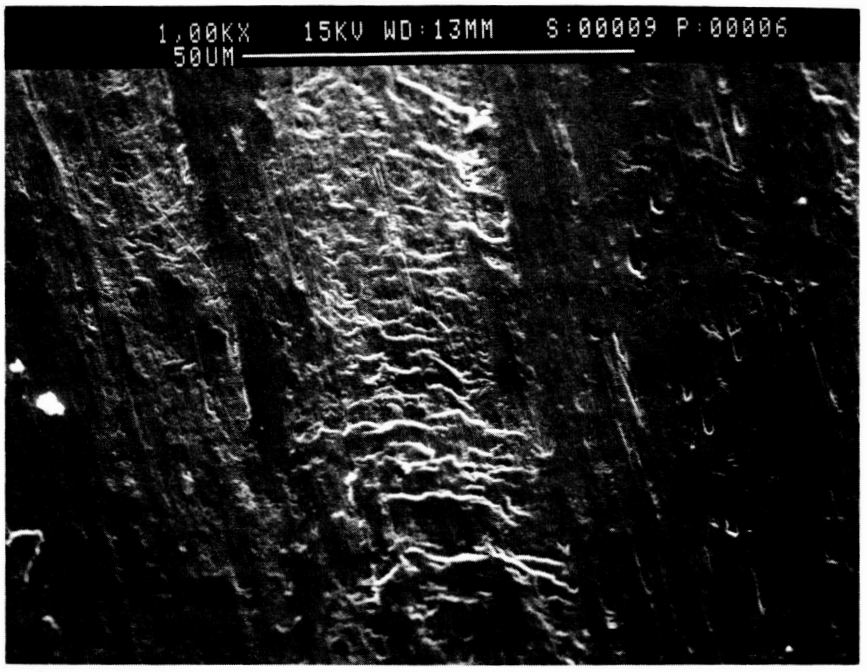

Fig. 3.51 Surface wear track magnified 1000x for grade 10 ball, 200 lb load, time study #2 - 90 min., 0.008 SRG 200 oil/freon concentration.

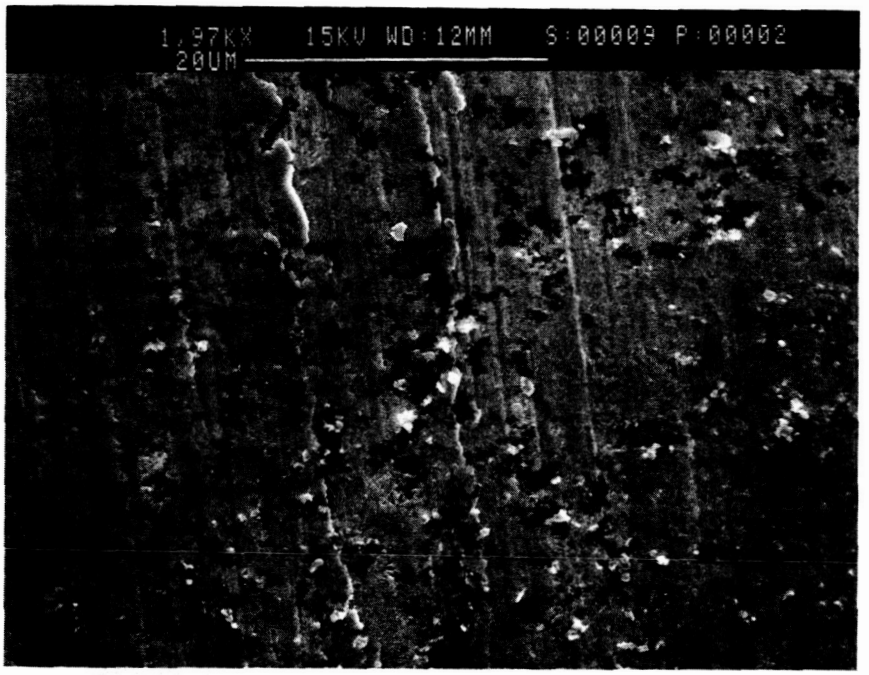

Fig. 3.52 Surface wear track magnified 1970x for grade 10 ball, 200 lb load, time study #2 - 90 min., 0.008 SRG 200 oil/freon concentration.

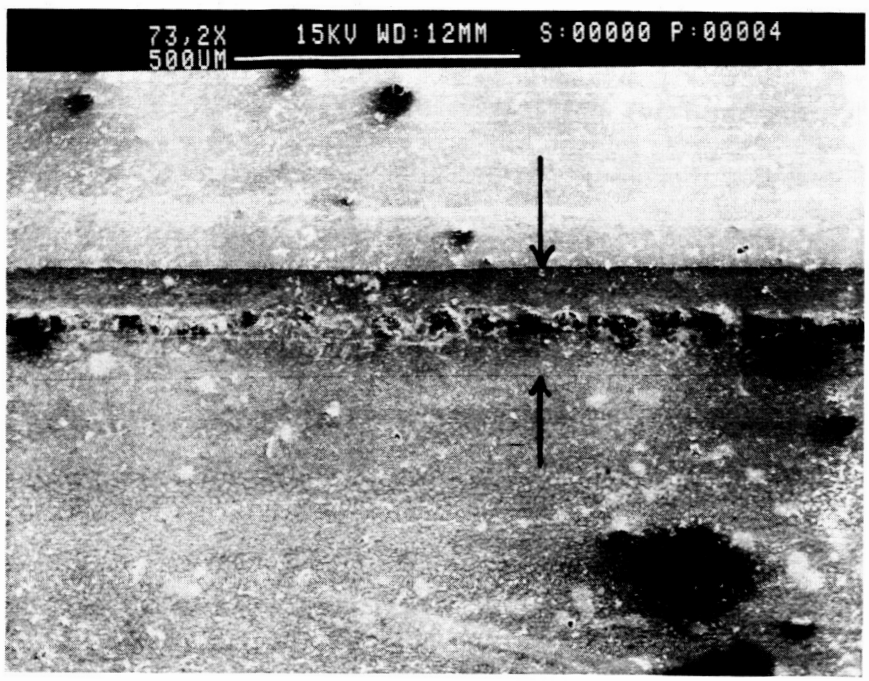

Fig. 3.53 Inner race polymer film magnified 73x for ITI 8990-A test bearing, 300 lb load, 0.002 SRG 200 oil/freon concentraion.

Fig. 3.54 Inner race polymer film magnified 254x for ITI 8990-A test bearing, 300 lb load, 0.002 SRG 200 oil/freon concentration.

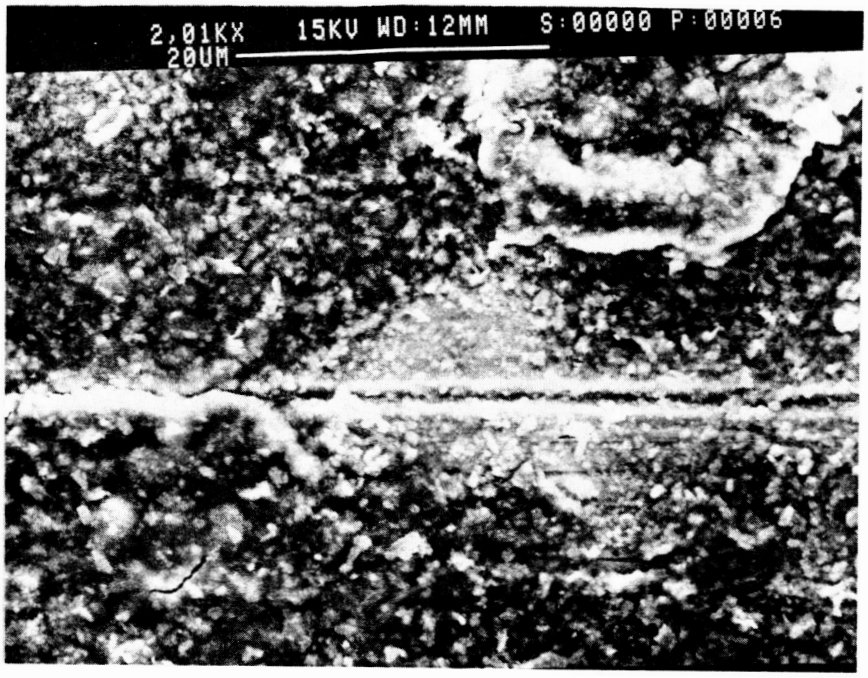

Fig. 3.55 Inner race polymer film magnified 2010x for ITI 8990-A test bearing, 300 lb load, 0.002 SRG 200 oil/freon concentration.

Fig. 3.56 End view of polymer film on inner race magnified 1990x for ITI 8990-A test bearing, 300 lb load, 0.002 SRG 200 oil/freon concentration. Lighter foreground is race surface.

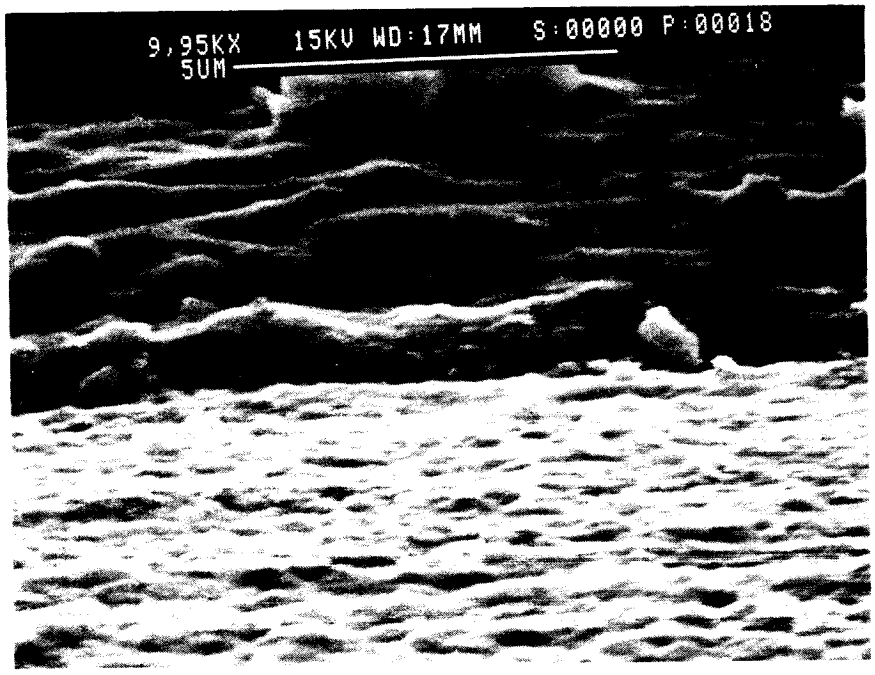

Fig. 3.57 End view of polymer film on inner race magnified 9950x for ITI 8990-A test bearing, 300 lb load, 0.002 SRG 200 oil/freon concentration. Lighter foreground is race surface.

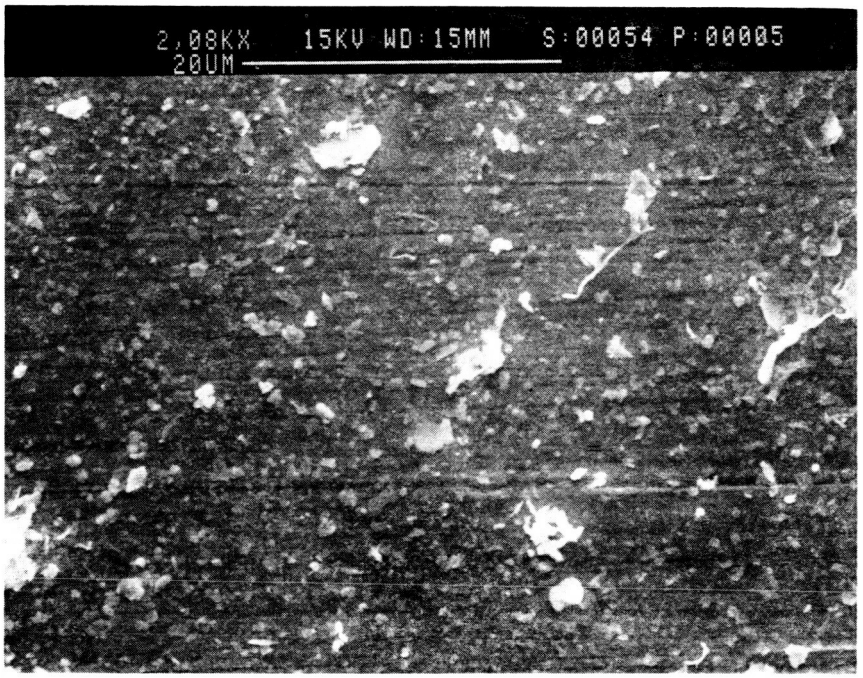

Fig. 3.58 Top view of polymer film on inner race magnified 2080x for ITI 8990-A test bearing, 300 lb load, 0.002 SRG 200 oil/freon concentration.

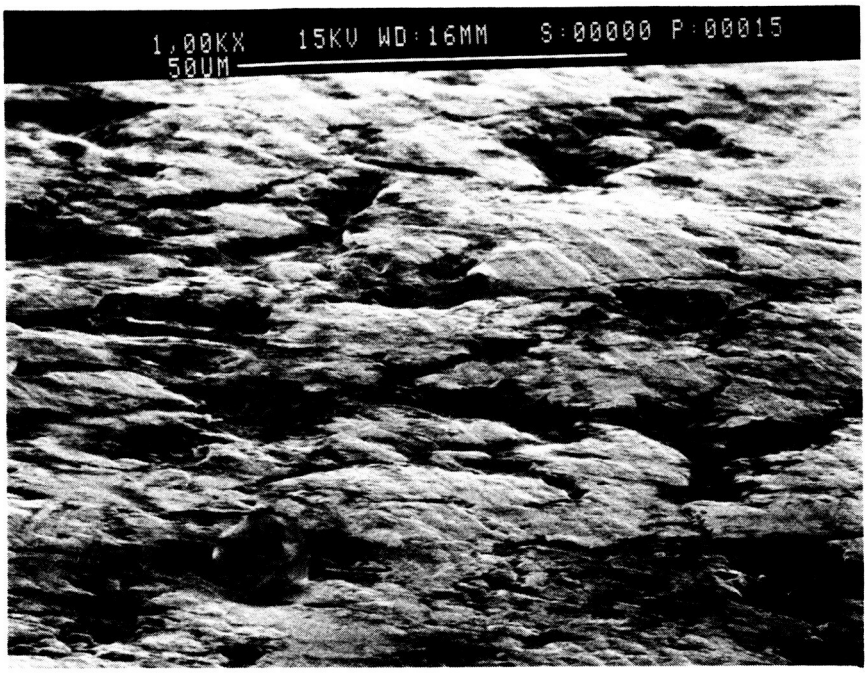

Fig. 3.59 Surface wear track magnified 1000x for grade 10 ball #1, 300 lb load, 0.002 SRG 200 oil/freon concentration.

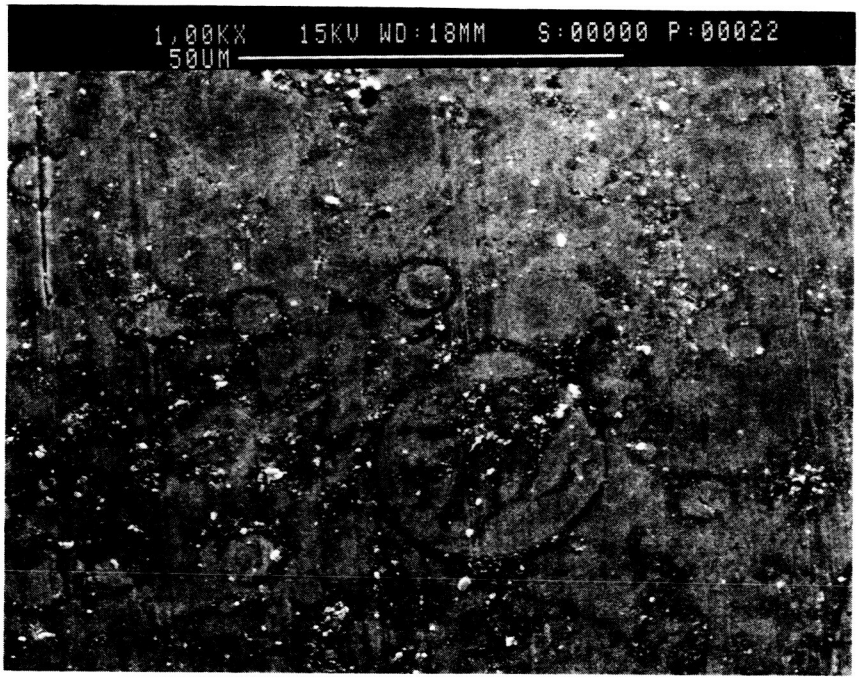

Fig. 3.60 Surface wear track magnified 1000x for grade 10 ball #2, 300 lb load, 0.002 SRG 200 oil/freon concentration.

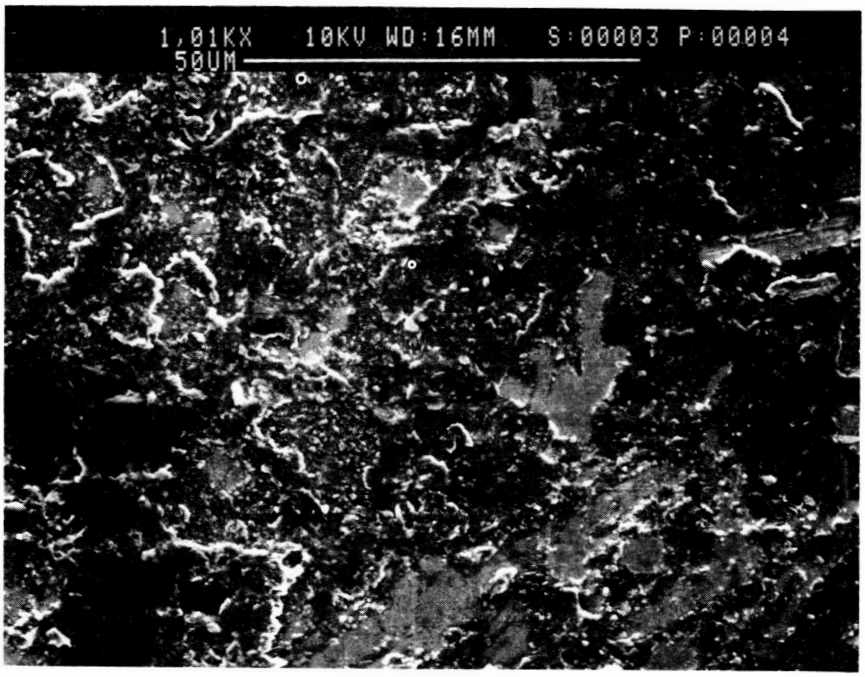

Fig. 3.61 Surface wear track magnified 1010x for grade 10 ball #3, 300 lb load, 0.002 SRG 200 oil/freon concentration.

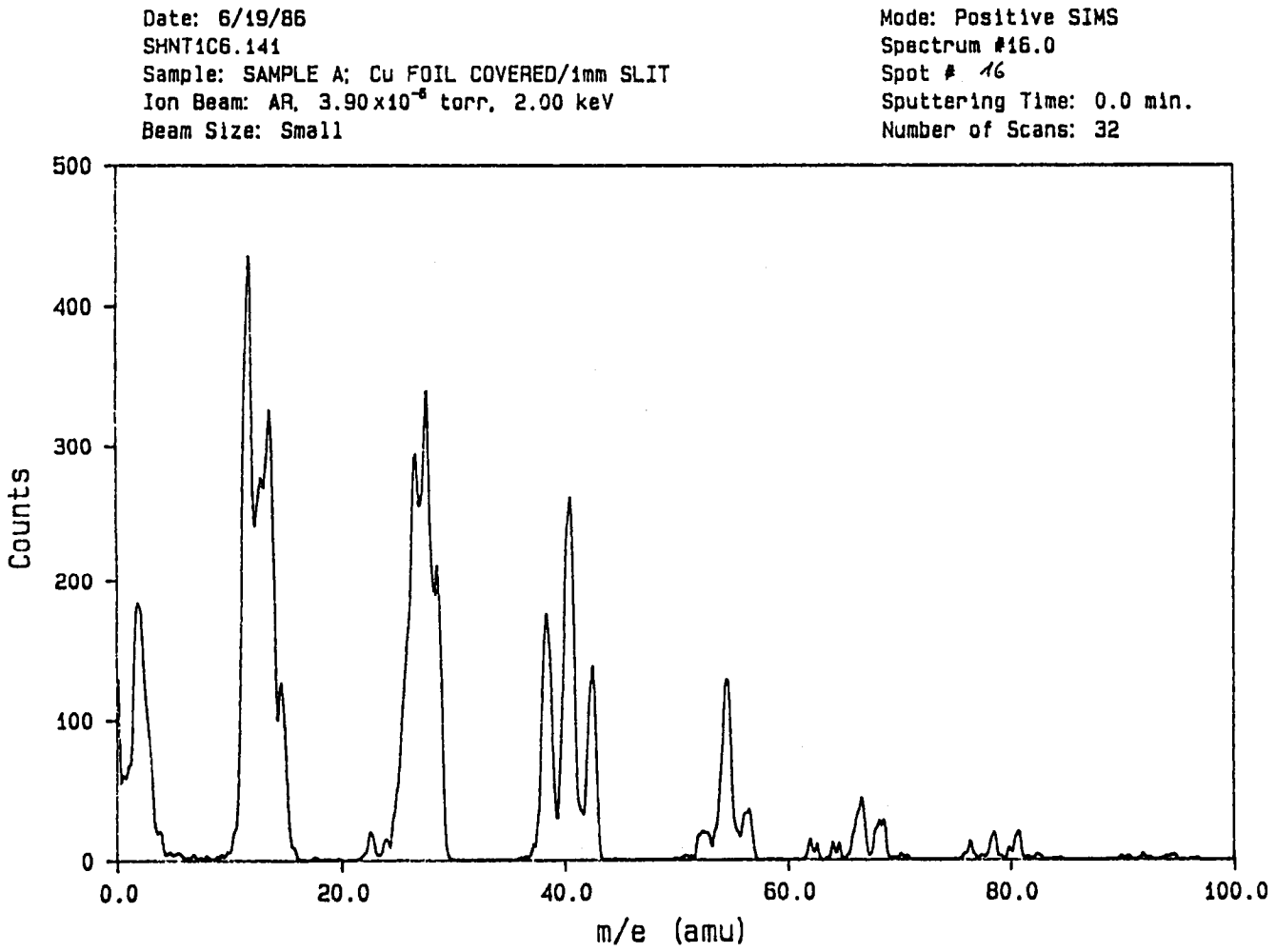

Fig. 3.62 SIMS spectrum versus atomic mass units for ITI 8990-A test bearing, 300 lb load, 0.002 SRG 200 oil/freon concentration.

TABLE III. - TABULATED VALUES FOR Y AND X FOR DETERMINATION OF THE CAPACITANCE OF THE INLET AND OUTLET SECTIONS

Relation between Y and X

$$X = \frac{b^2 \epsilon_0}{2Rh_0' \epsilon_1}$$

$$Y = \frac{(2X)^{1/2}}{4\pi} \int_0^1 \frac{d\zeta}{\zeta^2 + X\{|\sqrt{(1 - \zeta^2)}| - \zeta^2 \ln [|1/\zeta| + |\sqrt{(1/\zeta^2 - 1)}|]\}}$$

[Entries in the table are the values of Y for selected values of X given by the product of row and column headings. Precision is estimated as one part in 10^3.]

	10^{-3}	10^{-2}	10^{-1}	1	10	10^3	10^3
1	0.1735	0.1678	0.1548	0.1324	0.104 2	0.076 78	0.054 41
1.5	.1729	.1661	.1515	.1277	.099 11	.072 42	.051 08
2	.1723	.1648	.1490	.1242	.095 56	.069 42	.048 83
3	.1714	.1627	.1452	.1193	.090 64	.065 38	.045 80
4	.1707	.1610	.1424	.1157	.087 21	.062 61	.043 75
5	.1701	.1597	.1400	.1129	.084 60	.060 52	.042 22
6	.1695	.1585	.1381	.1106	.082 50	.058 87	↓
7	.1690	.1574	.1364	.1087	.080 74	.057 01	
8	.1686	.1565	.1349	.1070	.079 25	.056 32	
9	.1682	.1556	.1336	.1055	.077 94	.055 31	

TABLE IV. - SRG 200 DIELECTRIC CONSTANT EXPERIMENTAL DATA

Time, min	Temp., °C	Cap, pF	ϵ_o	Loss, μ℧
0	27	669.0	2.19	0.02
57	33	665.8	2.18	0.01
110	37	663.7	2.17	0.01
159	47	659.1	2.16	0.00
212	52	656.1	2.15	0.00
261	59	652.8	2.14	0.00
311	64	649.9	2.13	0.00
372	71	647.4	2.12	0.00
422	76	645.3	2.11	0.00
915	62	654.2	2.14	0.00
988	42	663.6	2.17	0.01

TABLE V. - TABULATED VALUES OF BSR FOR ITI 8990-A TEST BEARING AT VARIOUS APPLIED LOADS

Load	lbs				
	0	100	200	300	350
BSR Test 1	-----	2.6758	2.6776	2.6787	2.6792
BSR Test 2	-----	2.6763	2.6773	2.6784	------
BSR Test 3	-----	2.6755	2.6774	2.6786	------
BSR (No-Slip)	2.6826	2.6835	2.6840	2.6844	2.6846

REFERENCES

1. B.J. Hamrock, and D. Dowson, Ball Bearing Lubrication, Wiley, 1981.

2. O. Reynolds, On the Theory of Lubrication and Its Application to Mr. Beauchamp Tower's Experiments, Including an Experimental Determination of the Viscosity of Olive Oil, Philos. Trans. R. Soc. London, 177 (1886), 157-234.

3. E. Kingsbury, Parched Elastohydrodynamic Lubrication, J. Tribology 107 (1985), 229-233.

4. C.R. Singleterry, Some Factors Affecting the Movement of Oil Over Metal Surfaces, Gyro Spin Axis Hydrodynamic Bearing Symposium, Vol. 2, MIT Instrumentation Laboratory, 1966, Paper No. 12.

5. E.P. Kingsbury, Lubricant-Breakdown in Instrument Ball Bearings, J. Lubr. Technol. 100, (1978), 386-394.

6. B.O. Jacobson, and B.J. Hamrock, Non-Newtonian Fluid Model Incorporated into Elastohydrodynamic Lubrication of Rectangular Contacts, J. Tribology 106 (1984), 275-284.

7. E. Kingsbury, Pivoting and Slip in an Angular Contact Bearing, ASLE Trans., 27 (1984), 259-262.

8. E. Kingsbury, Transient EHL Effects in Starved Ball Bearings, Tribology in the 80's, NASA CP-2300, Vol. II, 1984, pp. 641-663.

9. A. Dyson, H. Naylor, and A.R. Wilson, The Measurement of Oil-Film Thickness in Elastohydrodynamic Contacts, Elastohydrodynamic Lubrication, Proc. Inst. Mech. Eng. (London), Vol. 180, pt. 3B, 1965-66, pp. 119-134.

10. G.E. Allen, L.A. Peacock, and W.L. Rhoads, Measurements of Lubricant Film Thickness in Hertzian Contacts, NASA CR-105378, 1968.

11. E.P. Kingsbury, Basic Speed Ratio of an Angular Contact Bearing, J. Lubr. Technol. 102 (1980), 391-394.

12. E. Kingsbury, Chemical Degradation in Parched Elastohydrodynamic Lubrication, Mixed Lubrication and Lubrication Wear, D. Dowson, ed., Butterworths, 1984, pp. 50-54.

13. B.B. Seth, and T. Willis, Techniques for Film Thickness Measurements in Elastohydrodynamic Lubrication, ASME Paper 76-DET-79, Sept. 1978.

14. J. Ferrante, Practical Applications of Surface Analytical Tools in Tribology, Lubr. Eng. 38 (1982), 223-236.

15. L.F. Fieser, and K.L. Williamson, Organic Experiments, D.C. Heath and Company, 1975.

16. R.S. Fein, and K.L. Kreuz, Chemistry of Boundary Lubrication of Steel by Hydrocarbons, ASLE Trans. 8, 1965, 29-38.

17. J.L. Lauer, Friction Polymers and Other Chemical and Physical Phenomena at Lubricant Boundaries, to be presented at the ASME-ASLE Lubrication Conference, Pittsburgh, PA, Oct. 1986.

18. B.J. Hamrock, Lubrication of Machine Elements," NASA RP-1126, 1984.

APPENDIX A

BASIC SPEED RATIO (BSR) CALCULATIONS

WITH NO SLIP

The angular velocity of the separator or cage in a ball bearing is

$$\omega_c = \frac{1}{2d_e}\left[(d_e - d\cos\beta)\,\omega_i + (d_e + d\cos\beta)\omega_o\right] \qquad (A.1)$$

where ω_i is the inner race angular velocity, ω_o is the outer race angular velocity, d is the ball diameter, d_e is the pitch diameter and β is the contact angle. See figs. A.1 and A.2. To measure the ball spin rate, the ball complement orbital velocity ω_c must be zero so that

$$\frac{\omega_i}{\omega_o} = -\frac{(d_e + d\cos\beta)}{(d_e - d\cos\beta)} \qquad (A.2)$$

The angular velocity of a ball about its own axis ω_B is

$$\omega_B = \frac{1}{2d}\left[(d_e - d\cos\beta)\omega_i - (d_e + d\cos\beta)\omega_o\right] \qquad (A.3)$$

Substituting this equation into eq. (A.2), the following is obtained:

$$\omega_B = -\frac{(d_e + d\cos\beta)}{d}\,\omega_o \qquad (A.4)$$

The BSR is equal to the ball spin rate divided by the difference in the inner and outer race angular velocities

$$BSR = \frac{\omega_\beta}{\omega_i - \omega_o} \qquad (A.5)$$

Substituting the expressions for ω_i and ω_o, the BSR becomes

$$BSR = \frac{-\left(\frac{d_e + d\cos\beta}{d}\right)\omega_o}{-\frac{(d_e + d\cos\beta)}{(d_e - d\cos\beta)}\omega_o - \omega_o} \qquad (A.6)$$

$$BSR = \frac{d_e^2 - d^2\cos^2\beta}{2d_e d} \qquad (A.7)$$

$$BSR = \frac{1 - \left(\frac{d}{d_e}\cos\beta\right)^2}{2\frac{d}{d_e}} \qquad (A.8)$$

For a given geometry, the only unknown is the contact angle β. The contact angle is a function of the load applied and so that a different BSR exists for different loads.

The contact angle β is found by first calculating the free contact angle β_f when no load is applied. From fig. A.1, the free contact angle is

$$\cos\beta_f = \frac{D - \frac{P_d}{2}}{D} \qquad (A.9)$$

$$\cos\beta_f = 1 - \frac{P_d}{2(f_i + f_o - 1)\,d} \qquad (A.10)$$

where D is the distance between race curvature centers, P_d is the diametral clearance and f_i and f_o are the inner and outer race conformity ratios, respectively. For the test bearings used, all of the quantities in eq. (A.10) are known.

There are two equations for β that must be solved. The first equation relates the applied load F_T to the load on one ball F:

$$F = \frac{F_T}{n \sin \beta} \tag{A.11}$$

where n is the number of balls.

The second equation comes from the geometry of the balls and races when a heavy load is applied as shown in fig. A.2:

$$\cos \beta = \frac{D - \frac{P_d}{2}}{D + \delta'} \tag{A.12}$$

where δ' is the total elastic deformation. Substituting eq. (A.9) into this equation yields:

$$\frac{D + \delta'}{D} \cos \beta = \cos \beta_f \tag{A.13}$$

Solving for δ':

$$\delta' = D\left(\frac{\cos \beta_f}{\cos \beta} - 1\right) \tag{A.14}$$

$$\delta' = \delta_i' + \delta_o' \tag{A.15}$$

where δ_i' and δ_o' are the inner and outer deformations, respectively. From Hamrock [18]

$$\delta_i' + \delta_o' = \left[\frac{F}{(k_j)_o}\right]^{1/j} + \left[\frac{F}{(k_j)_i}\right]^{1/j} \tag{A.16}$$

where $j = 1.5$ for ball bearings and

$$k_{1.5} = \pi k E' \left(\frac{R\epsilon}{4.5\mathcal{F}}\right)^{1/2} \tag{A.17}$$

For the case at hand, $\alpha = R_y/R_x \geq 1$ so that

$$k = \alpha^{2/\pi} \tag{A.18}$$

$$\varepsilon = 1 + \frac{q}{2} \tag{A.19}$$

$$q = \frac{\pi}{2} - 1 \tag{A.20}$$

$$\mathcal{F} = \frac{\pi}{2} + q \ln \alpha \tag{A.21}$$

$$R_{xi} = \frac{d(d_e - d \cos \beta)}{2d_e} \tag{A.22}$$

$$R_{xo} = \frac{d(d_e + d \cos \beta)}{2d_e} \tag{A.23}$$

$$R_{yi} = \frac{f_i d}{2} (f_i - 1) \tag{A.24}$$

$$R_{yo} = \frac{f_o d}{2} (f_o - 1) \tag{A.25}$$

$$\frac{1}{R_x} = \frac{1}{R_{xi}} + \frac{1}{R_{xo}} \tag{A.26}$$

$$\frac{1}{R_y} = \frac{1}{R_{yi}} + \frac{1}{R_{yo}} \tag{A.27}$$

where R_x and R_y are the effective radius in the x and y directions, respectively. Rearranging the deformation equations (A.14) and (A.16):

$$D^j \left(\frac{\cos \beta_f}{\cos \beta} - 1\right)^j = F\left(\left(\frac{1}{k_j}\right)_o^{1/j} + \left(\frac{1}{k_j}\right)_i^{1/j}\right)^j \tag{A.28}$$

$$F = K_j D^j \left(\frac{\cos \beta_f}{\cos \beta} - 1\right)^j \tag{A.29}$$

where

$$K_j = \frac{1}{\left[\left(\frac{1}{k_j}\right)_o^{1/j} + \left(\frac{1}{k_j}\right)_i^{1/j}\right]^j} \tag{A.30}$$

Substituting eq. (A.11) into eq. (A.29)

$$\frac{F_t}{\sin \beta} = K_j D^j \left(\frac{\cos \beta_f}{\cos \beta} - 1\right)^j \tag{A.31}$$

The only unknown in eq. (A.31) is β for a given bearing and load. Once β is found, the BSR for that load can be calculated from eq. (A.8).

NO SLIP BSR CALCULATION FOR TEST BEARINGS

Two 40 mm test bearings with 17 ball complements are used in this work - ITI 8990-A and ITI 11532-A.

ITI 11532-A

SPECIFICATIONS:

MATERIAL: 440C stainless steel

$f_i = 0.58$

$f_o = 0.54$

$d_e = 2.125$ in.

$P_d = 0.0025$ in.

$D = (f_i + f_o - 1)d = 0.045$ in.

BALLS USED: Grade 10, 440C stainless steel, 3/8 in. diameter. The modulus of elasticity and Poisson's ratio for 440C stainless steel are $29 \times 10^{+6}$ lb/in.^{2} and 0.3, respectively.

The free contact angle can be calculated from eq. (A.10)

$$\cos \beta_f = 1 - \frac{P_d}{2(f_i + f_o - 1)d} \tag{A.32}$$

$$\beta_f = 13.54° \tag{A.33}$$

The BSR with no slip as given by eq. (A.8) requires the contact angle β. The calculation procedure is as follows. As denoted by Hamrock [18], the radii of curvature for the different surfaces in a ball bearing are

ball-inner race contact

$$r_{ax_i} = r_{ay_i} = \frac{d}{2} = 0.1875 \text{ in.} \tag{A.34}$$

$$r_{bx_i} = \frac{d_e - d \cos \beta}{2 \cos \beta} = 0.9054 \text{ in.} \tag{A.35}$$

$$r_{by_i} = -f_i d = -0.2175 \text{ in.} \tag{A.36}$$

ball-outer race contact

$$r_{ax_o} = r_{ay_o} = \frac{d}{2} = 0.1875 \text{ in.} \tag{A.37}$$

$$r_{bx_o} = -\frac{d_e + d \cos \beta}{2 \cos \beta} = -1.280 \text{ in.} \tag{A.38}$$

$$r_{by_o} = -f_o d = -0.2025 \text{ in.} \tag{A.39}$$

where x is in the direction of the semiminor axis of the contact area when a load is applied and y the direction of the semimajor axis. The effective radii of curvature and radius ratios are:

ball-inner race contact

$$\frac{1}{Rx_i} = \frac{1}{r_{ax_i}} + \frac{1}{r_{bx_i}} \Rightarrow R_{xi} = 0.1553 \text{ in.} \tag{A.40}$$

$$\frac{1}{Ry_i} = \frac{1}{r_{ay_i}} + \frac{1}{r_{by_i}} \Rightarrow R_{yi} = 1.3594 \text{ in.} \tag{A.41}$$

$$\frac{1}{R_i} = \frac{1}{R_{xi}} + \frac{1}{R_{yi}} \Rightarrow R_i = 0.1395 \text{ in.} \tag{A.42}$$

$$\alpha_i = \frac{R_{yi}}{R_{xi}} = 8.753 \tag{A.43}$$

ball-outer race contact

$$\frac{1}{R_{xo}} = \frac{1}{r_{ax_o}} + \frac{1}{r_{bx_o}} \Rightarrow R_{xo} = 0.2197 \text{ in.} \tag{A.44}$$

$$\frac{1}{R_{yo}} = \frac{1}{r_{ay_o}} + \frac{1}{r_{by_o}} \Rightarrow R_{yo} = 2.531 \text{ in.} \tag{A.45}$$

$$\frac{1}{R_o} = \frac{1}{R_{xo}} + \frac{1}{R_{yo}} \Rightarrow R_o = 0.2022 \text{ in.} \tag{A.46}$$

$$\alpha_o = \frac{R_{yo}}{R_{xo}} = 11.521 \tag{A.47}$$

Eq. (A.28) can be written as

$$F = K_j D^j \left(\frac{\cos \beta_f}{\cos \beta} - 1\right)^j \tag{A.48}$$

where

$$K_j = \frac{1}{\left[\left(\frac{1}{K_j}\right)_o^{1/j} + \left(\frac{1}{K_j}\right)_i^{1/j}\right]^j} \tag{A.49}$$

α is greater than 1 so that Hamrock [18] suggests eqs. (A.17) through (A.27). For the ITI 8990-A test bearing:

$$K_i = 3.980 \qquad K_o = 4.740 \tag{A.50}$$

$$\mathcal{F}_i = 2.809 \qquad \mathcal{F}_o = 2.966 \tag{A.51}$$

$$\varepsilon_i = 1.0652 \qquad \varepsilon_o = 1.0495 \tag{A.52}$$

$$E' = 31.9 \times 10^6 \text{ lb/in}^2 \tag{A.53}$$

Substituting into eq. (A.30), K_j is $6.194 \times 10^{+6}$. The contact angle is calculated for various loads and shown in table A.1 with the BSR for loads of 0, 100, 200, and 300 lb .

ITI 8990-A

The calculations for the ITI 11532-A test bearing are the same as for the ITI 8990-A bearing. The only difference is that the ITI 11532-A bearing has an inner conformity ratio of 0.54, an outer conformity ratio of 0.58 and a pitch diameter of 2.076 in. Table A.2 shows the BSR and contact angle for the ITI 11532-A test bearing at various loads.

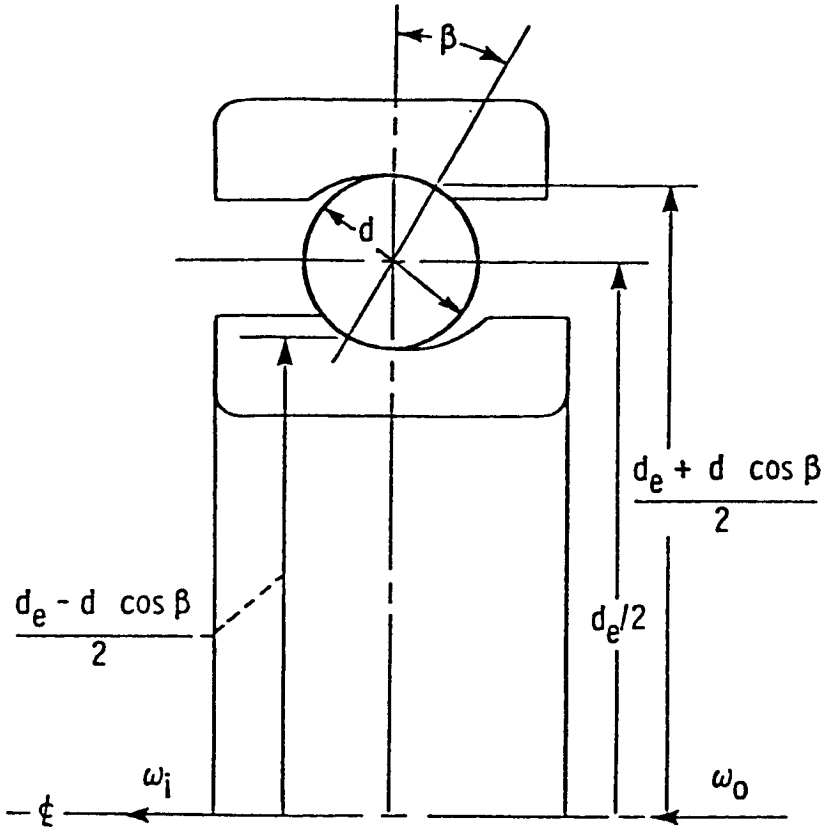

Fig. A.1 Cross section of shifted ball bearing.

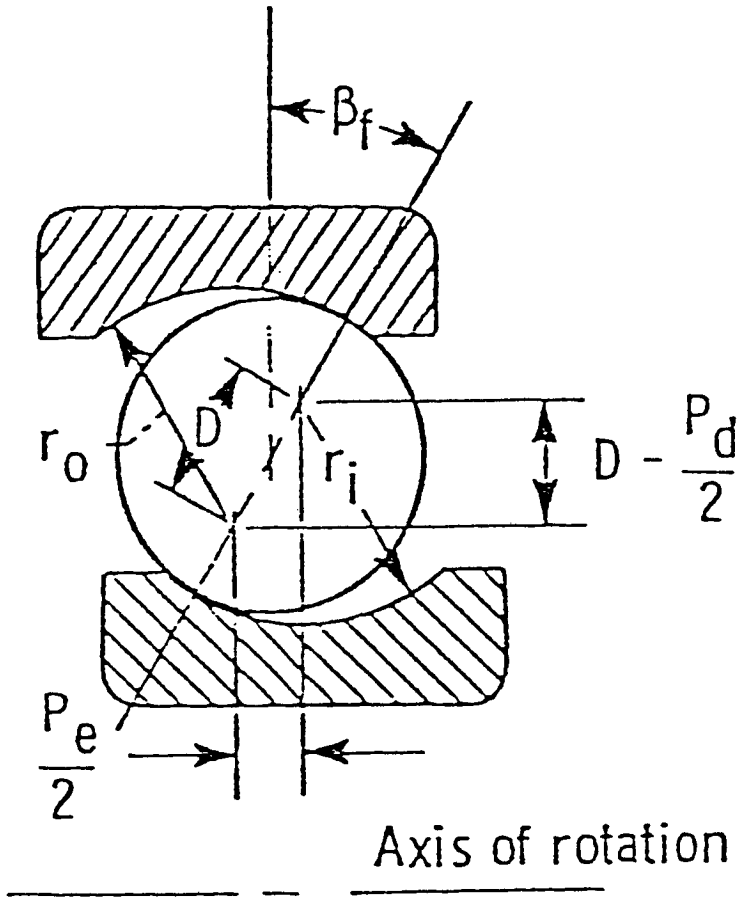

Fig. A.2 Cross section of shifted ball bearing showing ball-race contact.

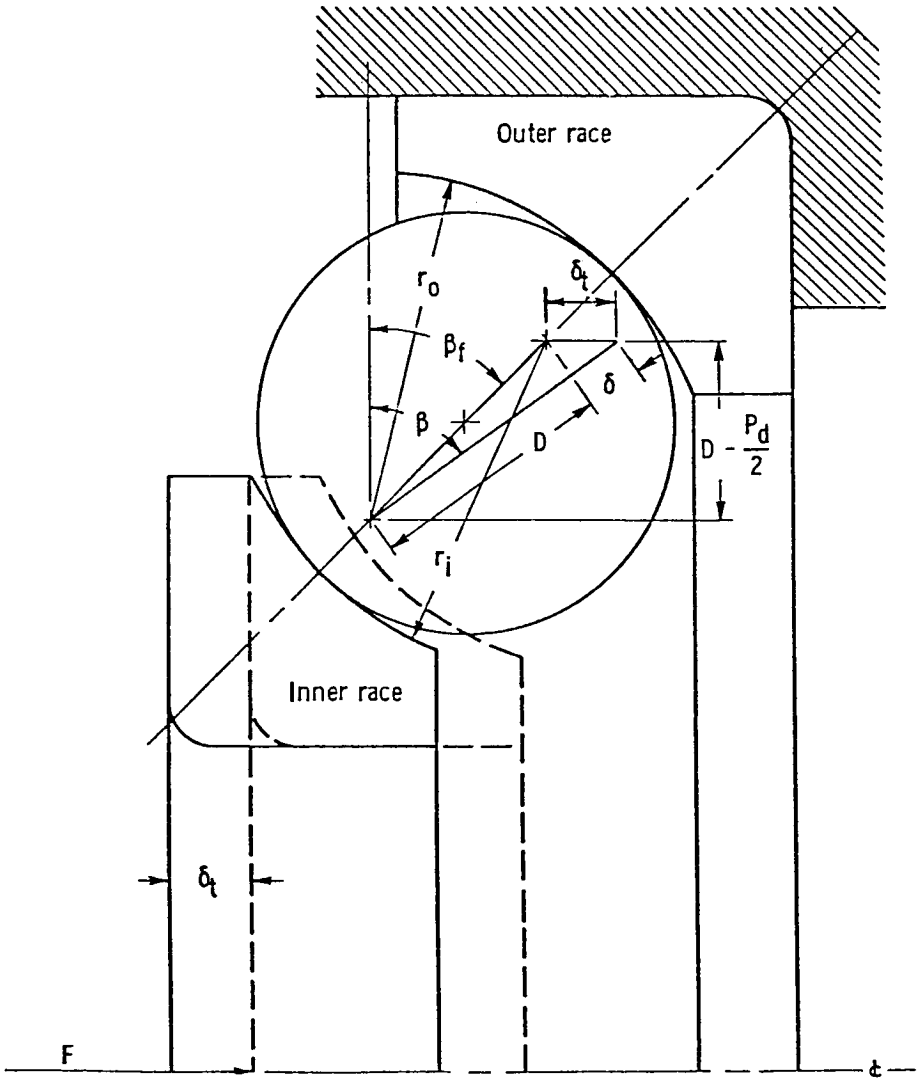

Fig. A.3 Angular contact bearing under thrust load.

TABLE A.1.- NO SLIP BSR
AND CONTACT ANGLE β
FOR ITI 11532-A
TEST BEARING

Load, lbs	BSR	β, degree
0	2.7499	13.54[a]
100	2.7508	14.75
200	2.7513	15.37
300	2.7517	15.85

[a]Free contact angle
by definition

TABLE A.2.- NO SLIP BSR
AND CONTACT ANGLE β
FOR ITI 8990-A
TEST BEARING

Load, lbs	BSR	β, degree
0	2.6826	13.54[a]
100	2.6835	14.75
200	2.6840	15.36
300	2.6844	15.84
350	2.6846	16.04

[a]Free contact angle
by definition

APPENDIX B

ERROR ANALYSIS FOR BALL SPEED MEASUREMENT AND BASIC SPEED RATIO

The BSR is defined as the ball spin rate divided by the difference in the inner and outer race speeds. The error for the BSR is

$$\frac{\hat{\delta}BSR}{BSR} = \left[\left(\frac{\delta\omega_B}{\omega_B}\right)^2 + \left(\frac{\hat{\delta\omega}_i}{\omega_i}\right)^2 + \left(\frac{\hat{\delta\omega}_o}{\omega_o}\right)^2\right]^{1/2} \qquad (B.1)$$

where ω_B, ω_i, and ω_o are the angular velocities of the ball, inner and outer races, respectively and $\hat{\delta}$ is the dimensional error associated with each quantity.

The error in the inner and outer race speed measurements comes from the digital counters which are connected directly to the oscillator of the power supplies. The inner race speed remains fixed during a test so that its error is $\pm$0.1 counts for a nominal reading of 66 000 counts. The outer race speed is adjusted to bring the ball complement to a stationary position so that its error is $\pm$0.4 counts for a nominal reading of 95 000 counts.

The ball speed error is not as straight forward and requires a calibration procedure. As mentioned in Chapter II, the ball speed measurement scheme is compared to a proximity probe in the measurement of the speed of a motor output shaft. Table B.1 shows the data from the counter and the proximity probe for the calibration test. The standard deviation is

$$\sigma = \left[\frac{\sum |\text{difference}|^2}{18 - 1} \right]^{1/2} = 0.333 \qquad \text{(B.2)}$$

The standard deviation of the mean is

$$\frac{0.333}{\sqrt{18}} = 0.079 \qquad \text{(B.3)}$$

The error in the ball speed measuring scheme is

$$e = \frac{0.079}{2475} = 0.00003 \qquad \text{(B.4)}$$

Substituting the calculated error values back into eq. (B.1), the error in the BSR is

$$\frac{\hat{\delta}BSR}{BSR} = \left[(0.00003)^2 + (0.0000041)^2 + (0.0000015)^2 \right]^{1/2} \qquad \text{(B.5)}$$

$$\frac{\hat{\delta}BSR}{BSR} = 0.00003 \Rightarrow 0.003 \text{ percent} \qquad \text{(B.6)}$$

TABLE B.2. - CALIBRATION DATA FOR
BALL SPEED MEASUREMENT SCHEME

Reading	Ball counter reading, rpm	Proximity probe counter reading, rpm	|Difference|, rpm
1.	2475.7	2475.0	0.7
2.	2475.2	2475.0	.2
3.	2475.5	2476.0	.5
4.	2476.7	2478.0	1.3
5.	2477.4	2478.0	.6
6.	2477.8	2478.0	.2
7.	2477.7	2478.0	.3
8.	2476.5	2476.0	.5
9.	2475.3	2475.0	.3
10.	2474.8	2476.0	1.2
11.	2477.5	2478.0	.5
12.	2478.2	2478.0	.2
13.	2478.1	2478.0	.1
14.	2477.9	2478.0	.1
15.	2478.6	2479.0	.4
16.	2479.3	2480.0	.7
17.	2479.8	2480.0	.2
18.	2477.6	2477.0	.6

APPENDIX C

ERROR ANALYSIS FOR

INITIAL OIL FILM THICKNESS

The initial oil film thickness is estimated from the following equation:

$$m_o = \rho_o \pi d^2 \delta \tag{C.1}$$

where m_o is the mass of the oil, ρ_o is the density of the oil, d is the diameter of the ball, and δ is the initial oil film thickness. From this equation, the error in the initial oil film thickness is:

$$\frac{\hat{\delta}\delta}{\delta} = \left[\left(\frac{\hat{\delta}m_o}{m_o}\right)^2 + 4\left(\frac{\hat{\delta}d}{d}\right)^2\right]^{1/2} \tag{C.2}$$

where $\hat{\delta}$ is the error for each given quantity. The error in the density is not known and is therefore not included.

The error in the ball size is stated by the manufacturer as $\pm$0.00004 in.

The error in the mass of the oil applied to the balls is introduced by the Mettler balance that is used. There are four measurements made in determining how much oil is placed on the balls. The two stainless steel screens that are used to hold the balls are cleaned with Freon and weighed. The clean balls are placed onto the screens and weighed as a unit. After the oil and Freon solution is mixed in an ultrasonic mixer, the clean balls are placed into the solution. The balls are lifted out of the solution with tygon wrapped tweezers, dried over a vacuum and placed back

onto the screens. The oiled balls and screens are weighed and then the balls are used in the assembling of a test bearing. The screens are reweighed to see how much oil is transferred from the balls to the screens. Each weight measurement is repeated at least four times and the error in each measurement is ± 0.0001 g.

The mass of the oil on the balls is the difference in the weight of the oiled balls and screens and the clean balls and screens

$$m_o = m_{\text{screens + balls + oil}} - m_{\text{screens + balls}} \tag{C.3}$$

The mass of oil left on the screens is typically between 0 and 0.0002 g and negative values are occasionally obtained so that the mass of oil on the screens is neglected. The error in the two quantities is the standard deviation divided by the square root of the number of points taken for each quantity N

$$\hat{\delta}m_{\text{screens + balls + oil}} = \frac{\sigma m_{\text{screens + balls + oil}}}{\sqrt{N}} \tag{C.4}$$

$$\hat{\delta}m_{\text{screens + balls}} = \frac{\sigma m_{\text{screens + balls}}}{\sqrt{N}} \tag{C.5}$$

The error of the mass of oil is

$$\hat{\delta}m_o = \left[(\hat{\delta}m_{\text{screens + balls + oil}})^2 + (\hat{\delta}m_{\text{screens + balls}})^2\right]^{1/2} \tag{C.6}$$

For the worst case of only one weight measurement per quantity, the error in the mass is

$$\hat{\delta}m_o = \left[(0.0001)^2 + (0.0001)^2\right]^{1/2} = \sqrt{2}\,(0.0001) \tag{C.7}$$

The balls are 3/8 in. in diameter and a typical value of m_o is 0.0020 g so that the error in the initial oil film thickness is

$$\frac{\hat{\delta}\delta}{\delta} = \left[\left(\frac{\sqrt{2}\ (0.0001)}{0.002}\right)^2 + 4\left(\frac{0.00004}{\frac{3}{8}}\right)^2\right]^{1/2} \qquad (C.8)$$

$$\frac{\hat{\delta}\delta}{\delta} = 0.071 \Rightarrow 7.1 \text{ percent} \qquad (C.9)$$

OIL/FREON SOLUTION ERROR ANALYSIS

The oil used in the test is diluted with Freon so that various amounts of oil may be applied to a test bearing. The oil is measured out into a beaker using a 2.0 ml syringe that can be read to $\pm$0.01 ml. A 100 ml graduated cylinder is used to measure out the 50 ml of Freon which is placed into a 100 ml beaker with the oil. The graduated cylinder can be read to $\pm$0.1 ml. A typical amount used in a test is 0.6 ml so that the error in the ratio of oil to Freon of the mixture is

$$\frac{\hat{\delta}(\text{concentration})}{\text{concentration}} = \left[\left(\frac{0.01}{0.6}\right)^2 + \left(\frac{0.1}{50}\right)^2\right]^{1/2} \qquad (C.10)$$

$$\frac{\hat{\delta}(\text{concentration})}{\text{concentration}} = 0.17 \Rightarrow 1.7 \text{ percent} \qquad (C.11)$$

APPENDIX D

EXPERIMENTAL DATA FOR

TEST TO FAILURE NO. 1

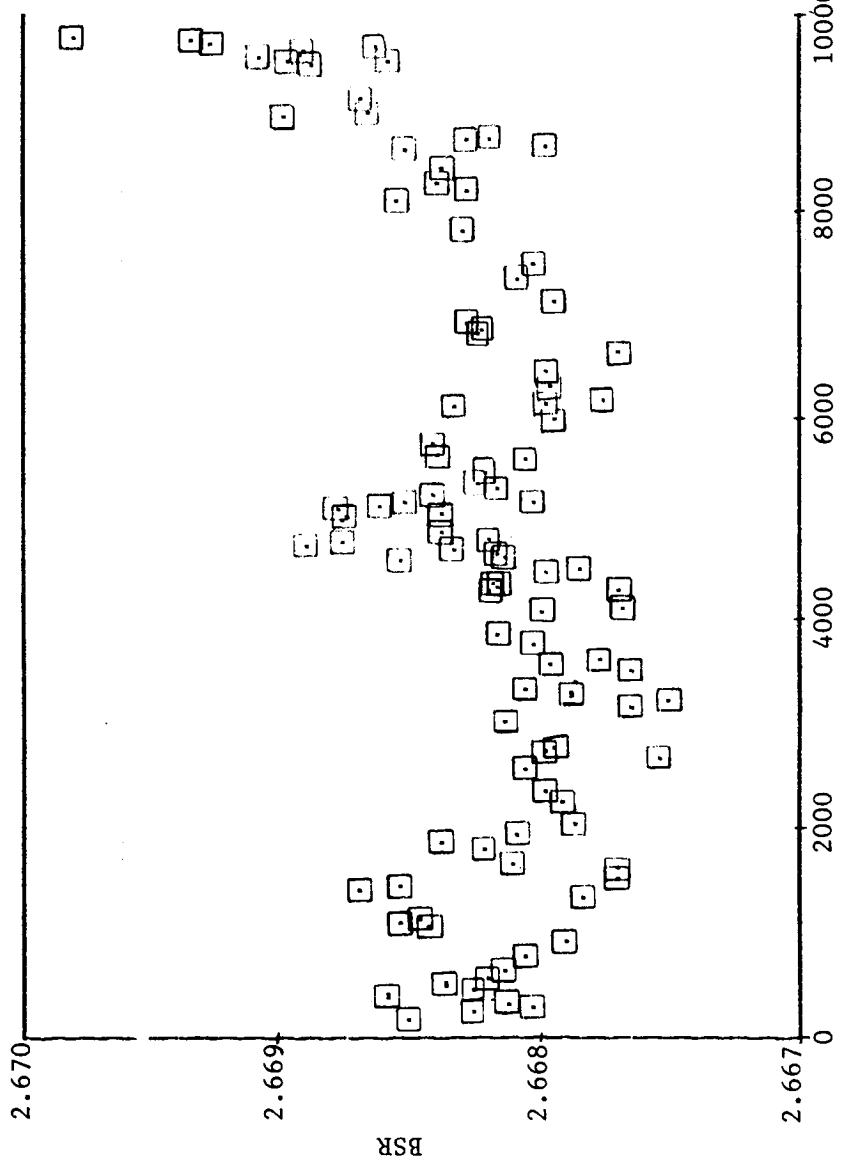

Fig. D.1 BSR vs. elapsed time for ITI 8990-A test bearing, 200 lb load, 0.014 SRG 200 oil/freon concentration.

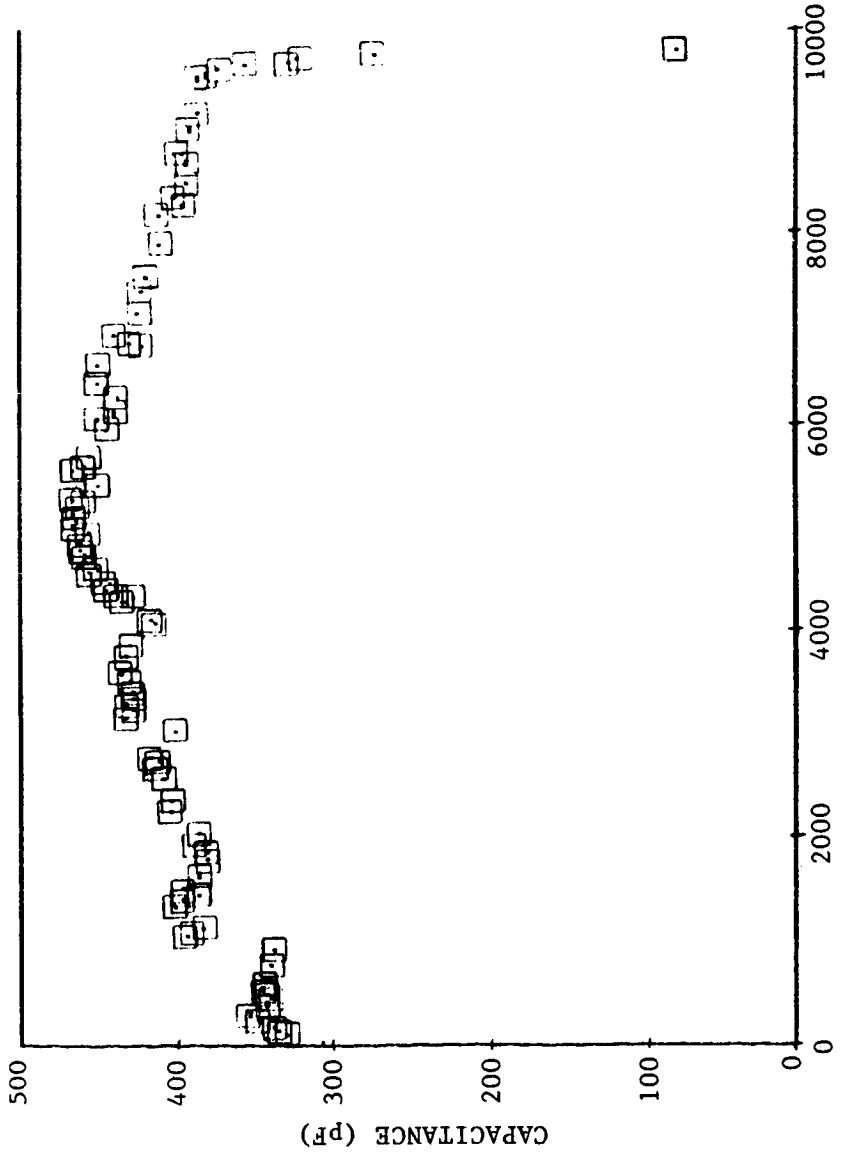

Fig. D.2 Capacitance vs. elapsed time for ITI 8990-A test bearing, 200 lb load, 0.014 SRG 200 oil/freon concentration.

Fig. D.3 Average film thickness vs. elapsed time for ITI 8990-A test bearing, 200 lb load, 0.014 SRG 200 oil/freon concentration.

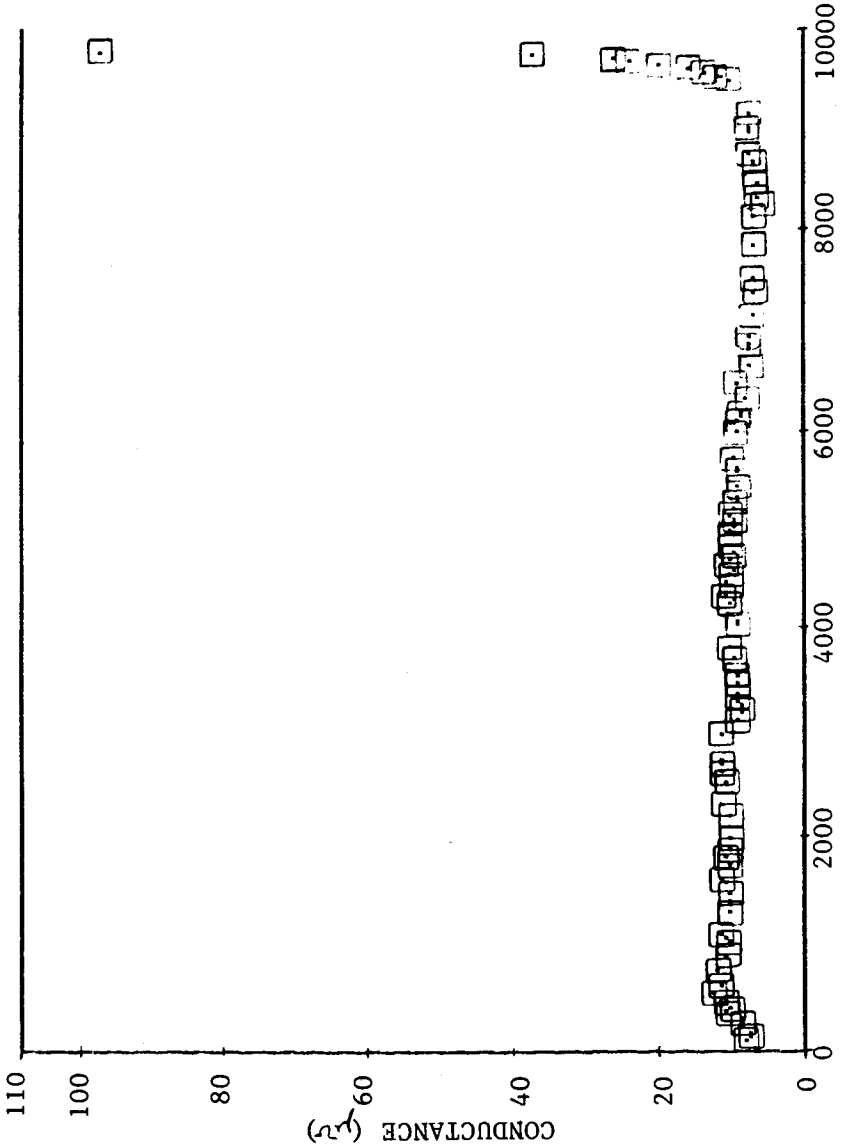

Fig. D-4 Conductance vs. elapsed time for ITI 8990-A test bearing, 200 lb load, 0.014 SRG 200 oil/freon concentration.

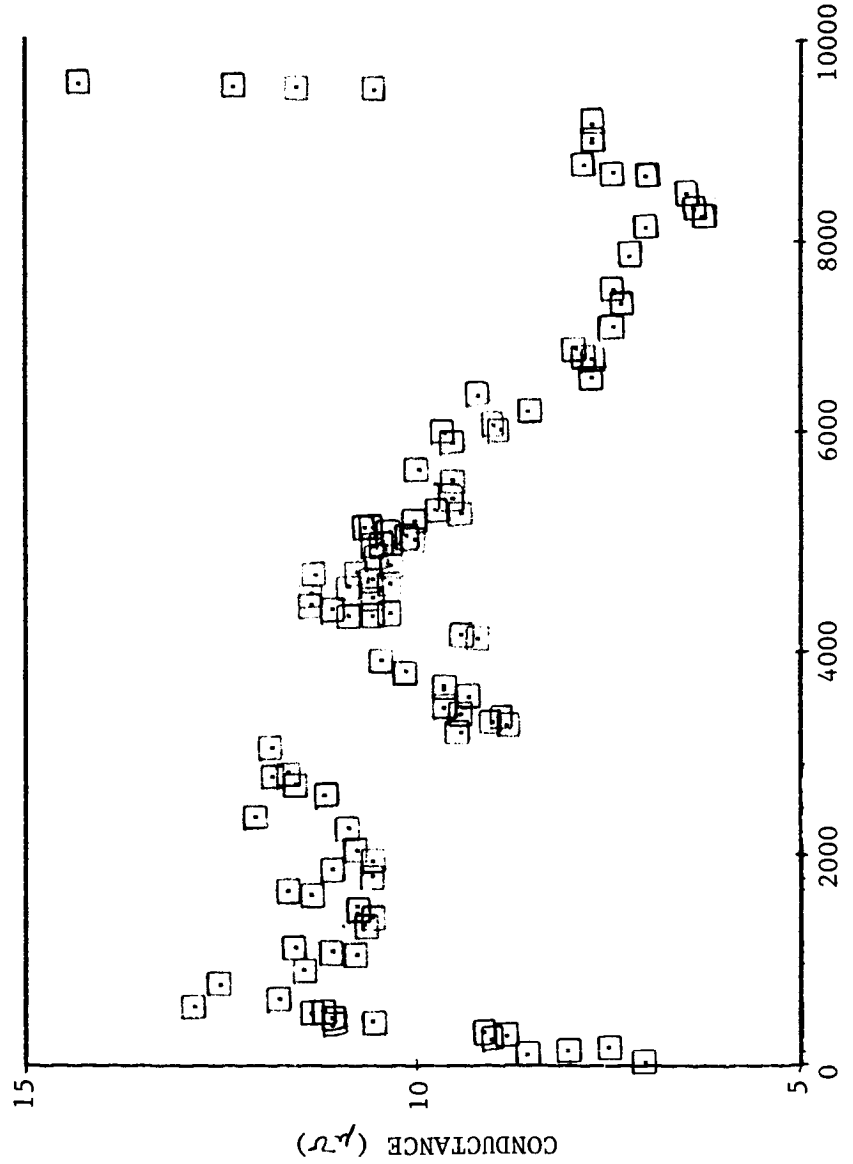

Fig. D-5 Conductance vs. elapsed time for ITI 8990-A test bearing, 200 lb load, 0.014 SRG 200 oil/freon concentration.

APPENDIX E

EXPERIMENTAL DATA FOR

TEST TO FAILURE NO. 2

TABULATED DATA FOR TEST TO FAILURE NO. 2

Elapsed time, sec	Inner race speed, rps	Outer race speed, rps	Ball race speed, rps	BSR	Capacitance, pF	Average film thickness, μin.	Conductance, μʊ
30	------	------	-------	-------	312	4.86	11.4
41	------	------	-------	-------	326	4.63	11.0
60	------	------	-------	-------	340	4.41	11.0
72	------	------	-------	-------	346	4.31	11.1
83	------	------	-------	-------	350	4.25	10.2
123	37.711	26.495	176.535	2.74949	352	4.23	10.0
142	37.711	26.494	176.547	2.74973	348	4.29	9.8
166	37.711	26.494	176.529	2.74943	351	4.24	9.7
212	37.711	26.505	176.547	2.74926	349	4.27	9.6
236	37.711	26.505	176.564	2.74952	353	4.21	10.2
255	37.711	26.510	176.581	2.74960	352	4.23	10.1
328	37.711	26.469	176.456	2.74939	334	4.49	10.0
348	37.711	26.482	176.406	2.74806	340	4.41	9.7
369	37.711	26.485	176.416	2.74810	338	4.43	9.9
394	37.711	26.483	176.393	2.74780	340	4.41	9.7
426	37.712	26.481	176.377	2.74762	338	4.43	9.7
443	37.712	26.480	176.380	2.74770	347	4.30	9.7
477	37.712	26.522	176.625	2.74974	345	4.33	9.3
492	37.712	26.522	176.638	2.74991	345	4.33	9.7
513	37.712	26.510	176.633	2.75036	348	4.29	9.5
528	37.712	26.511	176.623	2.75015	350	4.25	9.5
552	37.713	26.511	176.627	2.75019	356	4.18	9.6
570	37.713	26.515	176.633	2.75014	357	4.16	9.3
600	37.713	26.515	176.628	2.75001	357	4.16	9.5
622	37.713	26.517	176.636	2.75007	356	4.18	9.3
642	37.713	26.518	176.644	2.75017	355	4.20	9.5
692	37.713	26.519	176.653	2.75025	367	4.03	8.5
709	37.713	26.520	176.641	2.75000	365	4.06	8.5
725	37.713	26.520	176.641	2.75000	364	4.07	8.0
757	37.713	26.520	176.641	2.74999	365	4.06	8.5
773	37.713	26.518	176.631	2.74991	366	4.04	8.4
793	37.713	26.518	176.629	2.74989	367	4.03	8.5
814	37.713	26.518	176.635	2.74997	367	4.03	8.7
849	37.713	26.519	176.632	2.74991	366	4.04	8.5
935	37.714	26.526	176.695	2.75056	371	3.98	8.5
974	37.714	26.518	176.609	2.74955	371	3.98	8.6
1011	37.714	26.519	176.616	2.74960	371	3.98	9.1
1032	37.714	26.520	176.616	2.74957	367	4.03	9.3
1069	37.714	26.520	176.632	2.74981	365	4.06	9.6
1094	37.714	26.522	176.634	2.74976	364	4.12	9.1
1112	37.714	26.522	176.634	2.74977	360	4.14	9.6

TABULATED DATA FOR TEST TO FAILURE NO. 2 - CONTINUED

Elapsed time, sec	Inner race speed, rps	Outer race speed, rps	Ball race speed, rps	BSR	Capacitance, pF	Average film thickness, μin.	Conductance, μ℧
1132	37.714	26.524	176.636	2.74971	359	4.15	9.5
1149	37.714	26.524	176.637	2.74973	358	4.15	9.8
1167	37.714	26.522	176.632	2.74973	358	4.15	9.3
1206	37.715	26.523	176.648	2.74994	353	4.21	9.7
1228	37.715	26.523	176.646	2.74990	349	4.27	9.6
1247	37.715	26.523	176.648	2.74993	354	4.21	9.6
1268	37.715	26.523	176.646	2.74990	350	4.25	9.9
1292	37.715	26.524	176.645	2.74983	346	4.31	10.0
1339	37.715	26.524	176.642	2.74978	370	3.99	8.0
1362	37.715	26.524	176.648	2.74987	373	3.96	8.4
1404	37.715	26.524	176.634	2.74966	380	3.87	8.1
1465	37.715	26.523	176.636	2.74975	376	3.92	8.3
1550	37.714	26.522	176.616	2.74949	377	3.90	8.2
1588	37.714	26.520	176.625	2.74970	373	3.96	8.1
1623	37.714	26.520	176.622	2.74965	376	3.92	7.8
1635	37.714	26.520	176.623	2.74966	381	3.86	8.0
1792	37.713	26.515	176.562	2.74901	398	3.67	7.0
1815	37.713	26.515	176.562	2.74900	403	3.62	6.8
1842	37.713	26.515	176.553	2.74887	408	3.57	6.5
1869	37.713	26.513	176.555	2.74901	412	3.53	6.4
1905	37.712	26.512	176.548	2.74897	415	3.50	6.4
1932	37.712	26.511	176.547	2.74899	414	3.51	6.3
1979	37.712	26.515	176.553	2.74890	411	3.54	6.0
2041	37.712	26.515	176.471	2.74763	414	3.51	6.5
2057	37.712	26.515	176.494	2.74797	415	3.50	6.3
2095	37.712	26.519	176.514	2.74811	418	3.47	6.6
2124	37.712	26.519	176.513	2.74809	409	3.56	6.7
2180	37.711	26.519	176.558	2.74884	389	3.77	8.5
2200	37.711	26.520	176.566	2.74889	386	3.80	8.6
2218	37.711	26.520	176.566	2.74890	387	3.79	8.6
2234	37.711	26.520	176.563	2.74885	388	3.79	8.7
2250	37.711	26.520	176.557	2.74875	388	3.79	8.8
2314	37.711	26.519	176.563	2.74889	395	3.71	8.9
2347	37.711	26.519	176.551	2.74870	391	3.75	9.0
2372	37.711	26.520	176.576	2.74908	389	3.77	8.8
2393	37.711	26.519	176.572	2.74902	393	3.73	8.7
2411	37.711	26.520	176.571	2.74900	389	3.77	8.8
2499	37.711	26.520	176.567	2.74894	382	3.84	8.7
2582	37.711	26.521	176.580	2.74906	377	3.90	8.4
2615	37.711	26.522	176.574	2.74898	374	3.94	8.7
2713	37.711	26.521	176.571	2.74896	403	3.62	5.9
2773	37.711	26.524	176.541	2.74838	405	3.60	5.3

TABULATED DATA FOR TEST TO FAILURE NO. 2 - CONTINUED

Elapsed time, sec	Inner race speed, rps	Outer race speed, rps	Ball race speed, rps	BSR	Capacitance, pF	Average film thickness, μin.	Conductance, μ℧
2904	37.711	26.524	176.599	2.74929	407	3.58	3.8
2944	37.711	26.522	176.606	2.74946	409	3.56	4.0
3026	37.711	26.521	176.594	2.74932	409	3.56	4.4
3089	37.711	26.521	176.597	2.74938	409	3.56	4.2
3127	37.711	26.521	176.596	2.74937	409	3.56	4.2
3293	37.711	26.521	176.591	2.74930	405	3.60	4.1
3364	37.711	26.521	176.598	2.74940	406	3.59	4.3
3562	37.711	26.521	176.600	2.74944	403	3.62	4.2
3761	37.711	26.519	176.593	2.74940	402	3.63	4.1
3933	37.711	26.519	176.570	2.74902	408	3.57	4.4
4013	37.711	26.516	176.588	2.74944	417	3.48	4.0
4035	37.711	26.516	176.590	2.74947	417	3.48	4.7
4100	37.710	26.515	176.590	2.74954	420	3.45	4.5
4152	37.710	26.515	176.597	2.74965	417	3.48	5.1
4211	37.710	26.515	176.598	2.74966	413	3.52	5.0
4491	37.710	26.523	176.635	2.74988	408	3.57	3.3
4676	37.710	26.521	176.626	2.74984	406	3.59	3.4
4724	37.710	26.521	176.612	2.74961	408	3.57	3.3
5085	37.710	26.519	176.608	2.74965	424	3.41	3.1
5129	37.710	26.514	176.584	2.74947	423	3.42	3.4
5157	37.710	26.514	176.614	2.74993	421	3.44	3.1
5194	37.709	26.515	176.592	2.74964	421	3.44	3.5
5361	37.709	26.522	176.615	2.74970	402	3.63	3.4
5626	37.709	26.518	176.604	2.74969	406	3.59	4.0
5895	37.709	26.520	176.594	2.74947	408	3.57	4.4
6199	37.708	26.514	176.581	2.74957	403	3.62	3.9
6309	37.708	26.521	176.618	2.74982	411	3.54	3.0
6395	37.708	26.516	176.610	2.74990	416	3.42	2.5
6588	37.708	26.520	176.608	2.74974	416	3.49	2.5
6743	37.707	26.520	176.599	2.74962	409	3.56	2.6
7076	37.707	26.520	176.622	2.74998	405	3.60	2.7
7191	37.707	26.520	176.612	2.74982	408	3.57	2.8
7345	37.707	26.514	176.576	2.74952	417	3.48	2.9
7597	37.706	26.522	176.628	2.74999	407	3.57	2.8
7695	37.706	26.522	176.602	2.74960	419	3.46	3.3
7862	37.706	26.521	176.624	2.75000	414	3.51	3.2
8087	37.706	26.520	176.600	2.74965	406	3.59	4.7
8147	37.706	26.520	176.585	2.74942	417	3.48	3.2
8314	37.706	26.520	176.622	2.75000	422	3.43	2.9
8443	37.706	26.519	176.637	2.75027	420	3.45	3.0
8628	37.706	26.519	176.631	2.75017	417	3.48	2.9
8772	37.706	26.519	176.631	2.75012	422	3.43	3.8

TABULATED DATA FOR TEST TO FAILURE NO. 2 - CONCLUDED

Elapsed time, sec	Inner race speed, rps	Outer race speed, rps	Ball race speed, rps	BSR	Capacitance, pF	Average film thickness, μin.	Conductance, μ℧
8901	37.706	26.519	176.627	2.75016	407	3.58	3.8
8958	37.706	26.519	176.616	2.74994	406	3.59	4.0
8988	37.706	26.520	176.620	2.75001	409	3.56	3.9
9078	37.705	26.520	176.629	2.75016	416	3.49	4.0
9222	37.705	26.518	176.631	2.75027	408	3.57	4.6
9298	37.705	26.518	176.643	2.75046	407	3.58	4.5
9382	37.705	26.517	176.627	2.75023	406	3.59	4.8
9500	37.705	26.513	176.612	2.75021	413	3.52	5.0
9563	37.705	26.513	176.609	2.75015	400	3.65	5.1
9605	37.705	26.518	176.616	2.75004	408	3.57	5.3
9687	37.705	26.518	176.653	2.75063	408	3.57	5.3
9765	37.705	26.518	176.613	2.74999	408	3.57	5.7
9872	37.705	26.516	176.599	2.74983	411	3.54	5.4
10016	37.705	26.518	176.614	2.74998	405	3.60	5.1
10093	37.705	26.518	176.625	2.75019	412	3.53	5.0
10301	37.705	26.515	176.629	2.75036	411	3.54	4.5
10442	37.705	26.514	176.657	2.75085	412	3.53	5.8
10646	37.705	26.518	176.621	2.75014	413	3.52	5.6
10767	37.705	26.516	176.642	2.75057	410	3.55	6.5
10825	37.705	26.517	176.635	2.75042	418	3.47	6.1
10975	37.705	26.501	176.719	2.75240	443	3.25	8.0
10993	37.705	26.510	176.669	2.75124	457	3.14	9.2
11923	------	------	-------	-------	224	7.22	33.0
11030	------	------	-------	-------	177	9.61	48.0
11035	------	------	-------	-------	177	9.61	54.0
11040	------	------	-------	-------	160	----	51.0
11043	------	------	-------	-------	145	----	60.0
11046	------	------	-------	-------	135	----	65.0
11050	------	------	-------	-------	127	----	68.0
11053	------	------	-------	-------	118	----	72.0
11056	------	------	-------	-------	110	----	77.0
11059	------	------	-------	-------	100	----	82.0
11063	------	------	-------	-------	90	----	88.0
11066	------	------	-------	-------	65	----	96.0
11069	------	------	-------	-------	55	----	98.0

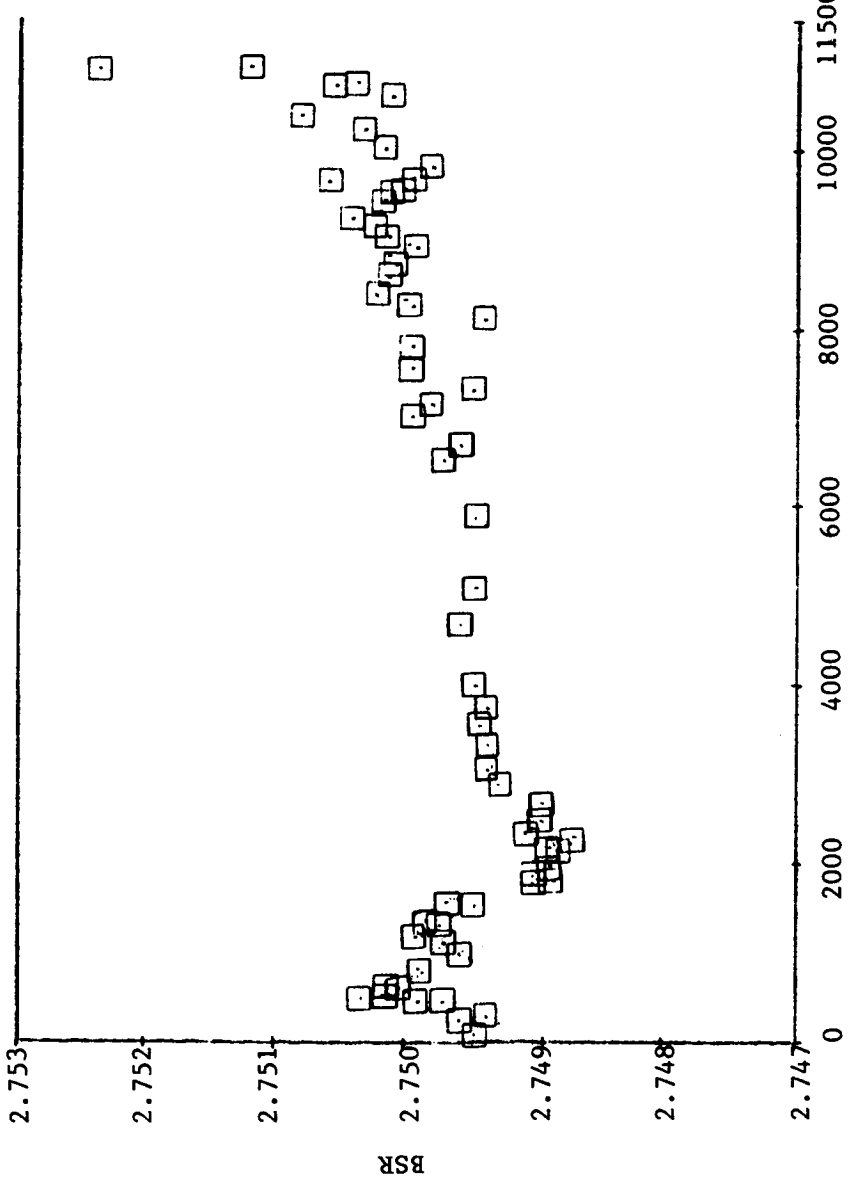

Fig. E.1 BSR vs. elapsed time for ITI 11532-A test bearing, 200 lb load, 0.008 SRG 200 oil/freon concentration.

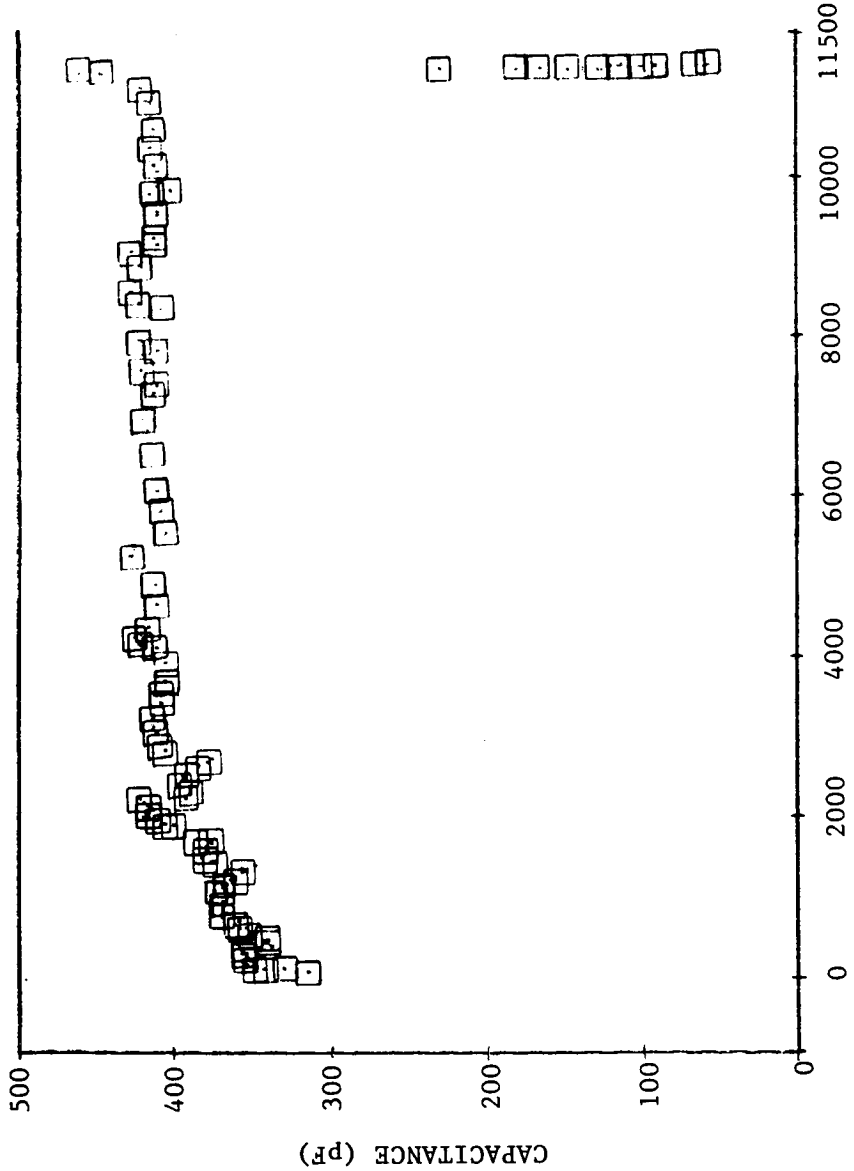

Fig. E.2 Capacitance vs. elapsed time for ITI 11532-A test bearing, 200 lb load, 0.008 SRG 200 oil/freon concentration.

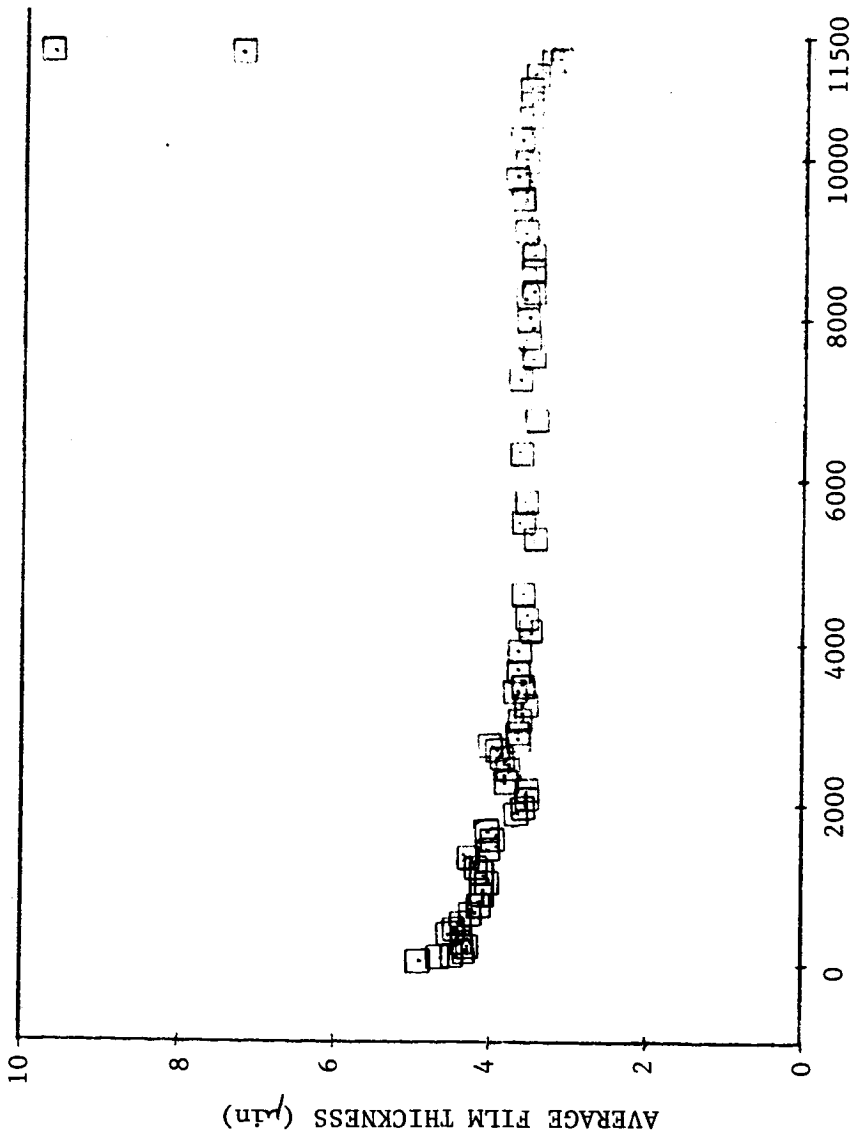

Fig. E.3 Average film thickness vs. elapsed time for ITI 11532-A test bearing, 200 lb load, 0.008 SRG 200 oil/freon concentration.

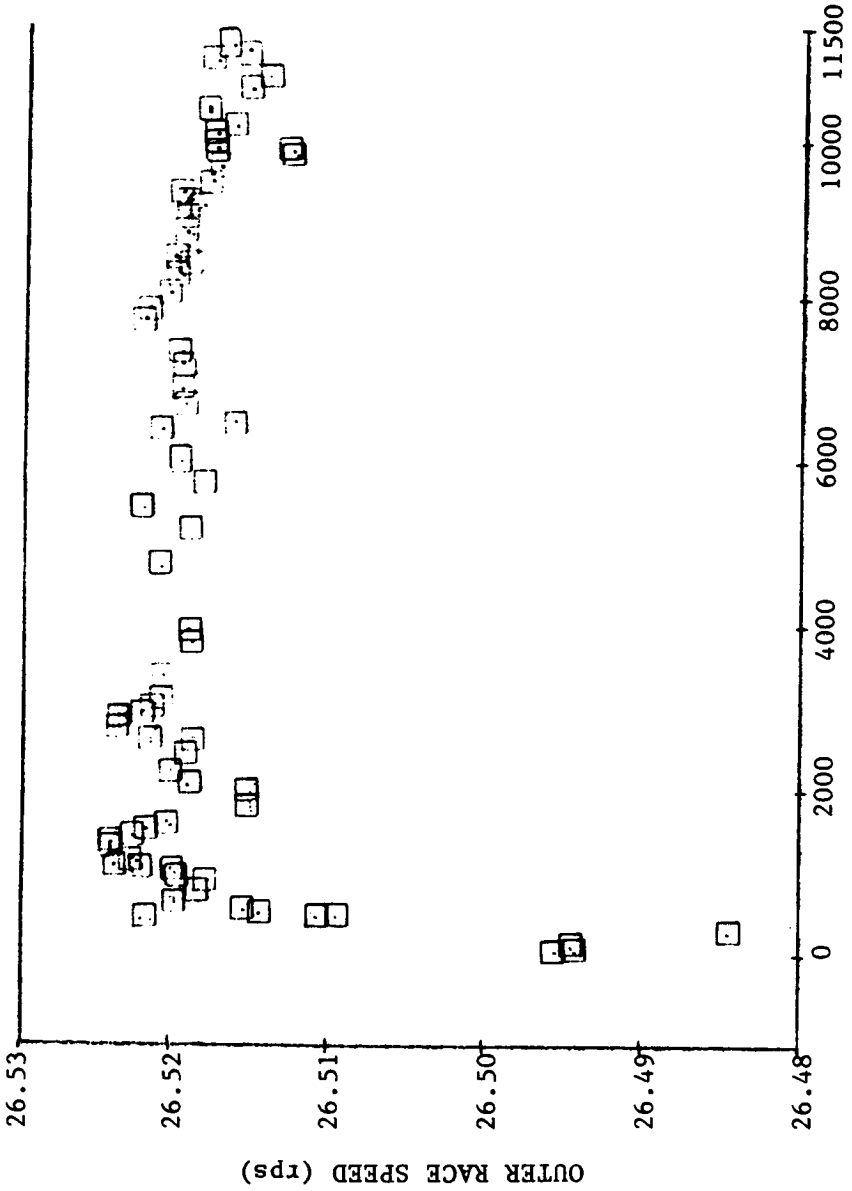

Fig. E.4 Outer race speed vs. elapsed time for ITI 11532-A test bearing, 200 lb load, 0.008 SRG 200 oil/freon concentration.

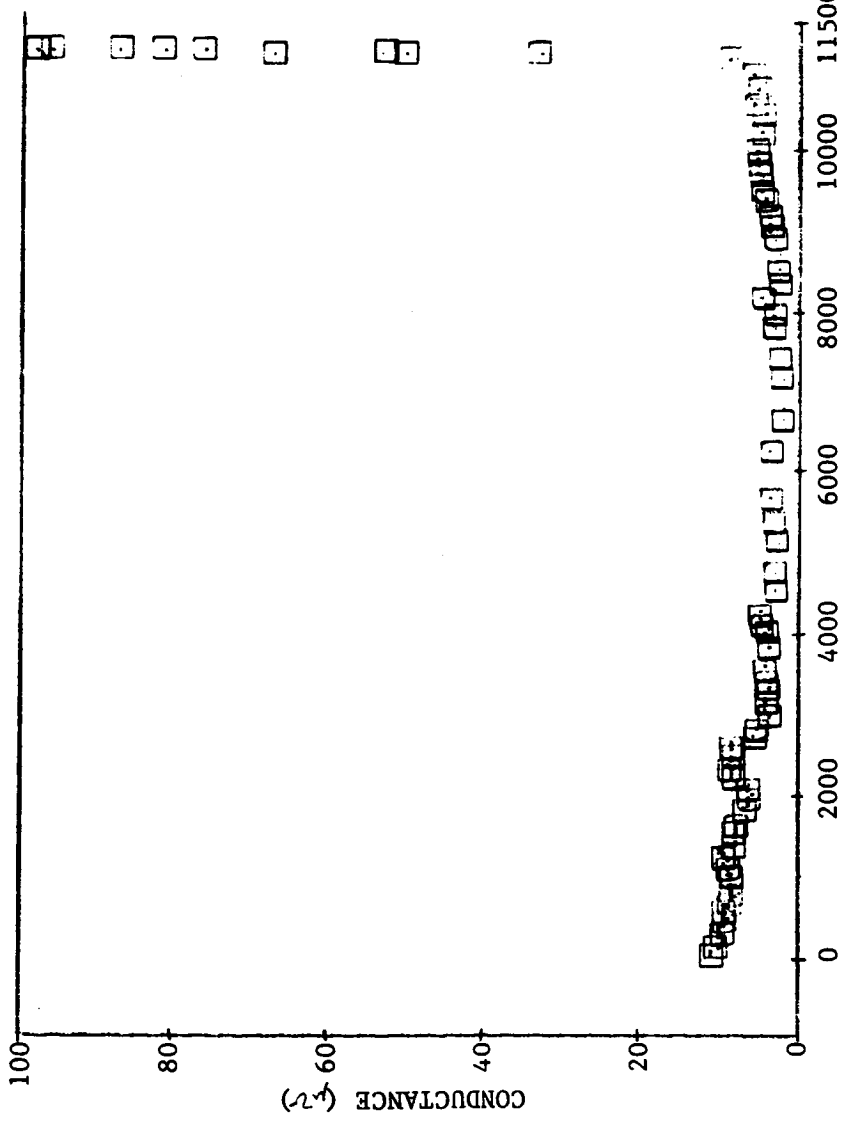

Fig. E.5 Conductance vs. elapsed time for ITI 11532-A test bearing, 200 lb load, 0.008 SRG 200 oil/freon concentration.

APPENDIX F

EXPERIMENTAL DATA FOR

BSR VERSUS OIL/FREON CONCENTRATION NO. 1

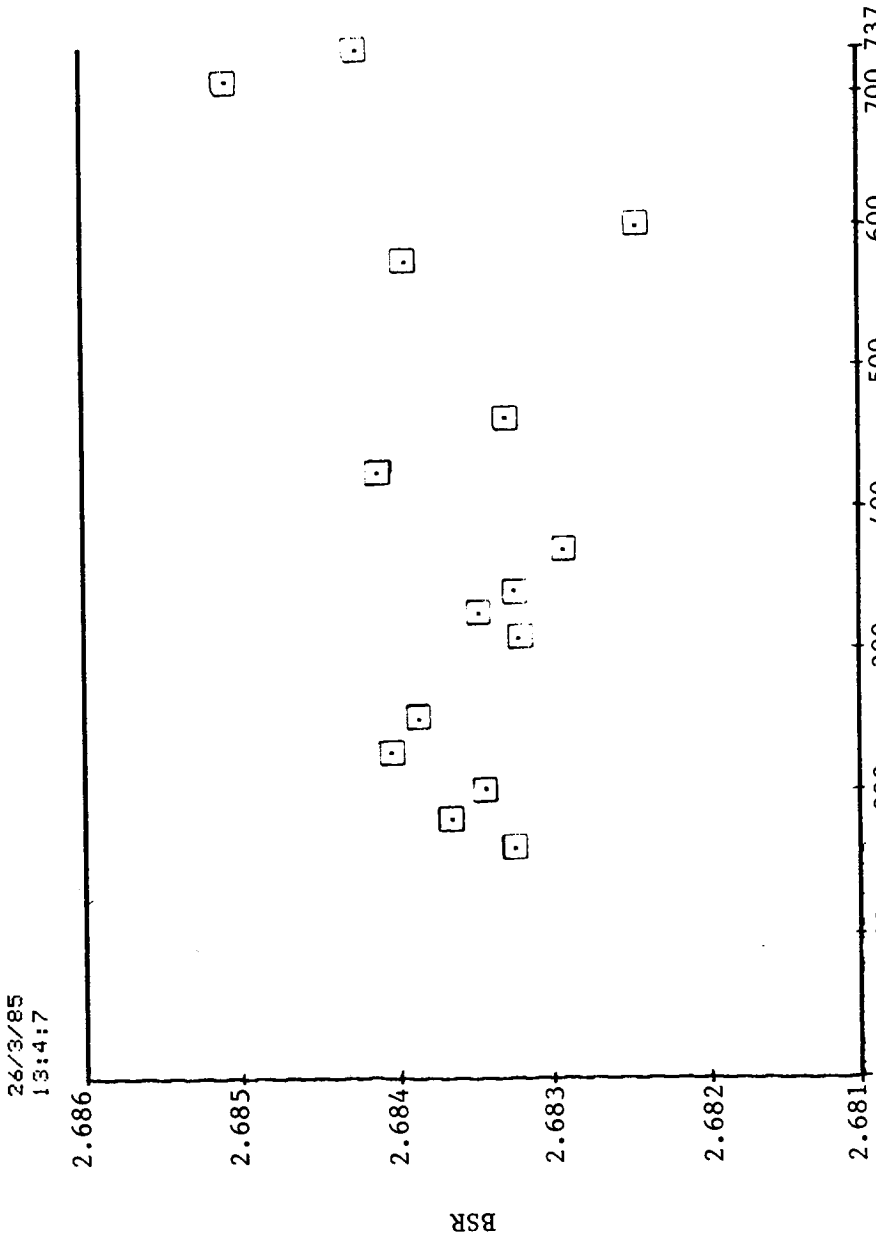

Fig. F.1 BSR vs. elapsed time for ITI 8990-A test bearing, 300 lb load, 0.002 SRG 200 oil/freon concentration.

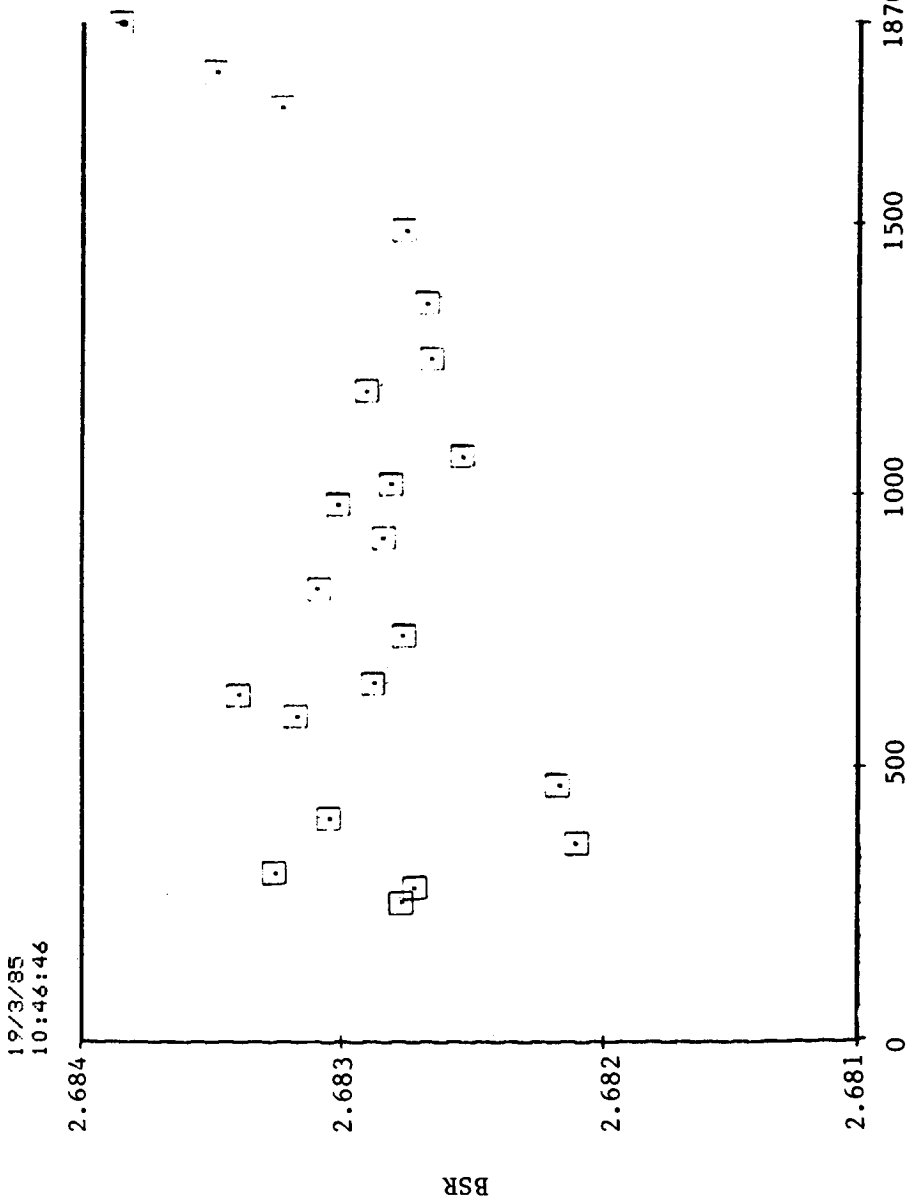

Fig. F.2 BSR vs. elapsed time for ITI 8990-A test bearing, 300 lb load, 0.004 SRG 200 oil/freon concentration.

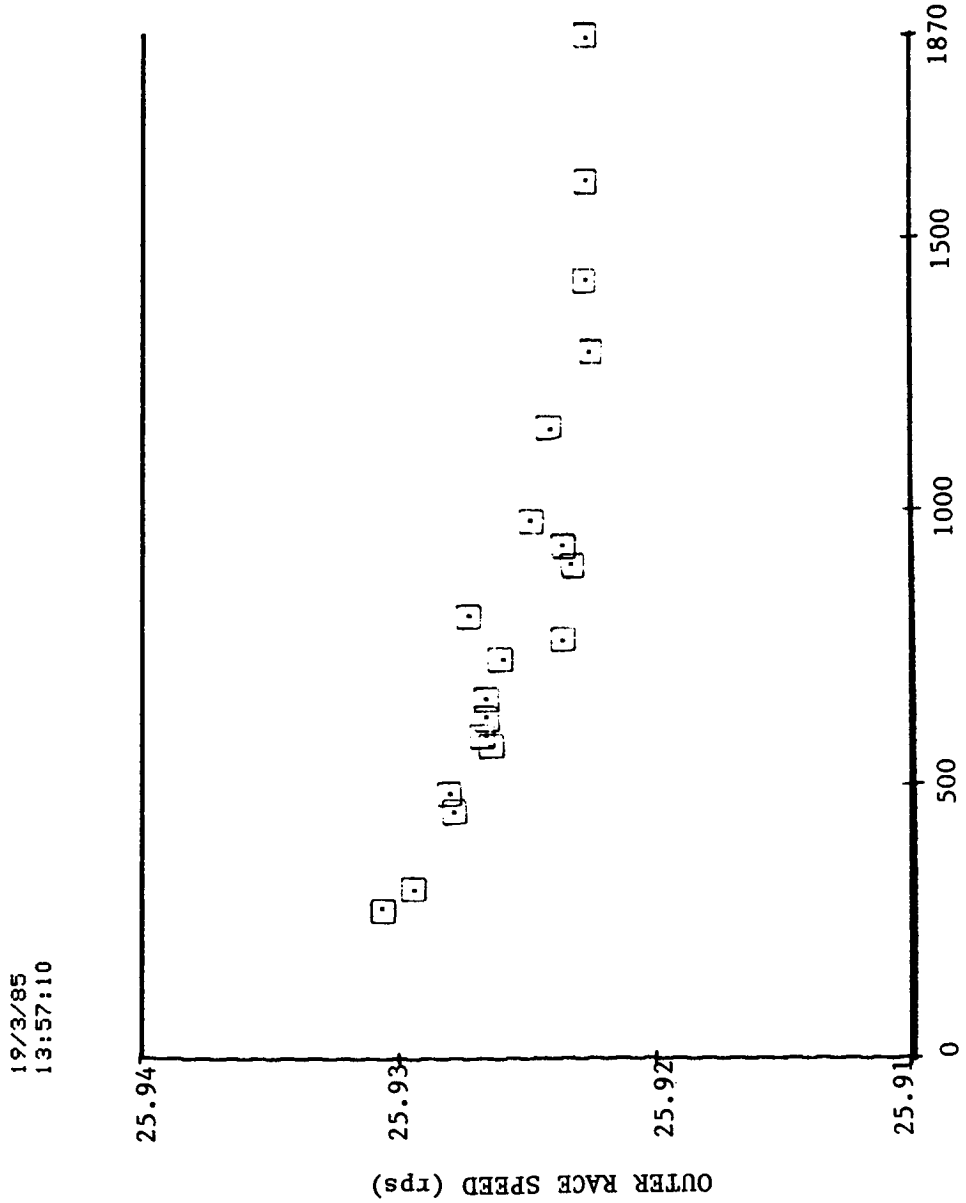

Fig. F.3 BSR vs. elapsed time for ITI 8990-A test bearing, 300 lb load, 0.004 SRG 200 oil/freon concentration.

C-3

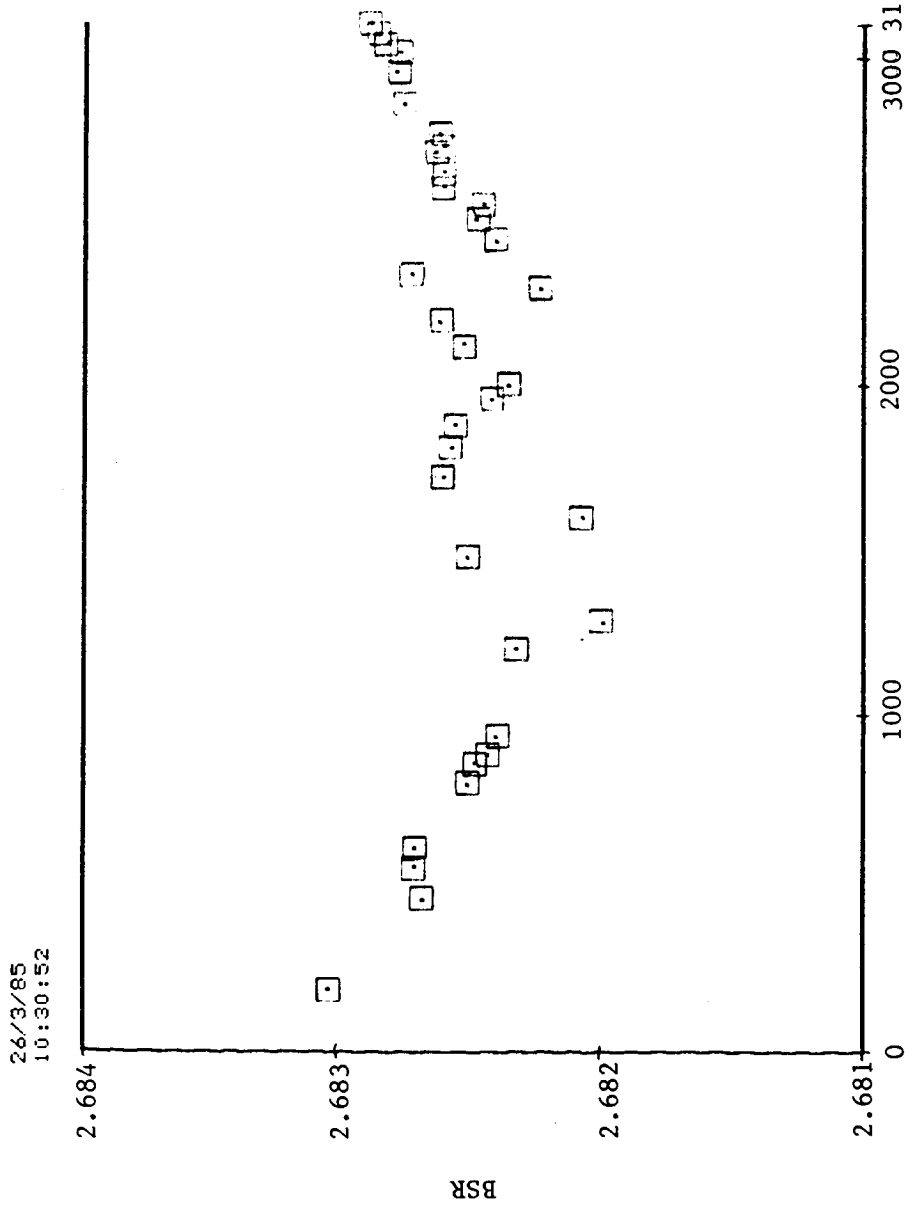

Fig. F.4 BSR vs. elapsed time for ITI 8990-A test bearing, 300 lb load, 0.006 SRG 200 oil/freon concentration.

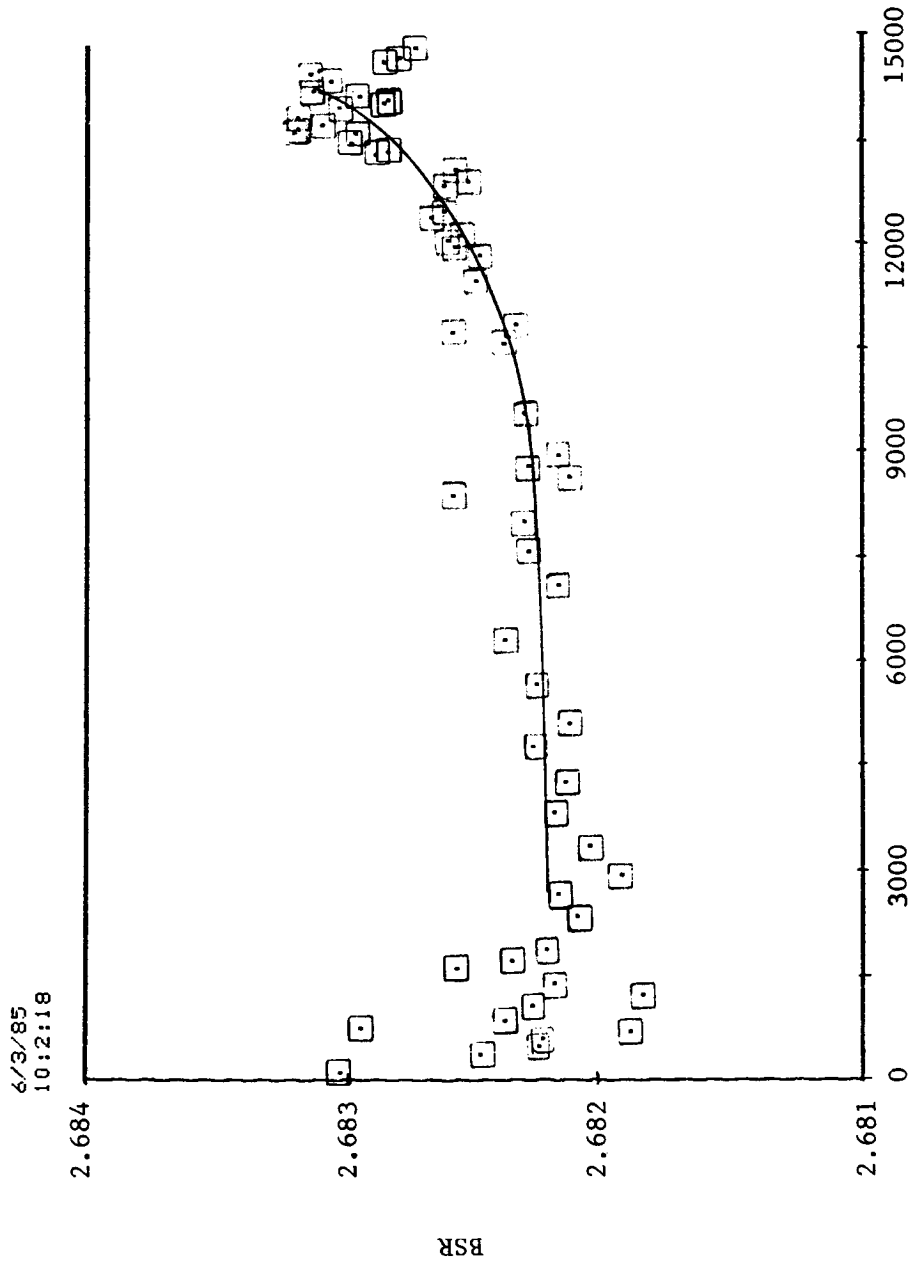

Fig. F.5 BSR vs. elapsed time for ITI 8990-A test bearing, 300 lb load, 0.010 SRG 200 oil/freon concentration.

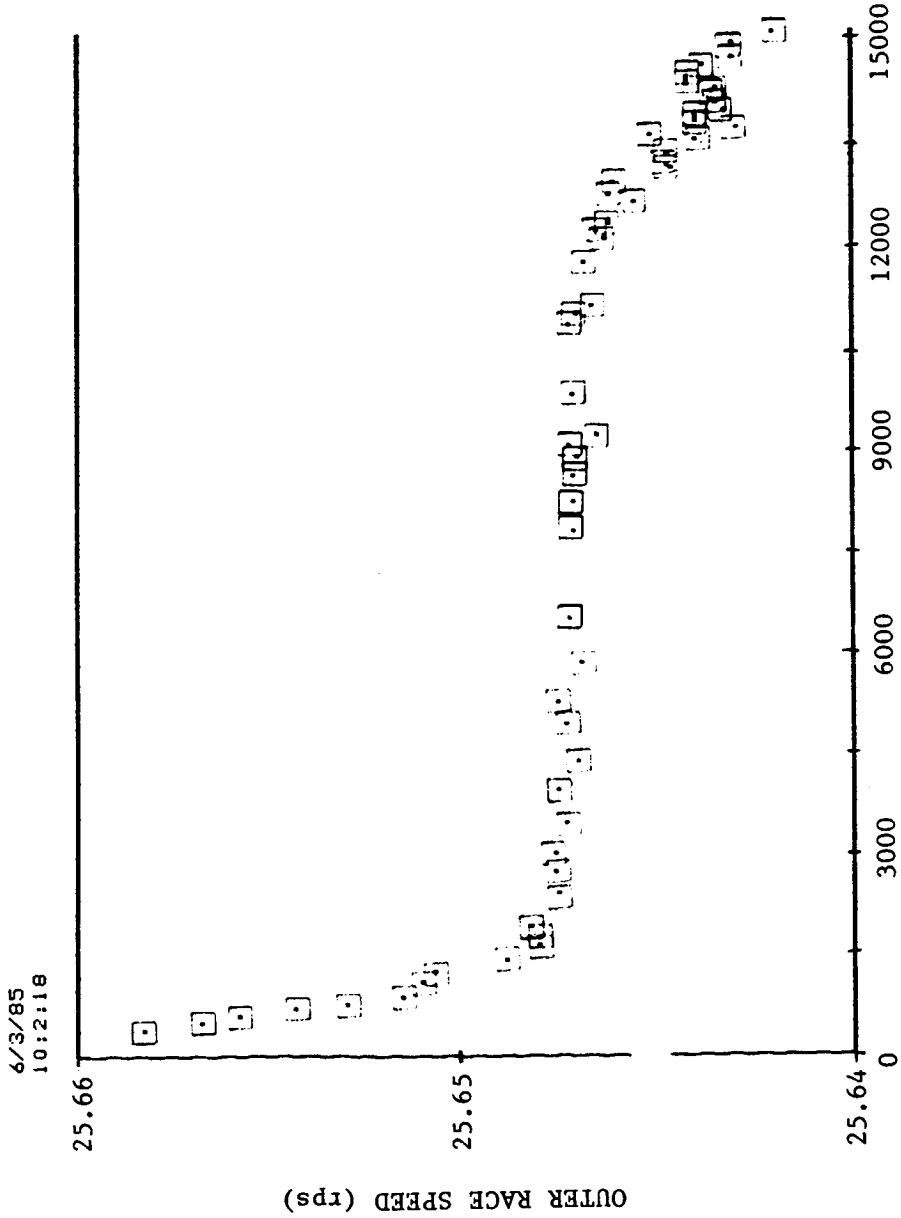

Fig. F.6 Outer race speed vs. elapsed time for ITI 8990-A test bearing, 300 lb load, 0.010 SRG 200 oil/freon concentration.

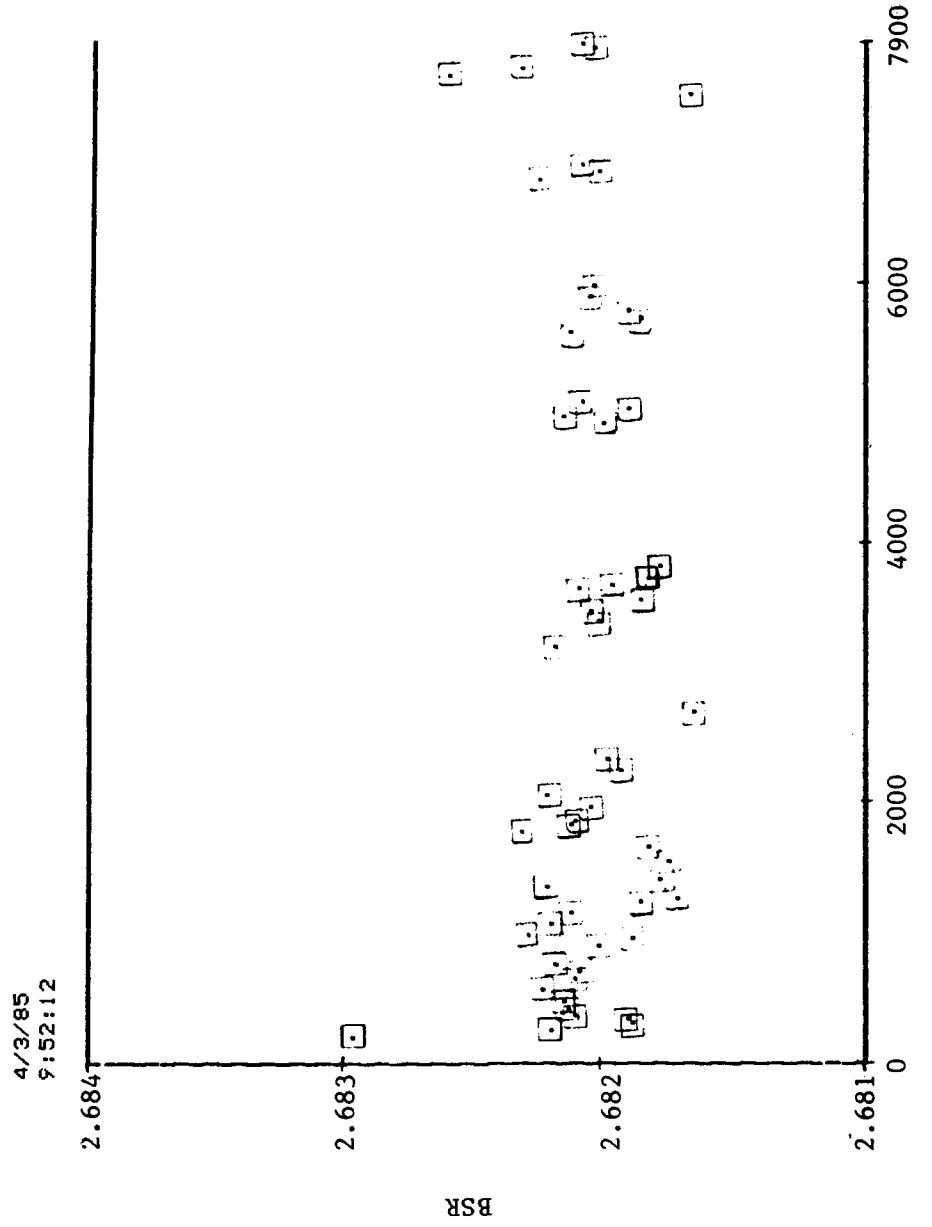

Fig. F.7 BSR vs. elapsed time for ITI 8990-A test bearing, 300 lb load, 0.010 SRG 200 oil/freon concentration.

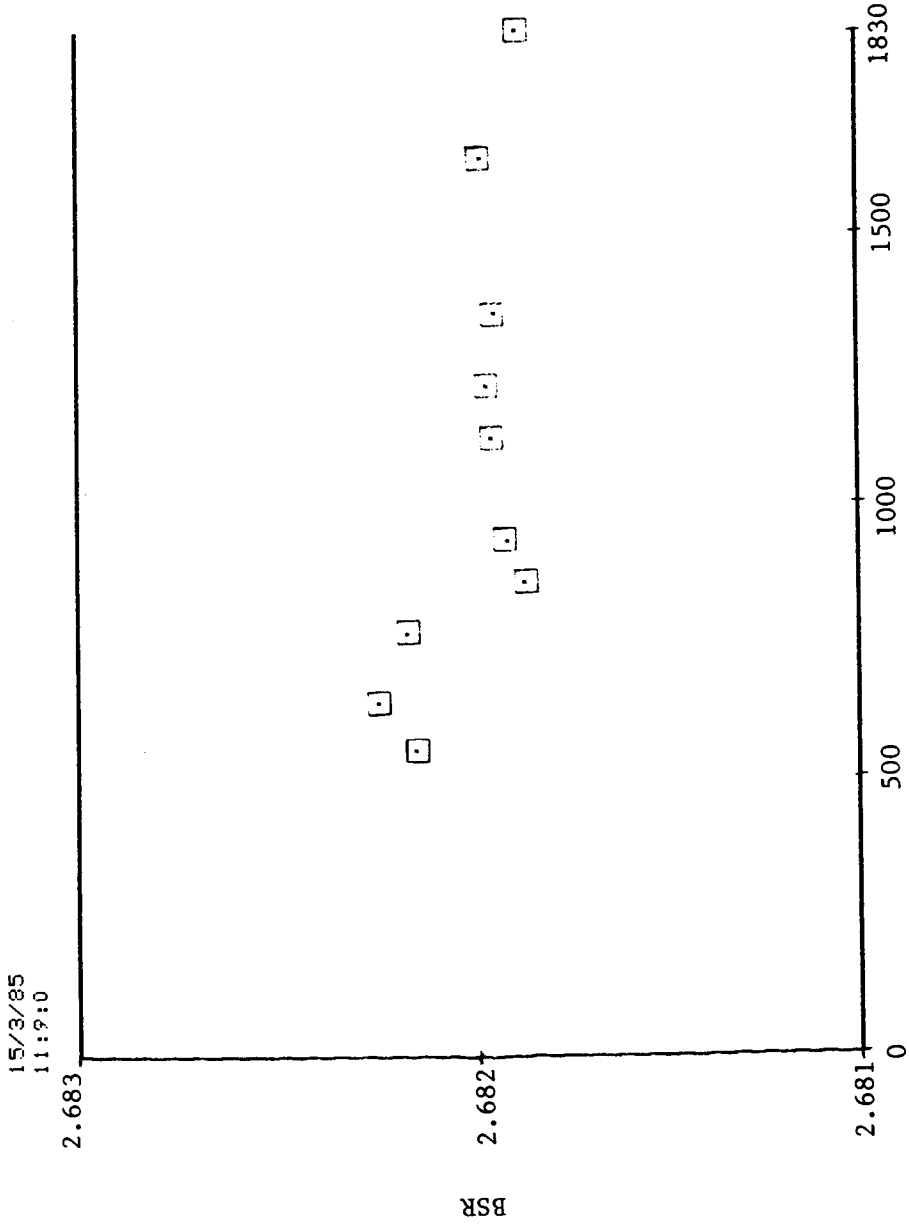

Fig. F.8 BSR vs. elapsed time for ITI 8990-A test bearing, 300 lb load, 0.010 SRG 200 oil/freon concentration.

ORIGINAL PAGE IS
OF POOR QUALITY

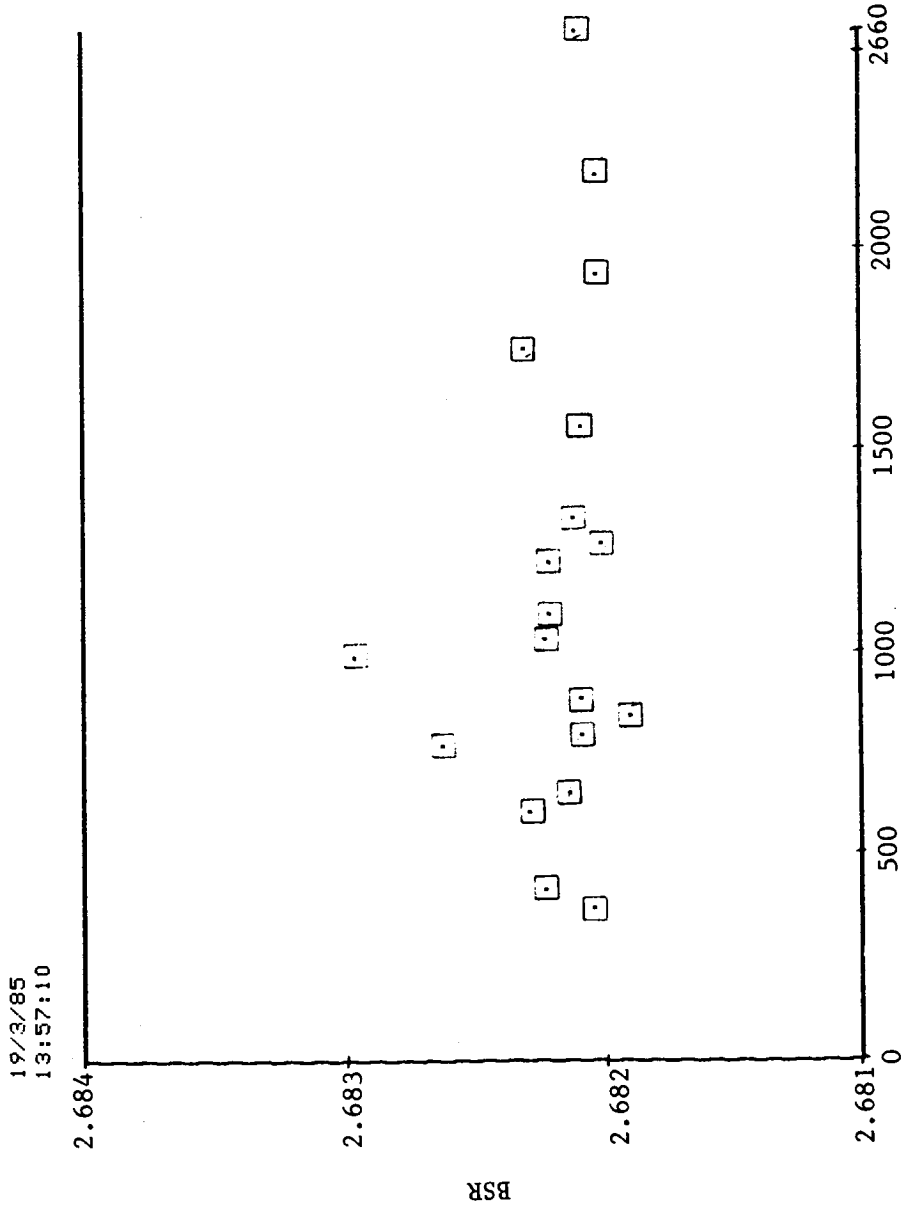

Fig. F.9 BSR vs. elapsed time for ITI 8990-A test bearing, 300 lb load, 0.014 SRG 200 oil/freon concentration.

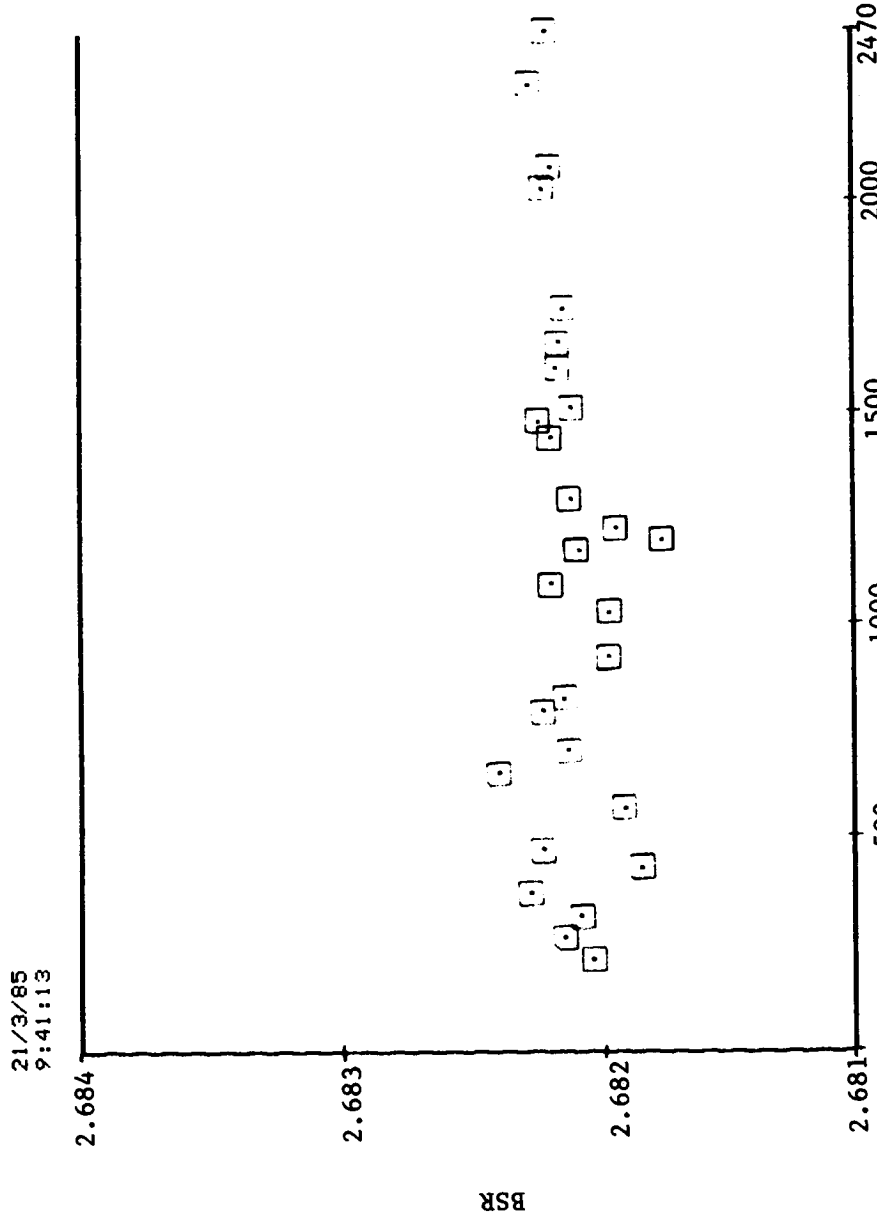

Fig. F.10 BSR vs. elapsed time for ITI 8990-A test bearing, 300 lb load, 0.020 SRG 200 oil/freon concentration.

APPENDIX G

EXPERIMENTAL DATA FOR

BSR VERSUS OIL/FREON CONCENTRATION NO. 2

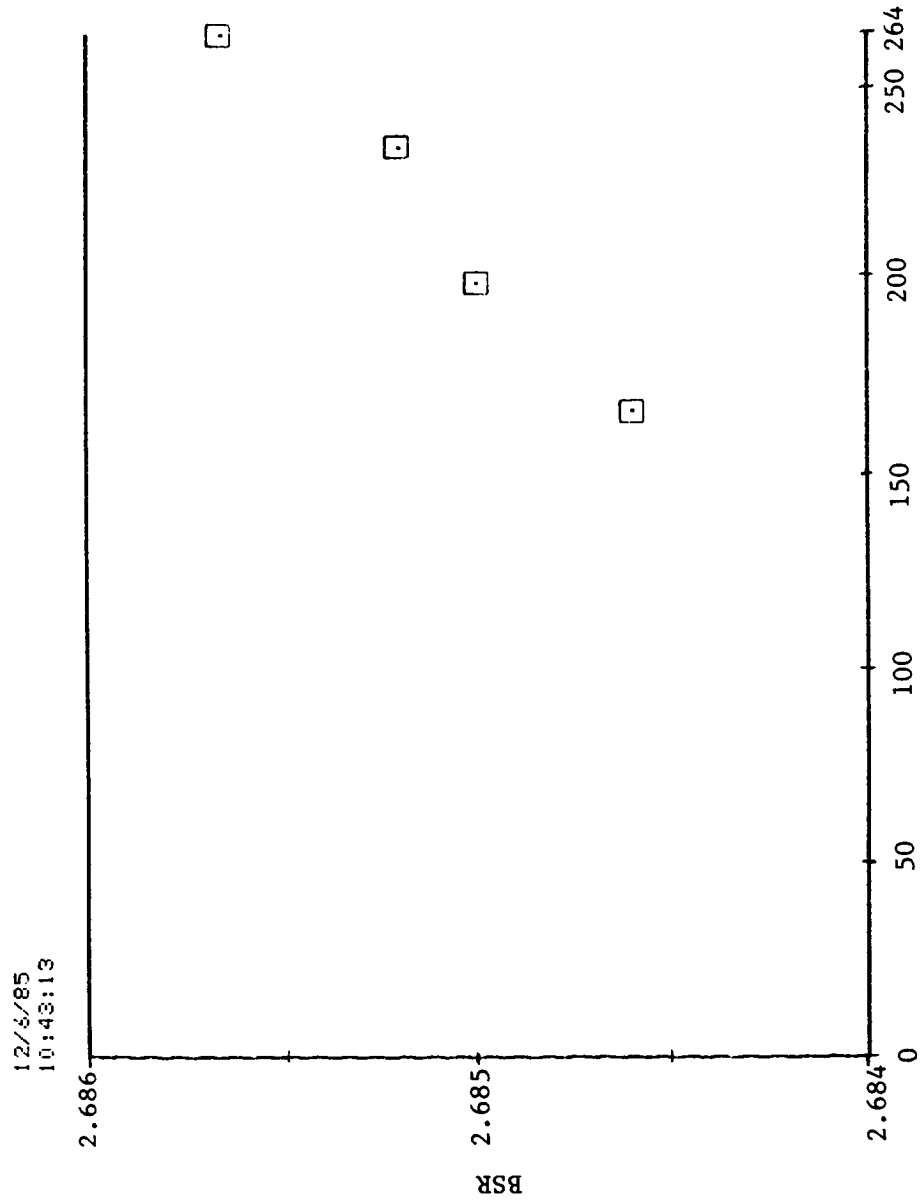

Fig. G.1 BSR vs. elapsed time for ITI 8990-A test bearing, 300 lb load, 0.002 SRG 200 oil/freon concentration.

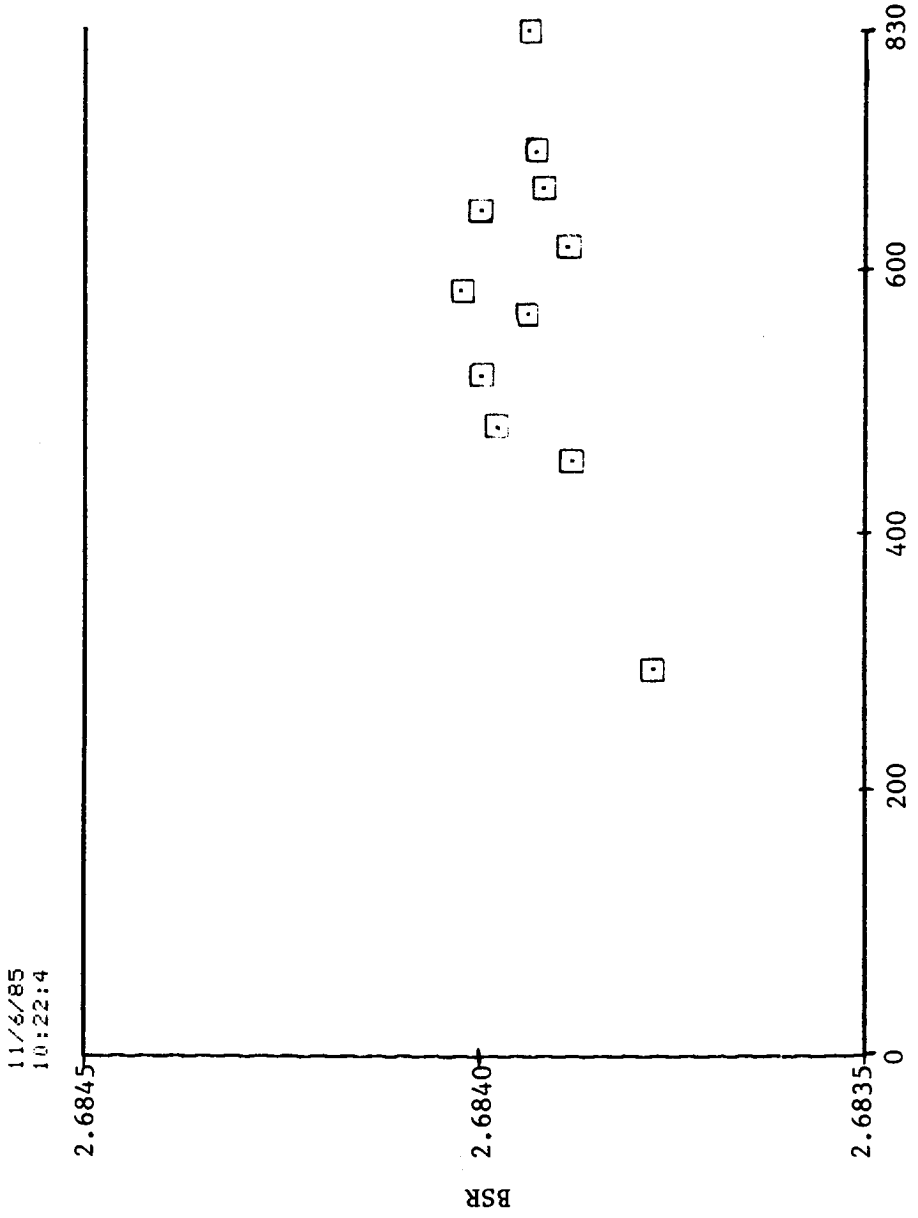

Fig. G.2 BSR vs. elapsed time for ITI 8990-A test bearing, 300 lb load, 0.004 SRG 200 oil/freon concentration.

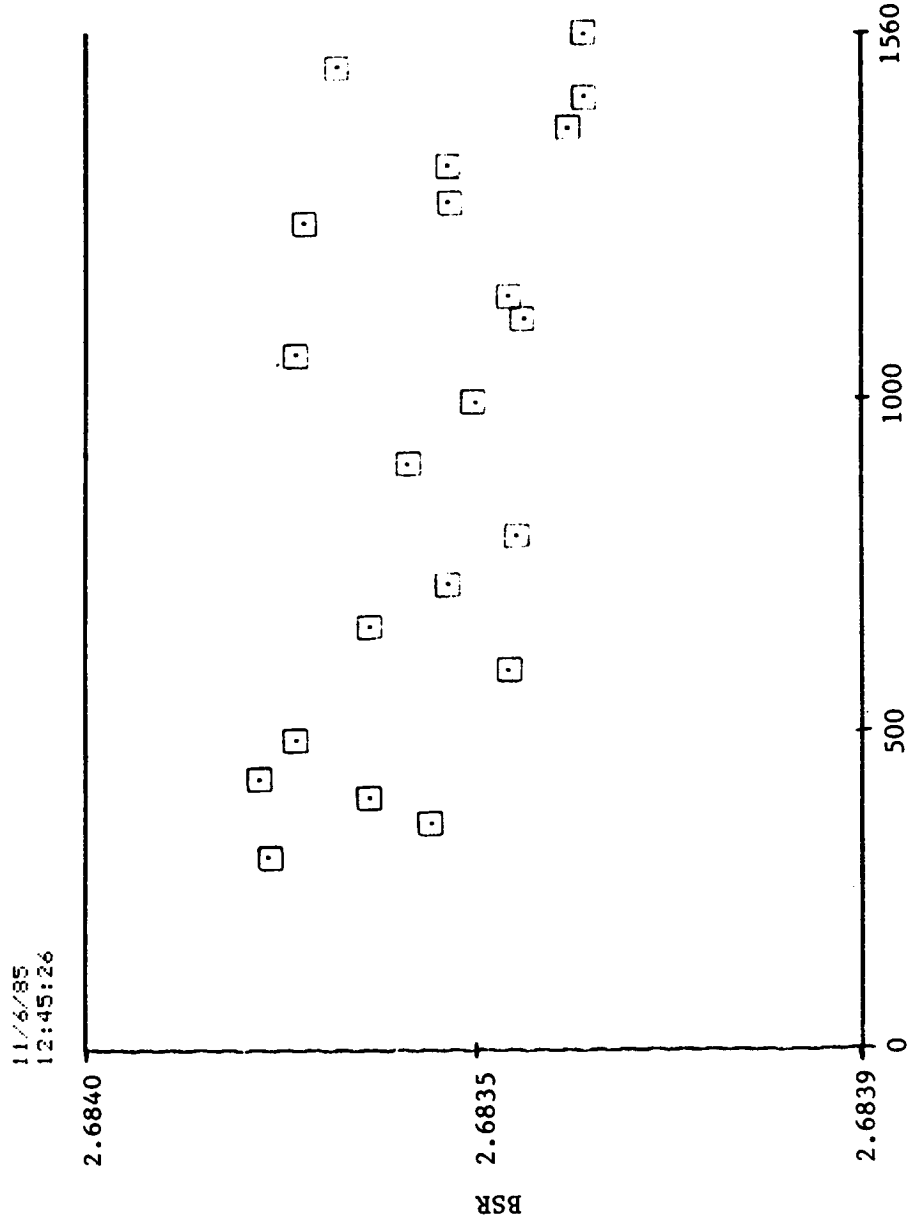

Fig. G.3 BSR vs. elapsed time for ITI 8990-A test bearing, 300 lb load, 0.004 SRG 200 oil/freon concentration.

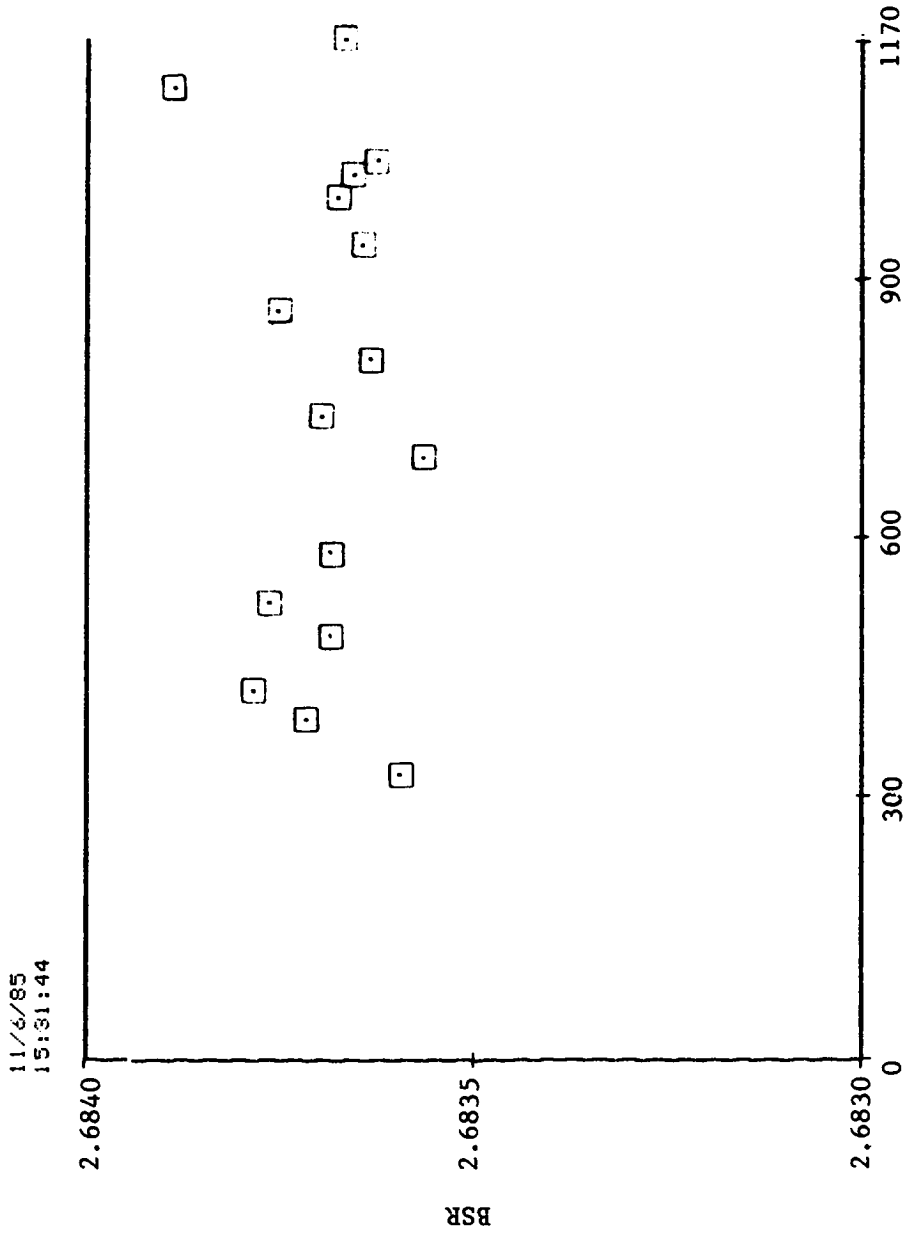

Fig. G.4 BSR vs. elapsed time for ITI 8990-A test bearing, 300 lb load, 0.004 SRG 200 oil/freon concentration.

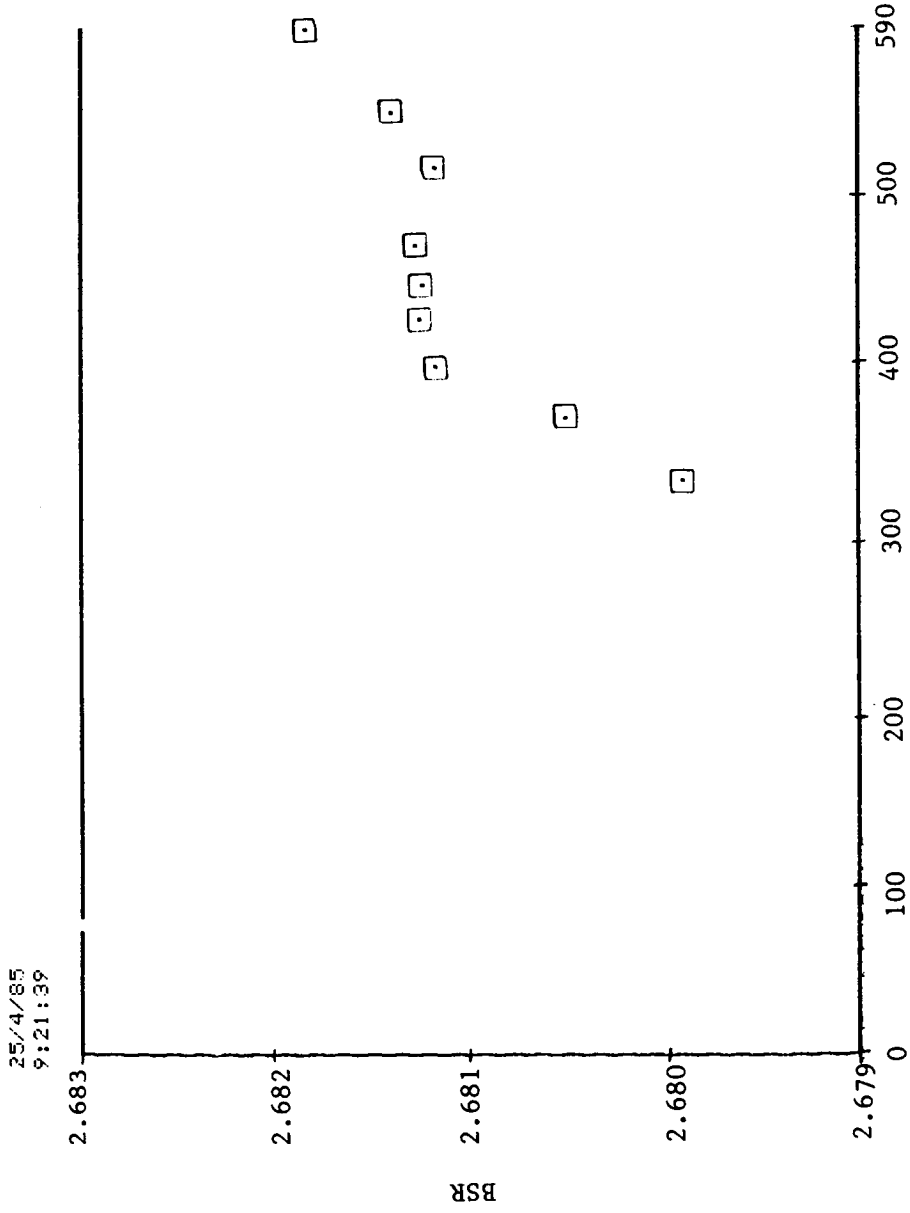

Fig. G.5 BSR vs. elapsed time for ITI 8990-A test bearing, 300 lb load, 0.004 SRG 200 oil/freon concentration.

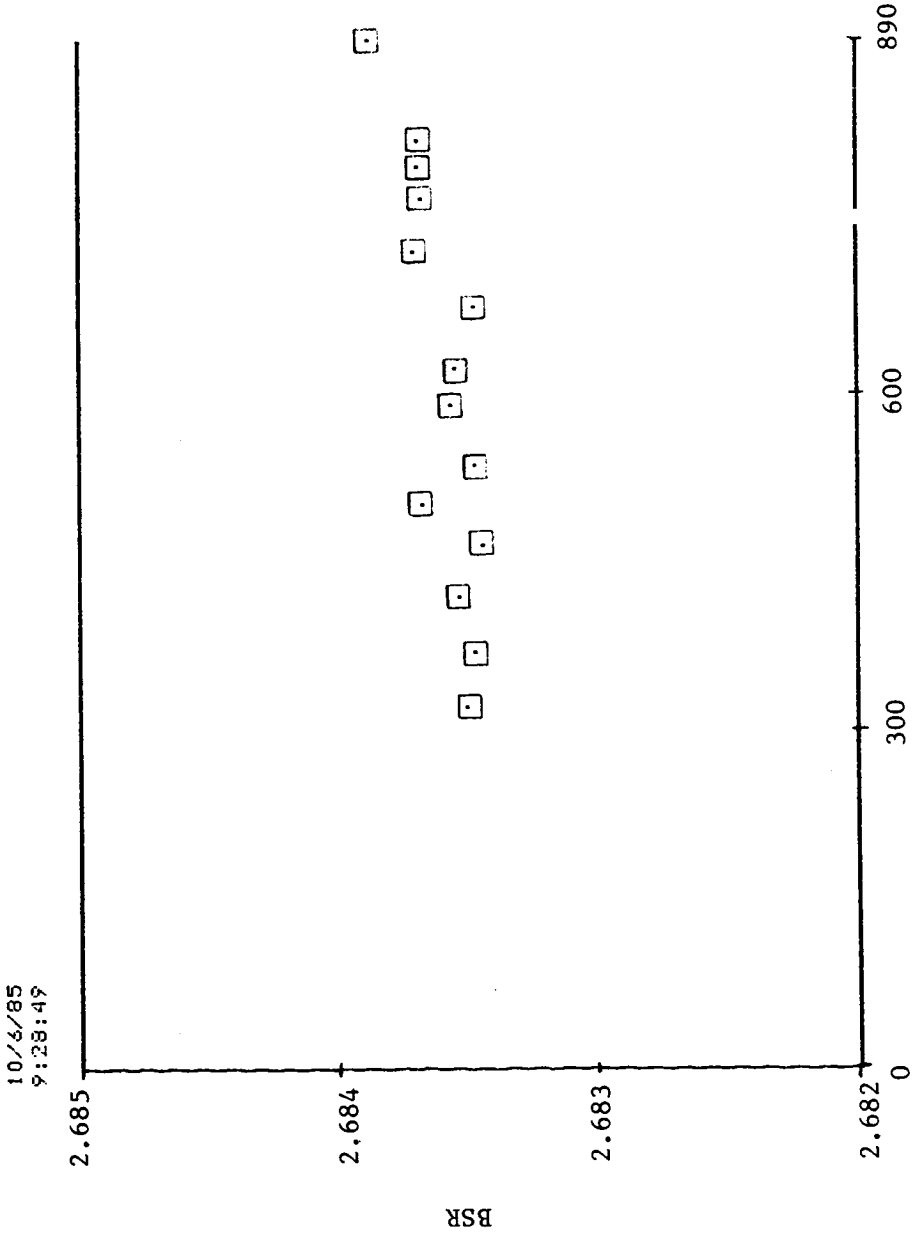

Fig. G.6 BSR vs. elapsed time for ITI 8990-A test bearing, 300 lb load, 0.006 SRG 200 oil/freon concentration.

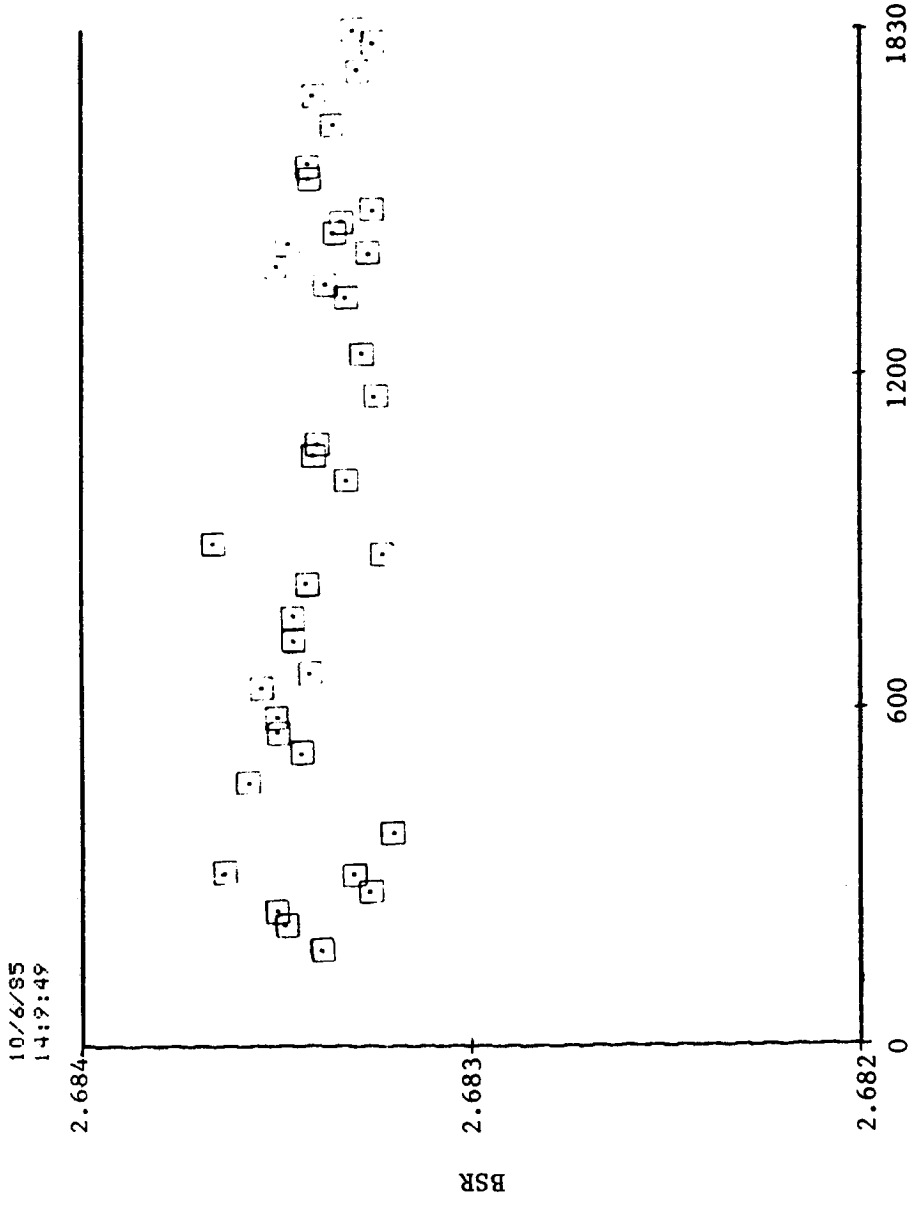

Fig. G.7 BSR vs. elapsed time for ITI 8990-A test bearing, 300 lb load, 0.006 SRG 200 oil/freon concentration.

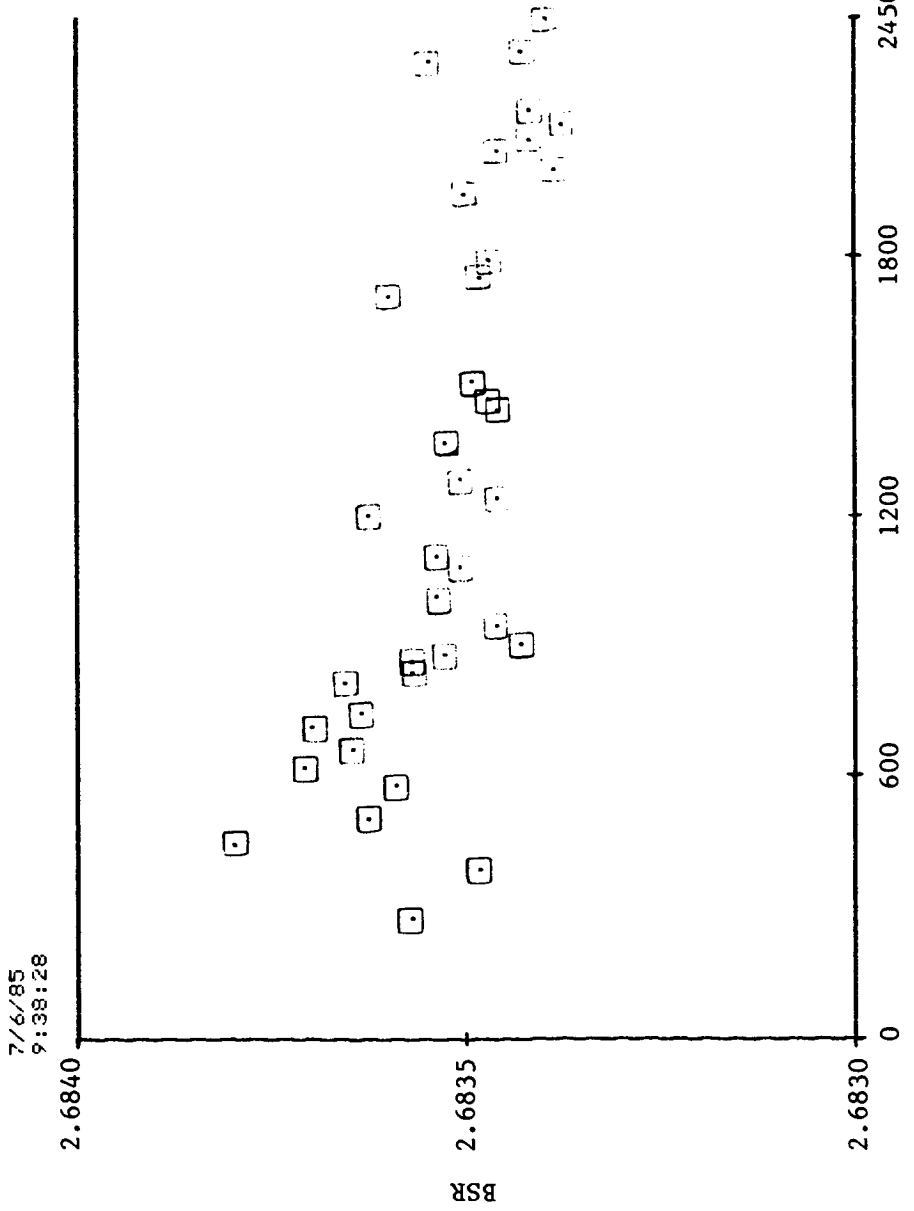

Fig. G.8 BSR vs. elapsed time for ITI 8990-A test bearing, 300 lb load, 0.008 SRG 200 oil/freon concentration.

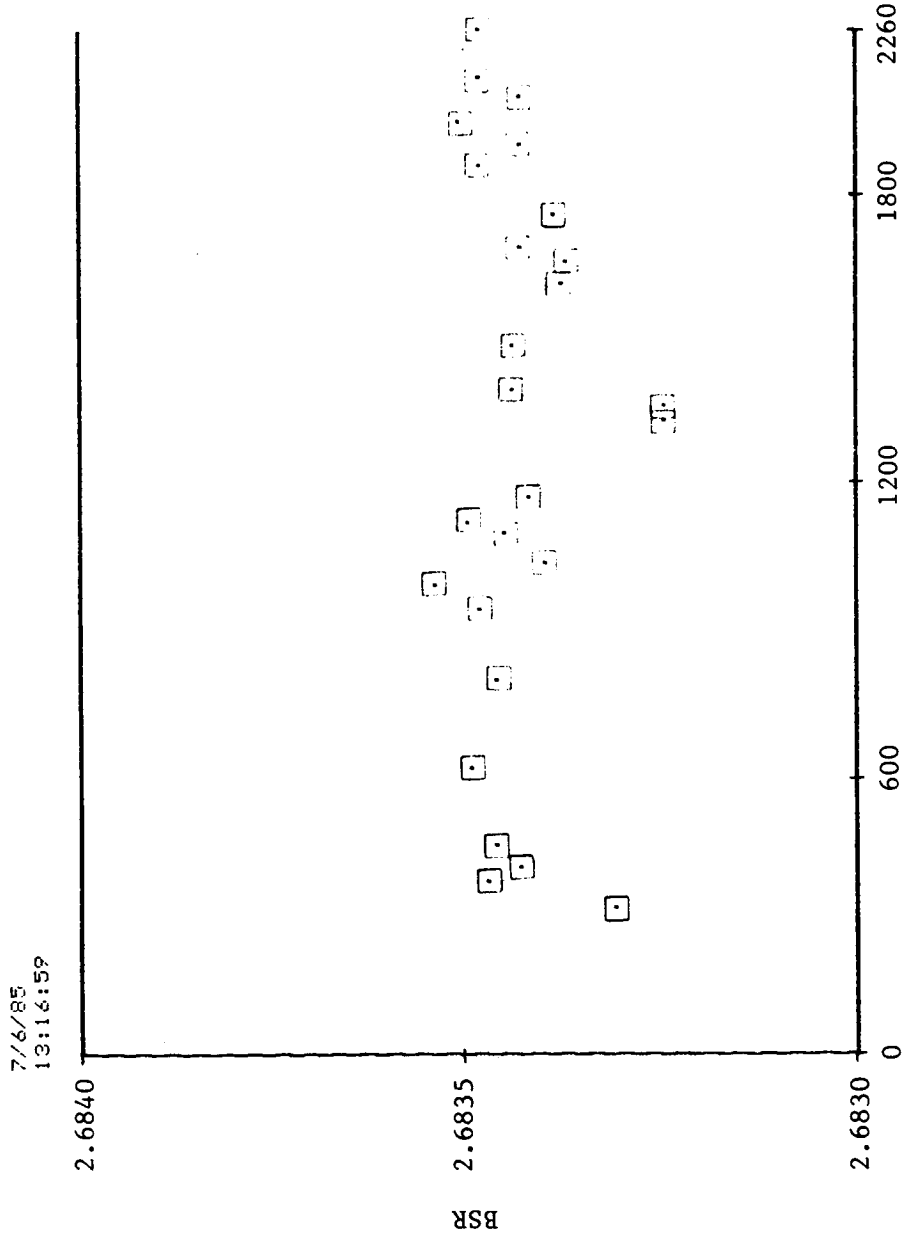

Fig. G.9 BSR vs. elapsed time for ITI 8990-A test bearing, 300 lb load, 0.008 SRG 200 oil/freon concentration.

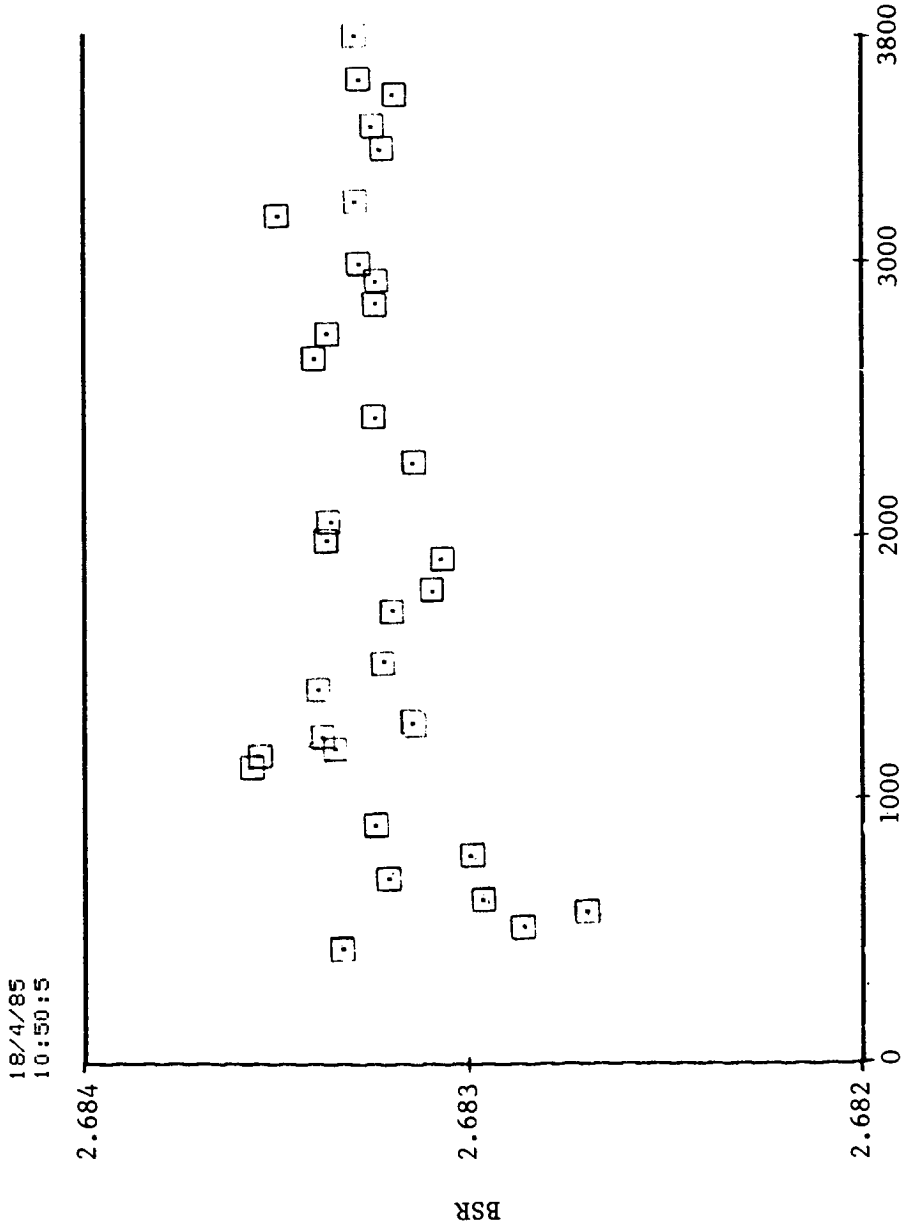

Fig. G.10 BSR vs. elapsed time for ITI 8990-A test bearing, 300 lb load, 0.008 SRG 200 oil/freon concentration.

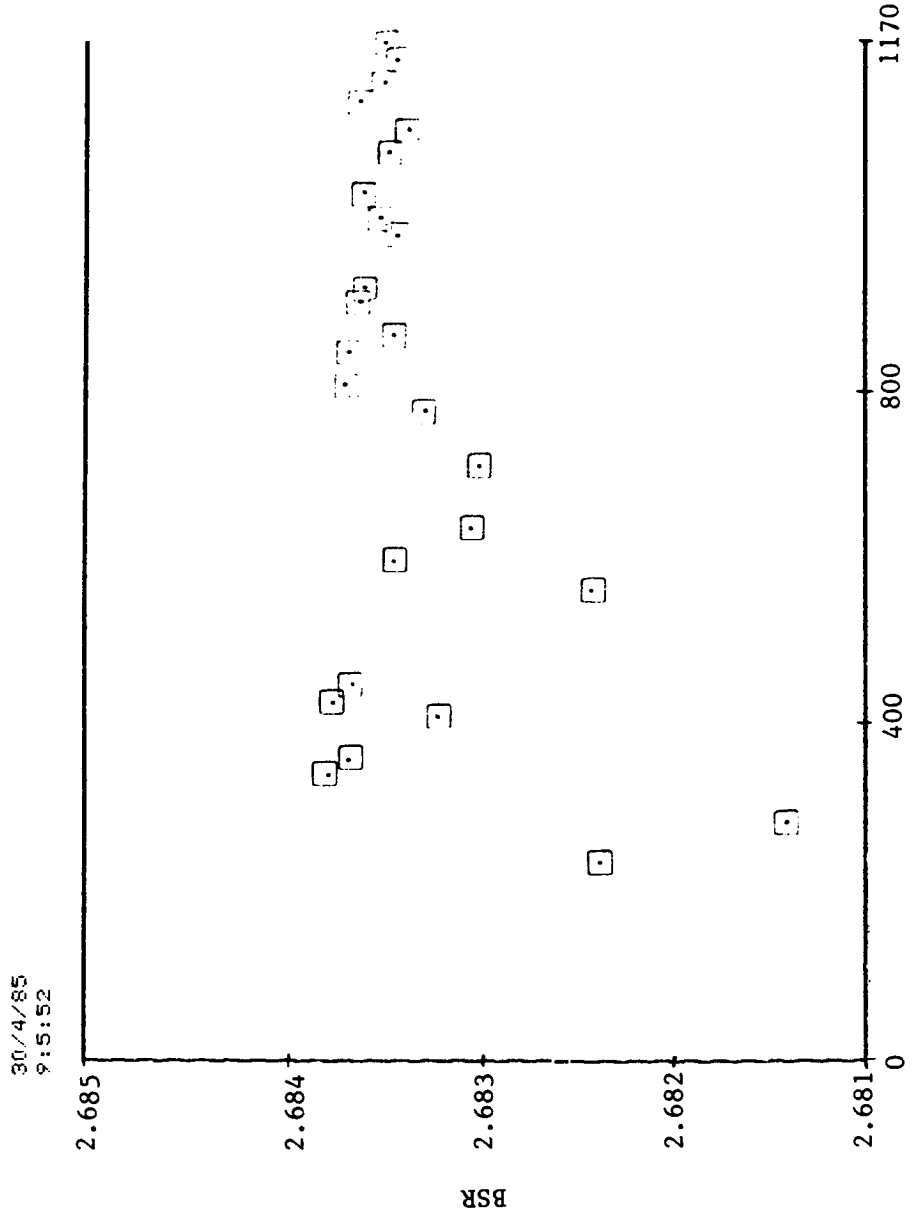

Fig. G.11 BSR vs. elapsed time for ITI 8990-A test bearing, 300 lb load, 0.001 SRG 200 oil/freon concentration.

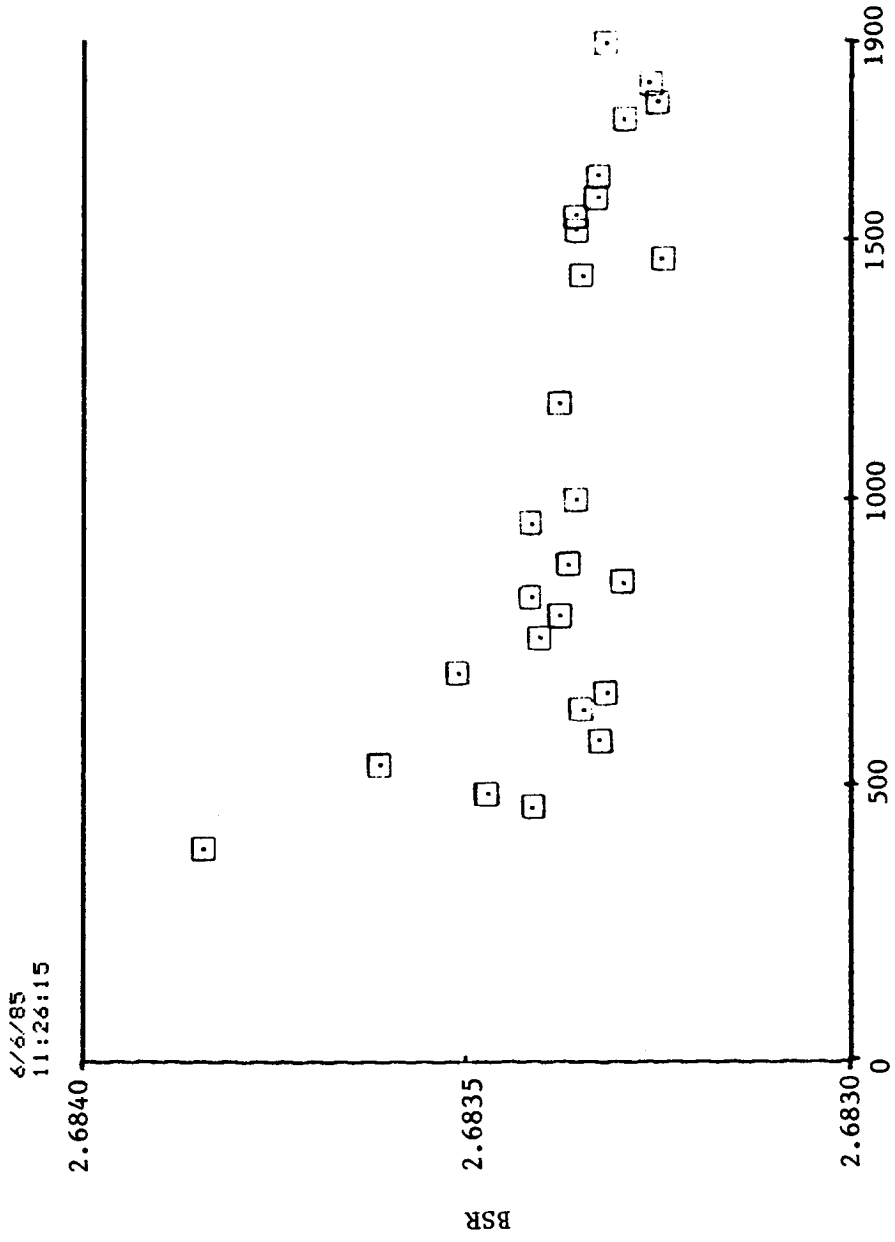

Fig. G.12 BSR vs. elapsed time for ITI 8990-A test bearing, 300 lb load, 0.01 SRG 200 oil/freon concentration.

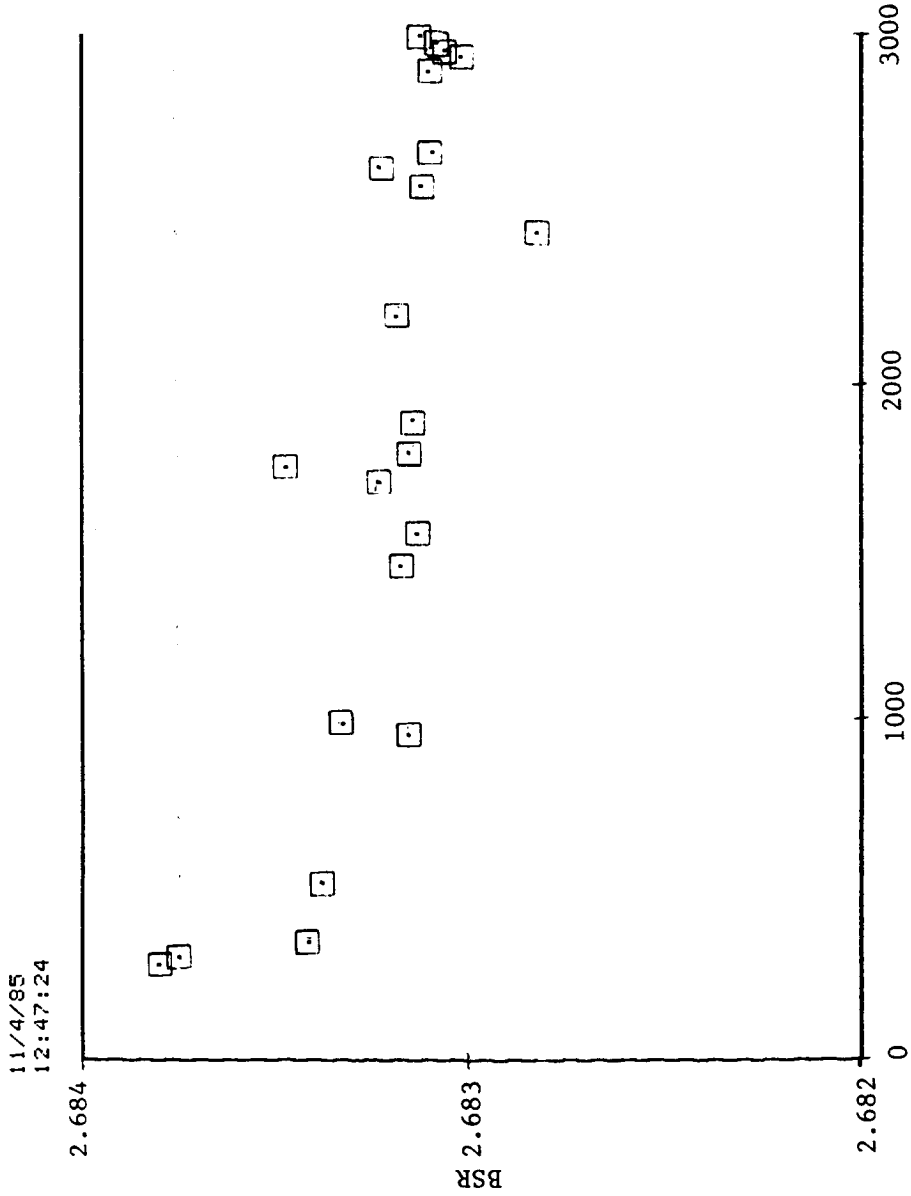

Fig. G.13 BSR vs. elapsed time for ITI 8990-A test bearing, 300 lb load, 0.01 SRG 200 oil/freon concentration.

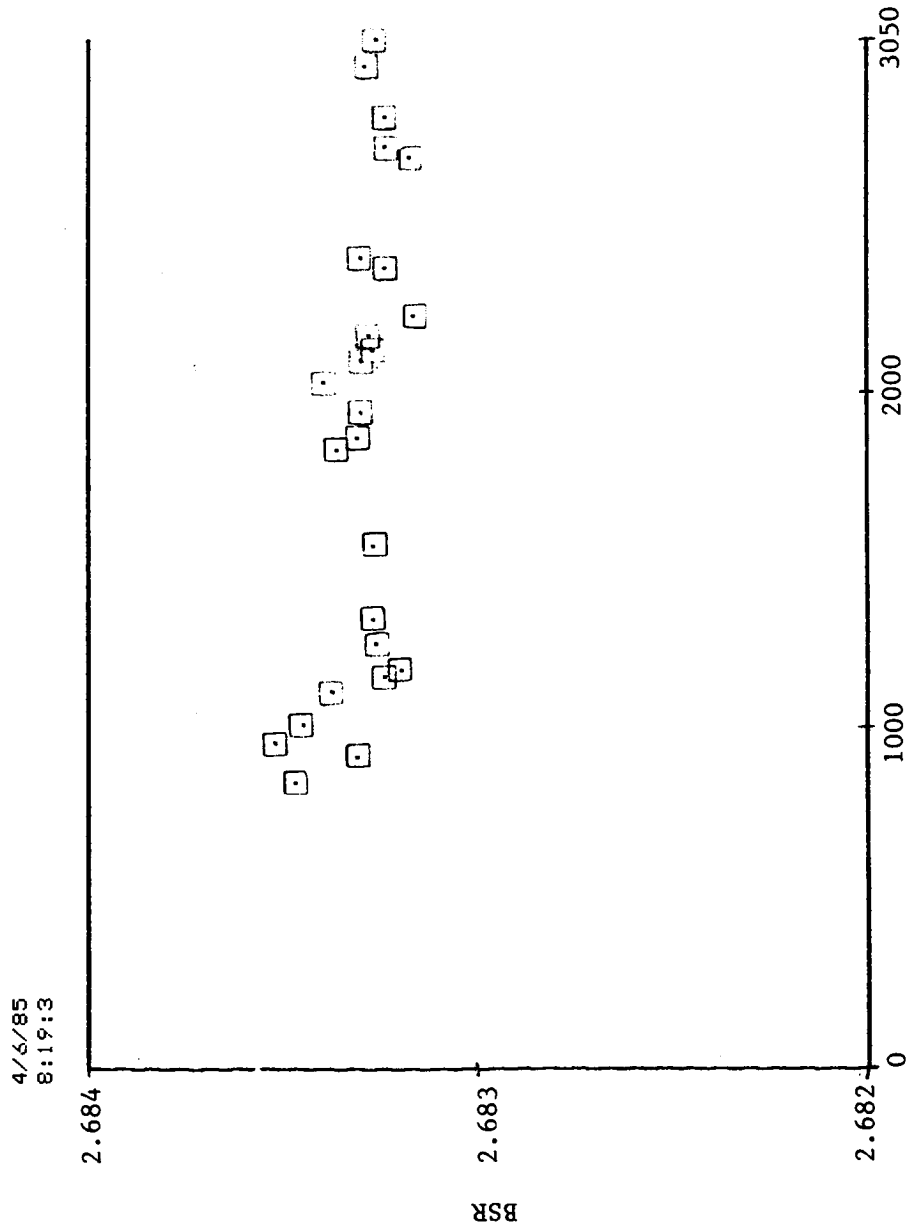

Fig. G.14 BSR vs. elapsed time for ITI 8990-A test bearing, 300 lb load, 0.013 SRG 200 oil/freon concentration.

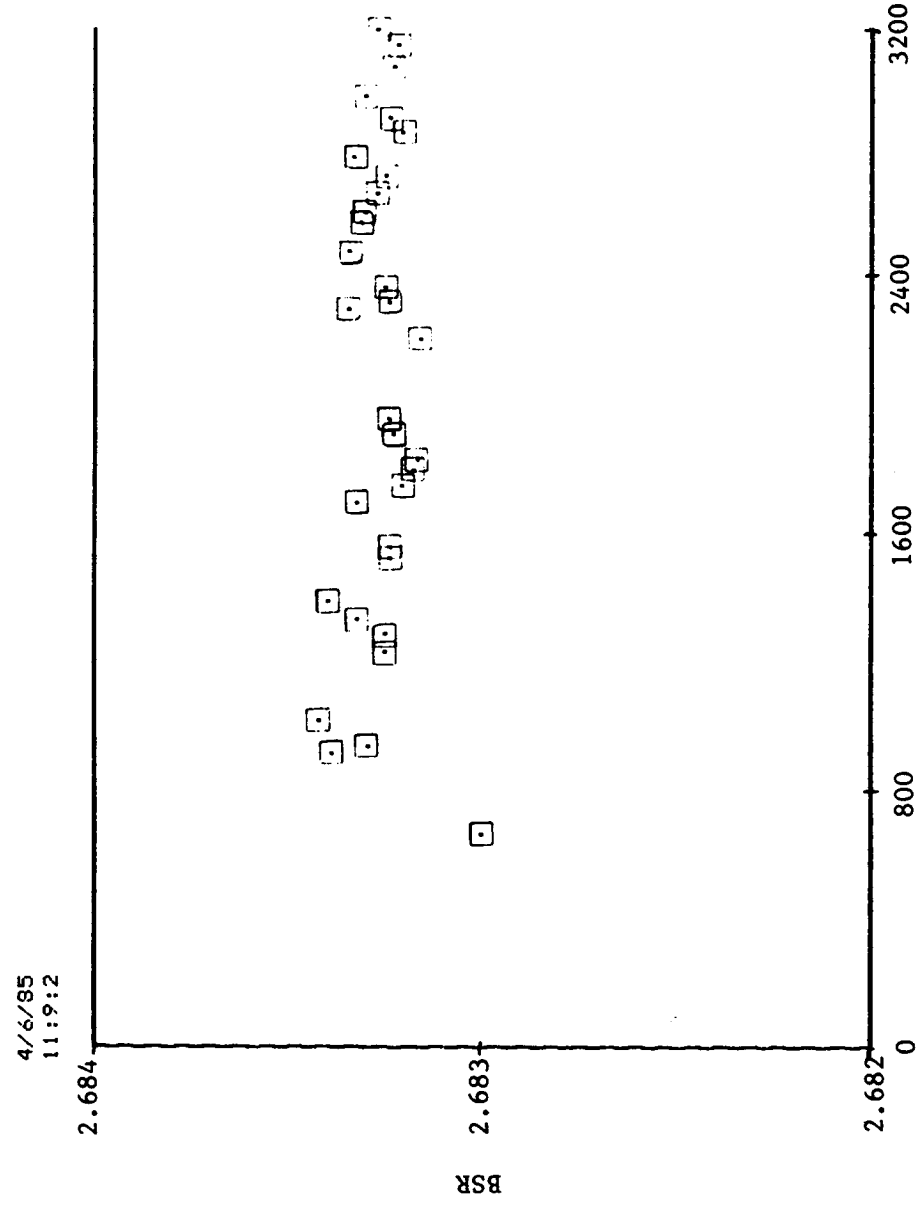

Fig. G.15 BSR vs. elapsed time for ITI 8990-A test bearing, 300 lb load, 0.013 SRG 200 oil/freon concentration.

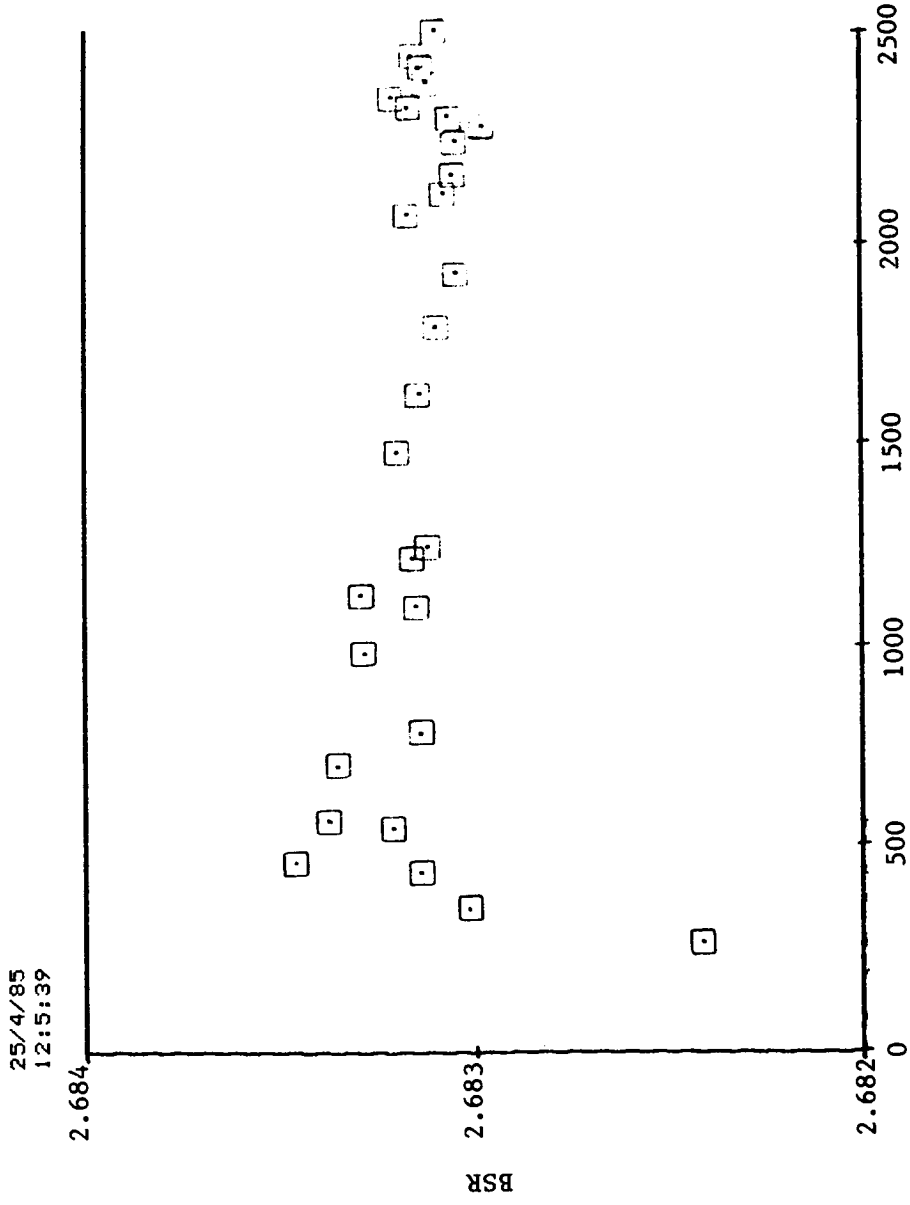

Fig. G.16 BSR vs. elapsed time for ITI 8990-A test bearing, 300 lb load, 0.014 SRG 200 oil/freon concentration.

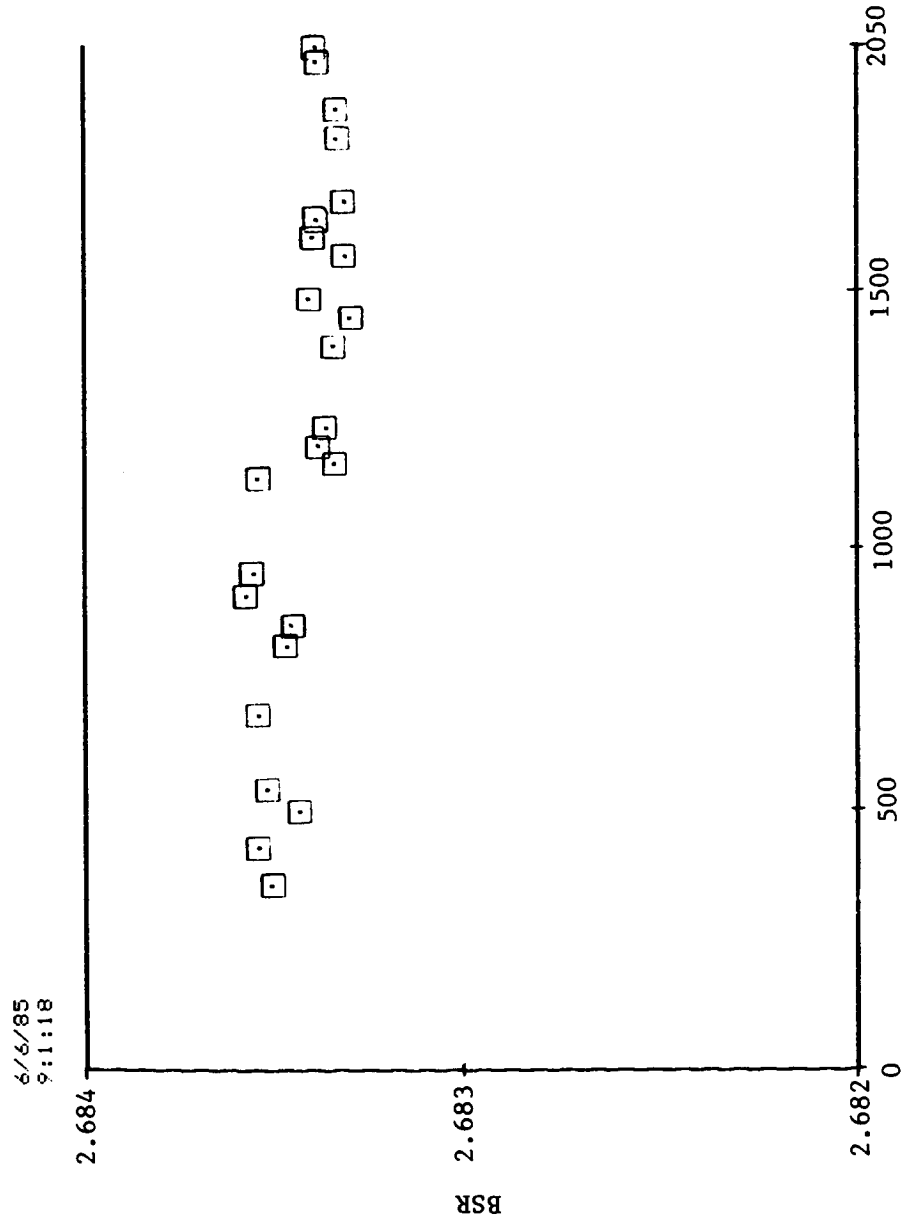

Fig. G.17 BSR vs. elapsed time for ITI 8990-A test bearing, 300 lb load, 0.016 SRG 200 oil/freon concentration.

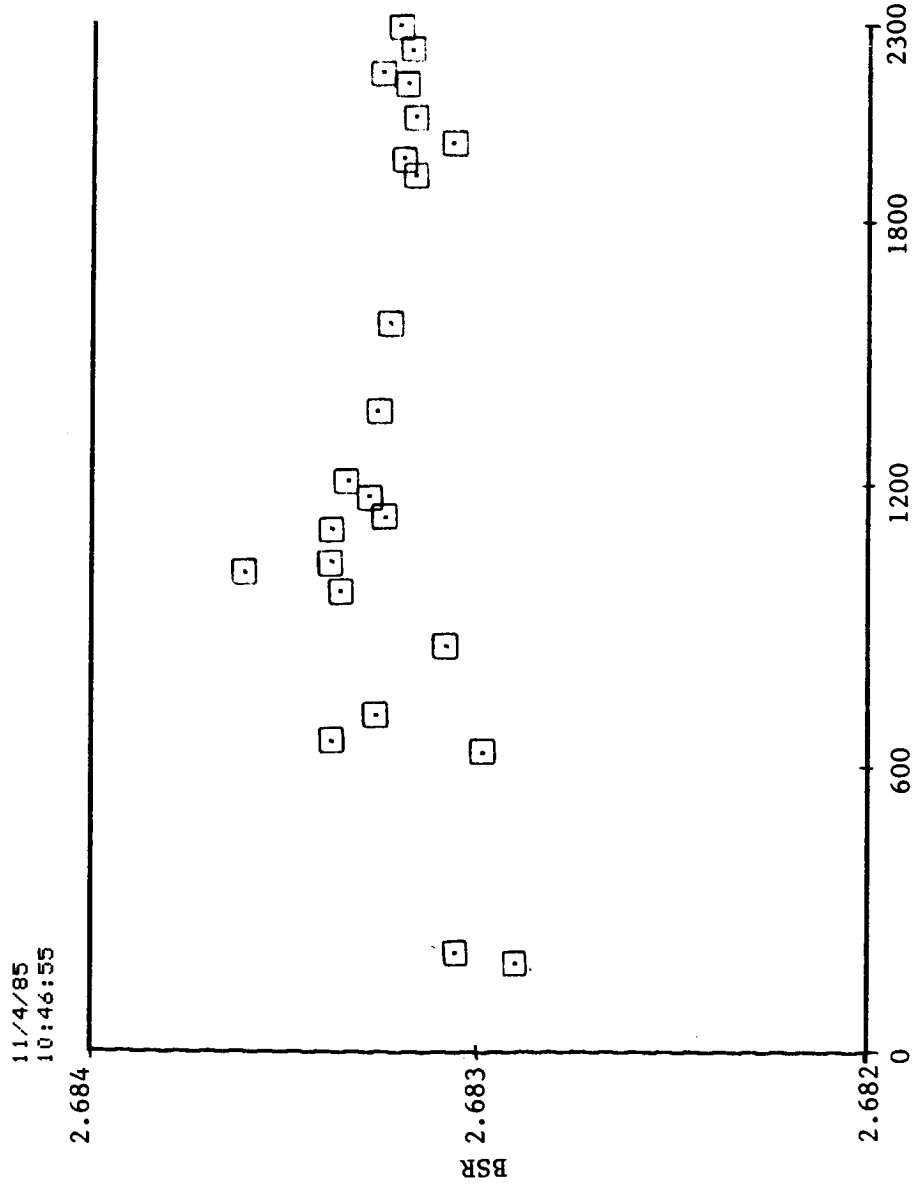

Fig. G.18 BSR vs. elapsed time for ITI 8990-A test bearing, 300 lb load, 0.016 SRG 200 oil/freon concentration.

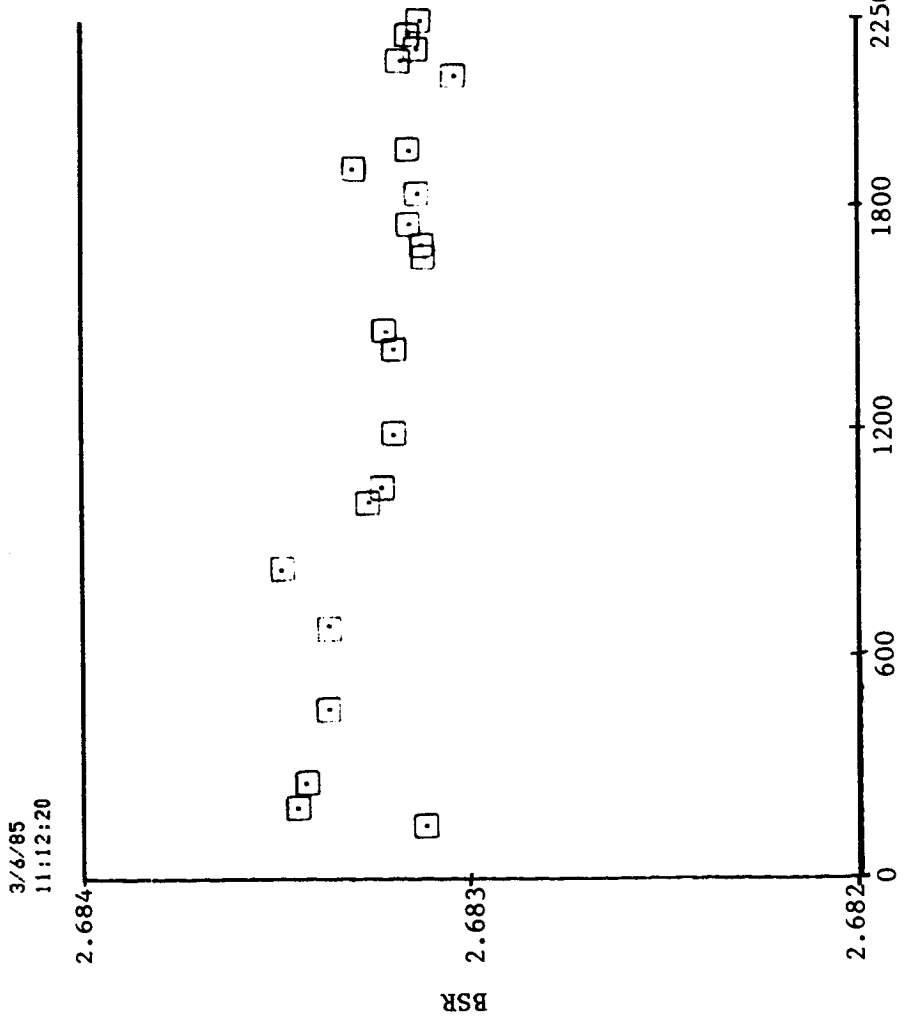

Fig. G.19 BSR vs. elapsed time for ITI 8990-A test bearing, 300 lb load, 0.020 SRG 200 oil/freon concentration.

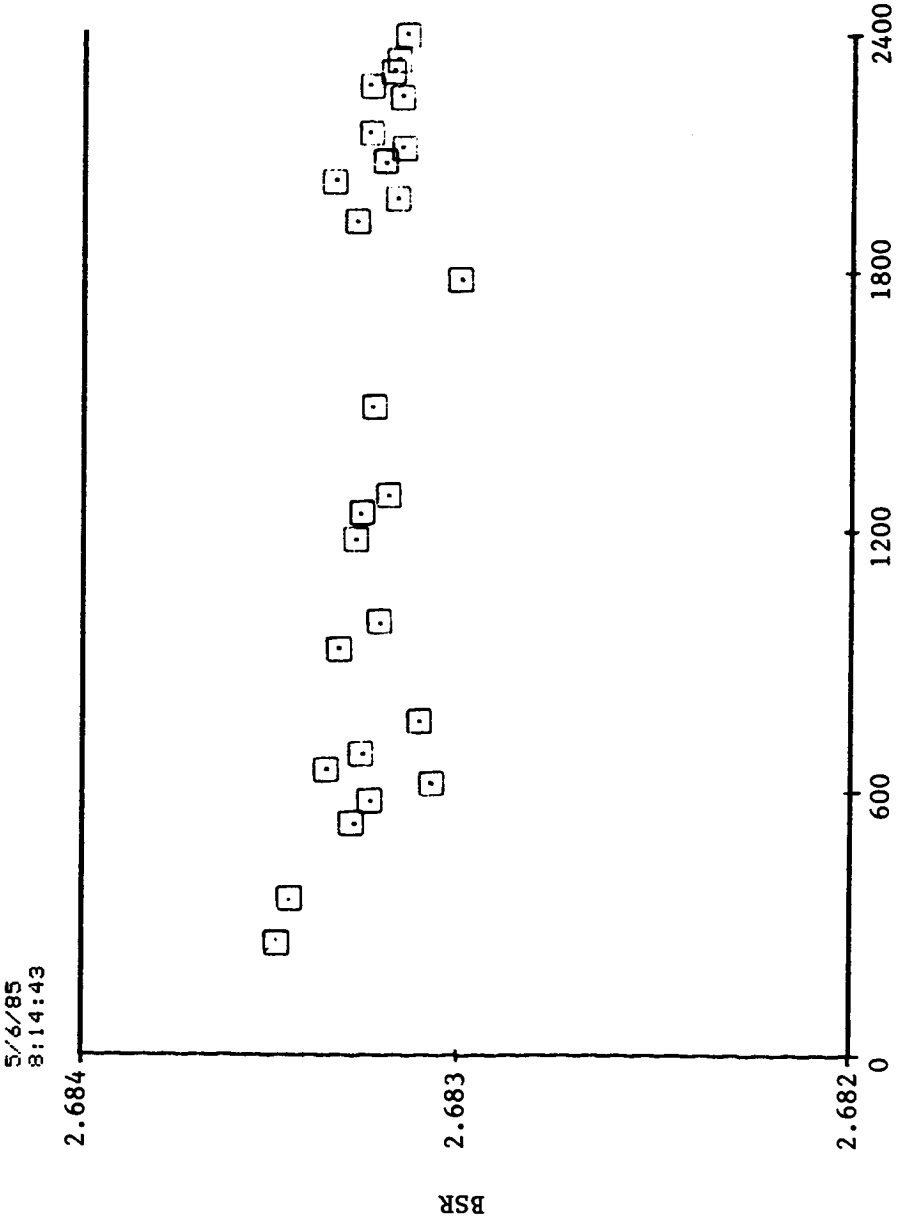

Fig. G.20 BSR vs. elapsed time for ITI 8990-A test bearing, 300 lb load, 0.022 SRG 200 oil/freon concentration.

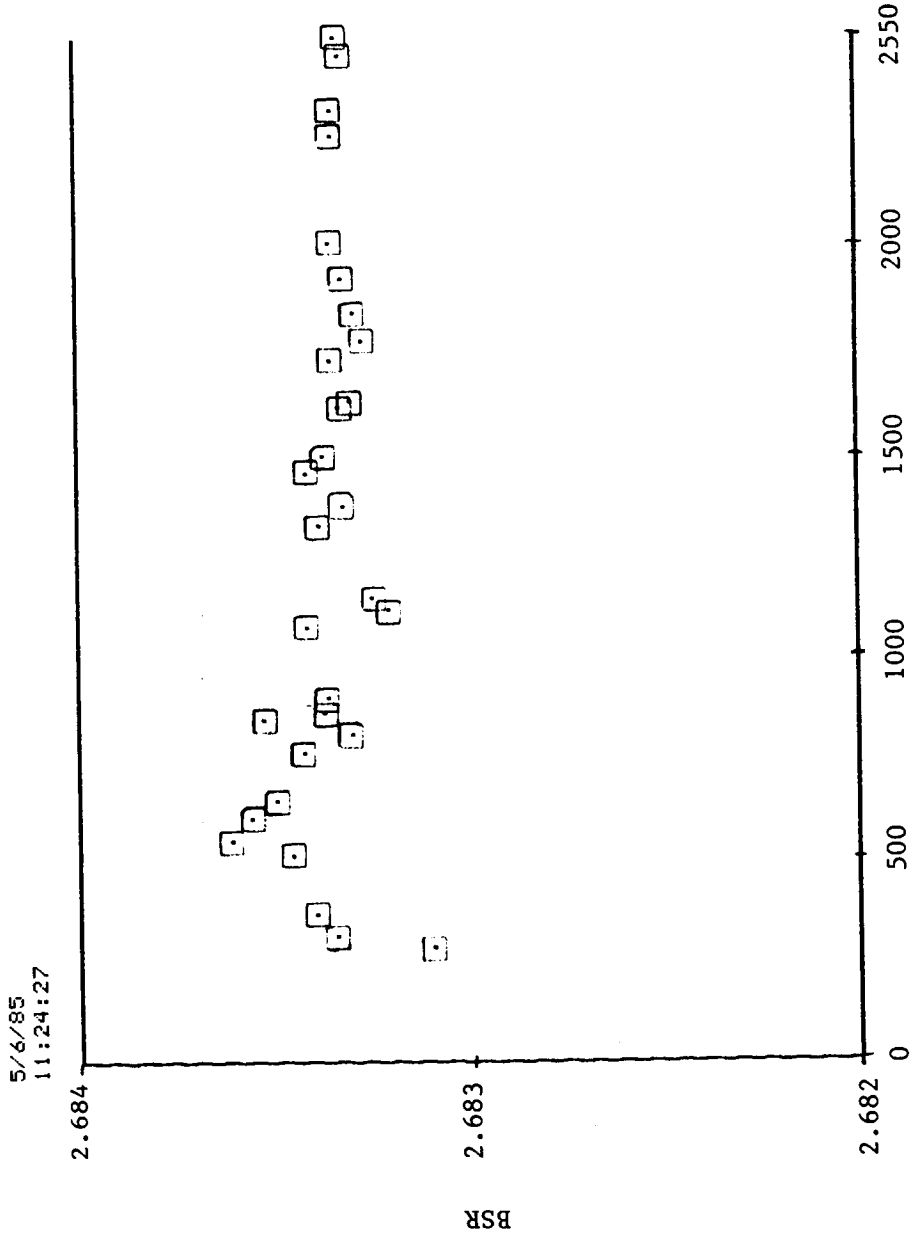

Fig. G.21 BSR vs. elapsed time for ITI 8990-A test bearing, 300 lb load, 0.022 SRG 200 oil/freon concentration.

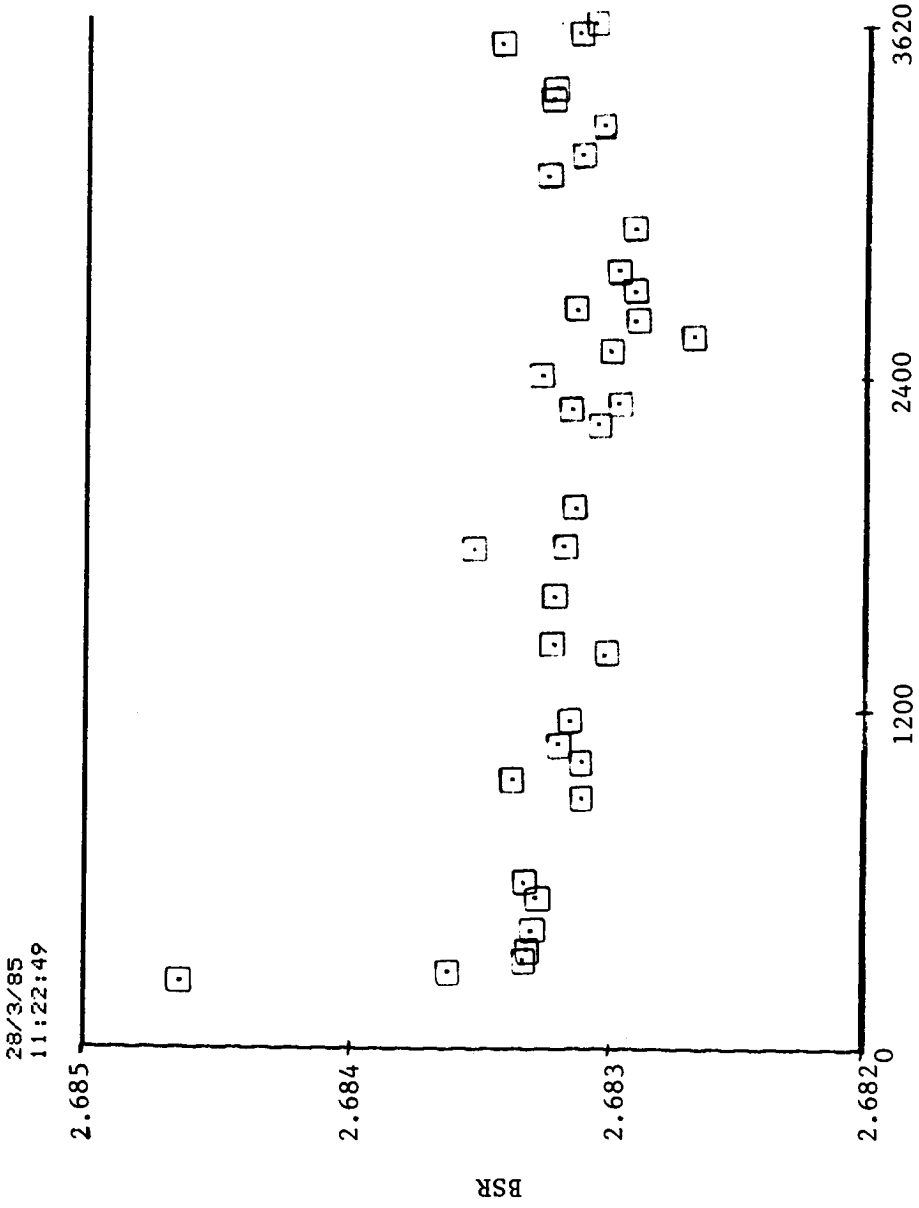

Fig. G.22 BSR vs. elapsed time for ITI 8990-A test bearig, 300 lb load, 0.026 SRG 200 oil/freon concentration.

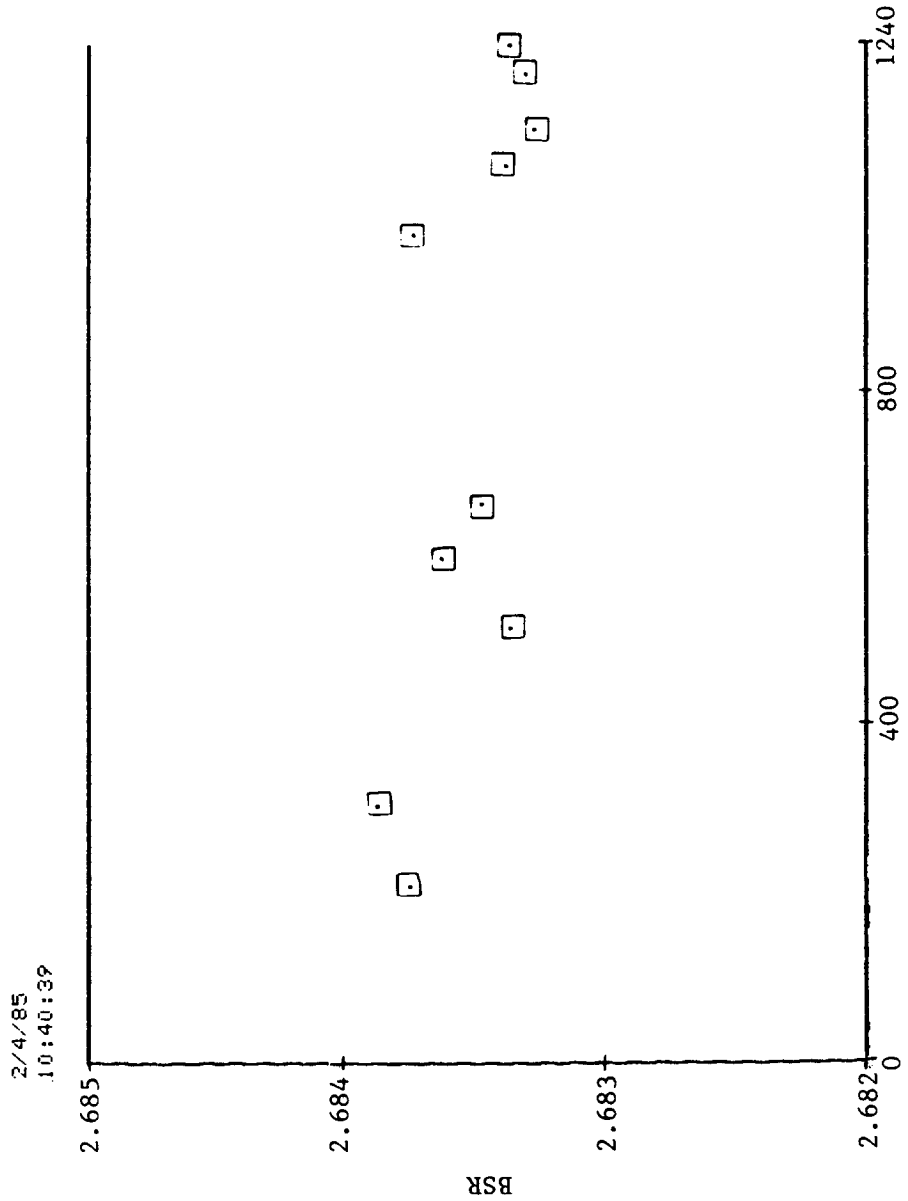

Fig. G.23 BSR vs. elapsed time for ITI 8990-A test bearing, 300 lb load, 0.026 SRG 200 oil/freon concentration.

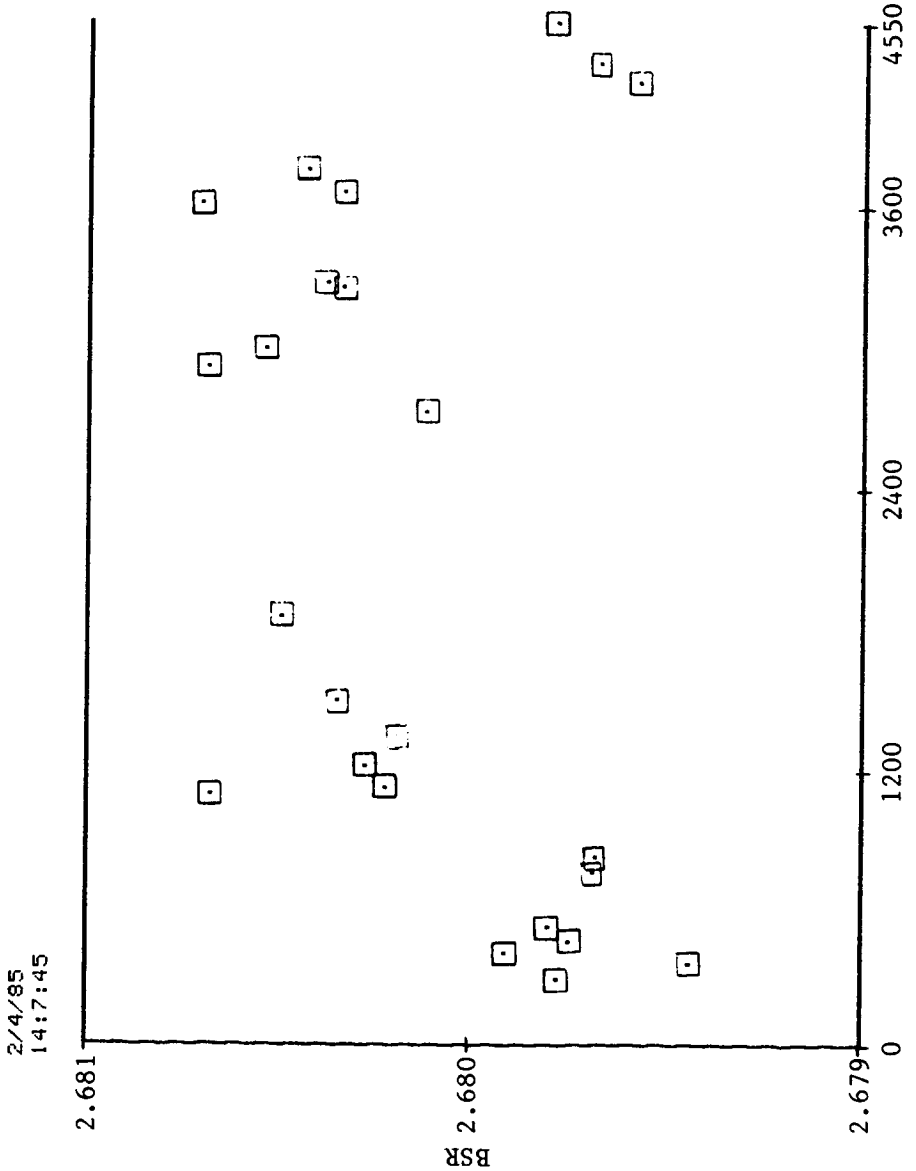

Fig. G.24 BSR vs. elapsed time for ITI 8990-A test bearing, 300 lb load, 0.026 SRG 200 oil/freon concentration.

APPENDIX H

EXPERIMENTAL DATA FOR

TIME STUDY NO. 1

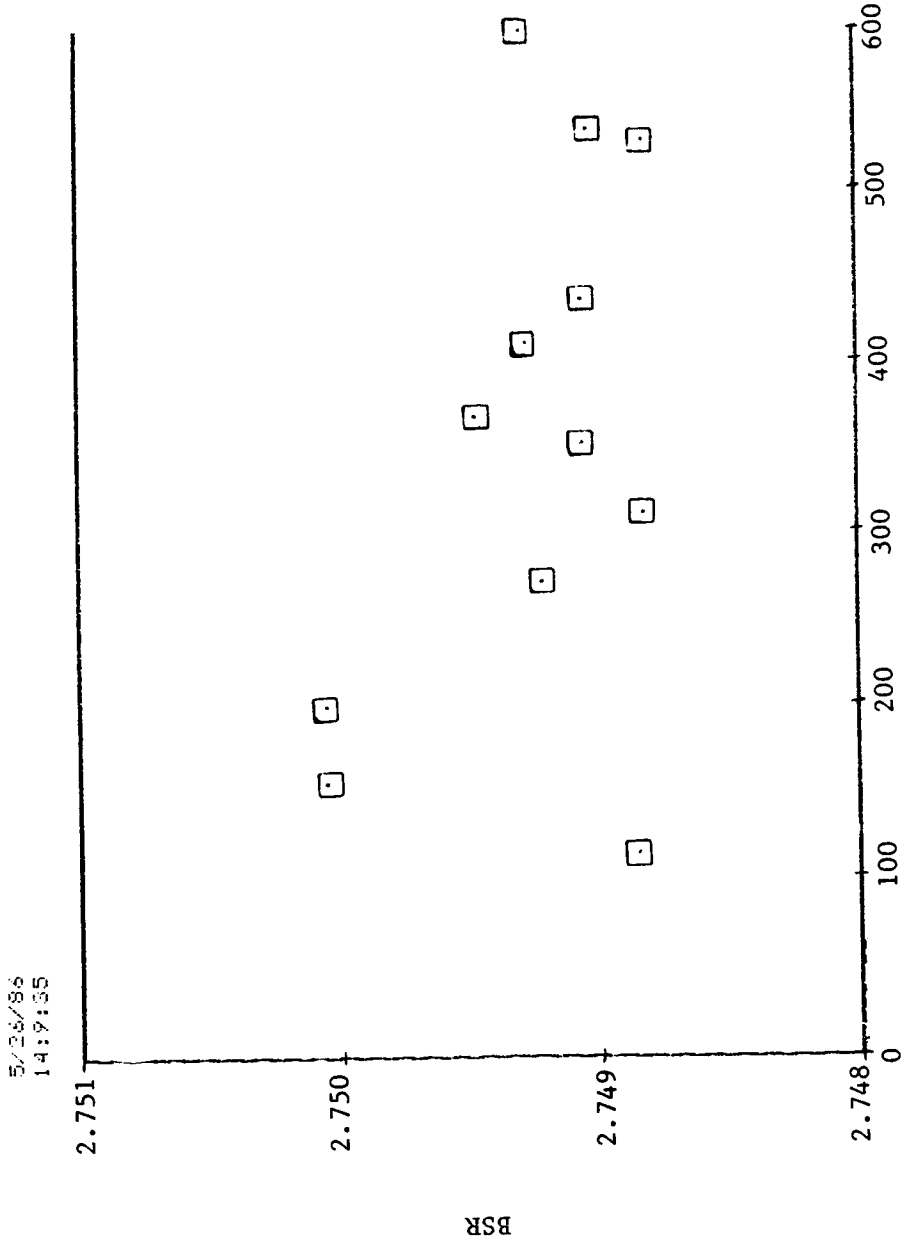

Fig. H.1 BSR vs. elapsed time for ITI 11532-A test bearing, 200 lb load, time study #1 - 10 min., 0.016 SRG 200 oil/freon concentration.

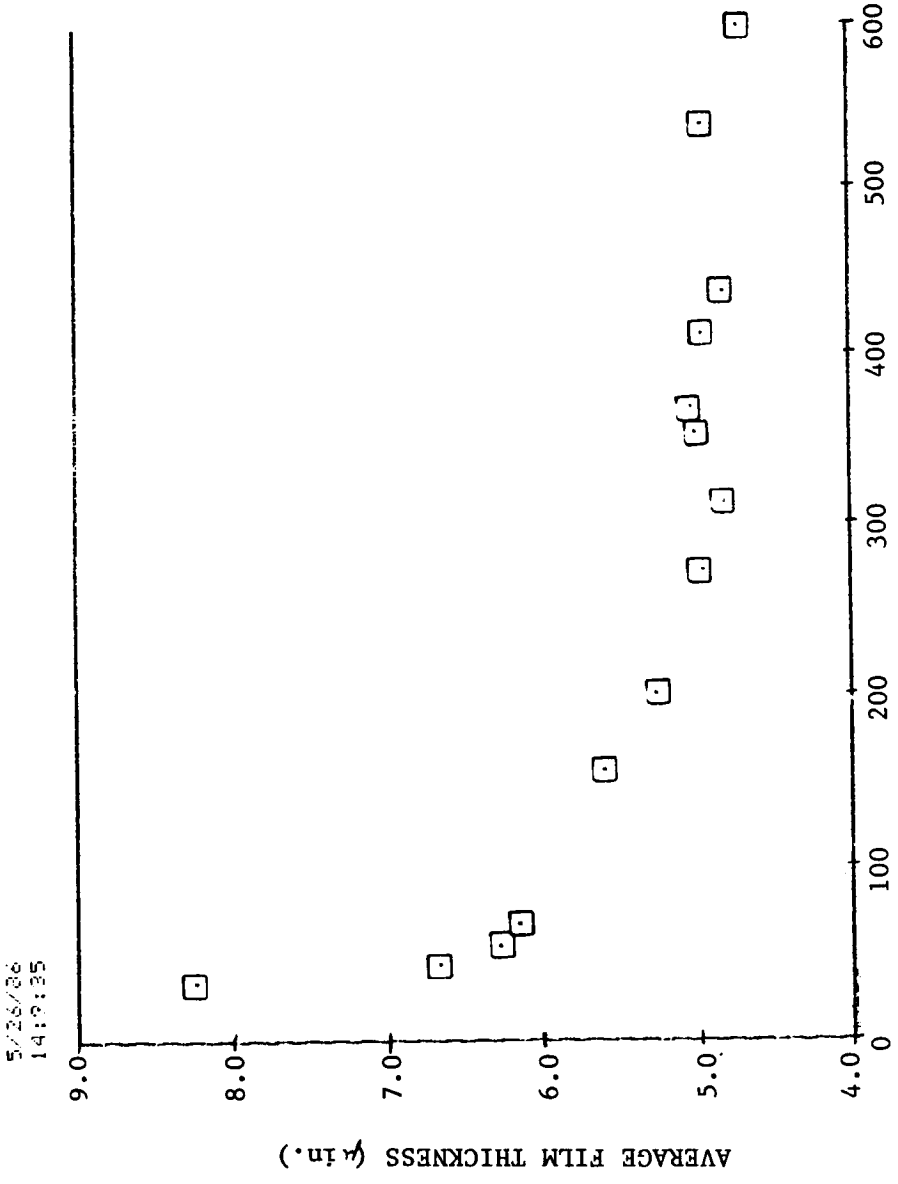

Fig. H.2 Average film thickness for ITI 11532-A test bearing, 200 lb load, time study #1 - 10 min., 0.016 SRG 200 oil/freon concentration.

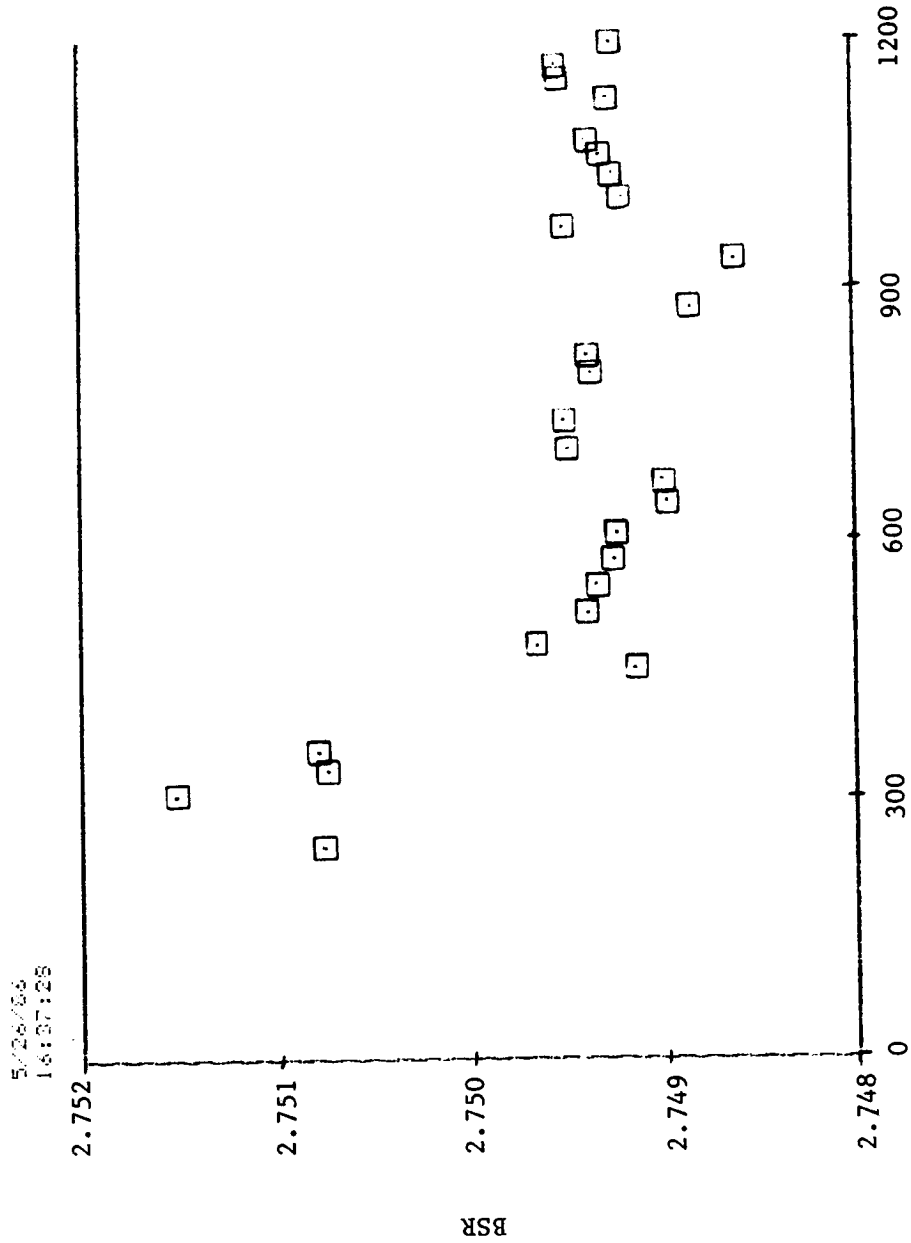

Fig. H.3 BSR vs. elapsed time for ITI 11532-A test bearing, 200 lb load, time study #1 - 20 min., 0.016 SRG 200 oil/freon concentration.

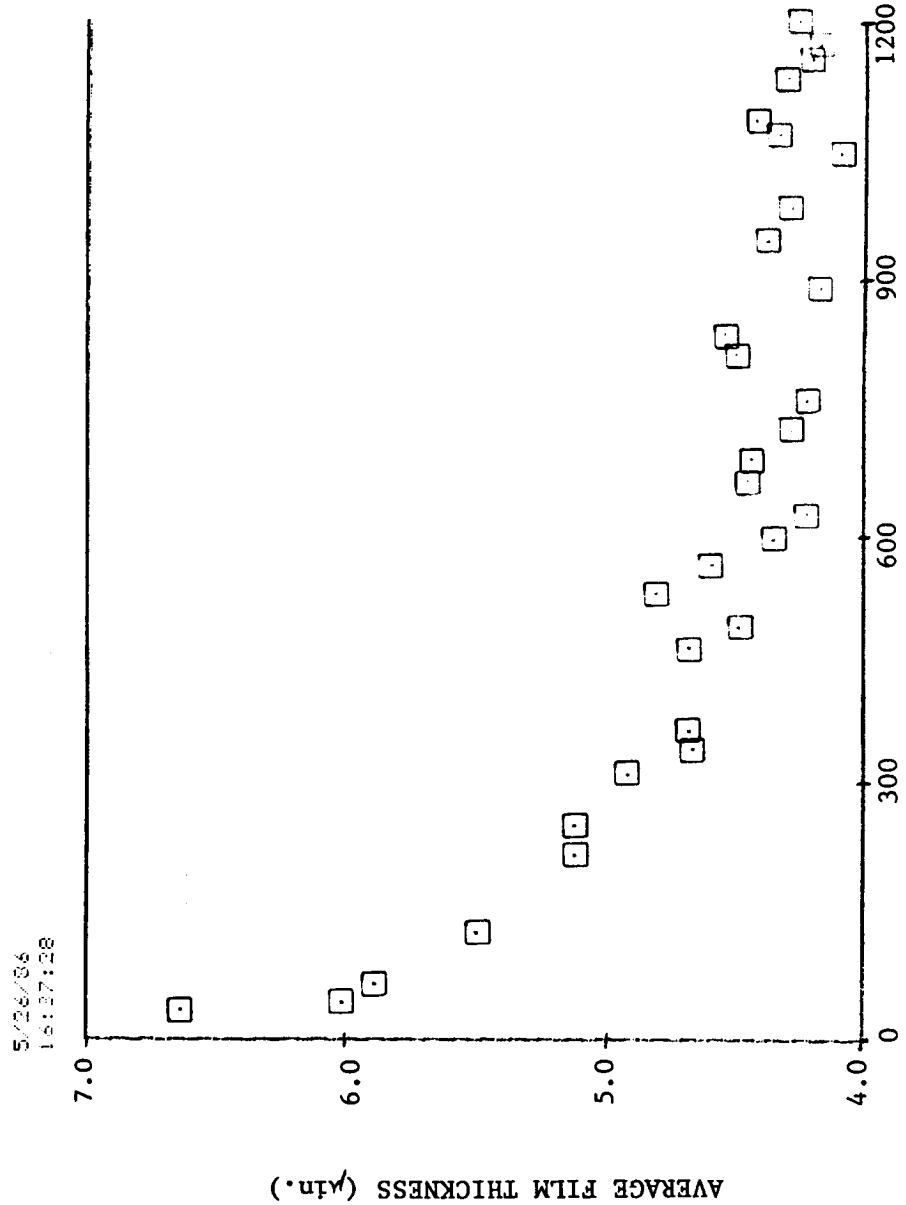

Fig. H.4 Average film thickness vs. elapsed time for ITI 11532-A test bearing, 200 lb load, time study #1 - 20 min., 0.016 SRG 200 oil/freon concentration.

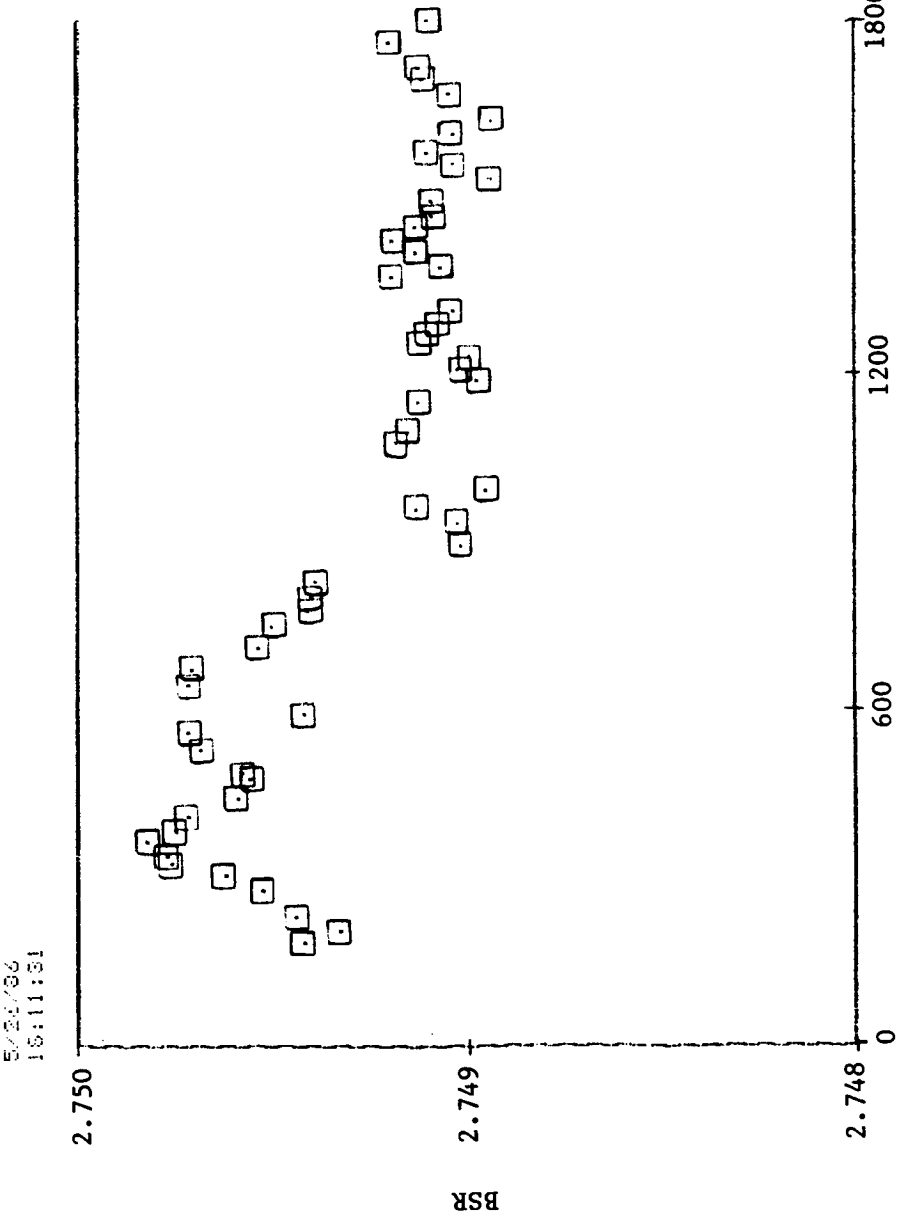

Fig. H.5 BSR vs. elapsed time for ITI 11532-A test bearing, 200 lb load, time study #1 - 30 min., 0.016 SRG 200 oil/freon concentration.

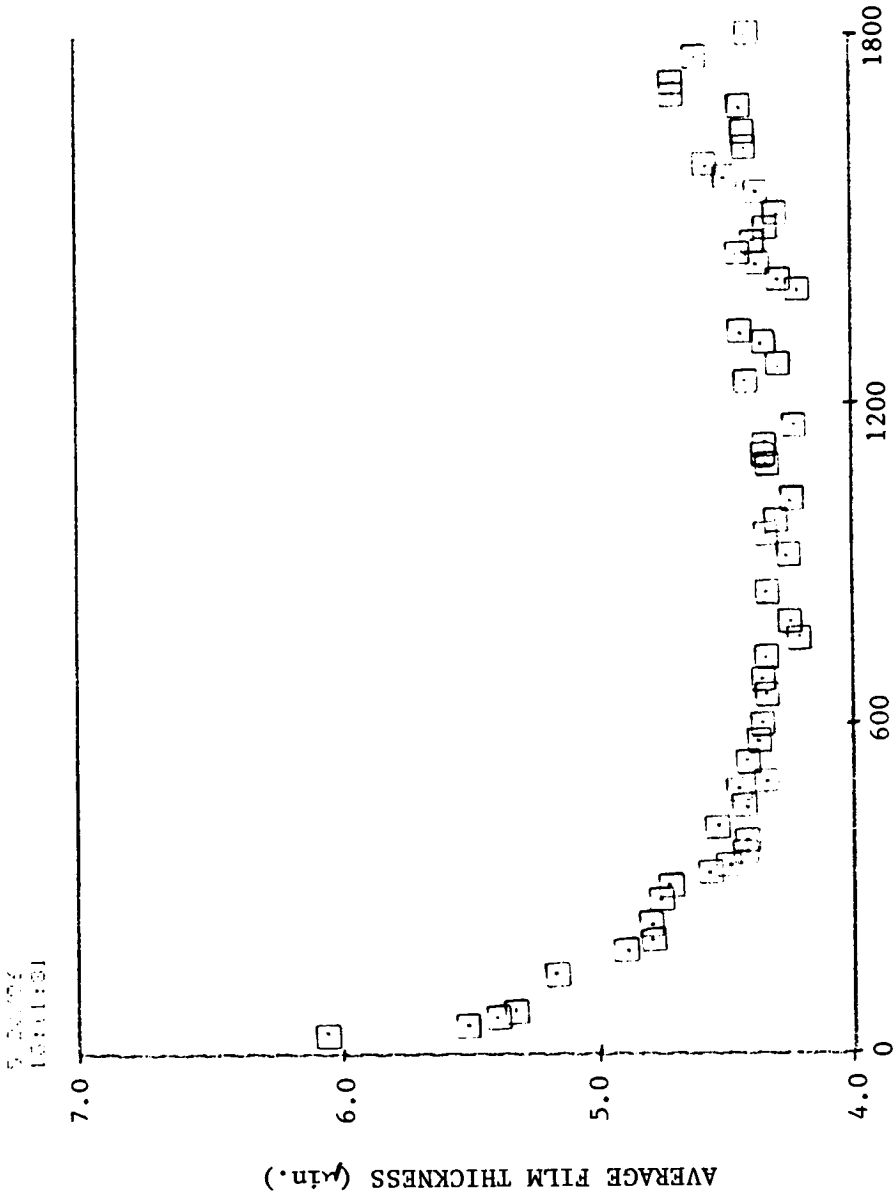

Fig. H.6 Average film thickness vs. elapsed time for ITI 11532-A test bearing, 200 lb load, time study #1 - 30 min., 0.016 SRG 200 oil/freon concentration.

ORIGINAL PAGE IS
OF POOR QUALITY

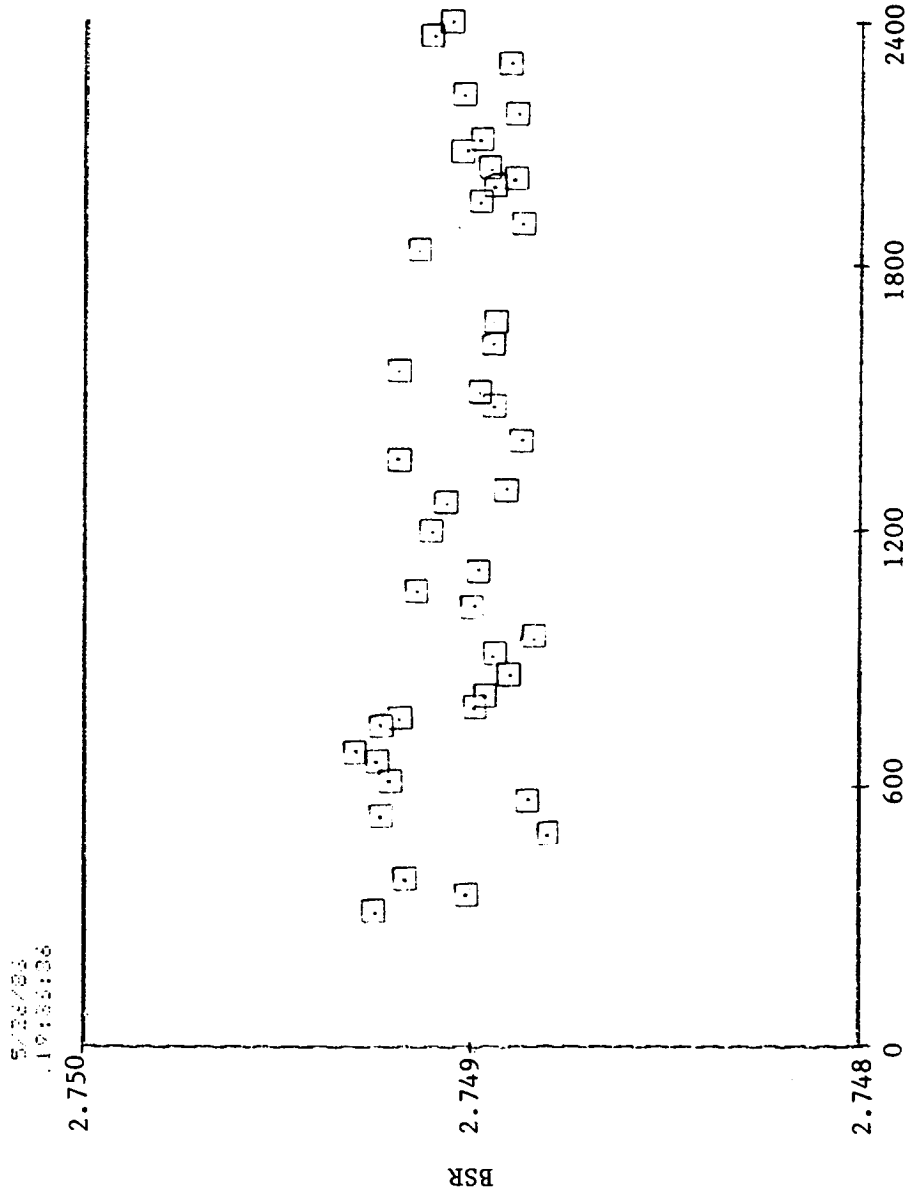

Fig. H.7 BSR vs. elapsed time for ITI 11532-A test bearing, 200 lb load, time study #1 - 40 min., 0.016 SRG 200 oil/freon concentration.

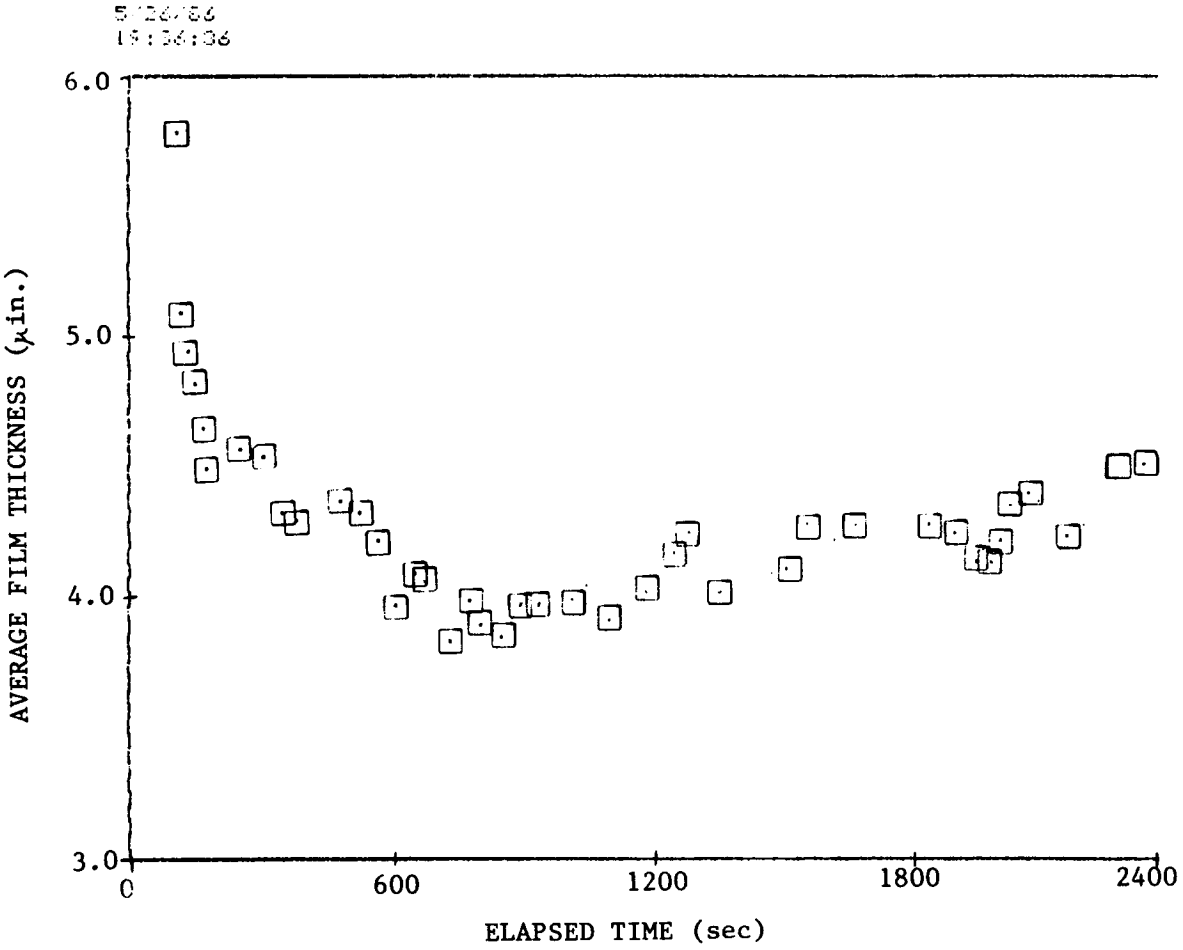

Fig. H.8 Average film thickness vs. elapsed time for ITI 11532-A test bearing, 200 lb load, time study #1 - 40 min., 0.016 SRG 200 oil/freon concentration.

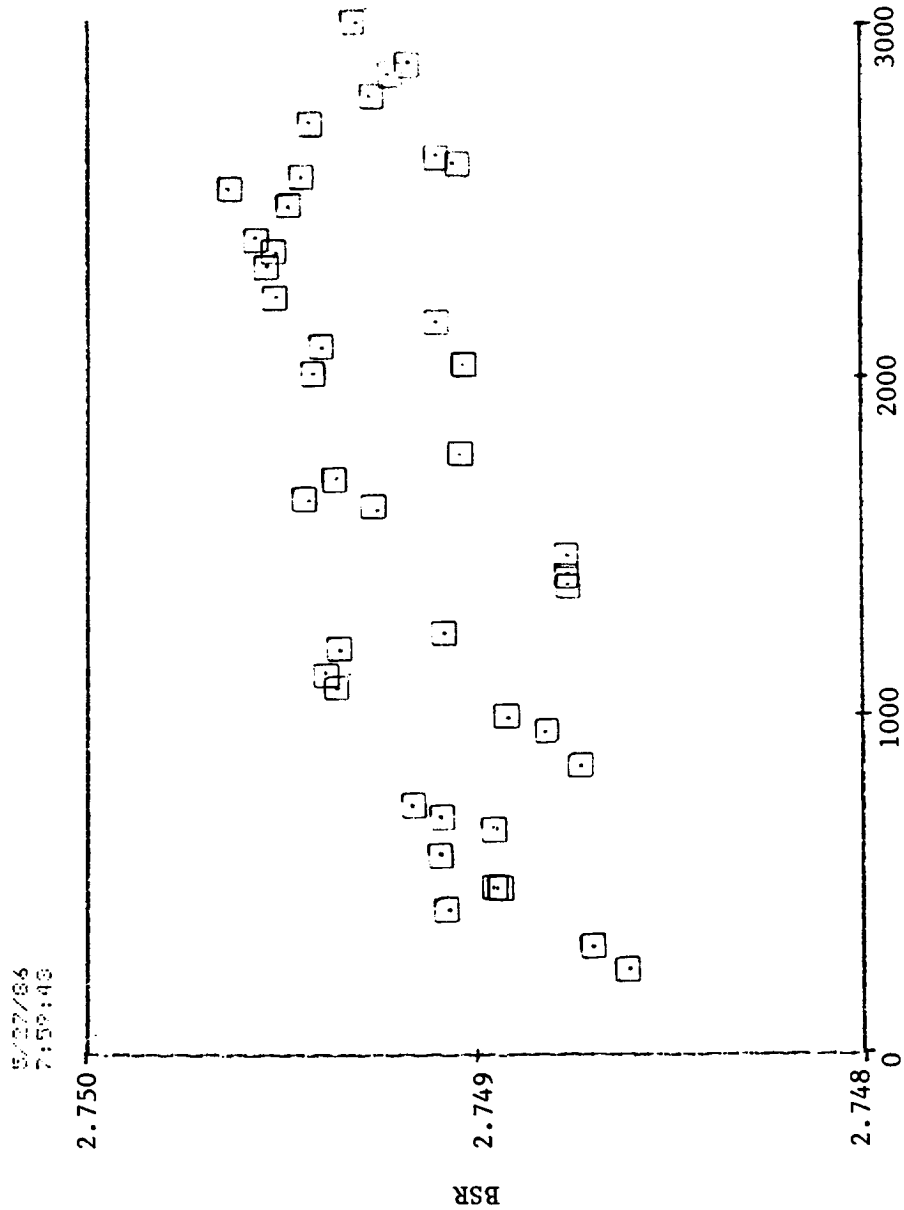

Fig. H.9 BSR vs. elapsed time for ITI 11532-A test bearing, 200 lb load, time study #1 - 50 min., 0.016 SRG 200 oil/freon concentration.

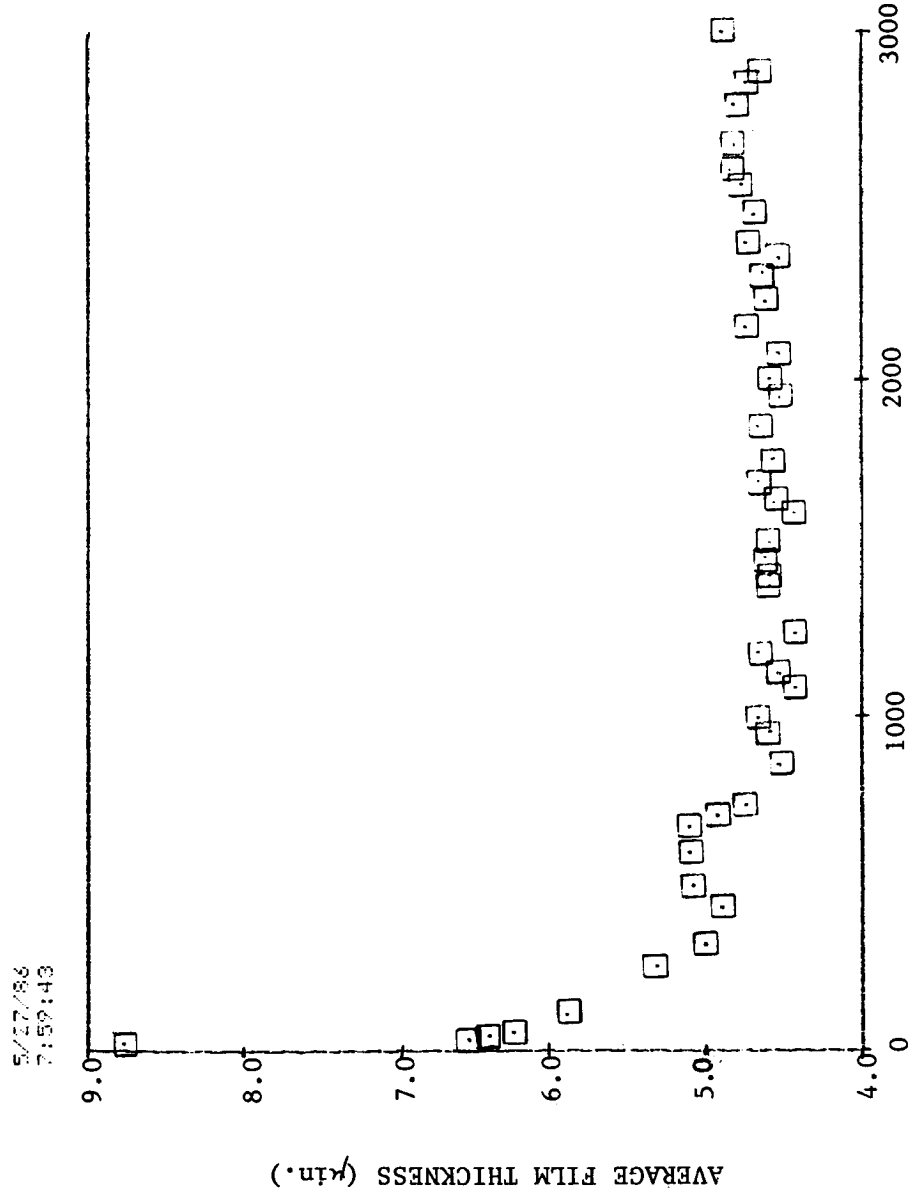

Fig. H.10 Average film thickness vs. elapsed time for ITI 11532-A test bearing, 200 lb load, time study #1 - 50 min., 0.016 SRG 200 oil/freon concentration.

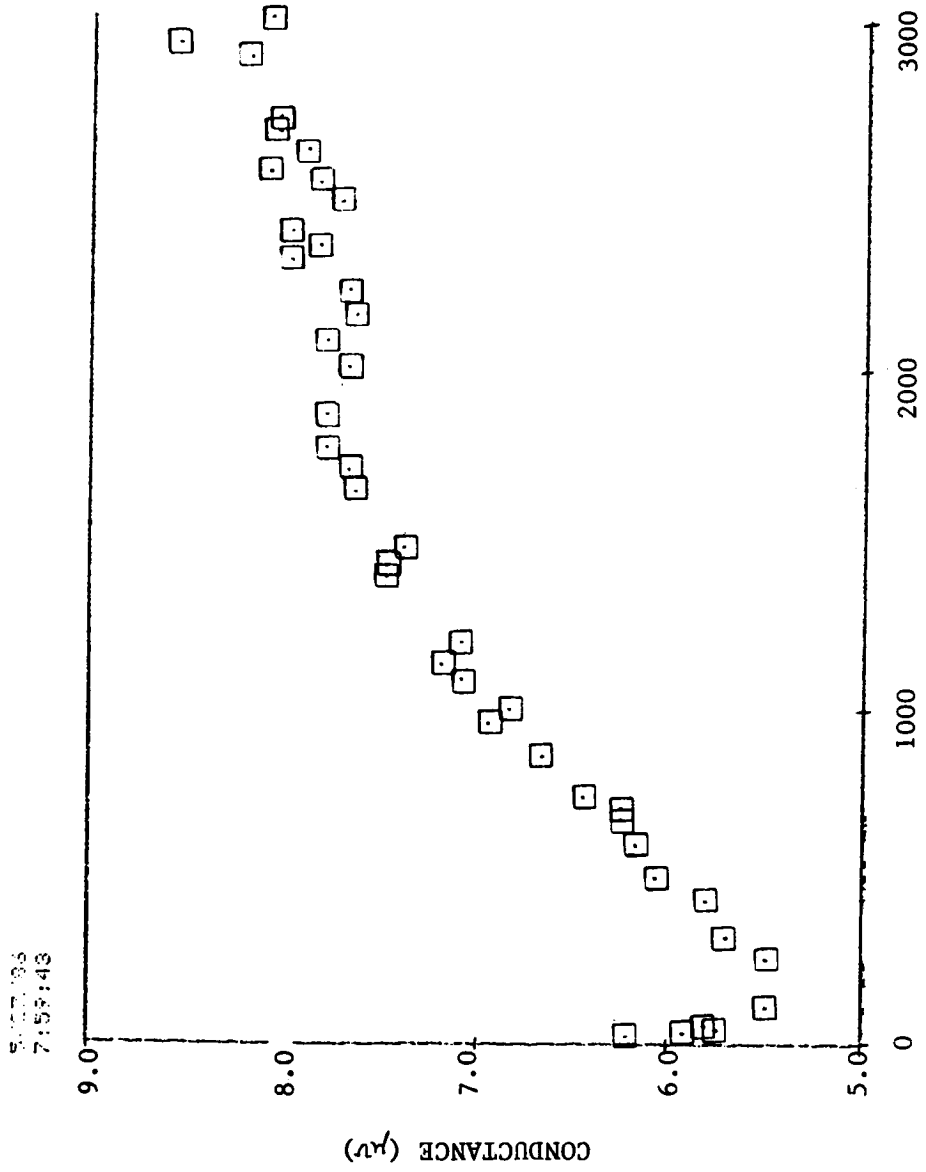

Fig. H.11 Conductance vs. elapsed time for ITI 11532-A test bearing, 200 lb load, time study #1 - 50 min., 0.016 SRG 200 oil/freon concentration.

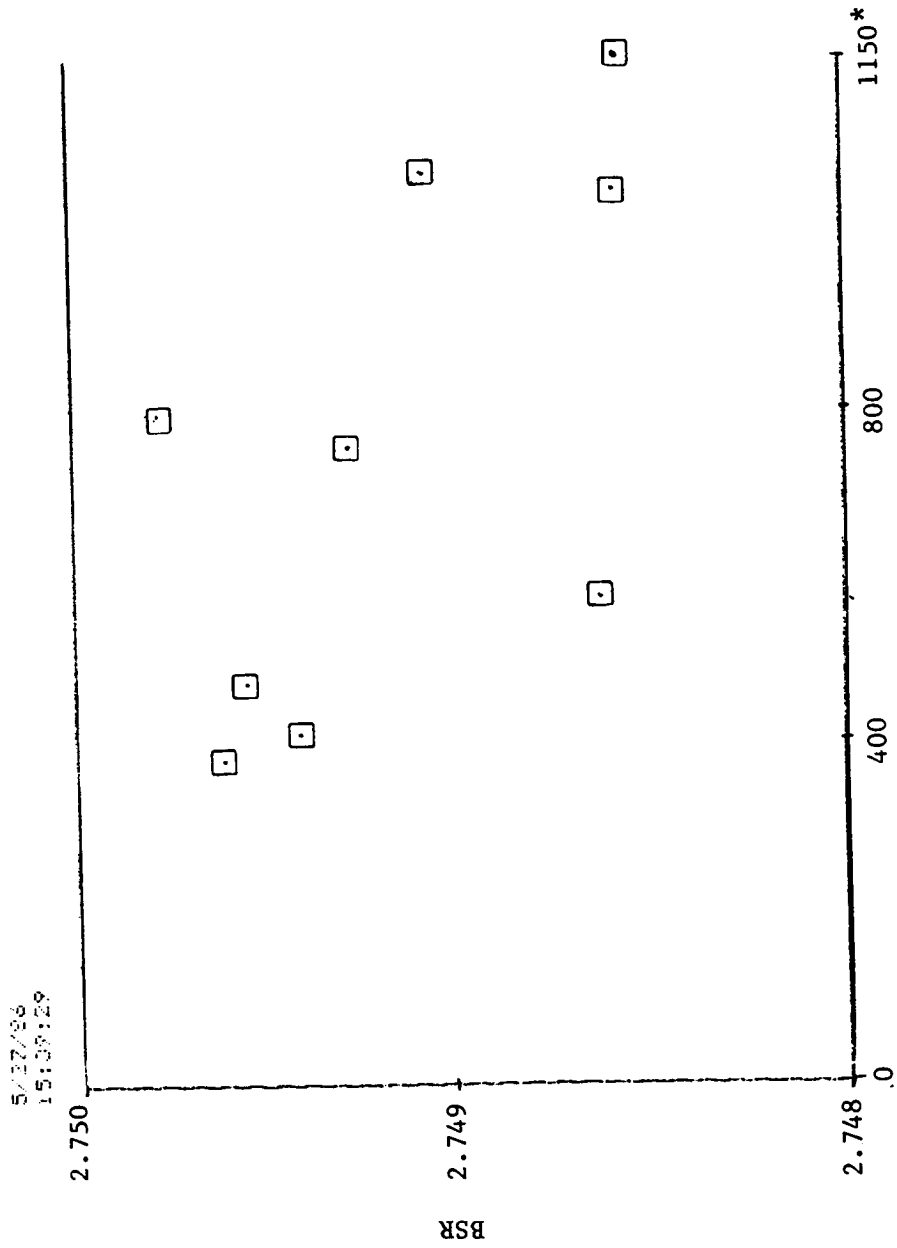

Fig. H.12 BSR vs. elapsed time for ITI 11532-A test bearing, 200 lb load, time study #1 - 60 min., 0.016 SRG 200 oil/freon concentration.

* - test bearing failed

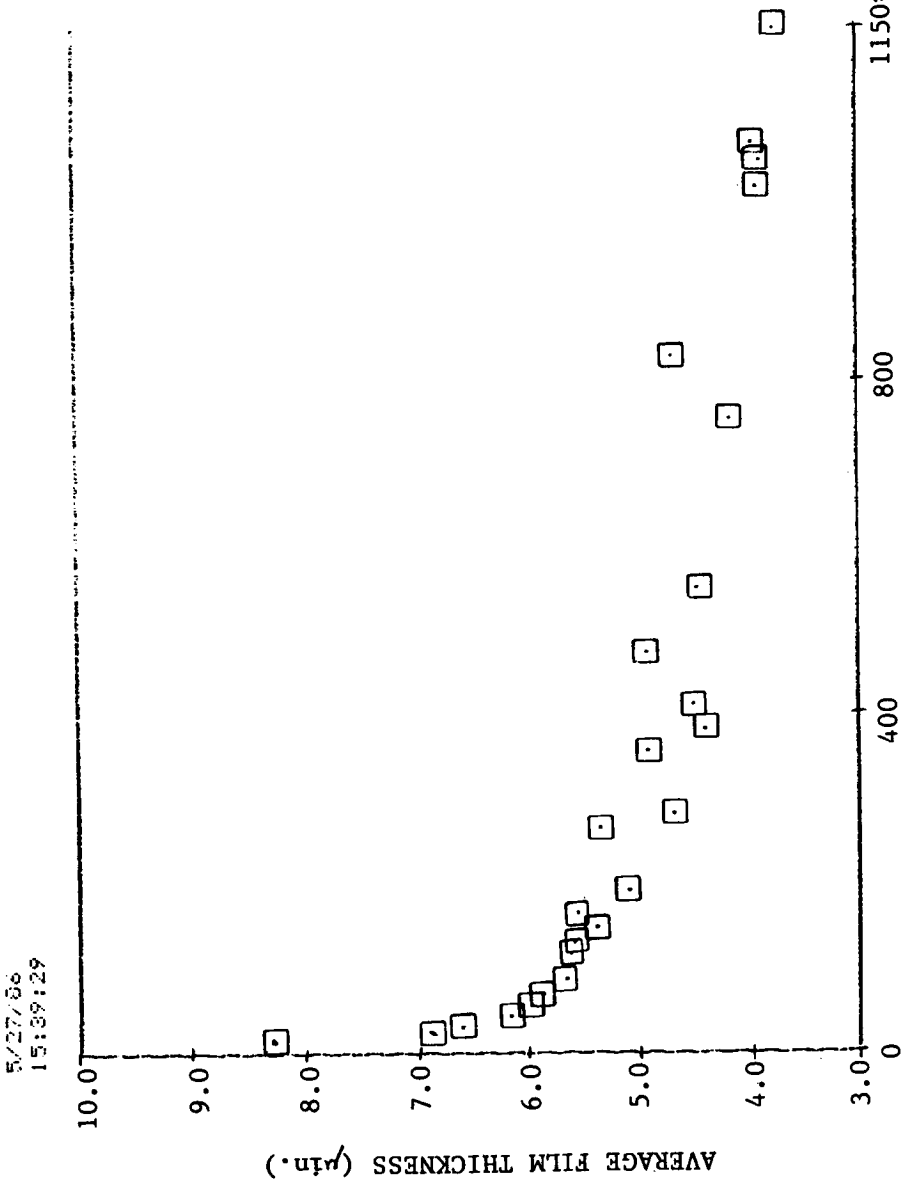

Fig. H.13 Average film thickness vs. elapsed time for ITI 11532-A test bearing, 200 lb load, time stucy #1 - 60 min., 0.016 SRG 200 oil/freon concentration.

* - test bearing failed

APPENDIX I

EXPERIMENTAL DATA FOR

TIME STUDY NO. 2

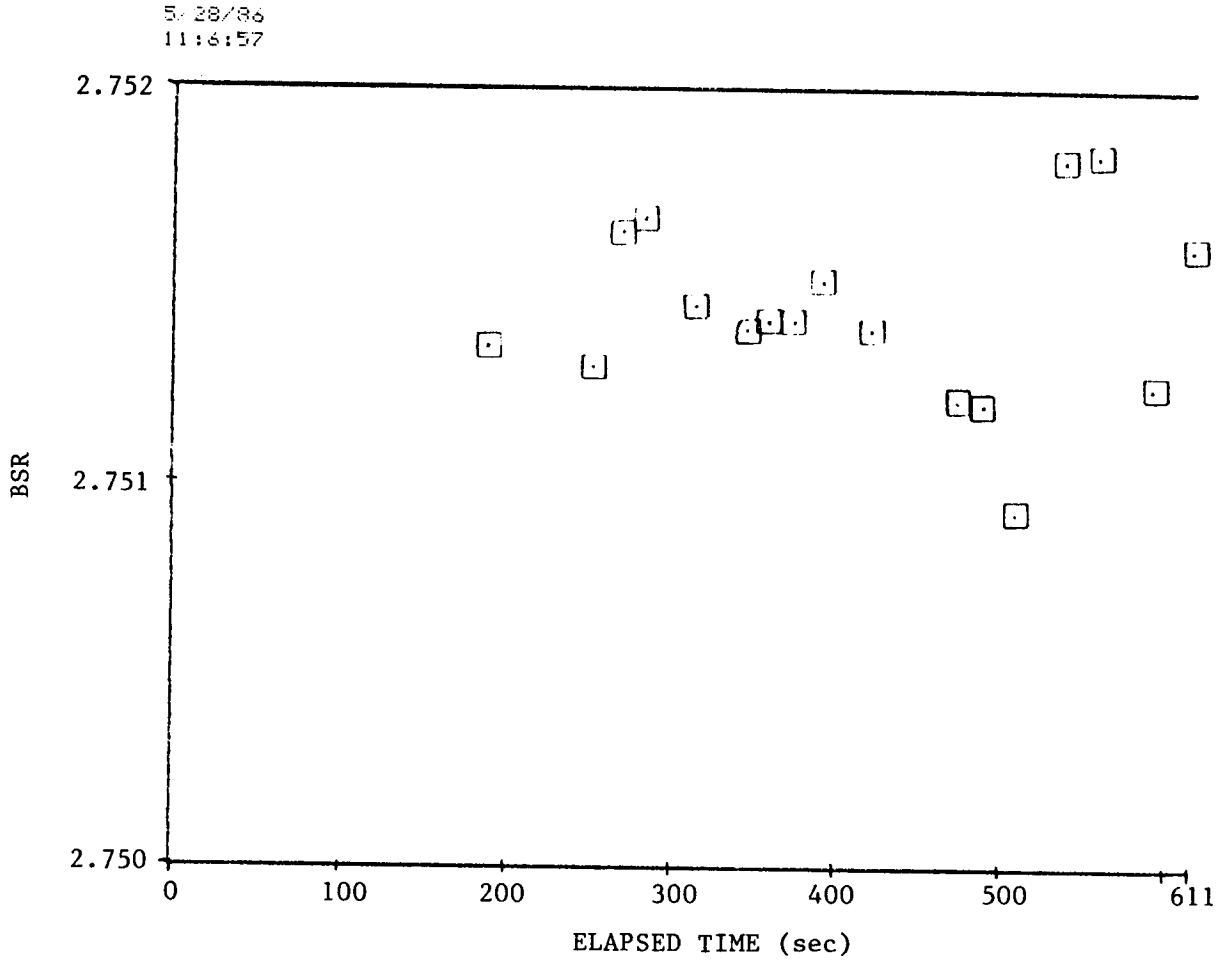

Fig. I.1 BSR vs. elapsed time for ITI 11532-A test bearing, 200 lb load, time study #2 - 10 min., 0.008 SRG 200 oil/freon concentration.

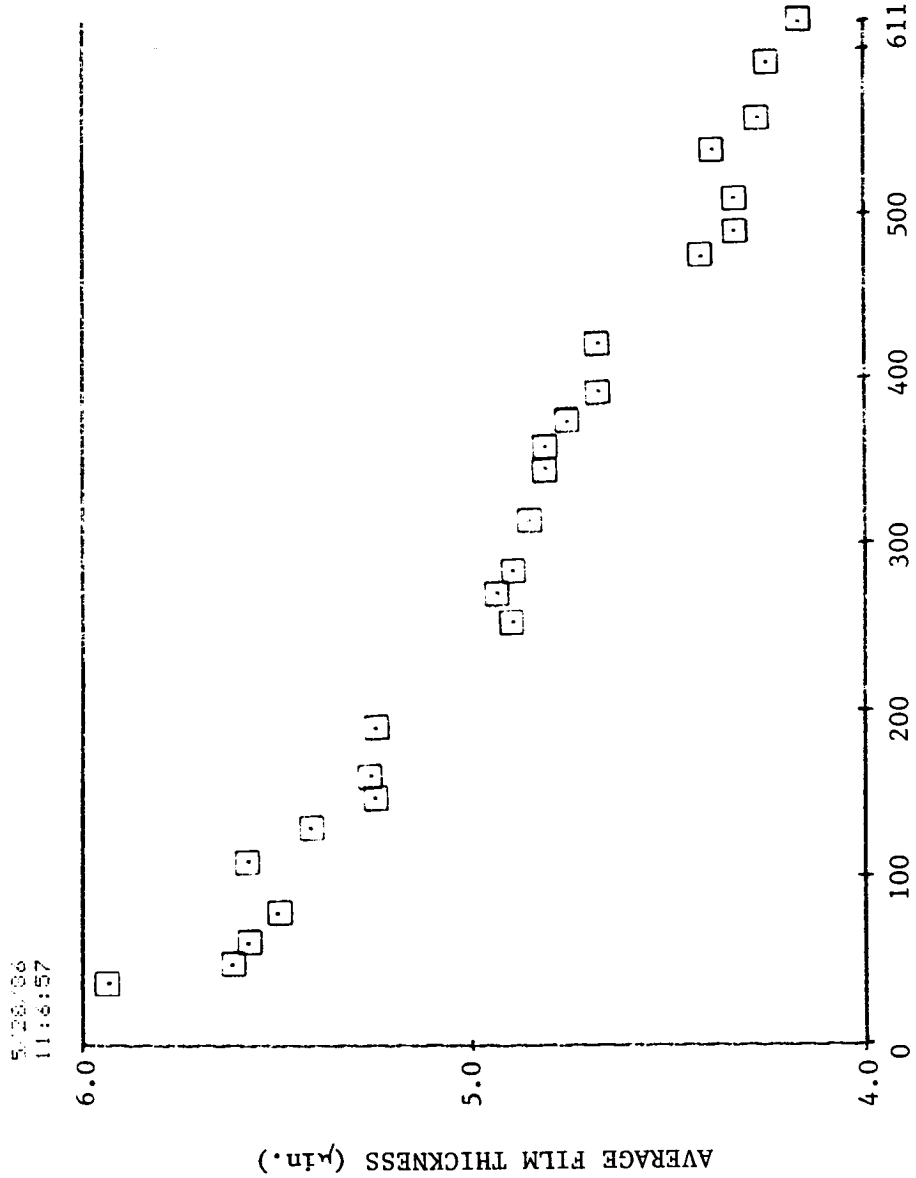

Fig. I.2 Average film thickness vs. elapsed time for ITI 11532-A test bearing, 200 lb load, time study #2 - 10 min., 0.008 SRG 200 oil/freon concentration.

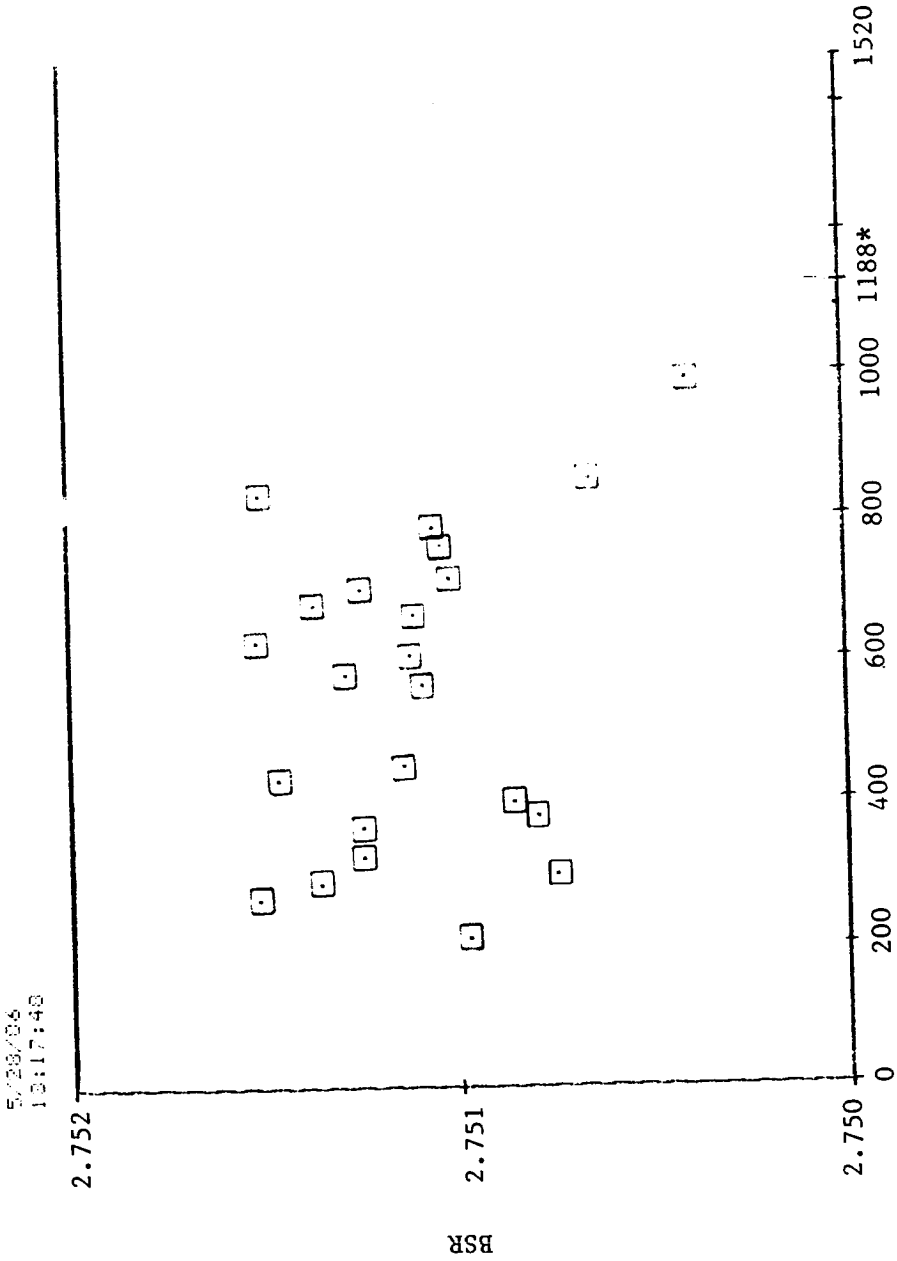

Fig. I.3 BSR vs. elapsed time for ITI 11532-A test bearing, 200 lb load, time study #2 - 20 min., 0.008 SRG 200 cil/freon concentration.

* - test rig stopped

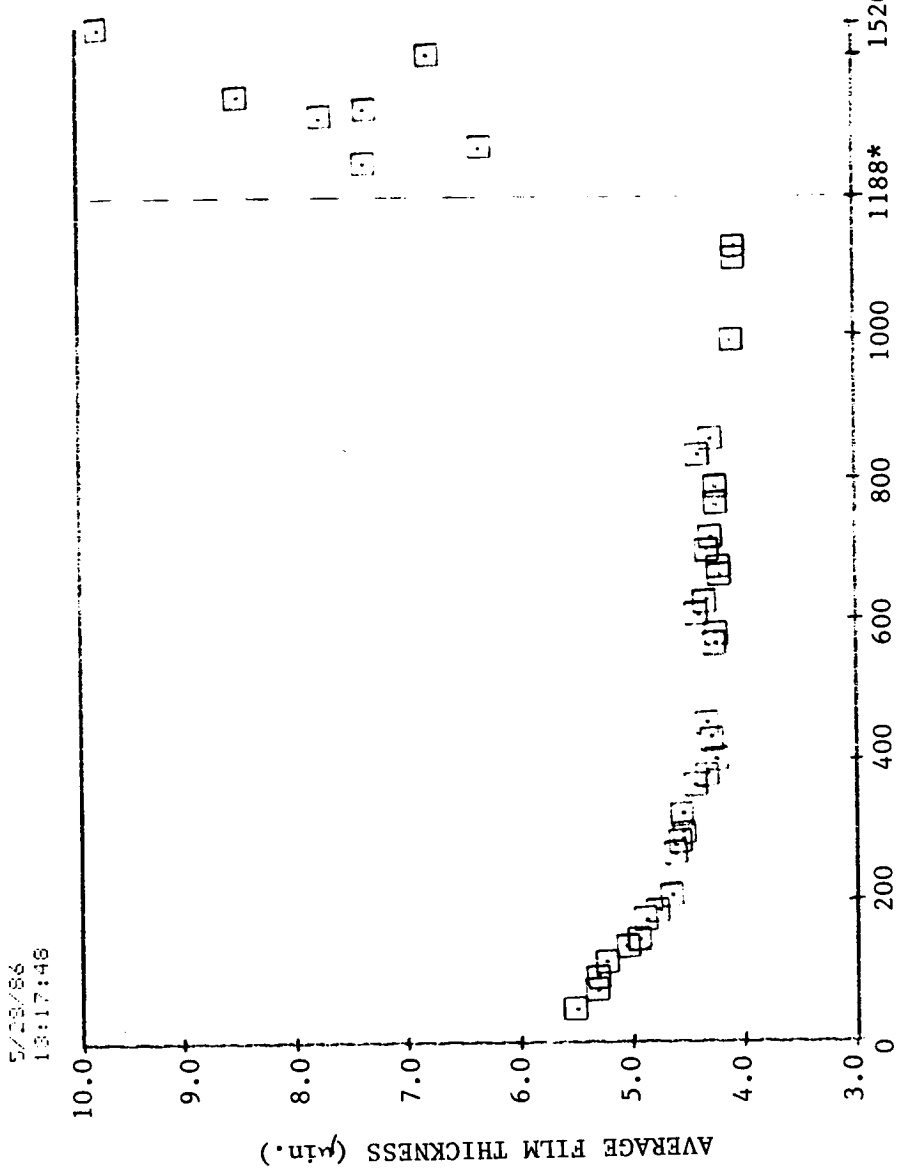

Fig. I.4 Average film thickness vs. elapsed time for ITI 11532-A test bearing, 200 lb load, time stud #2 - 20 min., 0.008 SRG 200 oil/freon concentration.

* - test rig stopped

ORIGINAL PAGE IS
OF POOR QUALITY

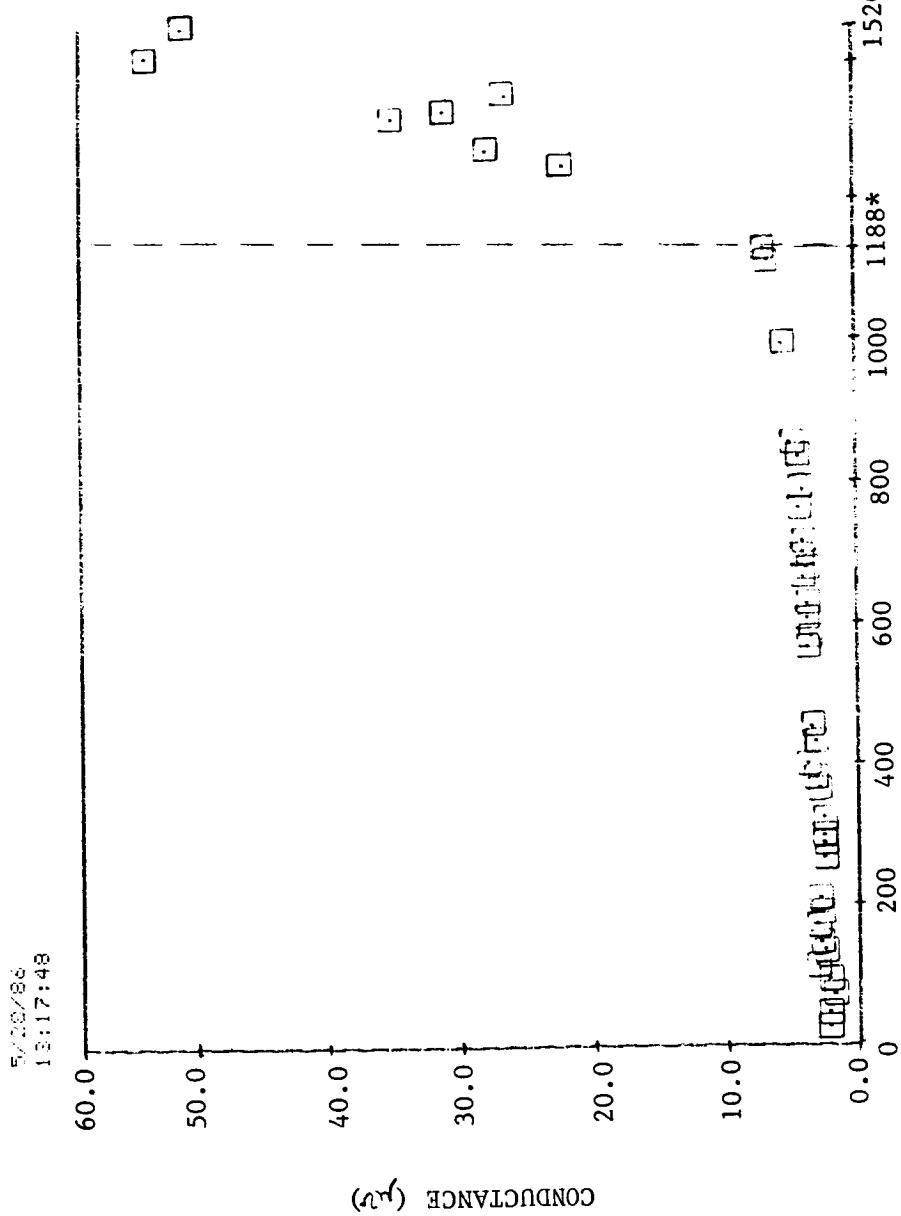

Fig. I.5 Conductance vs. elapsed time for ITI 11532-A test bearing, 200 lb load, time study #2 - 20 min., 0.008 SRG 200 oil/freon concentration.

* - test rig stopped

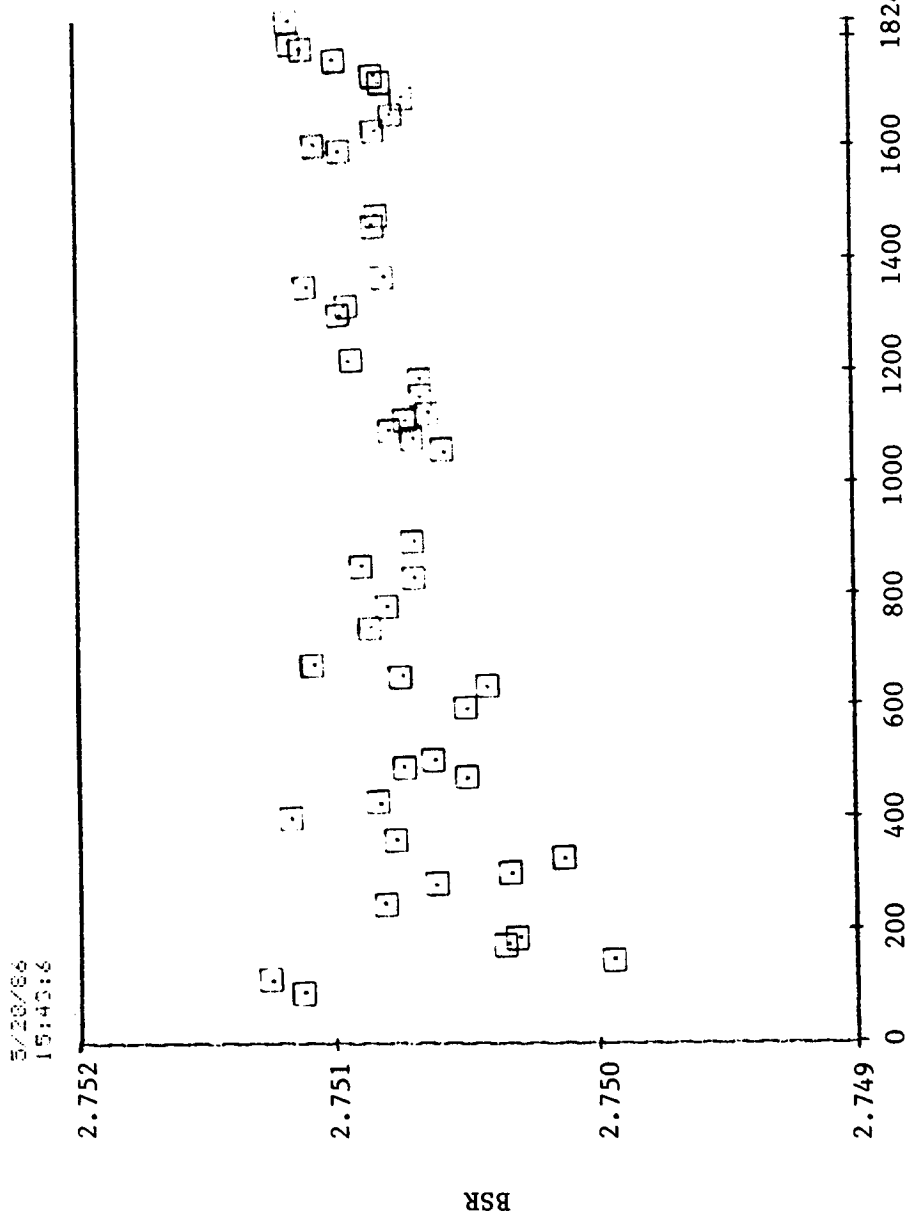

Fig. I.6 BSR vs. elpased time for ITI 11532-A test bearing, 200 lb load, time study #2 - 30 min., 0.008 SRG 200 oil/freon concentration.

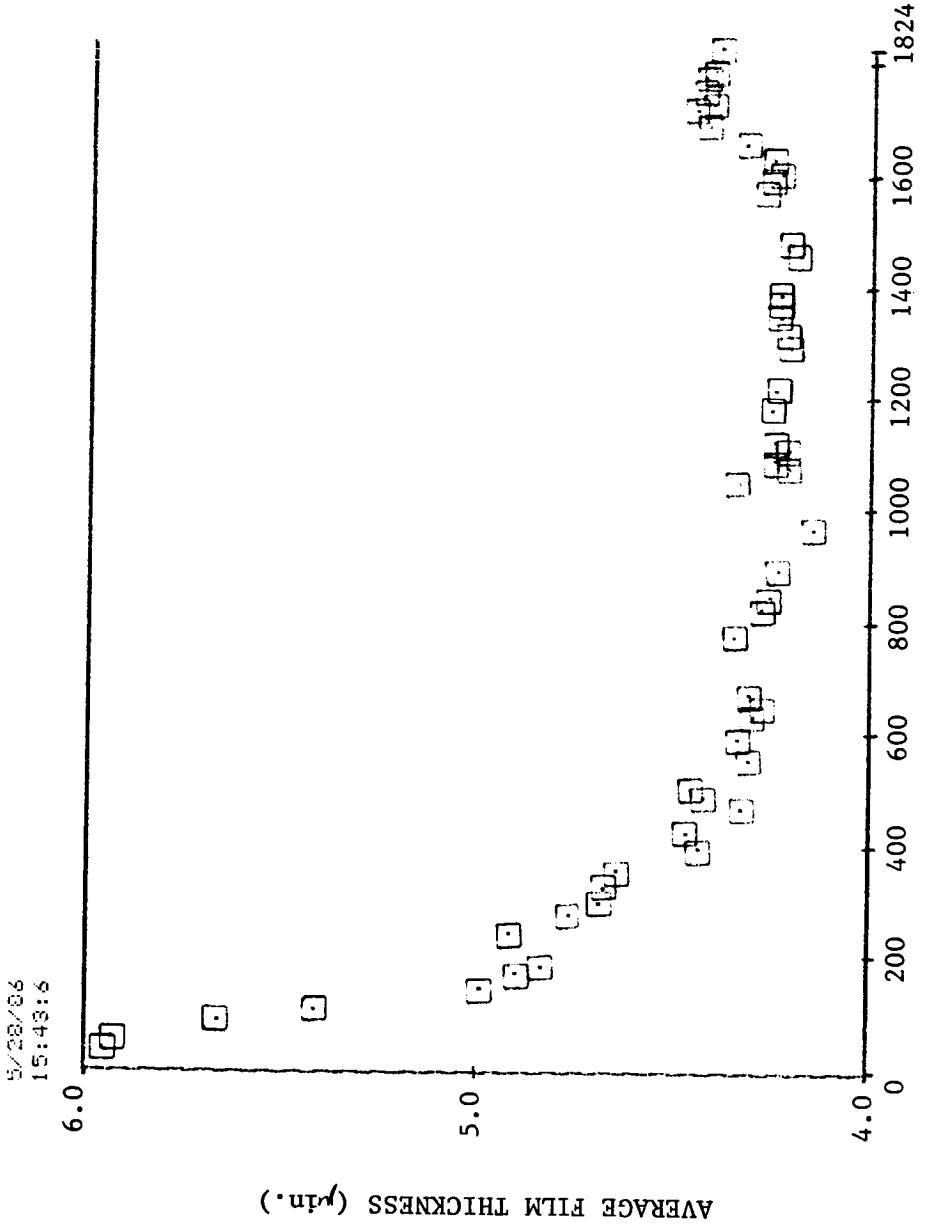

Fig. I.7 Average film thickness vs.elapsed time for ITI 11532-A test bearing, 200 lb load, time study #2 - 30 min., 0.008 SRG 200 oil/freon concentration.

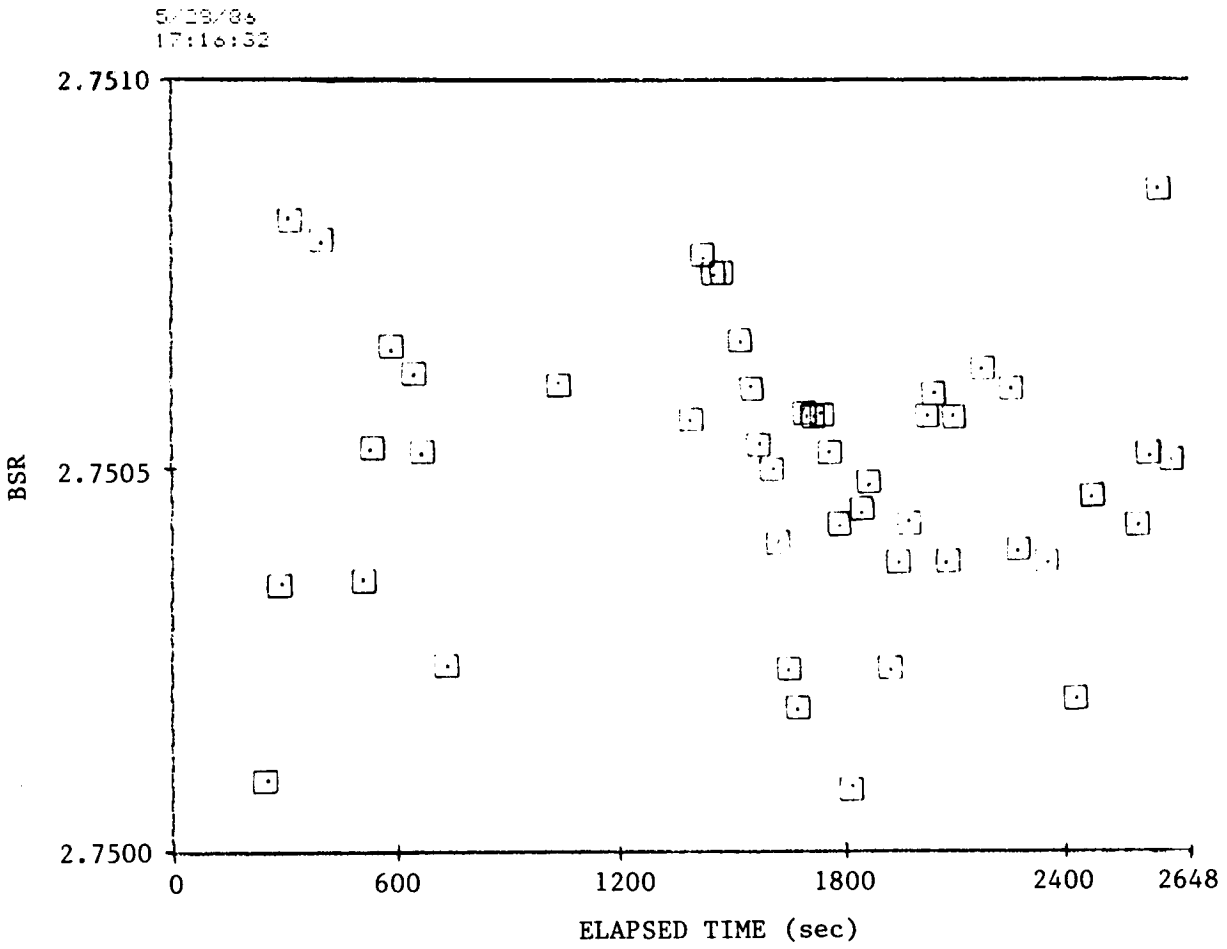

Fig. I.8 BSR vs. elapsed time for ITI 11532-A test bearing, 200 lb load, time study #2 - 40 min., 0.008 SRG 200 oil/freon concentration.

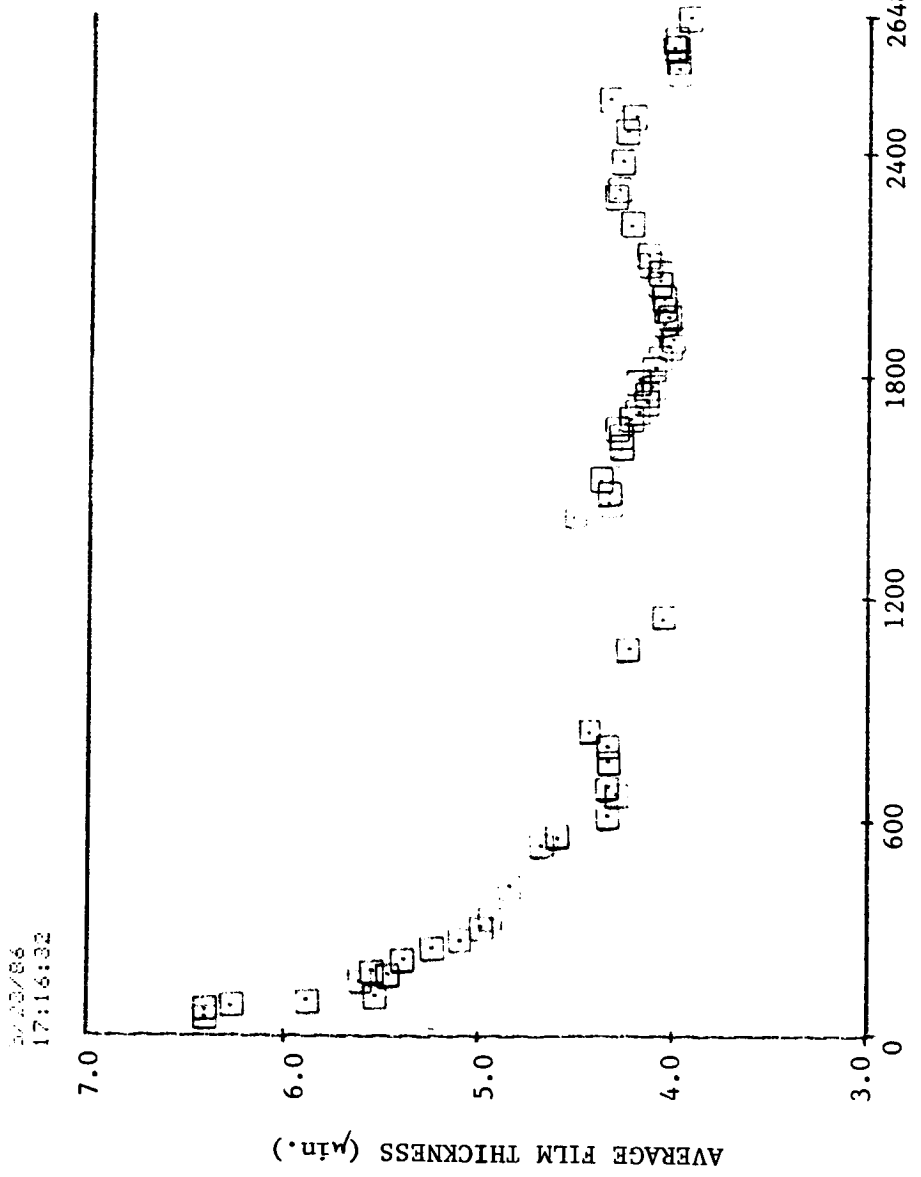

Fig. I.9 Average film thickness vs. elapsed time for ITI 11532-A test bearing, 200 lb load, time study #2 - 40 min., 0.008 SRG 200 oil/freon concentration.

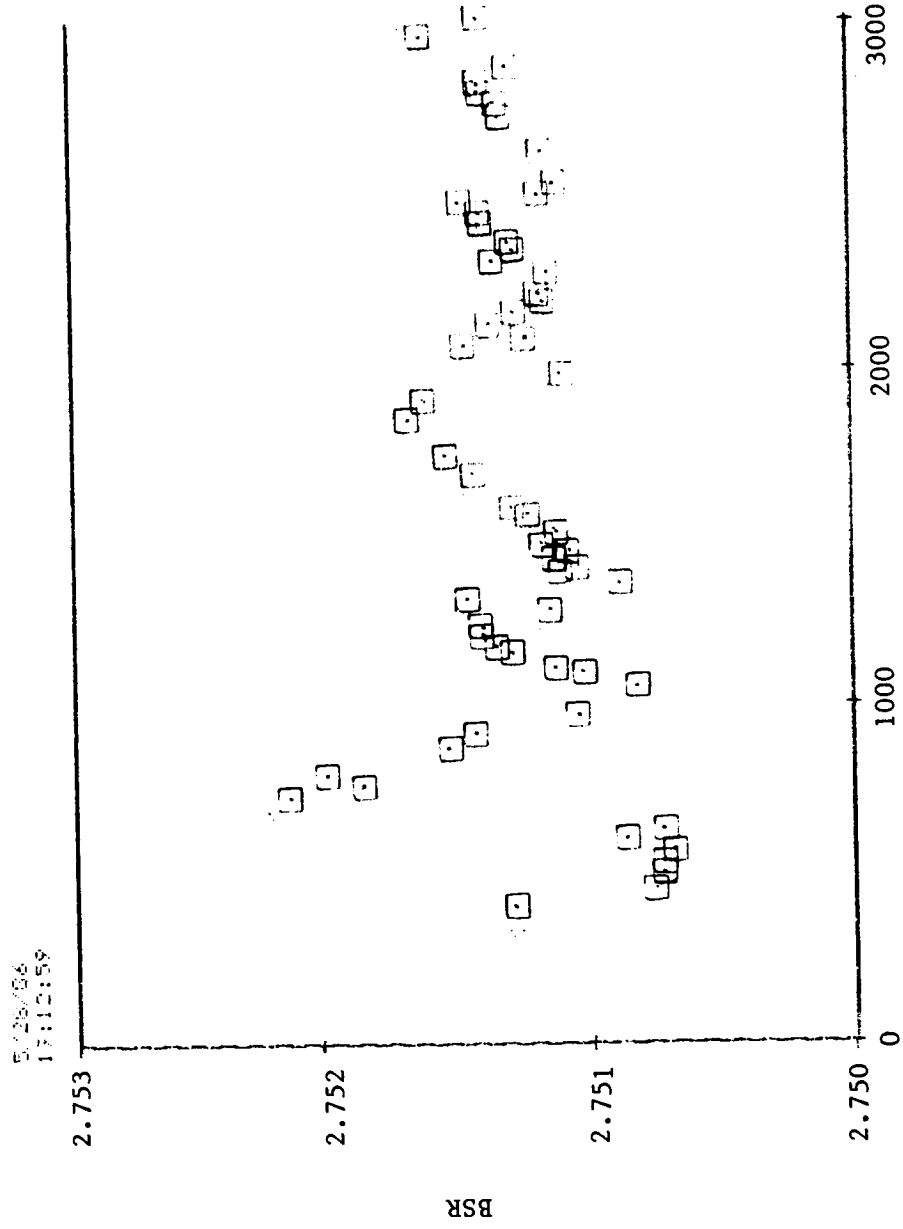

Fig. I.10 BSR vs. elapsed time for ITI 11532-A test bearing, 200 lb load, time study #2 - 50 min., 0.008 SRG 200 oil/freon concentration.

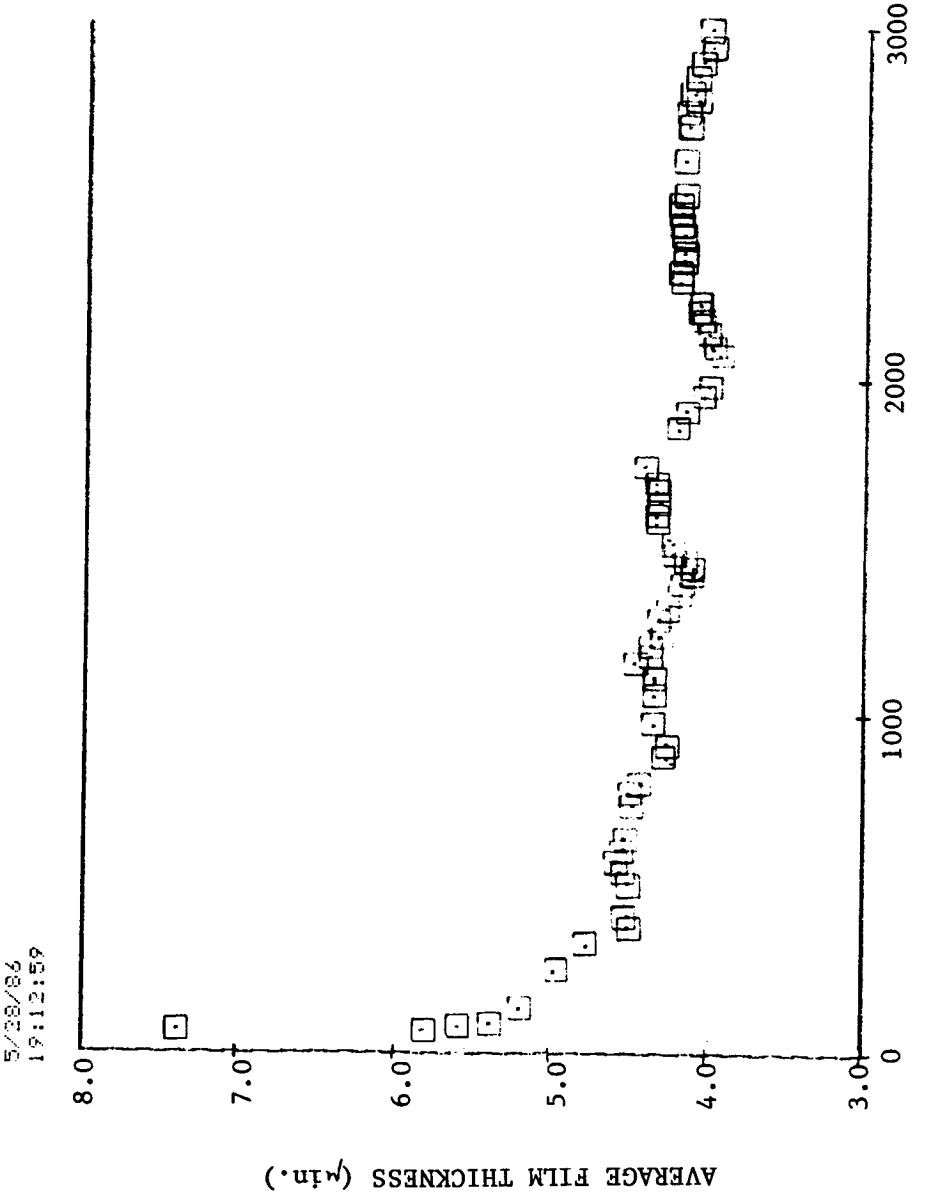

Fig. I.11 Average film thickness vs. elapsed time for ITI 11532-A test bearing, 200 lb load, time study #2 - 50 min., 0.008 SRG 200 oil/freon concentration.

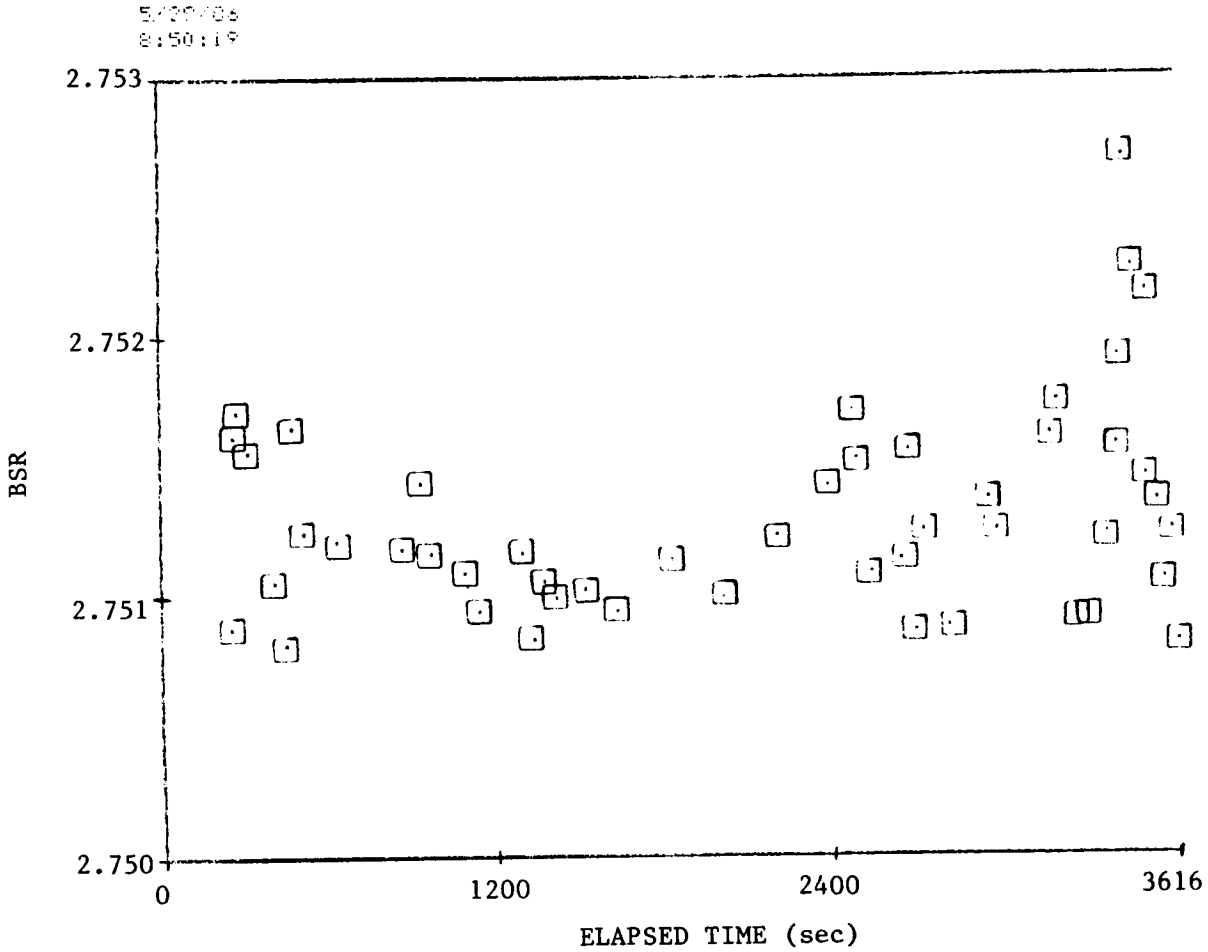

Fig. I.12 BSR vs. elapsed time for ITI 11532-A test bearing, 200 lb load, time study #2 - 60 min., 0.008 SRG 200 oil/freon concentration.

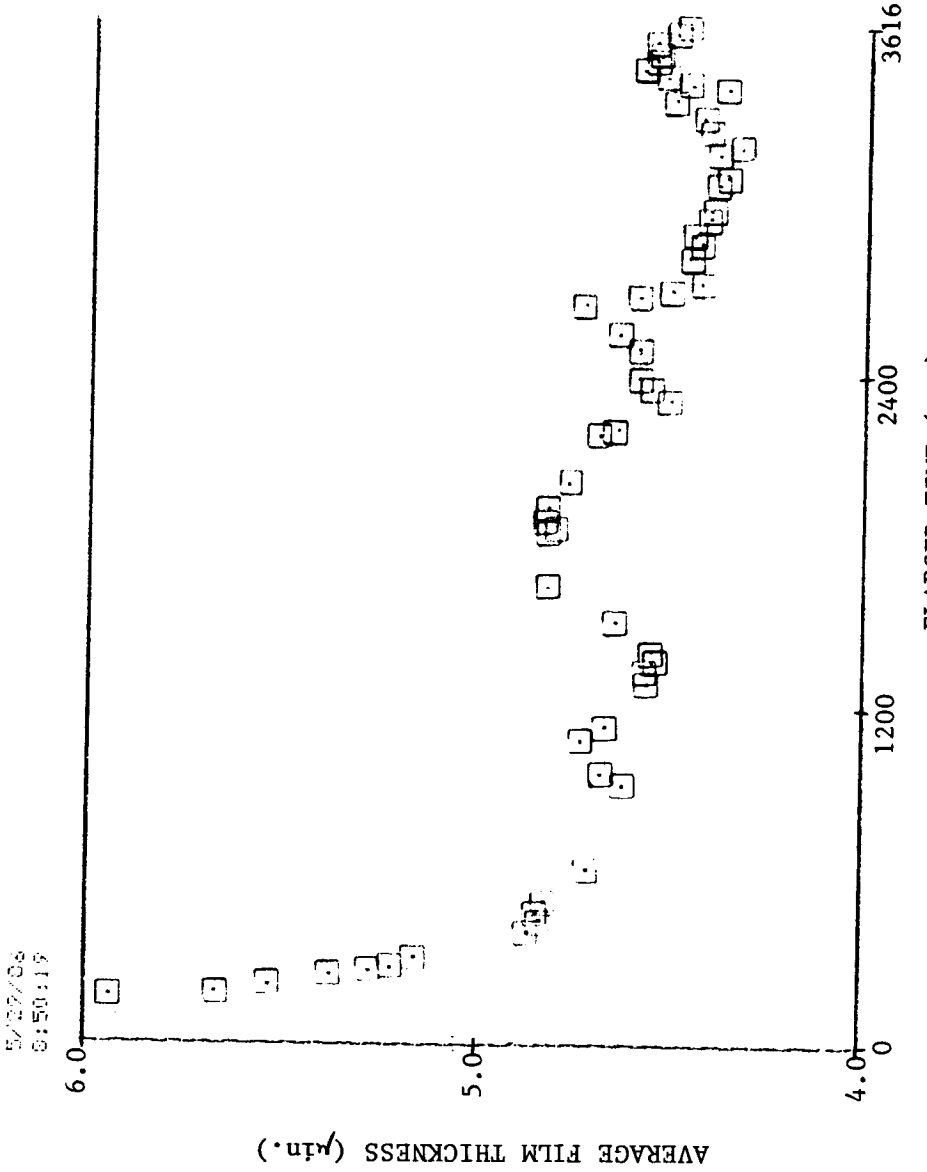

Fig. I.13 Average film thickness vs. elasped time for ITI 11532 test bearing, 200 lb load, time study #2 - 60 min., 0.008 SRG 200 oil/freon concentration.

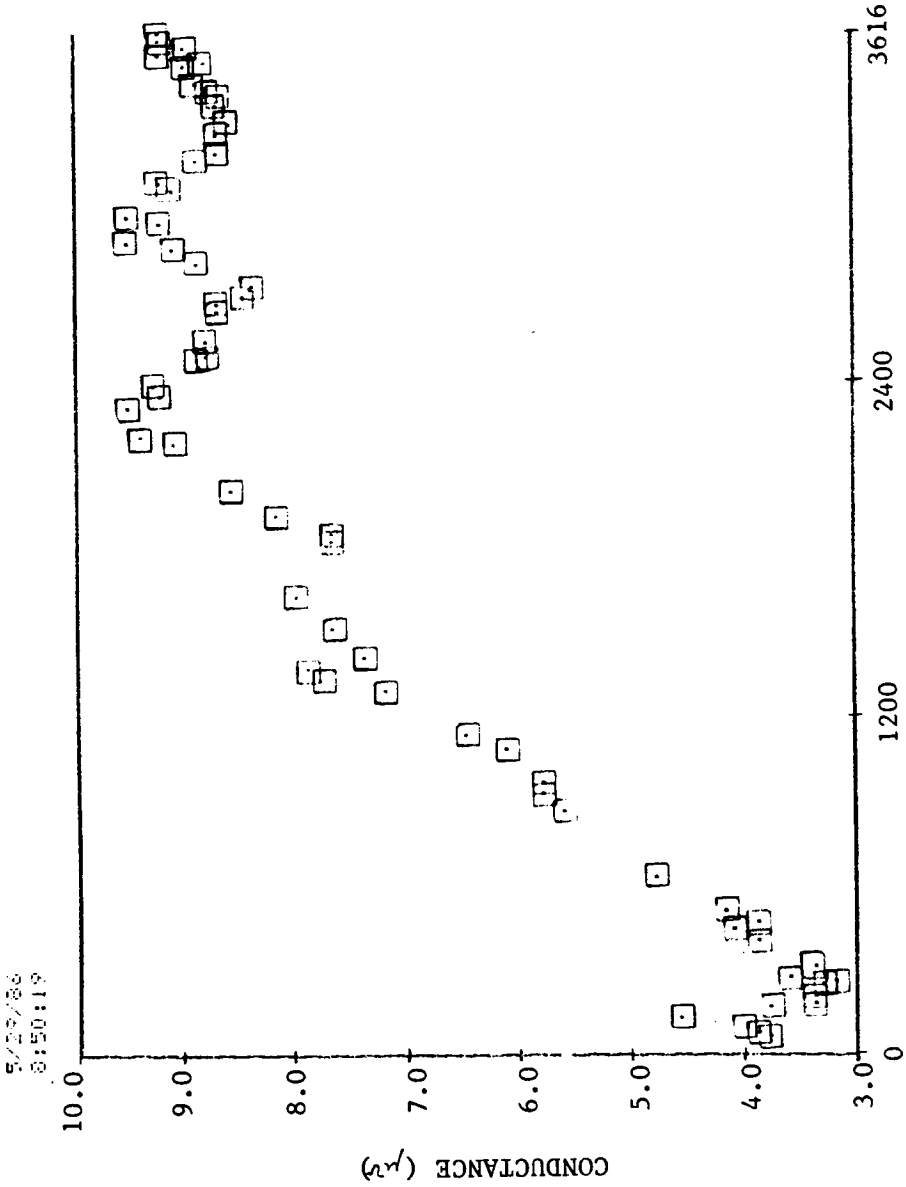

Fig. I.14 Conductance vs. elapsed time for ITI 11532-A test bearing, 200 lb load, time study #2 - 60 min., 0.008 SRG 200 oil/freon concentration.

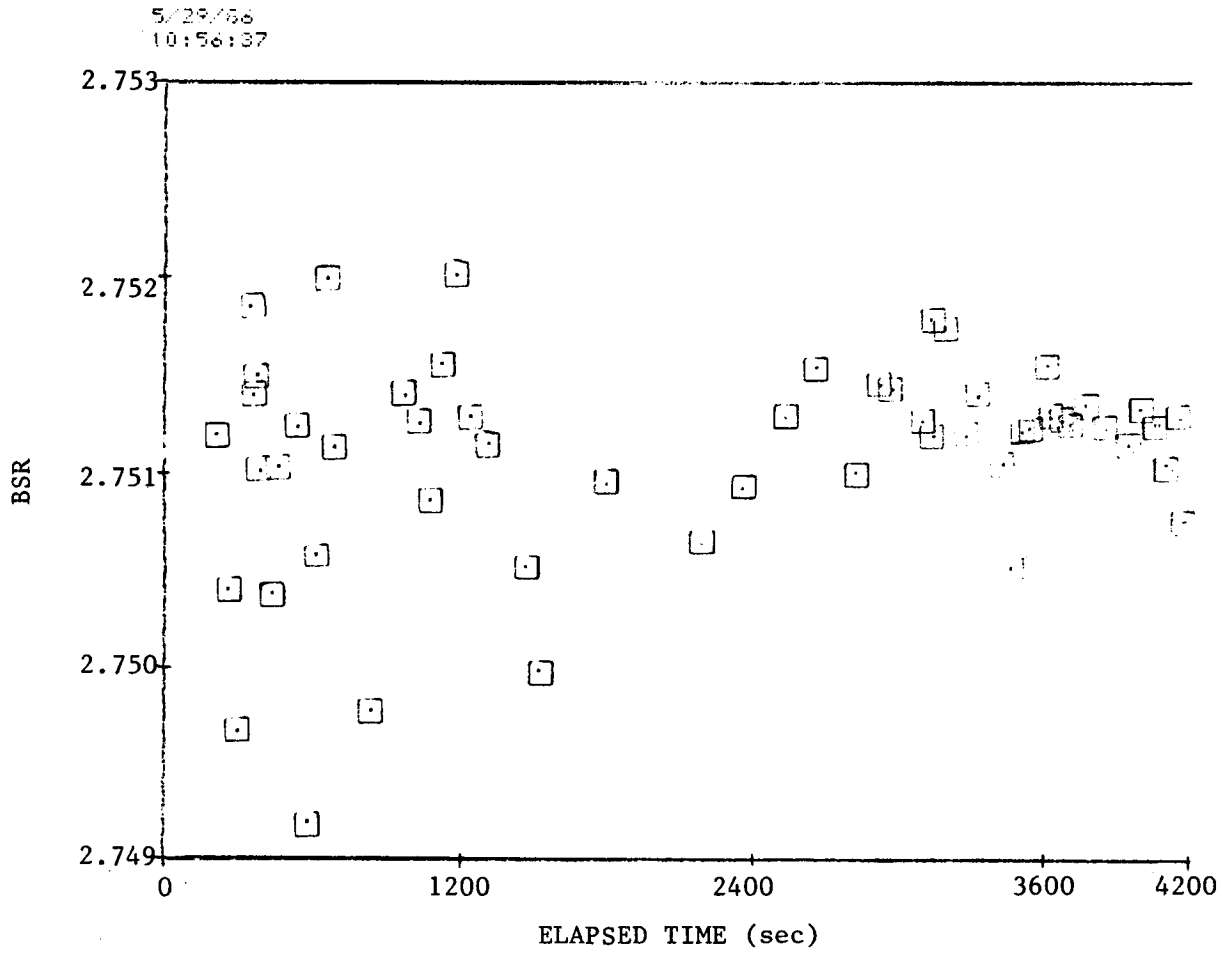

Fig. I.15 BSR vs. elapsed time for ITI 11532-A test bearing, 200 lb load, time study #2 - 70 min., 0.008 SRG 200 oil/freon concentration.

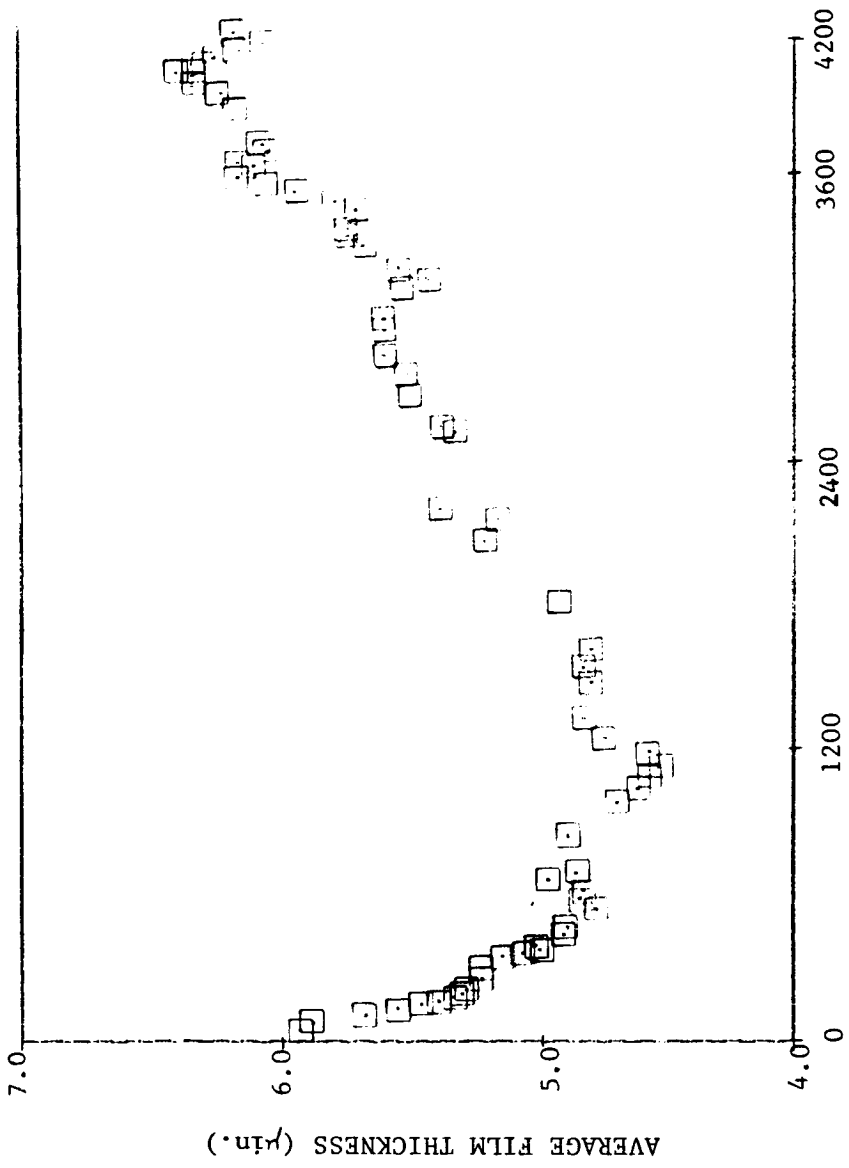

Fig. I.16 Average film thickness for ITI 11532-A test bearing, 200 lb load, time study #2 - 70 min., 0.008 SRG 200 oil/freon concentration.

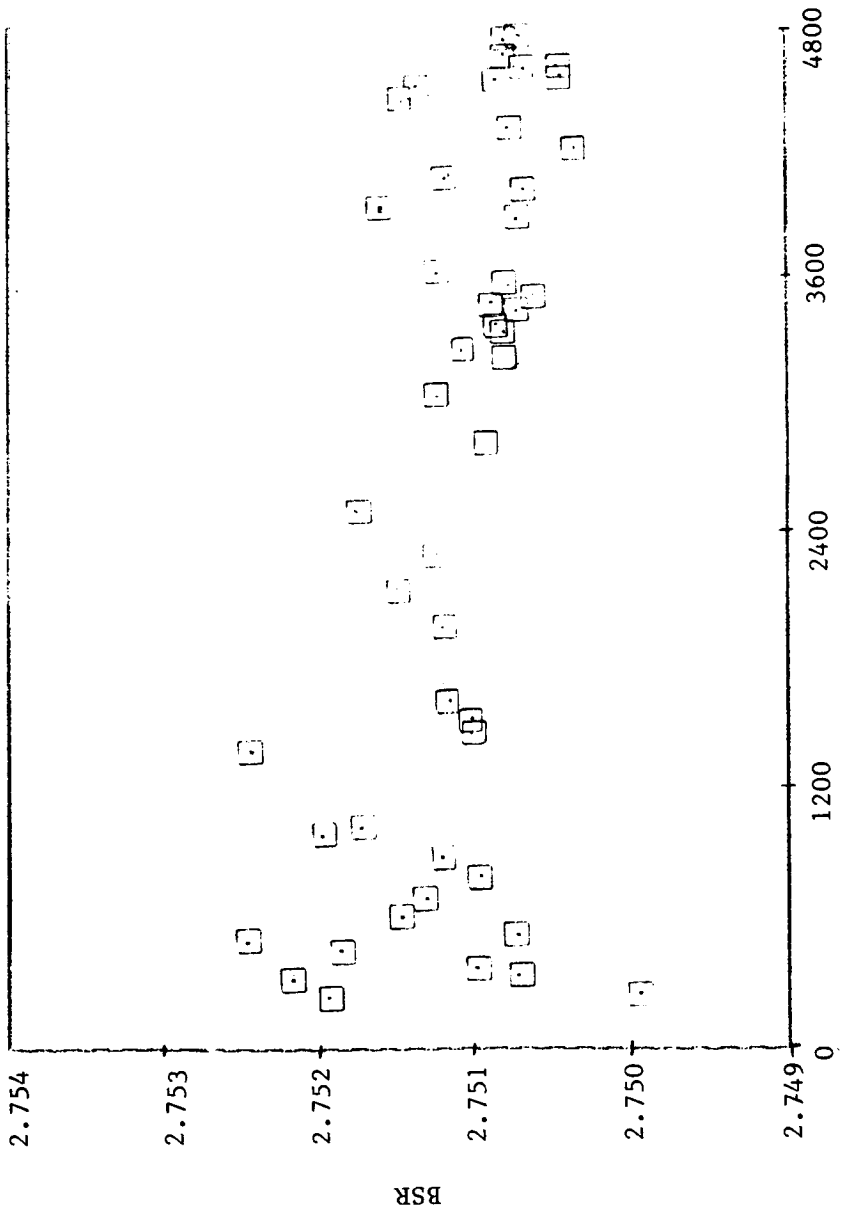

Fig. I.17 BSR vs. elapsed time for ITI 11532-A test bearing, 200 lb load, time study #2 - 80 min., 0.008 SRG 200 oil/freon concentration.

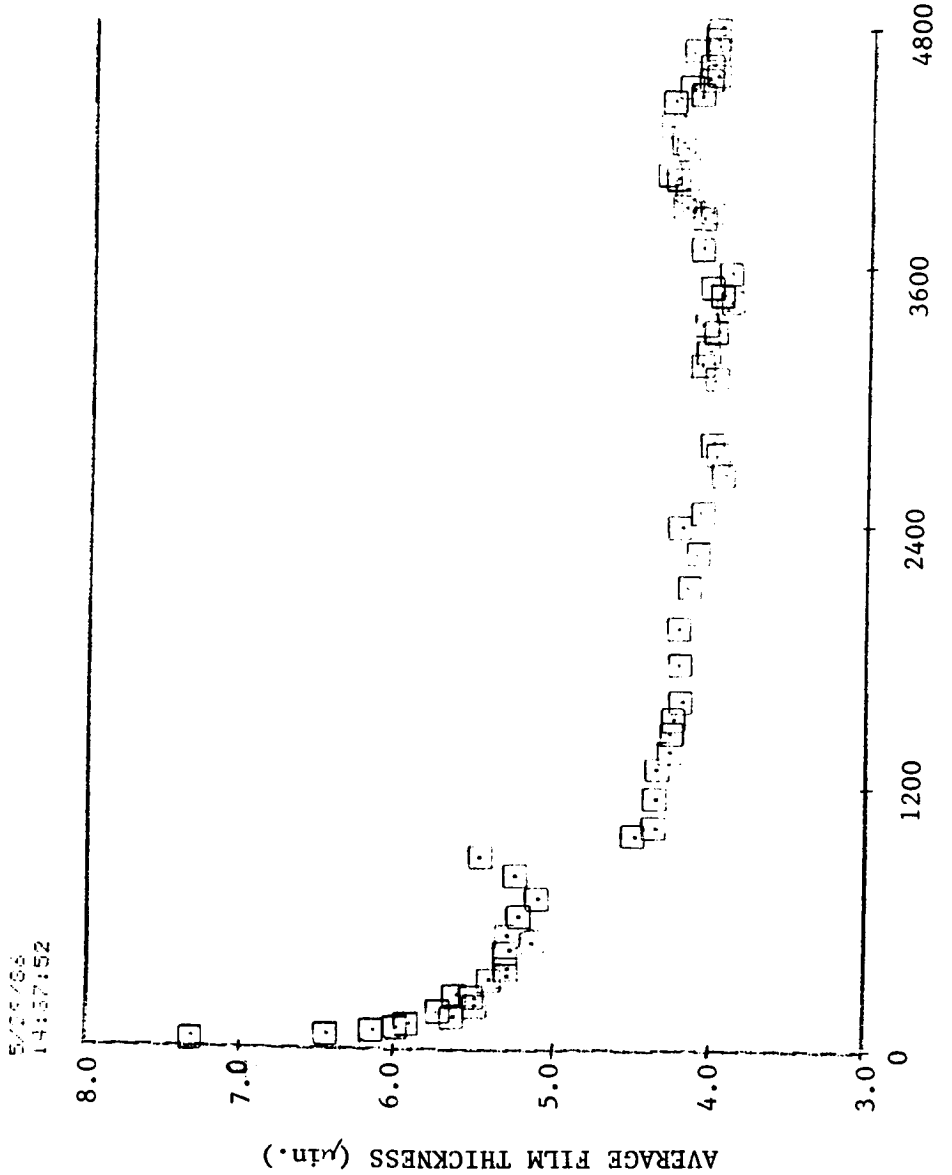

Fig. I.18 Average film thickness vs. elapsed time for ITI 11532-A test bearing, 200 lb load, time study #2 - 80 min., 0.008 SRG 200 oil/freon concentration.

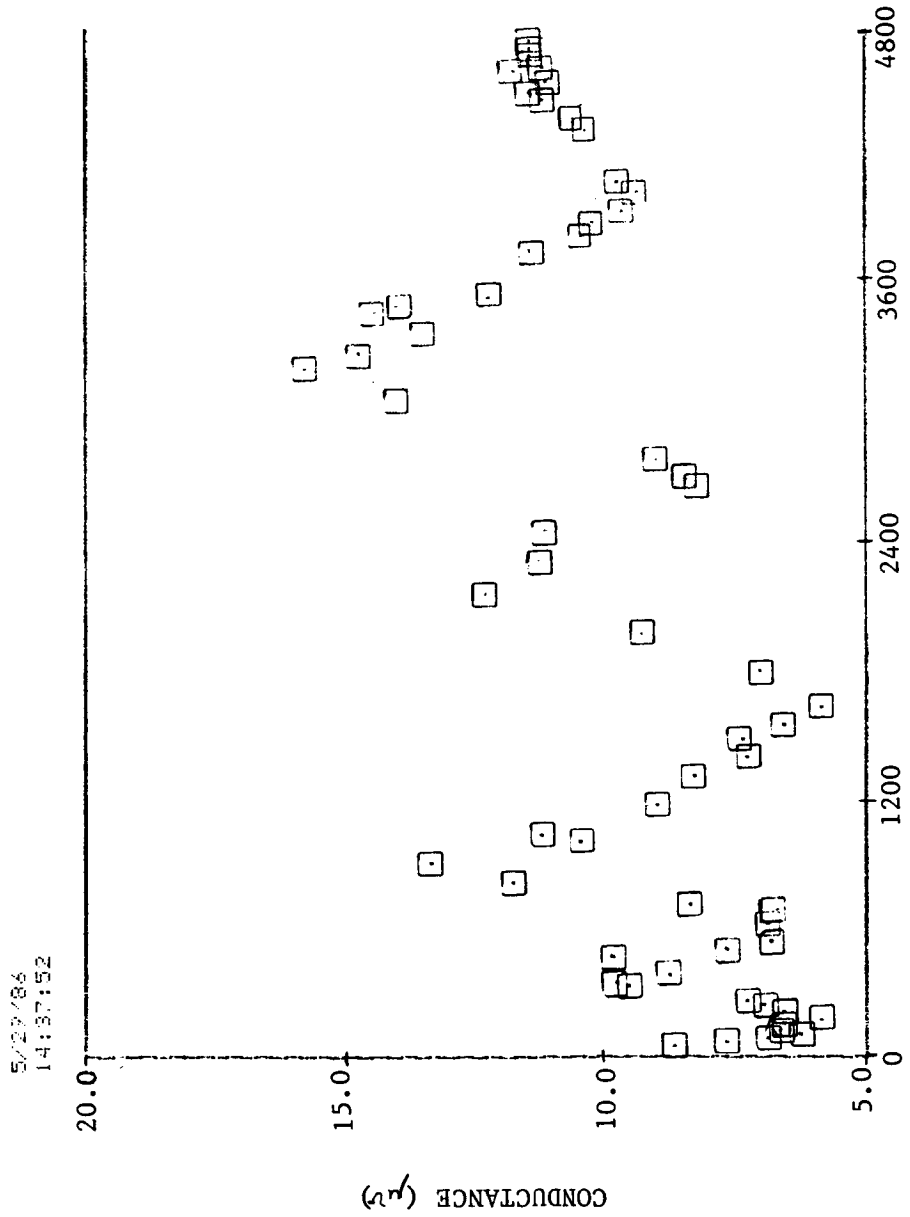

Fig. I.19 Conductance vs elapsed time for ITI 11532-A test bearing, 200 lb load, time study #2 - 80 min., 0.008 SRG 200 oil/freon concentration.

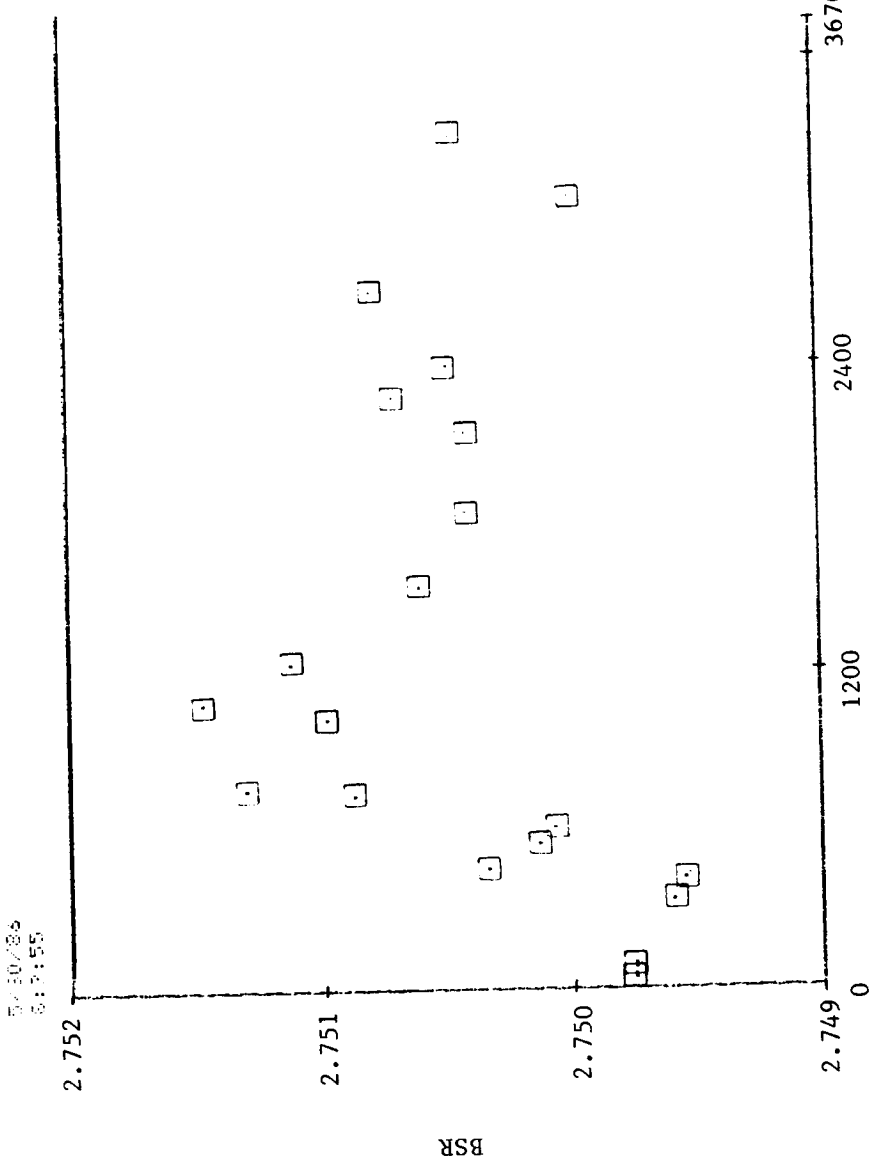

Fig. I.20 BSR vs. elapsed time for ITI 11532-A test bearing, 200 lb load, time study #2 - 90 min., 0.008 SRG 200 oil/freon concentration.

* - test bearing failed

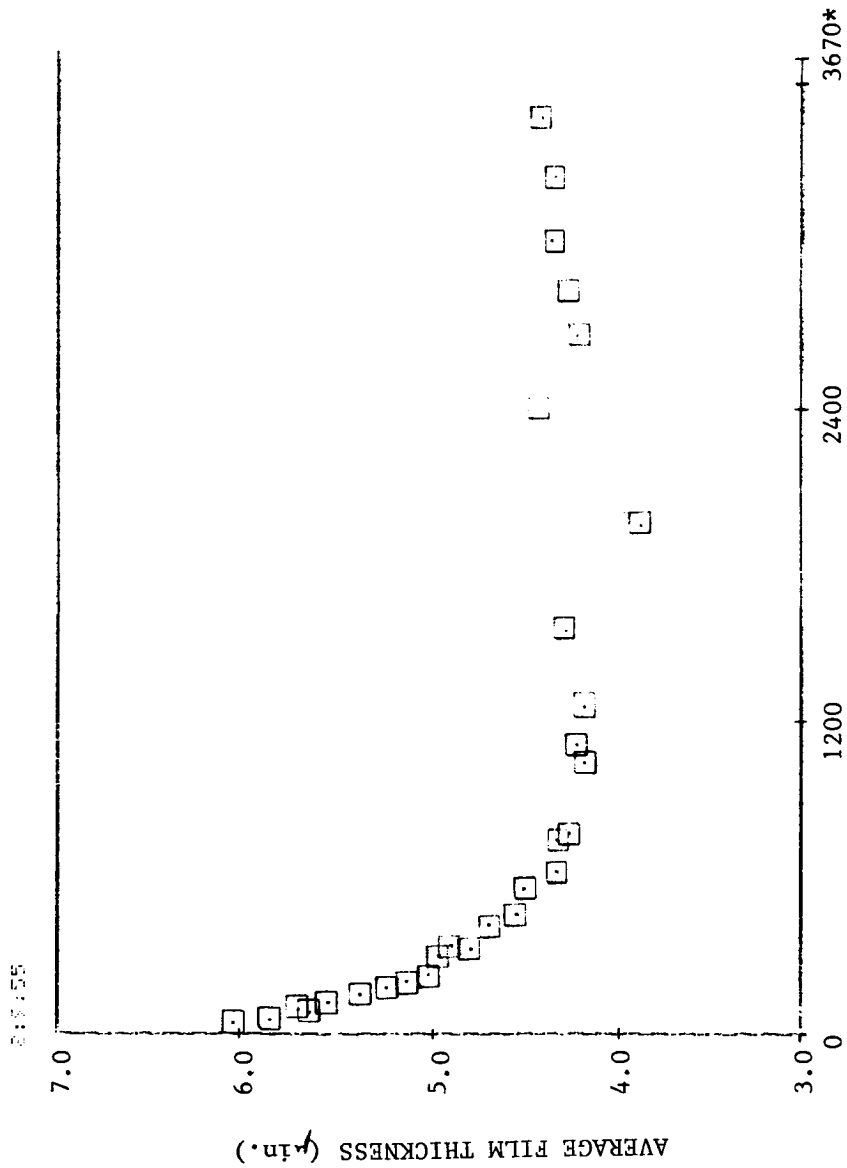

Fig. I.21 Average film thickness vs. elapsed time for ITI 11532-A test bearing, 200 lb load, time study #2 - 90 min., 0.008 SRG 200 oil/freon concentration.

* - test bearing failed

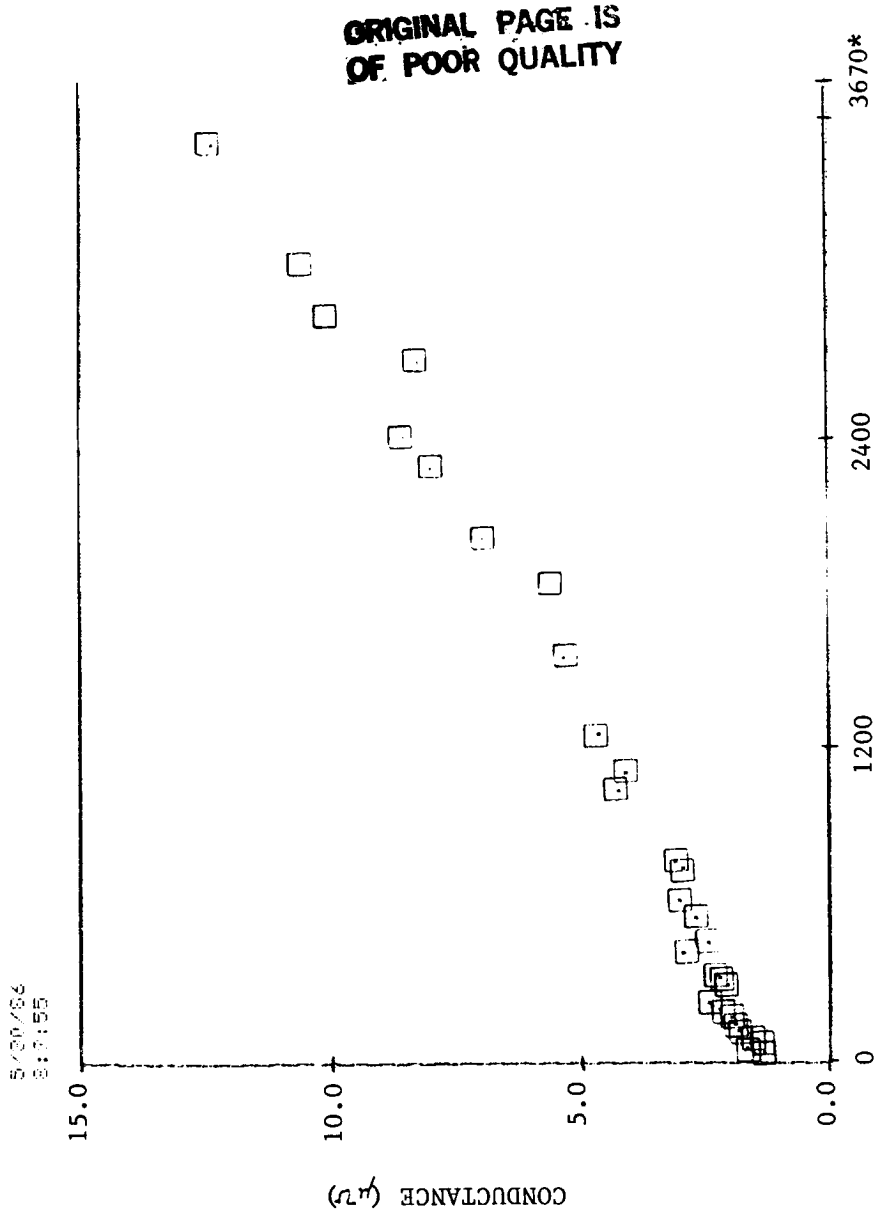

Fig. I.22 Conductance vs. elapsed time for ITI 11532-A test bearing, 200 lb load, time study #2 - 90 min., 0.008 SRG 200 oil/freon concentration.

* - test bearing failed

1. Report No.	2. Government Accession No.	3. Recipient's Catalog No.
NASA CR-179506		

4. Title and Subtitle	5. Report Date
Oil Film Thickness Measurement and Analysis for an Angular Contact Ball Bearing Operating in Parched Elastohydrodynamic Lubrication	September 1986
	6. Performing Organization Code
7. Author(s)	8. Performing Organization Report No.
Scott D. Hunter	None (E-3152)
	10. Work Unit No.
	505-63-81
9. Performing Organization Name and Address	11. Contract or Grant No.
Case Western Reserve University Dept. of Mechanical and Aerospace Engineering Cleveland, Ohio 44106	NCC 3-30
	13. Type of Report and Period Covered
12. Sponsoring Agency Name and Address	Contractor Report Final
National Aeronautics and Space Administration Lewis Research Center Cleveland, Ohio 44135	14. Sponsoring Agency Code

15. Supplementary Notes

Project Manager, David E. Brewe, Propulsion Directorate, U.S. Army Aviation Research and Technology Activity - AVSCOM, Lewis Research Center. This report was a thesis submitted in partial fulfillment of the requirements for the Degree of Master of Science in Mechanical and Aerospace Engineering to Case Western Reserve University in August 1986.

16. Abstract

The capacitance method is used to estimate the oil film thickness in the Hertzian contact zone of an angular contact ball bearing operating in parched elastohydrodynamic lubrication. The parched elastohydrodynamic lubrication regime is characterized by a transient film thickness and basic speed ratio (ball spin rate over combined race speed) and the formation of a friction polymer. The experimental apparatus tests 40 mm 108 H ball bearings in the counter rotating race mode at loads of 200 and 300 lb, a film parameter of 1.6 and nominal inner and outer race speeds of 38 and 26 rps, respectively. Experimental results are presented for the capacitance, thickness and conductance of the oil film as functions of elapsed time and for the basic speed ratio as a function of elapsed time, load and amount of lubricant applied to the test bearing. Results indicate that a friction polymer formed from the initial lubricant has an effect on the capacitance and basic speed ratio measurements. Based on a secondary ion mass spectroscopy and emission infrared spectroscopy analyses, the polymer contains carbon, carbon-hydrogen groups, possibly nitrogen and phosphate and forms a carboneous material during failure. The basic speed ratio shows a rapid increase before bearing failure due to the formation of the friction polymer which reduces the slip between the balls and races. The capacitance measurements also signify an approaching failure through a sudden decrease in capacitance and increase in conductance of the oil film due to the presence of surface metal in the film.

17. Key Words (Suggested by Author(s))	18. Distribution Statement
Oil film thickness measurement	Unclassified - unlimited STAR Category 23

19. Security Classif. (of this report)	20. Security Classif. (of this page)	21. No. of pages	22. Price*
Unclassified	Unclassified	265	A12

*For sale by the National Technical Information Service, Springfield, Virginia 22161